REPUBLIQUE ALGERIENNE DEMOCRATIQUE ET POPULAIRE

Ministère de l'Enseignement Supérieur et de la Recherche Scientifique

Université Ferhat Abbas Sétif 1

Institut d'Optique et de Mécanique de Précision

THESE DE DOCTORAT EN SCIENCES

Option :
Optique et mécanique de précision

Présentée par :

MR : BENTOUHAMI ABDERRAHMANE

Analyse expérimentale et numérique du comportement des structures sandwiches à âmes en nids d'abeille soumises à l'impact

Experimental and numerical analysis of behavior of honeycomb sandwiches panels subjected to impact.

Soutenue le: …/…/ ……
Devant la commission d'examen:

Jury

Président	BOUAOUADJA Nourdine	Professeur	Université Sétif 1
Directeur de thèse	KESKES	Boualem MCA	Université Sétif1
Examinateurs :	BOUSAID	Ouzin MCA	Université Annaba
	CHAOUI	Kamel	ProfesseurUniversité Annaba

إلى من أحبهم كل الحب

و أنا رضيع هواهم   والطفل يؤلمه الفطام

إلى أبي من وجهني وعلمني وأتاح لي فرصة العلم و السفر و البحث في وقت ما أحوج ما يكون فيه إلي.

إلى أمي التي كان لسان حالها الدعاء لي بالتوفيق و الإتمام.

اسأل الله سبحانه و تعالى أن يطيل في عمرهما على الطاعة و أن يمتعهما الصحة و العافية و أن يجعل عاقبتهما جنة عرضها السموات و الأرض و أن يكتب اجر هذا العمل في ميزان حسناتهما يوم العرض على ربي العالمين.

ACKNOWLEDGE

Scientific production

1- **Internationale publication :**

Experimental analysis and modeling of the buckling of loaded honeycomb sandwich composite.MTAEC 9, 49 (2), 2015

Meterials and Technology 49 (2015) 2, 235-242

2- **Matériaux 2015 Mahdia (Tunisie), 22-26 Mars 2015 :**

Study of honeycomb sandwich panel in low velocity impact.

3- **Second International Workshop on Frature Mechanics FRACT' 2 24-25 November 2013 Chlef, Alegria :**

Communication 1:

Honeycomb sandwich panel under compression and three point bending loading tests.

Communication 2:

Experimental study of foamed sandwiches structures loaded in three point bending.

4- **La 2eme journée des doctorants de l'IOMP le 29 mai 2013 :**

Etude comparative du comportement en statique et en dynamique des structures sandwiches

5- **Second Euro-Mediterranean Meeting on functionalized Materials EMM-FM 2013 Hammamet (Tunisie) March 24-28 ; 2013**

Communication 1:

Mechanical behavior during compressive and numerical analysis of buckling of honeycomb composite.

Communication 2:

Experimental study and numerical modelling on three point bending test of honeycomb sandwich panels.

6- **International Symposium of Aircraft Materials ACMA 2012 May 09-12, 2012 Fez, Morocco :**

Experimental analysis and numerical modeling of buckling behavior on honeycomb sandwich panels under compression.

7- **The International Congress for Applied Mechanics. La mécanique et les matériaux, moteurs du développement. JET 2012 Mai 02-04 mai, Marrakech-Morocco**

Communication 1 :

Modélisation en flambement et étude du comportement en compression des structures sandwichs à âmes en nids abeilles.

Communication 2 :

Homogénéisation analytique et numérique des structures sandwichs à âmes en nids d'abeilles.

8- Premier colloque national en aéronautique- first national congres on aeronautics CNA 2012 Mai2-3, Constantine- Algérie.

Communication 1 :

Analyse numérique et expérimentale du comportement en compression des structures sandwiches à âmes en nid d'abeilles.

Communication 2 :

Caractérisation des panneaux sandwichs à âmes en nid d'abeilles aluminium/aluminium.

9- 2eme Conférence Internationale sur les matériaux et les structures en composite , Novembre 28-30, 2011 ALGERIA, Oran

Communication 1 :

Modélisation en flambement et étude du comportement en compression des structures sandwiches à âmes en nid d'abeilles.

Communication 2 :

Modélisation numérique du comportement en flexion des panneaux à âmes en nid d'abeilles.

10- First international workshop on fracture mechanics FRACT'1 , 13-14 november 2011, Chlef, Alegria :

Experimental analysis and modelling of the buckling of loaded honeycomb sandwich panels.

Table of Contents

List of Symbols

W	displacement (mm)

α	indentation depth (mm)
ν	Poisson's ration
σ_c^{d}	dynamic crushing strength of the core material (MPa)
σ_c^{s}	static crushing strength of the core material (MPa)

List of Figures

XIV

List of Tables

Chapter I: Introduction and Overview

In recent years, numerous studies have been carried out to find lighter structures with better mechanical performance. Composite sandwiches are an excellent compromise when an optimal trade-off between light weight and high performance is required. Consequently these structures are being increasingly used in many industrial fields such as shipbuilding, automotive, aerospace and civil structures [1, 2]. In particular, the sandwich structure provides more bending stiffness and longer fatigue life cycles and is excellent in insulating applications [3, 4]. The use of these structures offers advantages in terms of reduction of the weight of transit, improvement of the speed, and increased energy efficiency.

A typical sandwich structure, as shown in Figure 1.1, is made of two thin, stiff and strong outer skins that are adhesively bonded and separated by a lightweight core. The skins are usually aluminum plates or fiber-reinforced composite laminates. Core material can be classified as being cellular, corrugated or honeycomb. By separating the skins through a low density core, the moment of inertia of the panel is increased so increasing bending stiffness. In fact, the geometric features and the mechanical properties of the core play an important role in depicting the loading capacity and energy absorption capability of sandwich structures. The core mainly ensures that a higher bending rigidity of the skins is maintained acting like the web in a structural 1- beam - while the skins, being relatively stronger and stiffer, carry most of the impact load. The bending rigidity of the structure is directly proportional to the thickness of the core. However, the maximum thickness is often dictated by the core's shear failure.By varying the cell geometry, density and mechanical properties of honeycombs, different combinations of curvature can be produced. Aluminum honeycomb sandwich structures having open cell structures are lighter than foam and balsa cores, but their impact characteristics are inadequate [5]. While polymeric foams have been applied for many years, currently there is a significant and growing interest in sandwich structures with aluminum foam core [6, 7] and with honeycomb core [8].Honeycomb cores with hexagonal cells are widely used in the aeronautics, aerospace and shipbuilding industries and are the subject of this study. A good alternative is the sandwich panels, made of aluminum alloys.
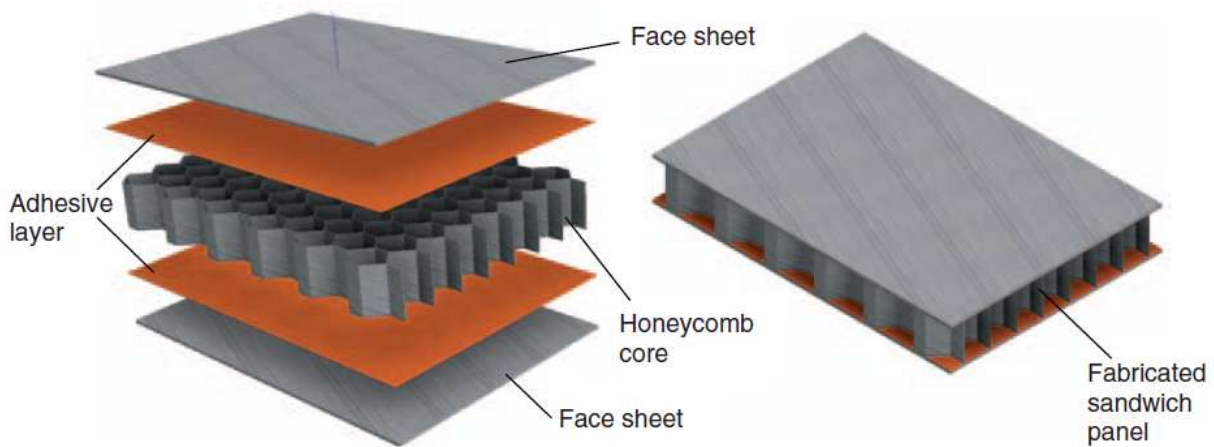
Figure 1.1: Sandwich structure with honeycomb core.

Theoretical analysis of sandwich panels has been developed by several authors [9–13] with general agreement on the formulation to be used, especially for linear behavior of sandwiches. Non-linear analysis of three-point bending of sandwich panels has also been described by Goutos et al. [13]. As a consequence of the capability of FEM codes in modeling sandwich structures, this has been the main focus of research topics on the analysis of failure of sandwich panels [12–13].

Sandwich structures are commonly subjected to severe impacts, such as those from runway and space debris, hailstones and birds. This can result in partial penetration or complete perforation of a structure. Although the impact event is a highly dynamic event, statistically determined contact laws can be used in the impact dynamics analysis of low-velocity impacts, because strain rate and wave propagation effects are negligible with commonly used material systems [14]. Many researchers have studied the mechanical properties of sandwiches with aluminum foam core and with honeycomb core. Gibson and Ashby [15] gave a thorough overview of the literature on cellular materials.

Many researchers have investigated the relationship between the failure mechanisms, the type of material used and the geometrical configuration of sandwich structures when subjected to bending, compression, quasi-static indentation and impact. Steeves and Fleck [16] devised a systematic procedure to compare the performance of sandwich beams with various combinations of materials. They identified the operative failure mechanisms and optimized the geometry of the sandwich structures to minimize the mass for a given load-bearing capacity. Petras and Sutcliffe [17] studied the failure mechanisms for GFRP skins/

honeycomb core sandwich beams under three points bending. They then constructed a failure mode map showing the dependence of failure mode and load on skin thickness to span length ratio and honeycomb density.

Yamashita and Gotoh [18] studied the impact behavior of honeycomb structures with various cell thicknesses and branch angles. They showed the effects of the cell shape and thickness on the crush strength by numerical simulations and experiments.

The strength of aluminum honeycomb-cored sandwich panels was evaluated in the same year by Paik et al. [19]in different loading conditions: three-point bending, axial compression and lateral crushing loads. Analytical and numerical (Finite Element) approaches have been used for the modeling of an aluminum honeycomb sandwich panel during a typical four-point bending test [20].

The failure mode and the damaged structure of the honeycomb panels have been also investigated by a Computed Tomography (CT) system, which allows a three-dimensional reconstruction of the analyzed object [21] and to obtain the data for Finite Element models of open-cell aluminum foam specimens [22]. Static and dynamic bending tests were carried out on AFS panels and simplified collapse models were developed [23] to explain the experimental observations. The failure mode and the damaged structure of the impacted panels have been also investigated by a Computed Tomography (CT) system [24]. An extensive series of experimental tests has been carried out by the authors for analyzing the mechanical behavior and collapse failure of the aluminum honeycomb sandwiches under static bending and low-velocity impact loading. Simplified collapse models were developed for honeycomb panels in order to define the bending collapse loads as a function of the support span values and a good agreement between predicted and experimental limit loads was achieved. The failure mode and the damaged structure of the impacted panels have been also investigated by a Computed Tomography (CT) system that allows a three dimensional reconstruction of the analyzed object. The CT system can detect the damage and internal flaws, including delamination and microcraking, in fiber-reinforced polymeric matrix composites [25]. Core deformation and failure are decisive factors for the energy absorption capability of sandwich structures. In the case of sandwiches, with aluminum honeycomb cores, damage consists of "buckling" of cell walls in a region surrounding the impact point, while, in foam cores, damage looks more like a crack for low-energy impacts [22-25].

[26] Simulation of the water impact (slamming) loading of sandwich boat structures has been presented. A weighted elastomer ball was dropped from increasing heights onto rigidly supported panels until damage was detected. Results from this test indicated that honeycomb

core sandwich panels, the most widely used material for racing yacht hulls, start to damage due to core crushing at impact energies around 550 J. Sandwich panels of the same areal weight and with the same carbon/epoxy facings but using a novel foam core reinforced in the thickness direction with pultruded carbon fibre pins, had not show signs of damage until above 1200 J impact energy. This suggests that these will offer significantly improved resistance to wave impact. Quasi-static test results cannot be used to predict impact resistance in their study as the crush strength of the pinned foam was more sensitive to loading rate than that of the honeycomb core.

An extensive study of the dynamic out-of-plane indentation of aluminum honeycombs at a range of different loading velocities. Dynamic and quasi-static mechanical properties of honeycombs were comparatively analyzed to investigate the strain rate effect on both mean plateau stress and energy absorption. Indentation and compression tests of three types of HEXCELL-5052-H39 aluminum hexagonal honeycombs were tested. The tearing energy was calculated as the difference in energy dissipated in indentation and compression of the same type of honeycomb. It was found that tearing energy was affected by strain rate and nominal density of honeycomb. Empirical formulae were proposed for tearing energy in terms of strain rate. [27]

Deformation of the sandwich panels has been studied by analyzing the deformation and the failure modes of the face sheets and the core for different core configurations, while the resistance of the sandwich panels has been studied by measuring the back-face deflection of the panels. The back-face deflection of the sandwich panels has also been compared with monolithic plates of equivalent mass and air sandwich panels. The air sandwich panel has a structure which consists of only two parallel plates (without core) at a distance similar to the core thickness of honeycomb sandwich panels. Finally the back-face deflection histories of the sandwich panels have been compared with the deflection histories of monolithic plates of equivalent mass to determine the benefit of using sandwich panels in reducing elastic spring-back. The histories of the back-face deflection have been captured experimentally by using a laser displacement sensor. The advantages and limitations of using sandwich panels in absorbing impact energy of foam projectile impact have been discussed [28].

They purpose in their research the characterization of honeycomb sandwich panels with two kinds of defects (Brinell ball, and drilling hole) on two types of honeycomb core (aluminum and aramide fibre) under fatigue loading. First, fatigue results of the characterization were compared to fatigue results of aluminum alloy skin which is the reference case. Second, Wöhler curve in the term of (load versus number of cycles) of honeycomb sandwich panels

with and without defects have been presented and discussed. Finally, damage and failure of sandwich panels with and without defects have been reported [29].

As described above, many studies have been conducted on the impact characteristics of the existing honeycomb sandwich panel with respect to the material quality, variation of thickness, and other parameters related to the face-sheet and the core. Therefore, this study is attempted to identify and investigate responses of these structures under static and dynamic loading and their damage mechanism according to the change of sum key parameters.

The goal of this present research is the experimental, analytical and numerical investigation of response of honeycomb panels under different loading (compression, quasi-static indentation and low velocity impact). Otherwise, we try to understand how geometrical configuration affects failure mechanisms for honeycomb sandwich structures subjected to different loadings. All structures tested in this work had an aluminum skin and honeycomb core (AHC and NHC). By varying the geometrical parameters (core's density, cell size, indenter geometry); core material (AHC and NHC) and loading conditions (velocity of solicitation) experimental tests were carried out. To optimize the use of the honeycomb sandwiches composites as structural elements, a theoretical approach was developed which will allowing parametric studies to be performed. In addition, the energy-balance model is used in conjunction with the law of conservation of momentum to solve for the impact load and deflection histories under low-velocity impacts. The theoretical results tallied with the experimental ones and consequently it was shown that the theoretical model is a reliable predictor of failure mechanisms in composite sandwiches with defined geometry. The critical buckling loads and failure modes of the sandwich panels have been determined by applying quasi-static and dynamic tests on these structures. A three-dimensional geometrically finite element model of the honeycomb sandwich plate and a rigid impactor is developed using the commercial software, ABAQUS. By adopting a discrete modeling approach where the cellular walls and the face sheets are explicitly modeled using shell elements, accurate prediction of the damage mechanisms and failure are possible. The obtained numerical buckling loads have been compared with the experimental results and presented in tables.

Chapter II: Literature Review

A literature review on composite sandwich construction is developed in this chapter. The review will begin with general exposure of the sandwich structure: the different components, the interest and advantages of its use and the different application areas. Secondly, the focus is set on experimental, theoretical and numerical results of previous works. Indeed, the term "buckling" is defined and the main damage mechanisms of a sandwich structure are presented. Finally, the influence of different structural parameters related to the core material of the sandwich structure and the influence of the experimental parameters related to the static and dynamic tests are explained.

II.1.   **Definition of composite** sandwich panels

In the aircraft industry every extra kilogram of structural mass taken off, means an increase in payload mass as well as a decrease in fuel mass, which trickles down to an increase in profit. Thus honeycomb sandwich panels were one of the outcomes of research into decreasing structural mass. Sandwich construction results in lower lateral deformations, higher buckling resistance and higher natural frequencies than monocoque constructions.

Amongst all possible design concepts in composite structures, the idea of sandwich construction has become increasingly popular because of the development of manmade cellular materials as core materials. Sandwich structures consist of (Figure 2.1) 1) a pair of thin stiff, strong skins (faces, facings or covers), 2) a thick, lightweight core to separate the skins and carry loads from one skin to the other; and 3) an adhesive attachment which is capable of transmitting shear and axial loads to and from the core [9]. The separation of the skins by the core increases the moment of inertia of the panel with little increase in weight, producing an efficient structure for resisting bending and buckling loads.

Figures 2.1 and 2.2 show the honeycomb sandwiches structure, which is used extensively in this thesis.
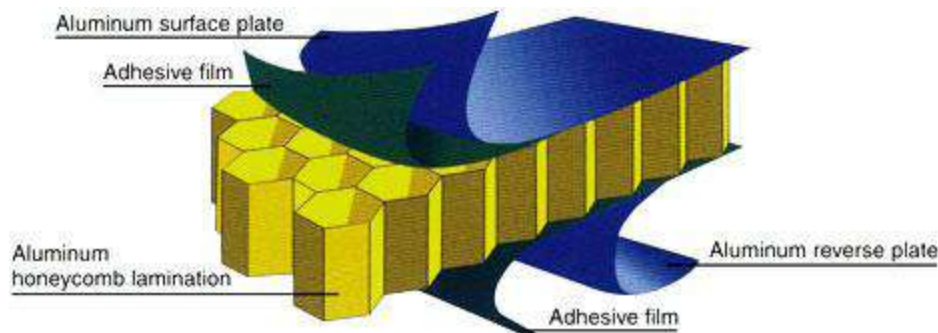
Figure 2.1: Honeycomb sandwich structure.
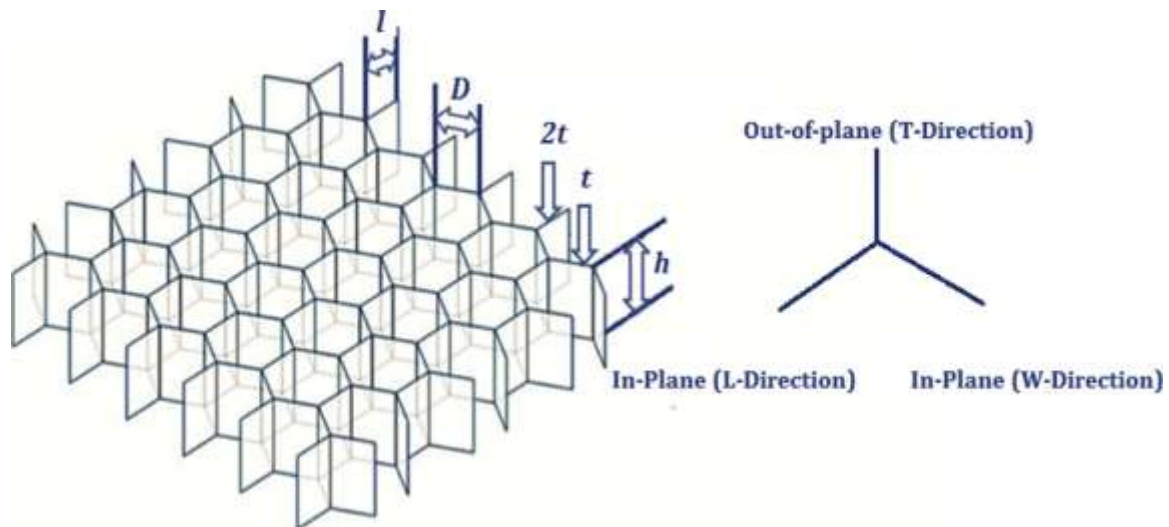
Figure 2.2: Schematic diagram of hexagonal honeycomb.

In structural sandwiches, face-sheets are mostly identical in material and thickness and they primarily resist the in-plane and bending loads. The face-sheets are strong and stiff in tension and compression compared to the low density core material whose primary purpose is to keep the face-sheets separated in order to maintain a high section modulus. These structures are called symmetric sandwich structures. However, in some special cases face-sheets may vary in thickness or material because of different loading conditions or working environment. This configuration is named as asymmetric sandwich structures. In general sandwich structures are symmetric; the variety of sandwich constructions basically depends on the configuration of the core. The core of a sandwich structure can be almost any material or architecture, but in general they are classified in four types; foam or solid core, honeycomb core, web core and corrugated or truss core (figure 2.3). The adhesion of face-sheets and core is another important criterion for the load transfer and for the functioning of the sandwich structure as a whole (ASM Handbook 1987). The core material has relatively low density (e.g., honeycomb or foam), which results in high specific mechanical properties, in particular, high flexural strength and stiffness properties relative to the overall panel density. Therefore, sandwich panels are efficient in carrying bending loads. Additionally they provide increased buckling resistance to shear panels and compression members.
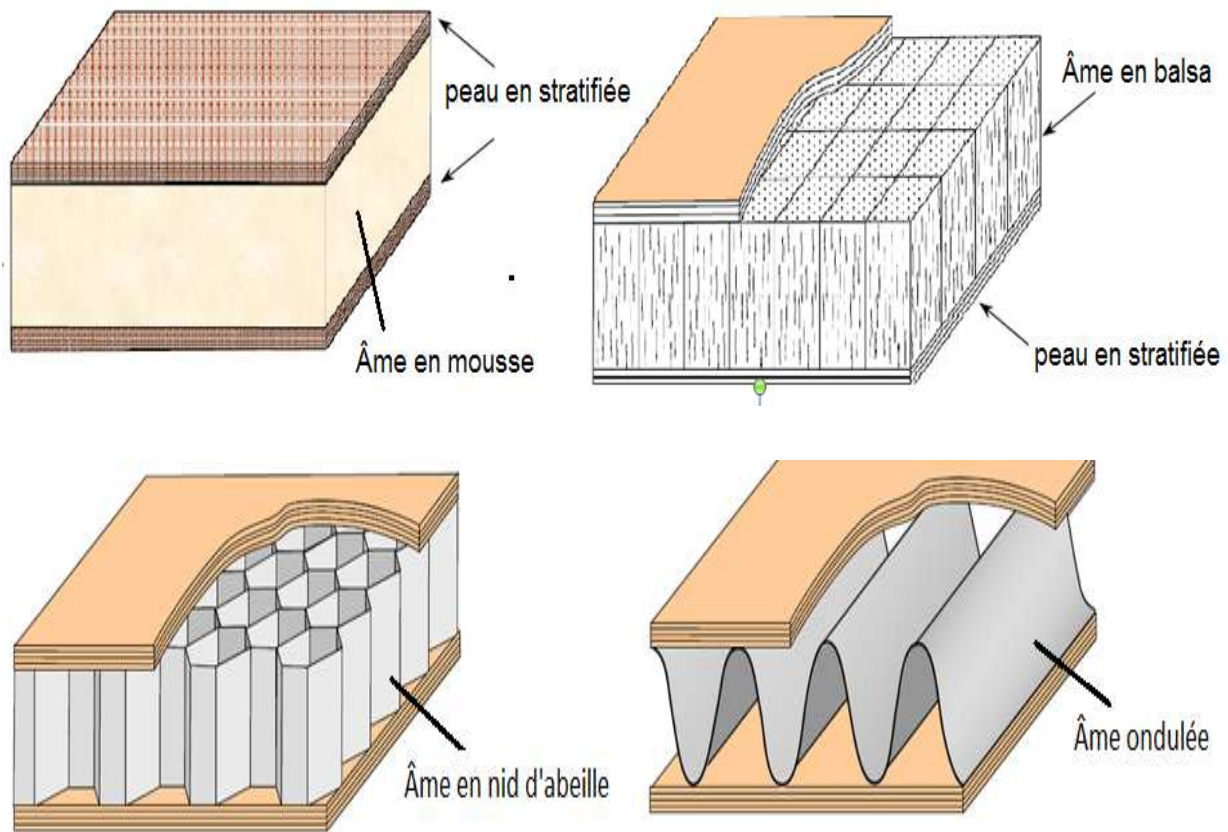
Figure 2.3: Sandwich panels with (a) corrugated (b) foam and (c) honeycomb core.

The relative separation of the stable face sheets result in high stiffness to weight ratios. Essentially the honeycomb was used as a shear web between two upper and lower skins, with the early honeycomb sandwiches made of balsa wood as the core and plywood as the skins. With the development of Epoxy resin, it was possible to bond aluminum skins to an aluminum honeycomb core. Since then, much advancement has been made in honeycomb studies, with the most commonly used honeycomb for aircraft structures being aluminum and Nomex Honeycomb which have been identified as one of the potential candidate protective structures as they have a high strength to weight ratio and have a good energy absorption capacity.

A sandwich structure operates in the same way with the traditional I-beam, which has two flanges and a web connecting the flanges (Figure 2.4). The connecting web makes it possible for the flanges to act together and resist shear stresses. Sandwich structure and an I-beam differ from each other that, in a sandwich structure the core and laminates are different materials and the core provides continuous support for the laminates rather than being concentrated in a narrow web. When the structure subjected to bending the laminates act

together, resisting the external bending moment so that one laminate is loaded in compression and the other in tension. The core resists transverse forces, at the same time, supports the laminates and stabilizes them against buckling and wrinkling.

Allen [9] and Plantema [10] presented the fundamental models of sandwich structures, assuming that the core is incompressible in the out-of-plane direction and does not have any bending rigidity, the skins only have bending rigidity, and the core has only shear rigidity. This approach is good for sandwich structures with incompressible cores, which are Anti-plane, like honeycomb cores.
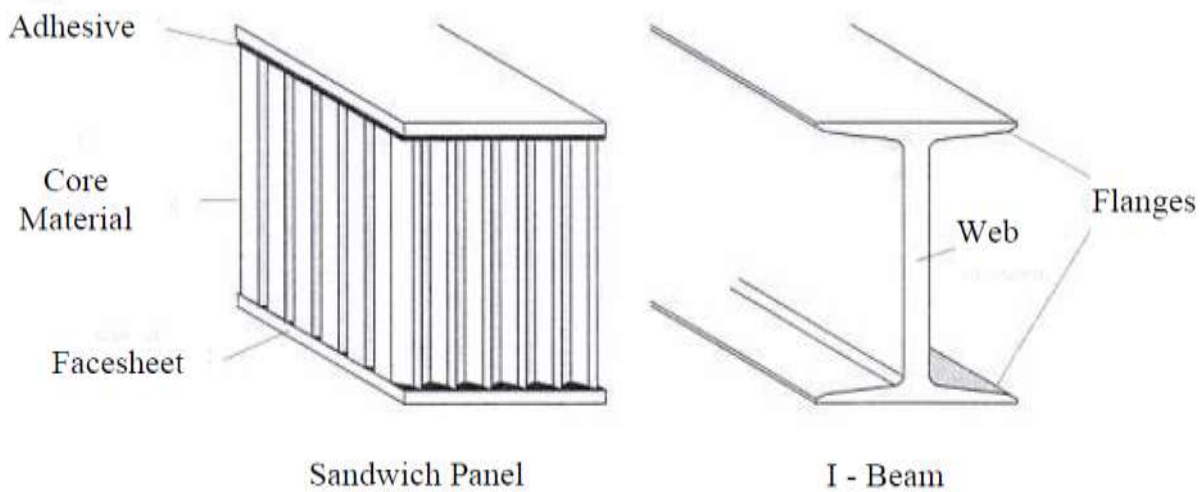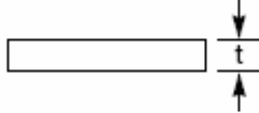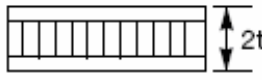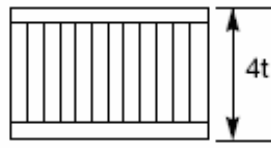
Figure 2.4: Sandwich structure in comparison with an I-beam.

Sandwich structures should be designed to meet the basic structural criteria such as the face-sheets should be thick enough to withstand the tensile, compressive and shear stresses and the core should have sufficient strength to withstand the shear stresses induced by the design loads. Adhesive must have sufficient strength to carry shear stress into core. The core should be thick enough and have sufficient shear modulus to prevent overall buckling of the sandwich under load to prevent crimping. Compressive modulus of the core and the face-sheets should be sufficient to prevent wrinkling of the face-sheets under design load. The core cells should be small enough to prevent the face-sheet dimpling under design load. The core should have sufficient compressive strength to resist crushing design loads acting normal to the panel face-sheets or by compressive stresses induced through flexure. The sandwich structure should have sufficient flexural and shear rigidity to prevent excessive deflections under design load (ASM Handbook1987).

II.2.   Advantages of Sandwich Composites

Sandwich structures utilize each of its constituent materials' properties. The thin face sheets' high stiffness combined with low-density cores give a sandwich structure of high stiffness to weight ratio when compared with a face sheet beam of same weight, and a high bending strength to weight ratio. In addition to the efficiency between stiffness and strength, honeycomb sandwich panels are fairly fatigue resistant, great insulators or radiators depending on the core material selection, highly serviceable and have smooth aesthetically pleasing surfaces.

Honeycomb sandwich panels are analogous to beams or plates. The use of honeycomb prevents buckling of the thin skins by providing the amount of shear strength to do so. Honeycomb panels are lightweight, easy to work with, and not labor intensive. By increasing the thickness of the core, the composite panel's strength and flexural stiffness increases much like increasing the height of a beam, but without the weight increase shown in Table 2.1. This is due to an increase in the panels' moment of inertia. Composite panels are designed such that failure occurs in the core of the panel, thus shear strength is the main factor in design, which is the core's predominant material property. Composite panels are designed to meet the application requirements. They have the same normal strengths that composites have, due to the face sheets being constructed from materials of high modulus of elasticity's (when compared with the core) like fiber-resin mixtures, metal alloys and plastics. The cores have low elastic moduli that yield without failure in the high deflection regimes. Cores usually consist of metallic and fibrous honeycomb structures to opened and closed cell structured foams.There are many standards, manufacturing techniques and accepted methods for constructing and testing materials such as metals. As sandwich composite structures are relatively new, there are not nearly as many standards for manufacturing and testing, particularly with the inclusion of honeycomb. Quality control thus is difficult to ensure correct integration into the strict design requirements of the aerospace industry. This results in a much higher safety factor when constructing the sandwich design, which is counterproductive to the main goal of reducing weight.

	Solid Metal Sheet	Sandwich Construction	Thicker Sandwich
Relative Stiffness	100 %	700 % 7 times more rigid	3700 % 37 times more rigid!
Relative Strength	100 %	350 % 3.5 times as strong	925 % 9.25 times as strong!
Relative Weight	100 %	103 % 3% increase in weight	106 % 6% increase in weight

II.3.   Application Areas of Sandwich Structures

The use of composite sandwich structures in aeronautical, automotive, aerospace, marine and civil engineering applications is getting wider as these structures have excellent stiffness to weight ratios that lead to weight reduction and fuel consumption. Also they have high structural crashworthiness because they are capable of absorbing large amounts of energy in a sudden collision. Various combinations of core and face-sheet materials are being studied by researchers worldwide in order to achieve improved crashworthiness.

Thus sandwich panels are popular in high performance applications where weight must be kept to a minimum, for example aeronautical structures, high-speed marine craft and racing cars (Fig2.5).
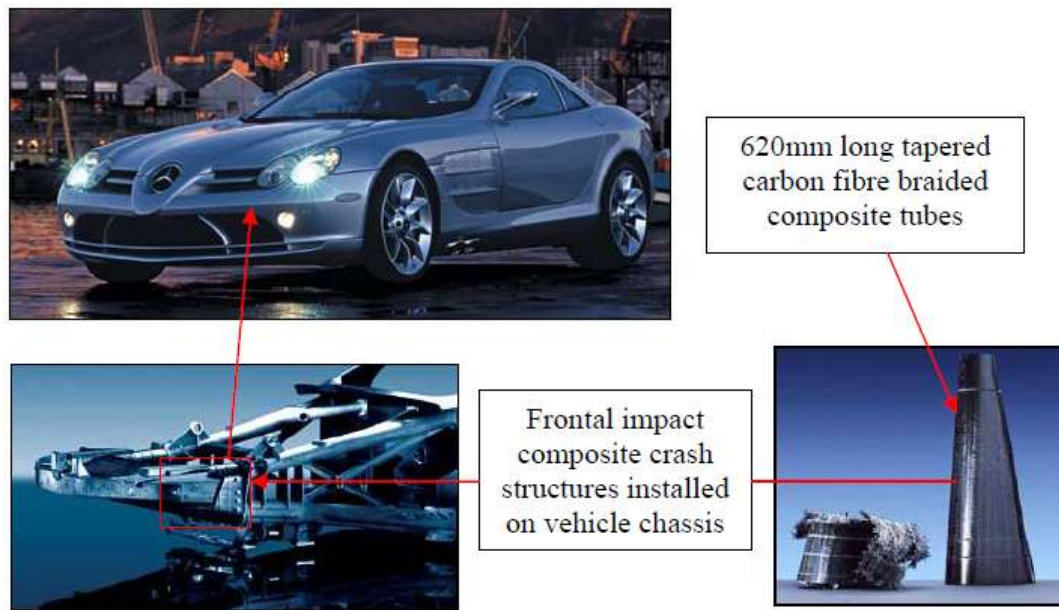
Figure 2.5: Mclaren Mercedes SLR bumper tube.

The application of composites is in high demand due to their favorable mechanical characteristics and material properties to current materials used, especially in the aerospace industry. In aerospace applications various honeycomb cored sandwich structures were used for space shuttle constructions also they are used for both military and commercial aircrafts. The U.S. Navy and the Royal Swedish Navy has used honeycomb sandwich bulkhead to reduce the weight of the ship and to withstand underwater explosions for more than 20 years. Moreover, locomotives are designed in order to resist the pressure waves occurring during the crossing of two high-speed trains in tunnels. More recently, sandwich constructions are commonly used in civil engineering projects such as bridge decks, wall and roof claddings for buildings because of their low cost and thermal performance. Also, railcars for rapid transit trains, busses, sailboats, racing boats, racing cars, snow skis, water skis and canoes are all employing sandwich constructions [12].

Composite sandwich structures have revolutionized the aerospace industry because of their high stiffness and lightweight attributes when compared with aluminum, the aviation standard. Sandwich structures have proven particular advancements in the latest spacecraft, automobiles, airplanes and racing yachts to name a few. In the civil industry, sandwich composites have revolutionized bridge and flooring structures. In the auto industry, companies have shifted to the use of fiberglass and carbon fiber to dramatically decrease weight, and thus directly increase performance. These advancements are accounted mostly to

15

the large weight reduction sandwich structures and composites offer over traditional materials. The aerospace and military industry has had the most dramatic advancements due to the use of sandwich composites. Aircraft performance, for the most part is directly affected by weight. Sandwich structures can be almost as stiff as steel whilst the low core density maintains the sandwich structure weight at a fraction of that compared with a comparable steel beam. Sandwich structures can be integrated into such aircraft parts as the wings, floor, ceiling, fuselage and cargo compartment paneling, and even control surfaces. Figure 2.4 shows the Boeing 787: the most recent aircraft to be constructed out of mostly composite materials, allowing for a 20% increase in fuel efficiency and 40% increase in engine efficiency over its' replacement, the Boeing 767 (Fig.2.6).

Figure 2.6: Over 50% composite commercial plane - Boeing's 787 Dreamliner.

II.4.   **Summary of Literature Review**

The buckling collapse of a honeycomb was analyzed in their study. A novel large deformation theory using a stiffness method has been introduced to compute the collapse surface for a honeycomb under in-plane biaxial stresses [30]. Otherwise, extensive experiments on a wide range of Nomex honeycombs have been reported, and the results compared with the model. It was founded that the magnitude of the buckling stress depends strongly on the density of the honeycomb and weakly on the shape of the unit hexagonal cell. On the other hand, the shape of the collapse surface depends strongly on the cell geometry and may be thought of as independent of the density of the honeycomb.

Figure 2.7 shows the dependence of the uniaxial collapse stress σ_{20}^*, normalized by $E_s(\rho/\rho_s)^3$, on the anisotropy ratio, R. The ratio, R, is defined by R = 0.58 $(1 + \sin\alpha)/\cos\alpha$ (it measures the deviation of the cell shape from a regular hexagon, for which R = 1). The solid line in the figure shows the prediction from this study while the dashed line shows the

16

prediction from Gibson *et al.* [15]. The diagram clearly shows that the large-deformation model agrees better with the experimental data.
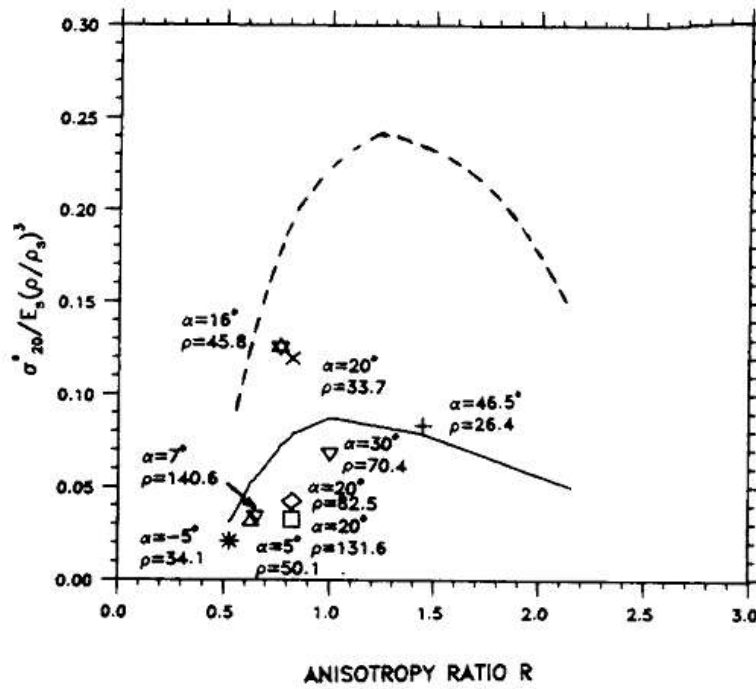
Figure 2.7: The graph shows the dependence of try on cell geometry. The solid line shows the prediction from the large-deformation model, and the dashed line shows the results from the small deformation model. The anisotropy ratio r = 0.58 (1 + sinα)/cosα [30].

[31]The mechanical behavior and failure mechanism of honeycomb composite consisting of Nomex honeycomb core and 2024Al alloy face-sheets were investigated in their work. The compressive and shear deformation behaviors of honeycomb composite were analyzed at temperatures ranged 25–300∘C. The compressive and shear strengths of honeycomb composite decreased continuously with increasing temperature up to 300∘C. The stress-strain curves obtained from the compressive and shear tests showed that the stress increased to a peak value and then decreased rapidly to a steady state value, which is nearly constant up to failure with increasing strain. The compressive deformation behavior (figure 2.8) of honeycomb composite was progressed by an elastic and plastic buckling of cell walls, debonding fracture at the interfaces of cell walls, and followed by a fracture of resin layer on cell walls.
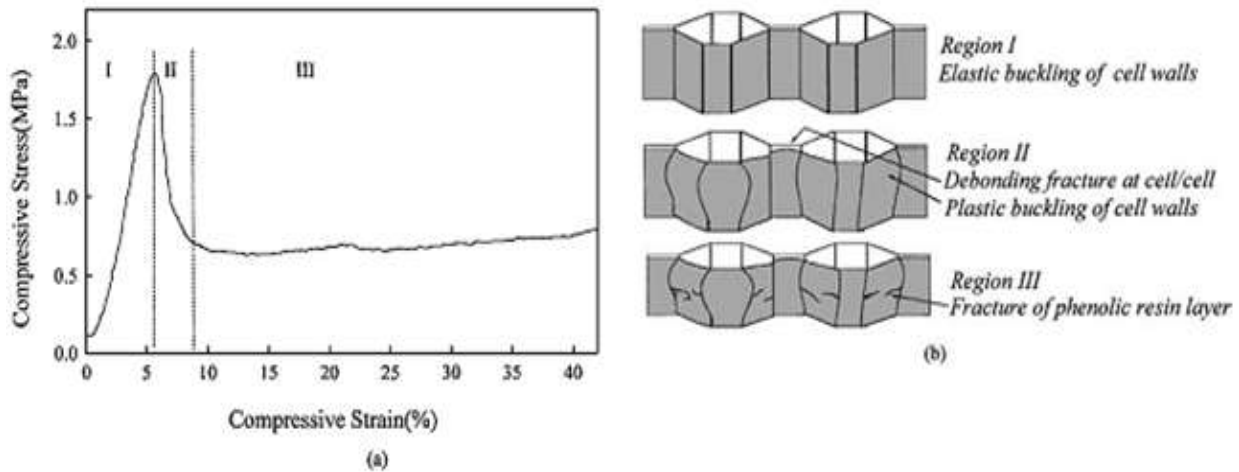
Figure 2.8: Typical stress-strain curve obtained from the compressive test: (a) typical stress-strain curve, (b) schematic microstructural change during the compressive deformation of specimen [31].

Figure 2.9 shows the variation of compressive strength calculated from the maximum value in stress-strain curve with increasing temperature. The measured compressive strengths of 1.7 MPa were compared with the calculated compressive strengths of 1.97 MPa based on Zhang and Ashby's model [30].
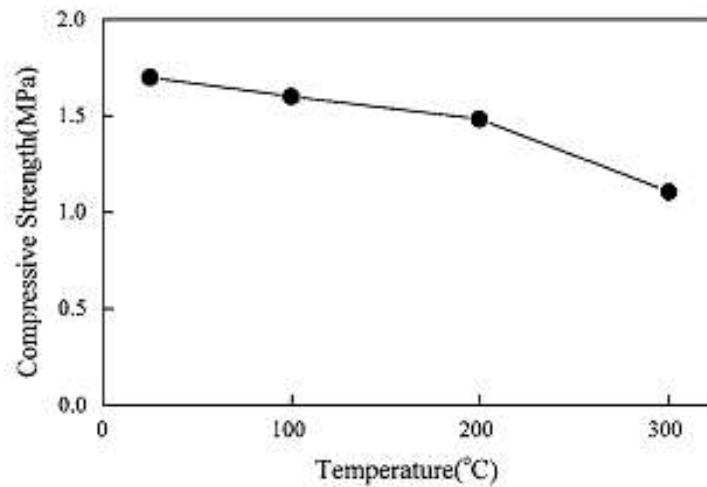
Figure 2.9: Variation of compressive strength of honeycomb composites with increasing temperature [31].

[32] In their work several numerical techniques for modelling the transverse crush behavior of honeycomb core materials have been developed and compared with test data on aluminum and Nomex honeycomb. The methods included a detailed honeycomb micromechanics model, a homogenized material model suitable for use in FE code solid elements, and a homogenized discrete/finite element model used in a semi-adaptive numerical coupling (SAC) technique. The micromechanics model has shown to be suitable for honeycomb design, since it may be used to compute crush energy absorption for different

18

honeycomb cell sizes, cell wall thicknesses and cell materials. However, the very fine meshes required have been making it unsuitable for analysis of large sandwich structures. The homogenized FE model may be used for such structures, but gives poor agreement when failure is due to core crushing. The SAC model has shown to be most appropriate for use in structural simulations with extensive compression core crushing failures, since the discrete particles are able to model the material compaction during local crushing. Figure 2.8 shows the typical stages of the quasi-static compression test on aluminium honeycomb material. Three different regimes can be observed: at low strains a linearly elastic region and buckling, followed by progressive folding and final densification.
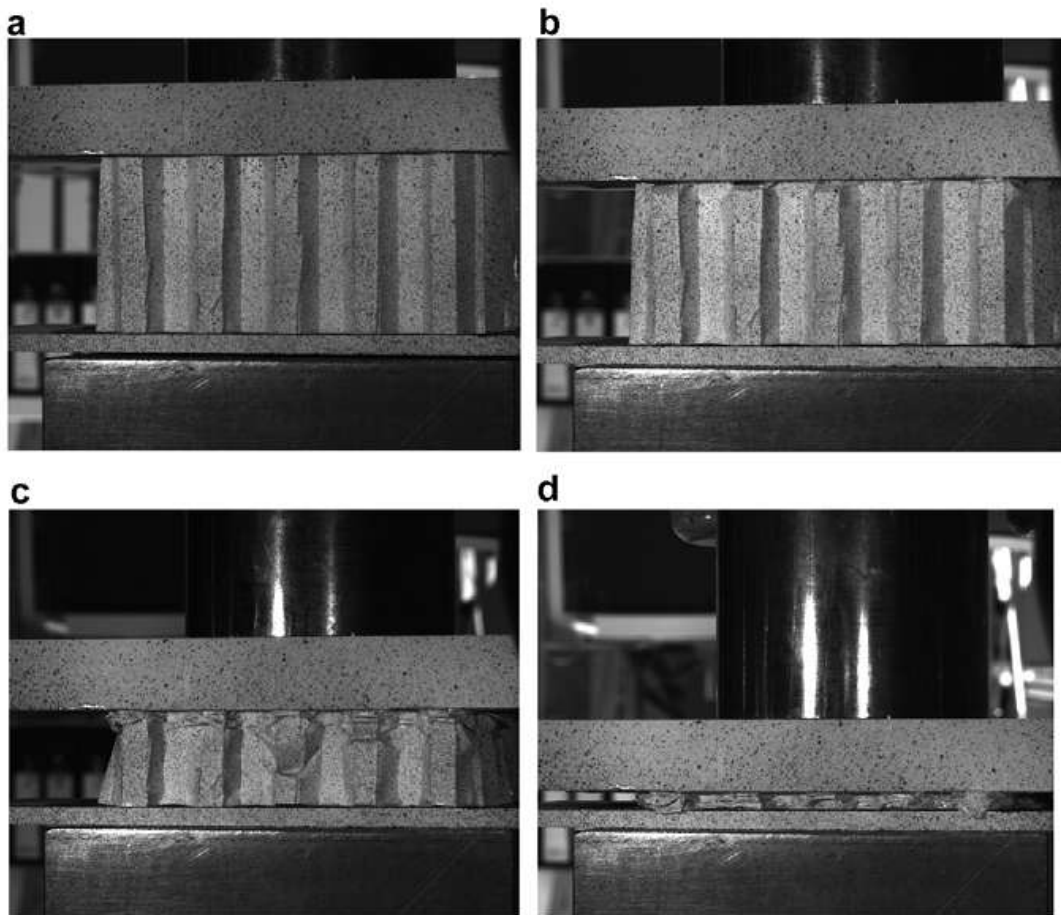
Figure 2.10: Stages of quasi-static compression test of aluminum honeycomb: (a) initial state, (b) buckling initiation, (c) progressive folding and (d) densification [32].

Initial studies on modeling the crush behavior have showed that these micro buckling/failure problems have typically meshing sensitive, so that a mesh sensitivity analysis was conducted. Three different mesh sizes have been chosen: 0.5, 1 and 2 mm, respectively. Figure 2.11shows that the deformation modes at 30% and 60% change slightly with three different mesh sizes. In experimental work, the aluminum honeycomb starts collapsing after

buckling. The collapse behavior was a mixture of global and local deformation. At 30% deformation the collapsed mode was the mixture of global (starts approximately from the middle of the honeycomb) and local collapse from the upper side of the honeycomb. However 2 mm mesh size produces pure global collapse.
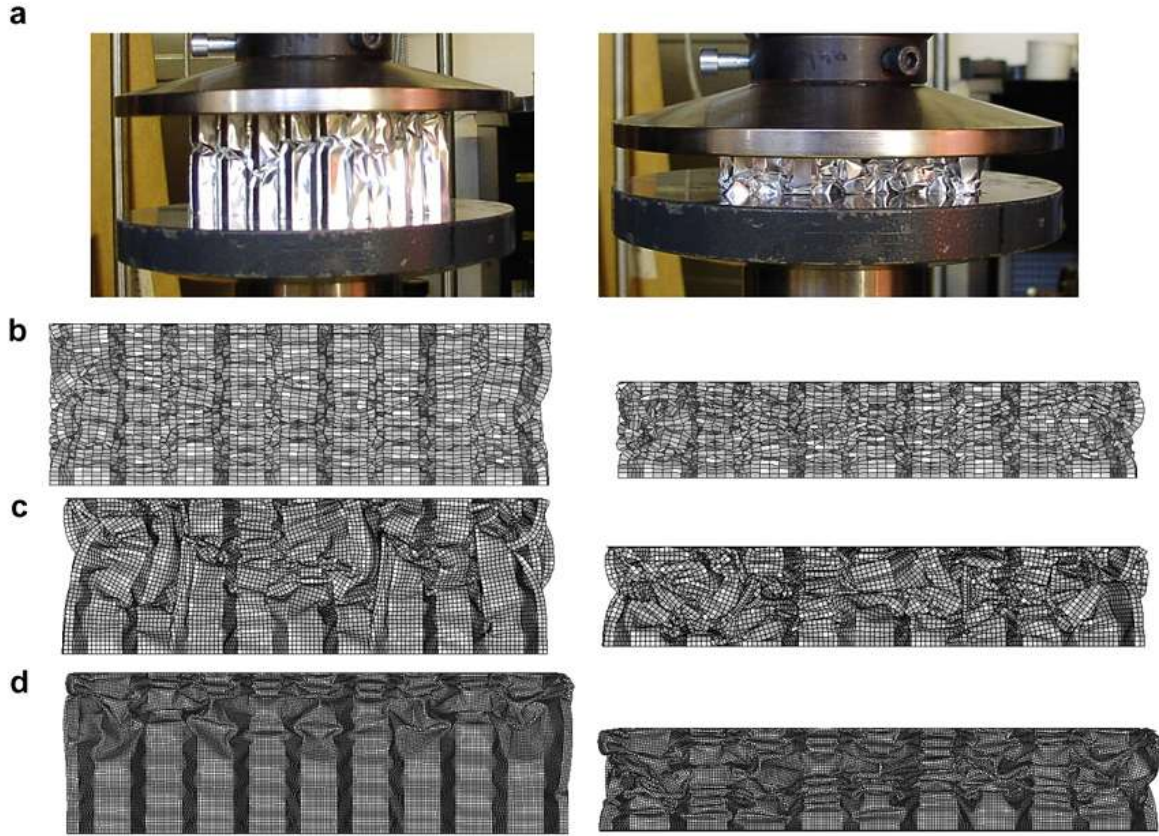
Figure 2.11: Stages of quasi-static compression of aluminum honeycomb at 30% and 60% compressive strain: (a) experiment, and FE analysis with (b) 2 mm, (c) 1 mm and (d) 0.5 mm element size.

The numerical model with 2 mm mesh size was given higher load response than the numerical models with 1 mm and 0.5 mm mesh sizes. The difference has been get higher when the aluminum honeycomb has been get near to the densification region. This shows that the number of elements through the core thickness can change the global and local deformation responses and the load–deformation history (figure 2.12-13).
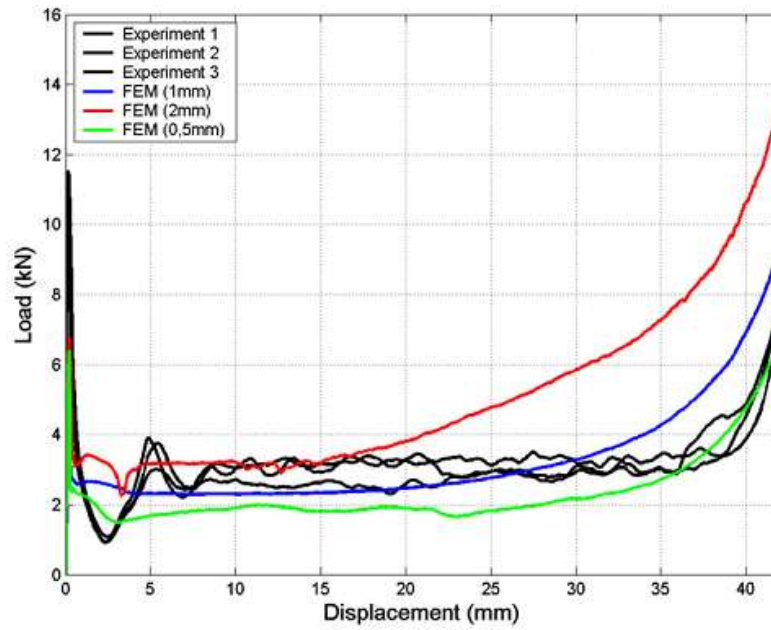
Figure 2.12: Numerical (three different mesh sizes) and experimental load–displacement responses of aluminum honeycomb under compression.
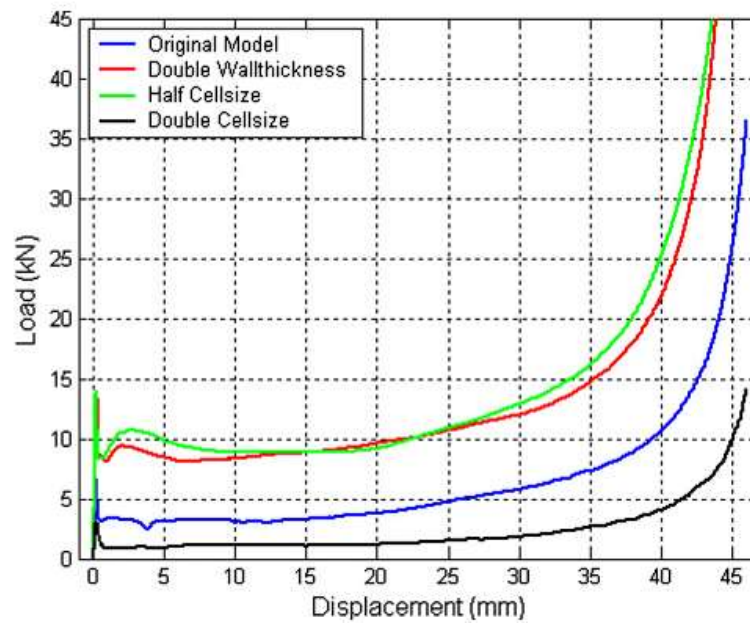
Figure 2.13: Effect of cell size and cell wall thickness on crush response on aluminum honeycomb in compression.

[33]Their work describes the results of experiments and numerical simulation studies on the impact and indentation damage created by low-velocity impact subjected onto honeycomb sandwich panels for application to the BIMODAL tram. The tested panels were subjected to low-velocity impact loading using an instrumented testing machine at six energy levels. Contact force histories as a function of time were evaluated and compared. The extent of the damage and depth of the permanent indentation was measured quantitatively using a 3-dimensional scanner. An explicit finite element analysis based on LS-DYNA3D was focused on the introduction of a material damage model and numerical simulation of low-velocity impact responses on honeycomb sandwich panels. Extensive material testing was conducted to determine the input parameters for the metallic and composite face-sheet materials and the effective equivalent damage model for the orthotropic honeycomb core material. Good agreement was obtained between numerical and experimental results; in particular, the numerical simulation was able to predict impact damage area and the depth of indentation of honeycomb sandwich composite panels created by the impact loading.
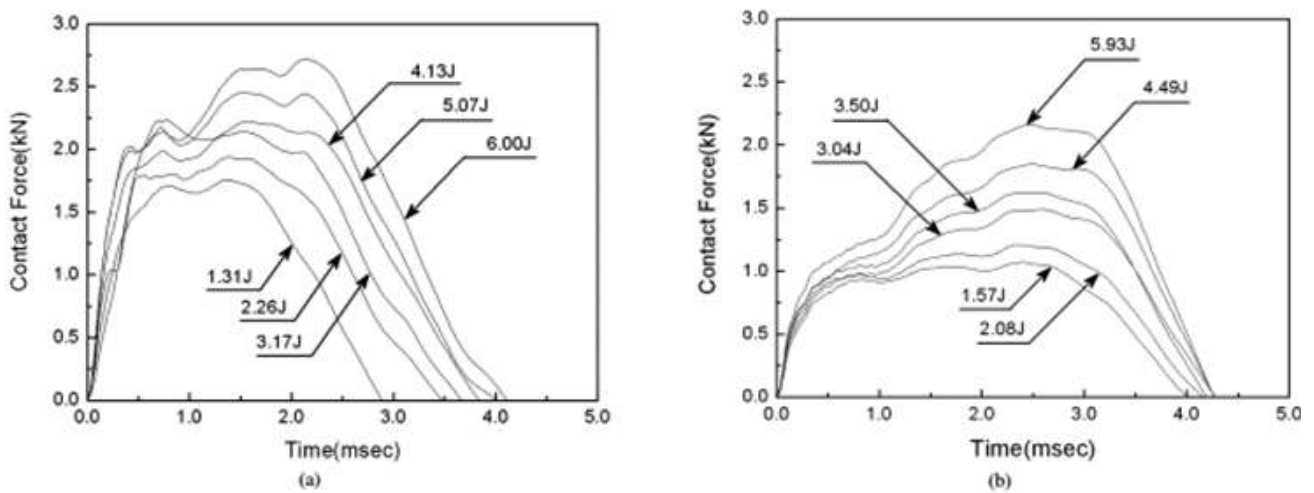
Figure 2.14: Force–time histories with impact energy for the sandwich specimens. (a) body-shell sandwich panels (GE/AH) and (b) floor sandwich panels (AL/AL) [33].
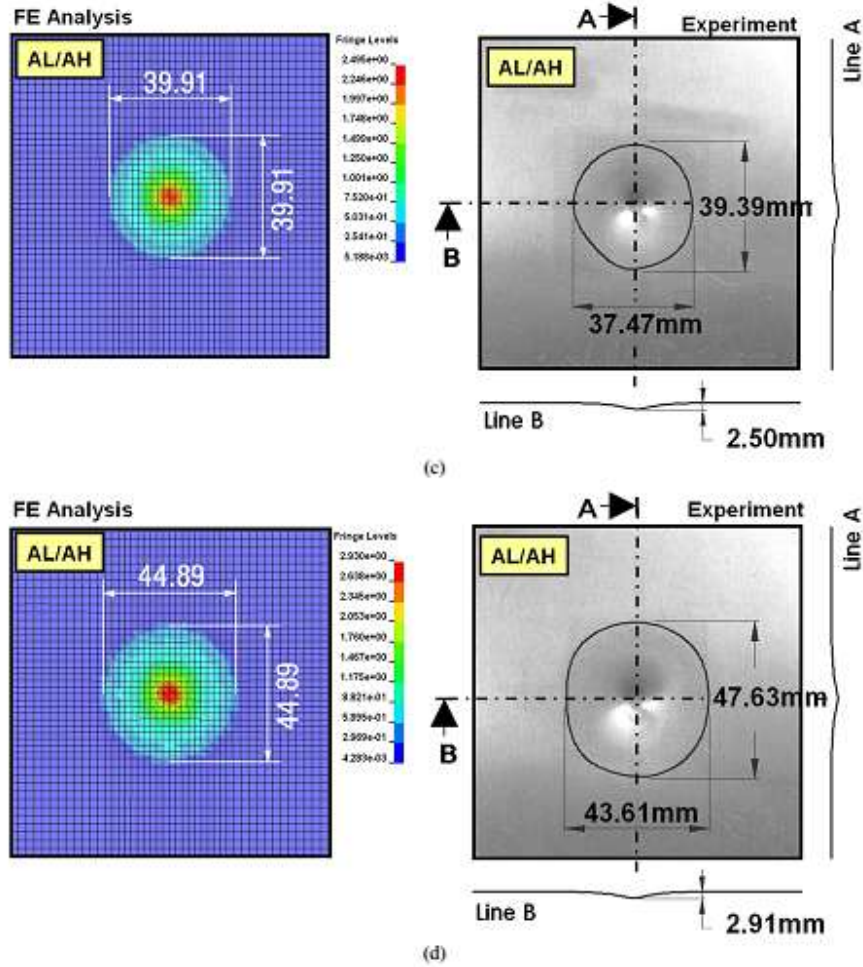
Figure 2.15: Comparison of impact damage areas for floor sandwich panels (al/ah) after impact loading. (a) 1.57 j, (b) 3.04 j, (c) 4.49 j and (d) 5.93 j [33].
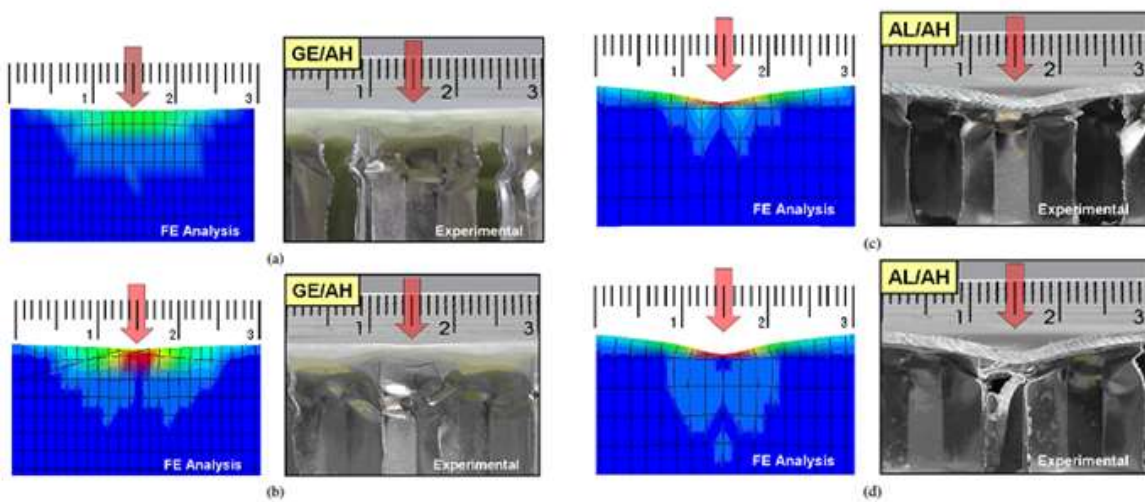
Figure 2.16: Comparison of post-impact damage for sectioned sandwich panels after impact loading. (a) GE/AH specimens (4.13 j), (b) GE/AH specimens (6.00 j), (c) al/ah specimens (4.49 j) and (d) AL/AH specimens (5.93 j) [33].

23

[34]They presented results from a test developed to simulate the water impact (slamming) loading of sandwich boat structures. A weighted elastomer ball was dropped from increasing heights onto rigidly supported panels until damage was detected. Results indicated that honeycomb core sandwich panels start to damage due to core crushing at impact energies around 550 J. Sandwich panels of the same areal weight and with the same carbon/epoxy facings but using a novel foam core reinforced in the thickness direction with pultruded carbon fiber pins, did not showed signs of damage until above 1200 J impact energy.

Two examples from the preliminary tests, shown in Figure 2.17, enable the influence of sandwich thickness and density to be examined. The damage energy is the energy at which damage was observed, defined simply as E=mgh. Thinner cores may provide improved impact performance due to improved deflection resulting in higher stored energy, Figure 2.14 a. Increasing density can improve the energy absorbed before damage is observed, as resistance to local crushing is improved, but there may be a plateau to this improvement as higher flexural rigidity results in lower deflection, Figure 2.17 b. It should be noted that the thicker sandwich panels did not show the same damage mechanism as thin panels. For the latter core crushing was apparent, while thicker panels also showed skin/core delamination.
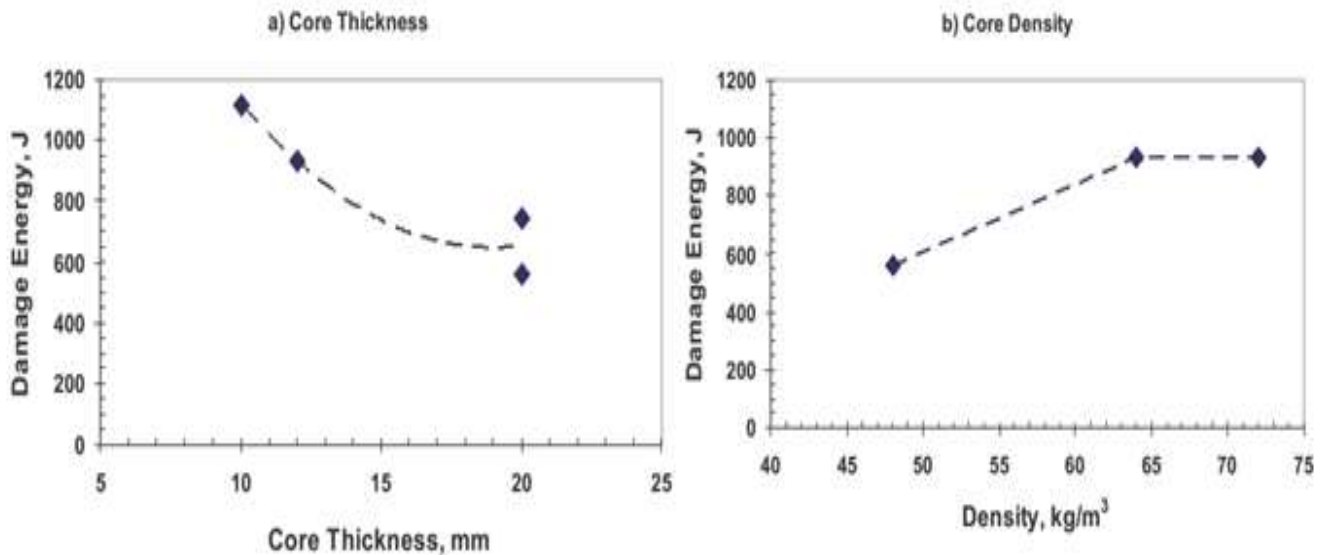
Figure 2.17: Influence of core thickness and core density on energy to first damage, honeycomb core, a) OX 64 kg/m3, b) OX 20mm thick [34].

Four fully instrumented panels were tested, two honeycomb, one pinned foam core and one unreinforced core sandwich. Panels were loaded at drop height increments of one meter. In

24

order to examine repeatability the two meter drop height test was repeated three times on each honeycomb panel. Figure 2.18 summarizes the tests performed on the three materials.
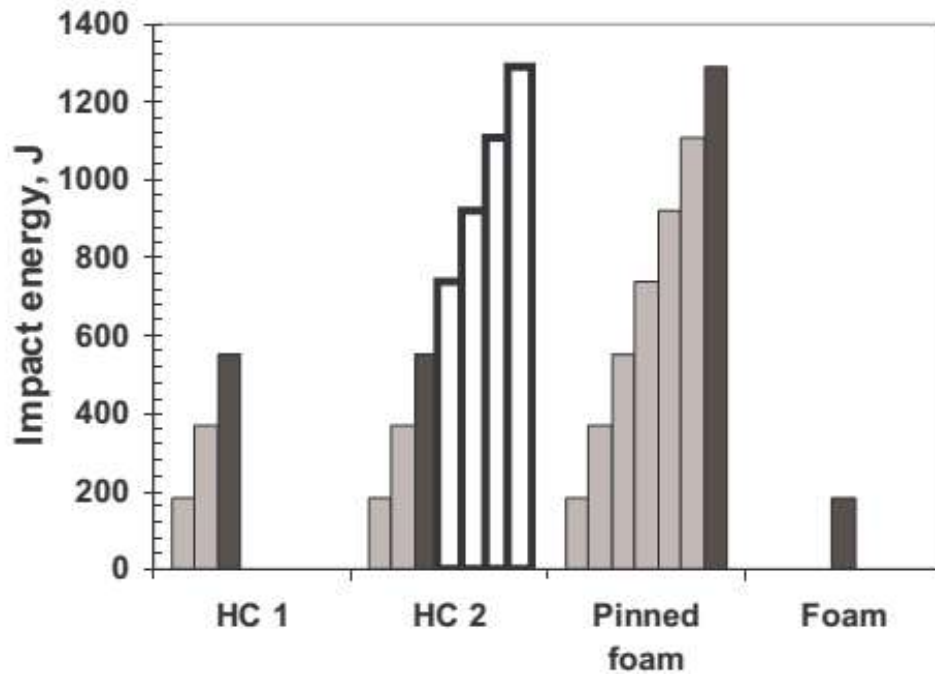
Figure 2.18: Impact tests performed; HC: honeycomb. Grey indicates undamaged, black indicates first panel damage noted [34].

Figure 2.19 shows the damage incurred. The first damage of the standard (64 kg/m3) material was noted visually after a drop from 3 meters, and sectioning revealed this to be permanent crushing of the core (Figure 2.19 a). No skin debonding was noted. A second identical panel was then tested to confirm this result and again first damage was noted at 3 meters. Tests were continued on this second panel up to final complete failure, which occurred at around 1.3 kJ. Figure 2.20 presents the maximum loads and displacements recorded during the instrumented test series. For the honeycomb, the displacements ware very similar initially but beyond the energy required for core crushing there was a break in the plots of both force and displacement, suggesting that the damage introduced has modified the response of the structure.
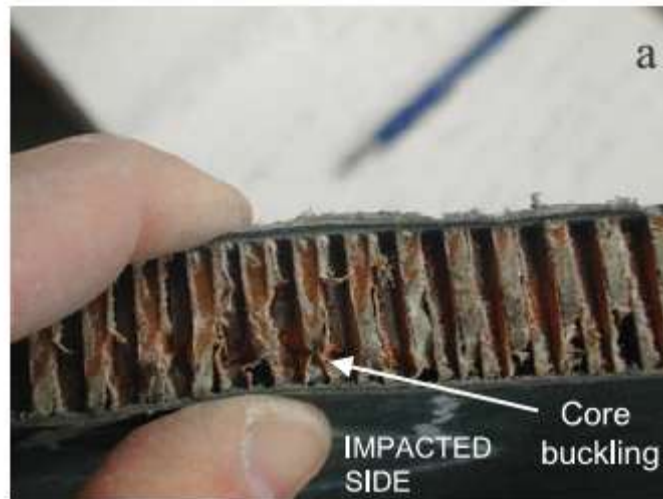
Figure 2.19: Damage observed after impact: honeycomb, 3m 18.8 kg [34]
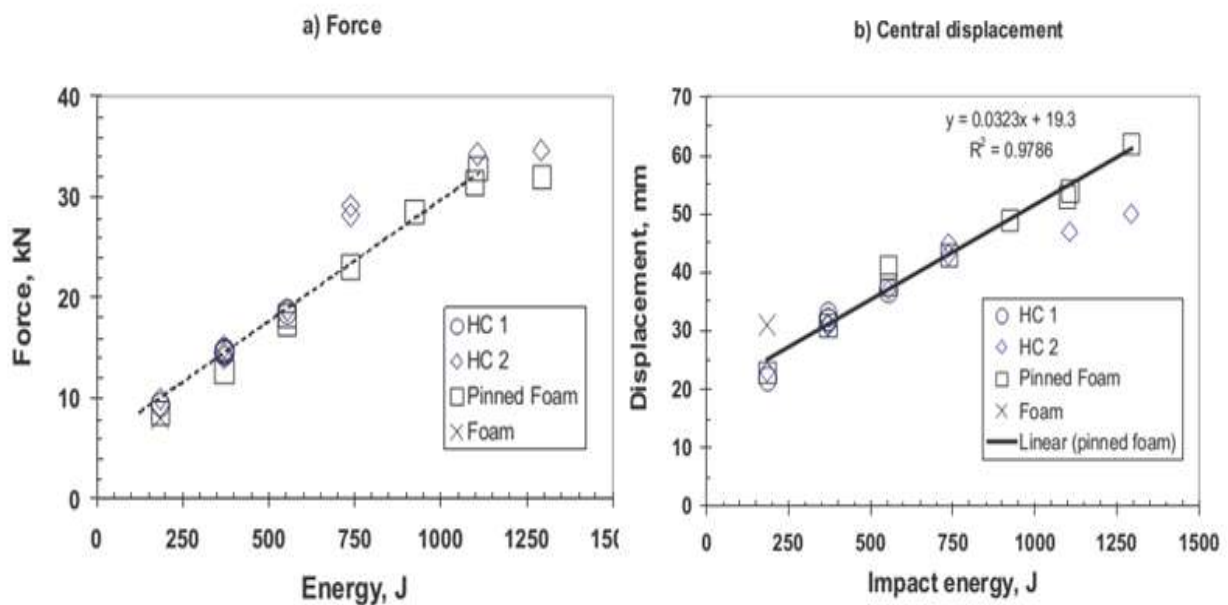
Figure 2.20: Recorded data from tests versus impact energy. a) Maximum loads (sum of four load cells) and b) central displacements [34].

[35] Perforation response and failure of sandwich panels with composite face sheets and aluminum foam core are investigated experimentally in their study. Quasi-static perforation and low-velocity impact tests were carried out by using a material test system and a drop weight machine, respectively. The load-displacement response, energy absorption and energy-absorbing effectiveness of sandwich panels were obtained and compared for quasi-static and impact tests. Effects of some key parameters on the overall energy absorption behavior of the panels were explored, such as impact energy, face sheets and core thickness, core density and indenter nose shape.
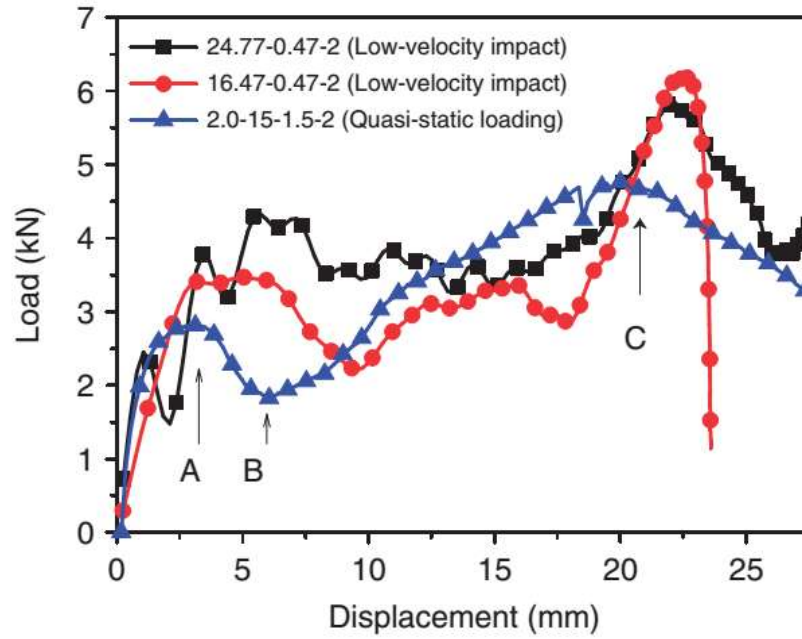
Figure 2.21: Force–displacement curves of sandwich specimens under conical indenter [35].
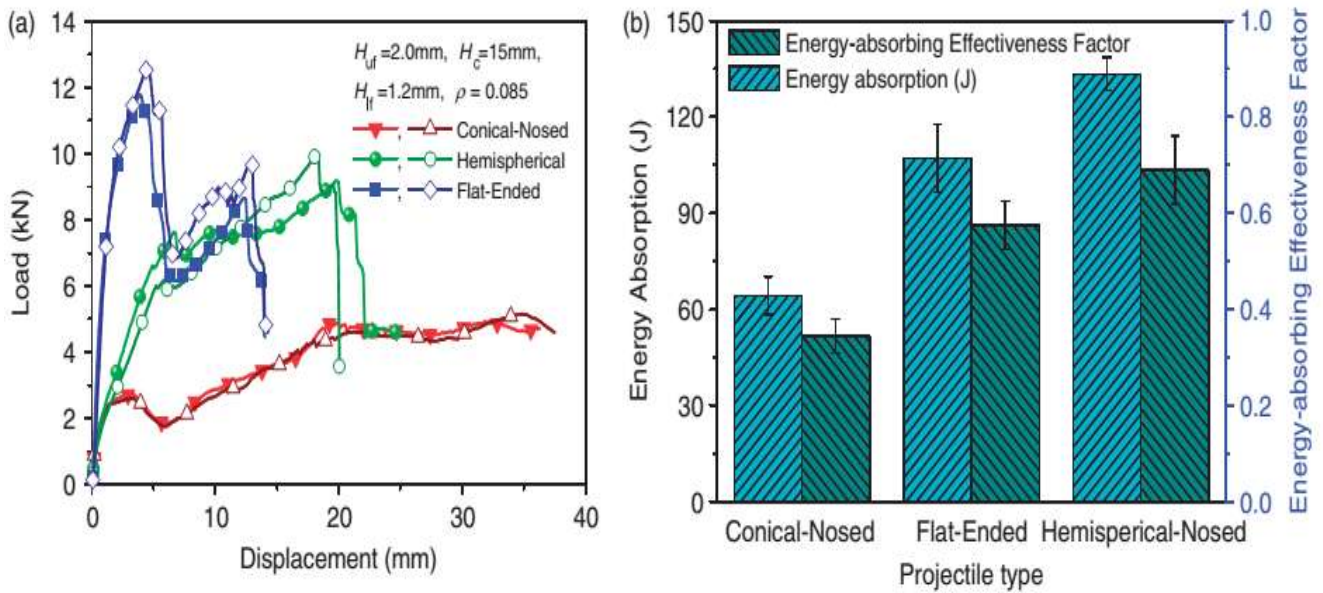
Figure 2.22: Effects of projectile nose shape on: (a) force–displacement curves and (b) energy absorption and energy-absorbing effectiveness (the error bars denote the standard deviations in replicate experiments) [35].

It is important to fully understand the resistance of the sandwich panels subjected to impact loading conditions. For this reason [28] were studied the resistance of sandwich panels with different aluminum honeycomb cores, air sandwich panels (no core between the two face sheets) and monolithic plates of equivalent mass subjected to impact from foam projectiles. The deformation and the elastic spring-back of the honeycomb sandwich panels and the monolithic plates have been compared and discussed. The resistance of the panels and plates has been quantified by their back-face deflection with respect to the projectile impulse. Five different types of aluminum honeycombs have been used as the core material. The front-face sheet and the back-face sheet of the honeycomb sandwich panels are made of aluminum plate with 1 mm thickness. Cylindrical ALPORAS aluminum foams with a relative density between 9% and 11% were employed as the metal foam projectiles. They have been fired at several hundred meters per second towards the center of the panels and plates using a gas gun. The deflection histories of the back-face have been measured using a laser displacement sensor. From the deflection histories, the maximum deflection and the final deflection of the back-face has been distinguished. Deformation modes and failure modes of the individual component have been observed and classified into several categories. Moreover, the deflections of the honeycomb sandwich panels have been compared with deflections from air sandwich panels. It has been found that the honeycomb sandwich panels outperform both the air sandwich panels and the monolithic plates within an impulse range of 2.25 kNsm^2∼ 4.70 kNsm2. Outside this operational range, the advantages associated with employing the honeycomb sandwich panels as a protective structure upon impact of foam projectiles diminishes.

Initial shape   After tests: front-face   After tests: back-face
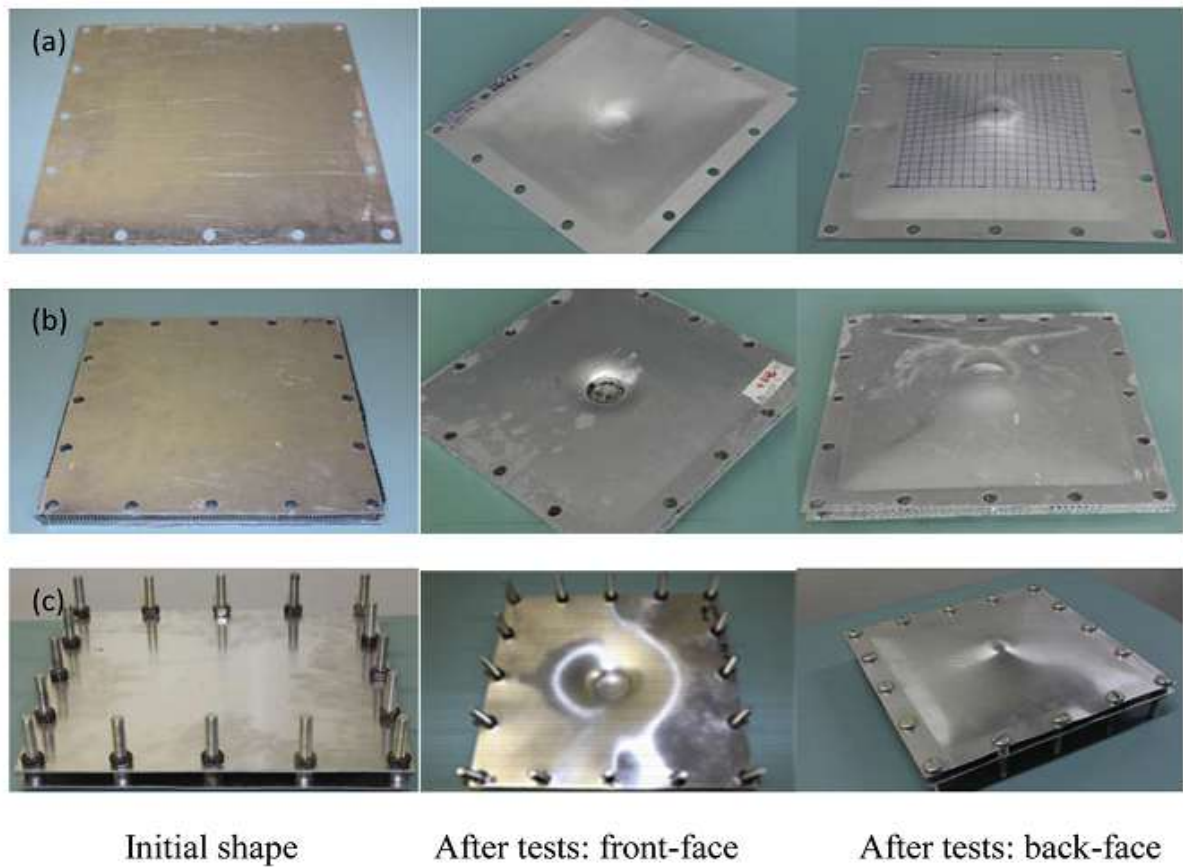
Figure 2.23: Photographs showing typical deformation of (a) a monolithic plate (sample m1-2); (b) a honeycomb sandwich panel (sample b4); (c) an air sandwich panel (sample g6) [28].

In order to study the deformation of the core, samples A2, B2, C2 and D2, which were tested at similar impulses, were sectioned along the central axis as shown in figure 2.21.
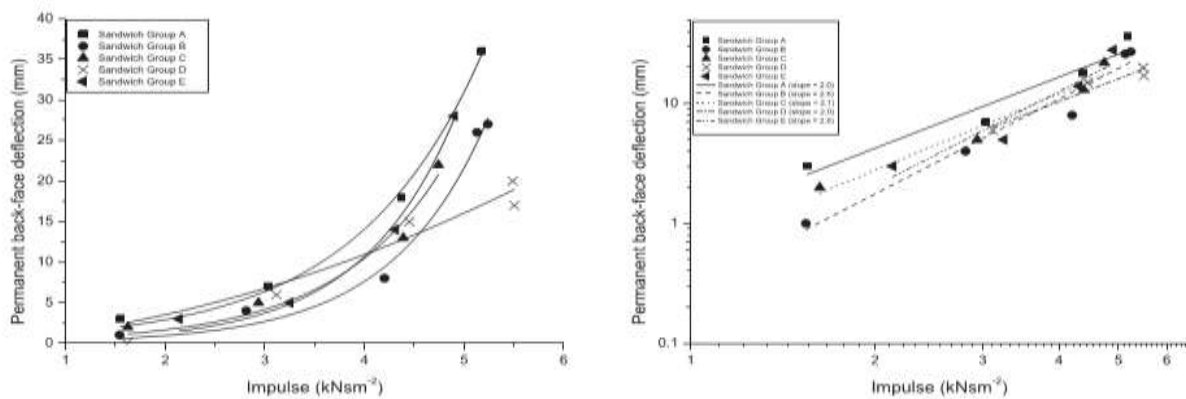
Figure 2.24: Four specimens showing core compression ratio reduces from the center towards the edges of the sandwich panels. From top to bottom: samples a2, b2, c2 and d2 [28].

The permanent back-face deflections of all the honeycomb sandwich panels against impulses are shown in figure 2.25. Sandwich Group D behaved differently from the other honeycomb sandwich panels as the fitting line shows almost a linear line. The density of the honeycomb core in sandwich Group D is almost 4 times the density of the honeycomb core in sandwich Group A, which is the weakest sandwich group.
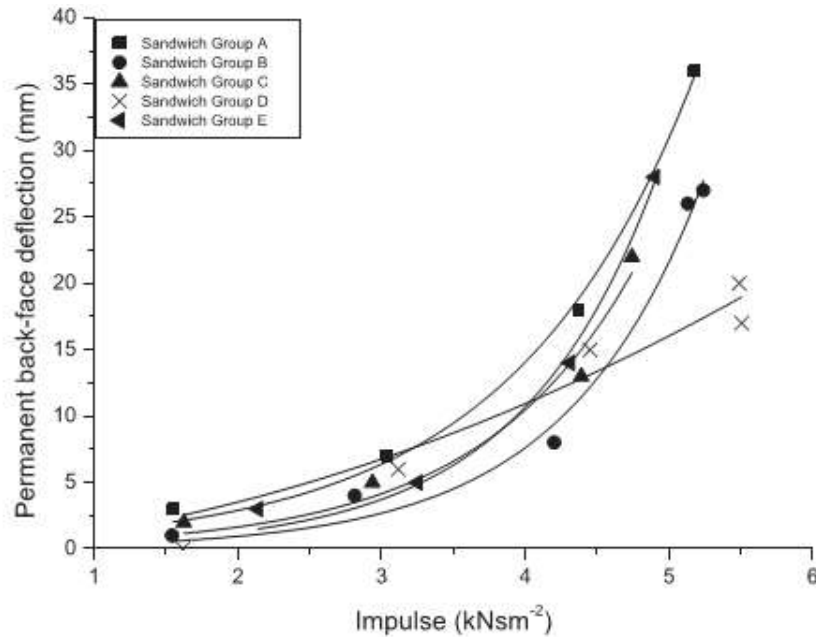
Figure 2.25: Permanent back-face deflection of honeycomb sandwich panels at various impulse levels [28].

In order to check the relation between the permanent back-face deflection and impulse, a logelog graph of the deflection is drawn as shown in figure 2.26. The slopes of the graphs vary from 2 to 2.6, which indicate that the back-face deflection and the impulse are related by a power relation. In-depth theoretical analysis was required in order to determine the relationship between the back-face deflection and the applied impulse accurately.
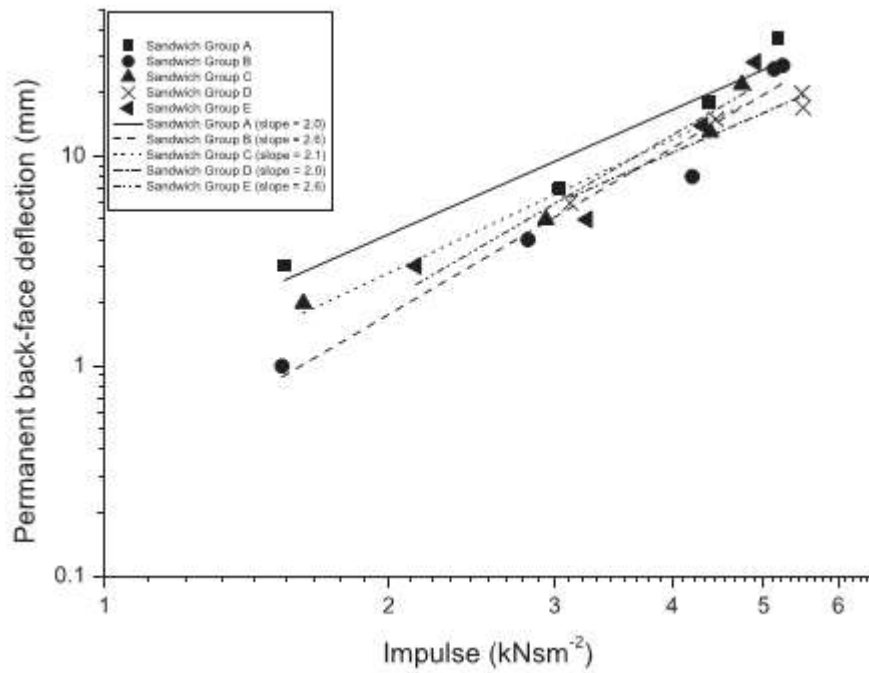
Figure 2.26: The logelog graph of the permanent back-face deflection of honeycomb
sandwich panels vs. Impulse [28].

II.5.   **Mechanical Properties and The theoretical models in literature**

The mechanical properties are a consequence of folding (buckling) and collapse processes taking place in the cell walls. Numerous analytical models have been developed to predict the overall properties of honeycomb based on the geometry of the cells and properties of the base material. In researched studies and literature, the analysis of honeycomb is often separated into two groups, the mechanics of in-plane and out-of-plane deformation.

The ultimate strength of the honeycombs describes the maximum resistance under compressive load. Many researchers noticed that the compressive strength is not mainly correlated to the compressive strength of the solid cell wall materials, but critically to the buckling behavior of the honeycomb cell walls [4–15].

II.5.1.   **In-Plane Properties**

Ashby and Gibson [15] and Zhang and Gibson [30] have established predictive methods to determine in-plane properties. This work reduced the complexity of the honeycomb cells to a single wall and resolving the forces and moments, Figure 2.27, so that in-plane properties can be predicted.

31
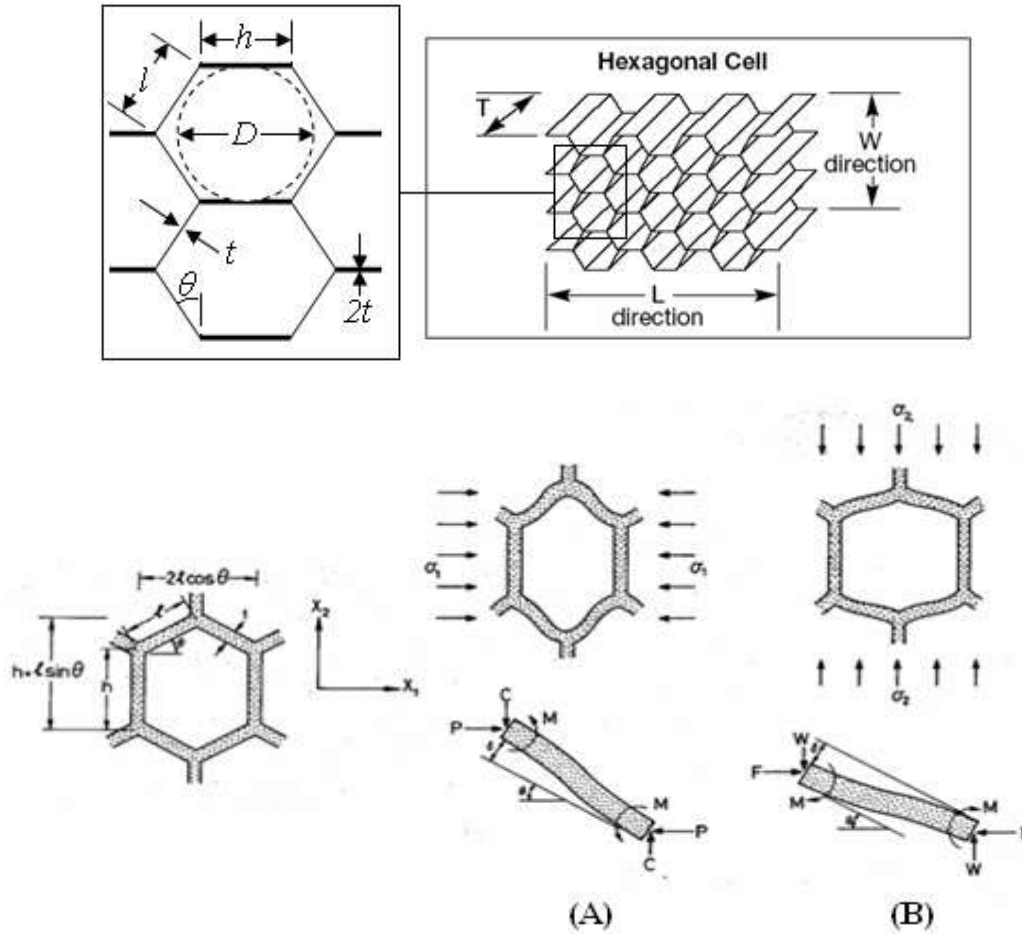
Figure 2.27: Elastic deformation, (a) 'W' compression, (b) 'L' compression [15].

From [15], the in-plane elastic modulus of honeycomb can be determined using equations 2-1 and 2-2:

$$\frac{E_w}{E_s} = \left(\frac{t}{l}\right)^3 \frac{\cos \theta}{(\frac{h}{l}+\sin \theta) \sin 2\theta} \tag{2.1}$$

$$\frac{E_L}{E_s} = \left(\frac{t}{l}\right)^3 \frac{(\frac{h}{l}+\sin \theta)}{\cos 3\theta} \tag{2.2}$$

Where θ is the internal angle of the hexagonal, t is the thickness of the cell wall, h and l the lengths of the cell wall and are shown in 2-27. When the hexagonal shape is regular, when h=l and $\theta=30^0$ shown in Figure 2-27, equations 2-1 and 2-2 become identical and produce equation 2-3:

$$\frac{E_w}{E_s} = \frac{E_L}{E_s} = 2.3 \left(\frac{t}{l}\right)^3 \tag{2.3}$$

This equation states that a regular hexagon honeycomb arrangement will produce an identical elastic modulus in both in-plane directions. The in-plane plastic collapse strength, $(\sigma_{PL})_L$ and $(\sigma_{PL})_W$, can also be shown to be identical in both in-plane directions for a regular hexagonal cell and reduces to produce equation 2-4:

$$\left(\sigma_{pL}\right)_L = \left(\sigma_{pL}\right)_w = \frac{1}{4}\left(\frac{t}{l}\right)^2 \frac{\sigma_{\gamma s}}{\cos\theta} \tag{2.4}$$

Where σys is the tensile yield stress of the base material. These equations were shown to produce a good agreement with experimental studies on rubber honeycomb samples.

These equations produce an indication of bulk properties which are not dependent on sample dimensions. Onck et al. [62] Investigated size effect on in-plane properties and developed relationships linking the ratio between cell size and sample width with in-plane compression and shear properties. The parameter ζ was introduced as a ratio between the sample width, L, and cell diameter, d, and indicates the number of cells along the width of the sample. An example of the variation in compression properties is shown in Figure 2-28 and was later compared with experimental research using foam materials [63], shown in Figure 2-29, which showed the estimated trends to be applicable to alternative foam materials.
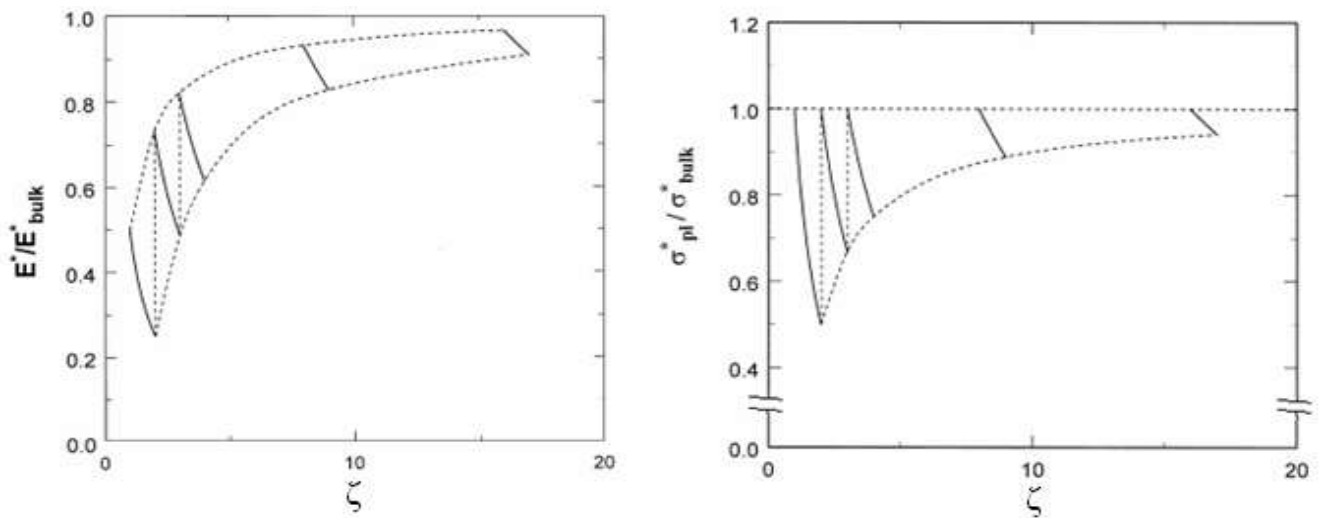
Figure 2.28: Example of the variation between in-plane compression properties depending on sample size [62]
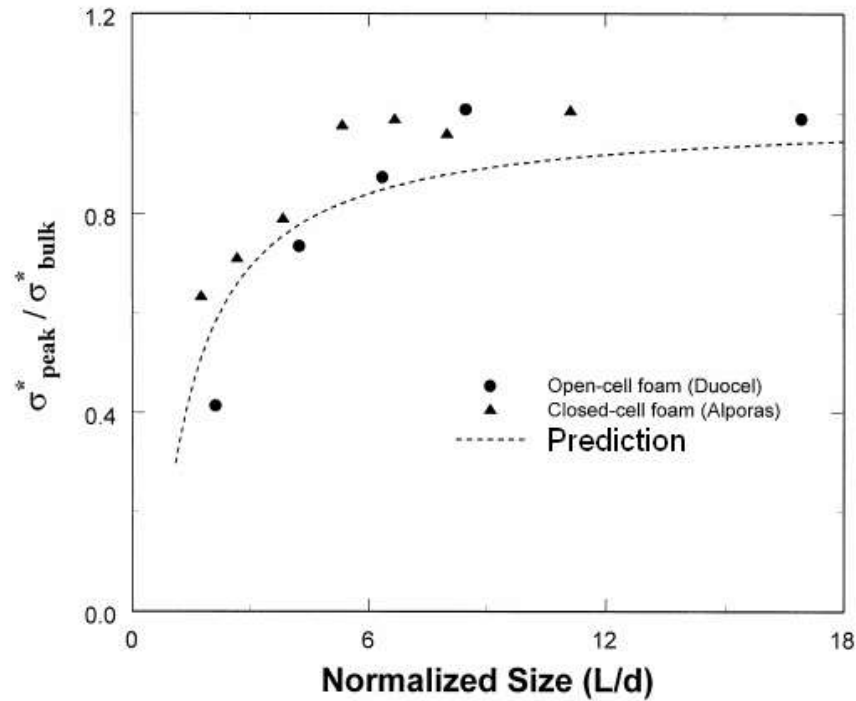
Figure 2.29: Comparison between theoretical size dependency influence on peak crushing strength and foam compression results [63].

II.5.2.   Out-of-Plane Properties

The mechanics of deformation in the 'T' direction are based on the mechanics of folding walls. Figure 2-30 shows the regular folding pattern of a honeycomb cell under out-of-plane loading.
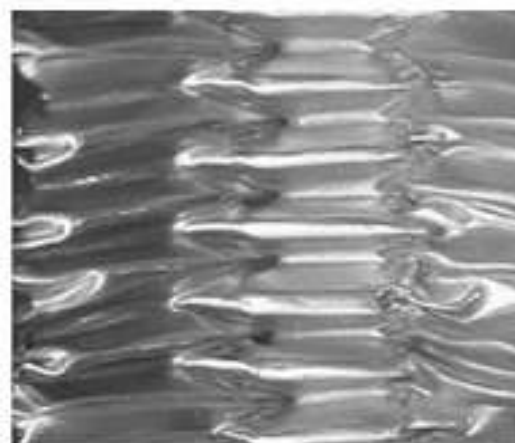
Figure 2.30: Deformed honeycomb due to out-of-plane compression loading [30]

Early research studies to determine the folding (buckling) and energy absorbing mechanisms similar to those in honeycomb cells were confined to thin-walled cylinders; one such example was conducted by Alexander [31], producing the model shown in Figure 2-31. The Alexander model [31] mathematically describes the crushing process for cylindrical structures; however, it did contain unrealistic assumptions concerning the folding profile and under-predicts the crushing strength of the structure.
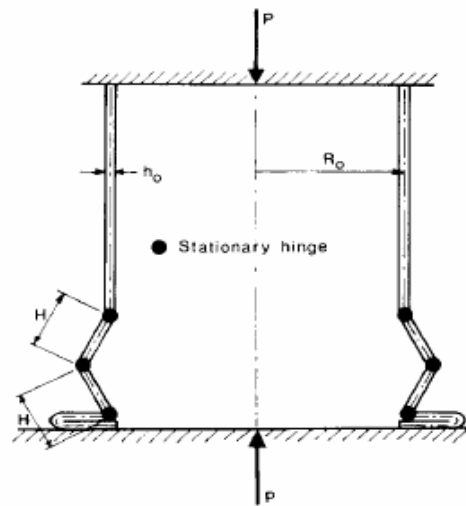
Figure 2.31: Alexander's model: folding of thin walls in a cylinder [31]

In a later work, McFarland [32] presented a predictive method to determine the crushing strength in the out-of-plane direction based on a hexagonal cell structure. McFarland idealized the crushing mode to determine the mechanisms of collapse. The collapse profile, as shown in Figure 2-32, was used to relate the energy involved in the bending deformation to the mean crushing strength. This mechanism was simplified to introduce the effect of in-plane shearing during the 'T' direction crushing process.
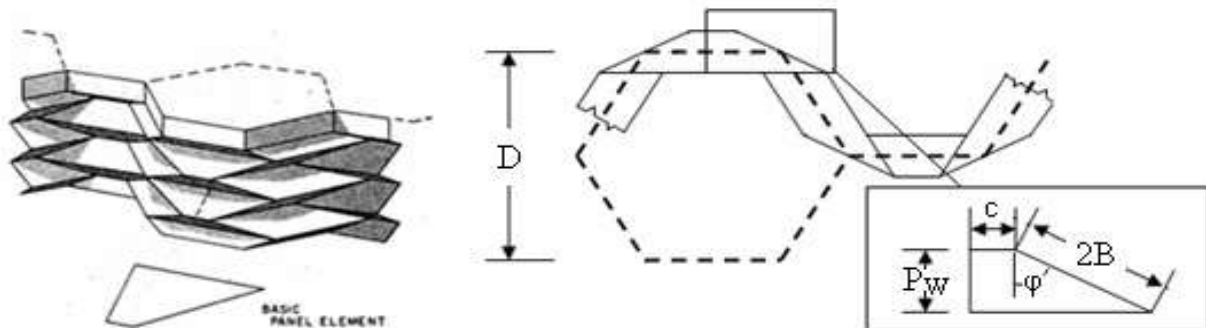
Figure 2.32: Mcfarland model: 'T' direction crushing mechanism [32]

Wierzbicki [33] also developed a method of determining the axial crushing of honeycomb cells. The model was further developed by including an analysis of the bond and thickness change between cells. Wierzbicki introduced an improved folding mechanism to the cell walls and comments on the effect of shear at the interface between the cell walls. The research concluded that delamination must occur between adjacent cells for the folding mechanism to continue and proposed equation 2-5 to determine the plateau stress for a honeycomb:

$$\sigma_{p(T)} = 6.6 \, \sigma_{\gamma s} \left(\frac{t}{l}\right)^{\frac{2}{3}}$$
(2-5)

Where σ_{YS} is the yield strength of the base material. In the same paper Wierzbicki also derived an equation to calculate the average fold wavelength λ, where $\lambda = 2H$ in Figure 2-33:

$$\lambda = 1.642 \sqrt[3]{th^2}$$
(2-6)

Out-of-plane shear, defined as 'TW' and 'TL', can also be predicted using the geometry of the cell and base material properties. The difficulty with predicting shear in this direction is that each surface cannot deform uniformly due to constraints imposed by surrounding cells. The 'unit load' method considers the individual flexibilities of each of the cell walls in a unit area, Figure 2-33, and focuses on the shear stresses at four of the cell walls, where q is the shear flow in each wall, suffices a, b, c and d identify each wall, β is the direction of loading and τ is the shear stress. The 'unit displacement' method focuses on strains in the structure to determine the force required to deform the structure.
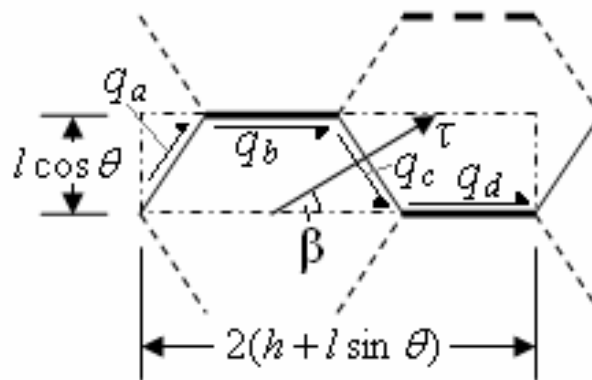
Figure 2.33: Shear flows in cell walls when honeycomb sample subjected to out-of plane shear stresses [22]

Assuming regular hexagonal cells, the two methods produce the equations:

$$\frac{G_F}{G_S} \frac{\rho_S}{\rho} = \frac{9}{8(2 + \sin 2\beta)}$$
(2-7)

$$\frac{G_D}{G_S}\frac{\rho_S}{\rho} = \frac{15}{8(3+2\sin 2\beta)} \qquad (2\text{-}8)$$

Where suffices F and D are the load and displacement methods respectively and the suffix S represents the base material. When $\beta = 0^0$ the calculated shear is in the 'TL' direction; at $\beta = 90^0$ the calculated shear is in the 'TW' direction.

Gibson and Ashby [15] also comment on the calculation of out-of-plane shear modulus. The theorems presented in [15] specify upper and lower bounds for shear modulus. The lower boundary for shear in the 'TW' and 'TL' direction are:

$$\frac{G_{TW}}{G_S} \leq \frac{\cos\theta}{(\frac{h}{l}+\sin\theta)}\left(\frac{t}{l}\right) \qquad (2\text{-}9)$$

$$\frac{G_{TL}}{G_S} \leq \frac{1}{2}\frac{\frac{h}{l}+2\sin 2\theta}{(\frac{h}{l}+\sin\theta)\cos\theta}\left(\frac{t}{l}\right) \qquad (2\text{-}10)$$

The upper boundaries are:

$$\frac{G_{TW}}{G_S} \geq \frac{\cos\theta}{(\frac{h}{l}+\sin\theta)}\left(\frac{t}{l}\right) \qquad (2\text{-}11)$$

$$\frac{G_{TL}}{G_S} \geq \frac{1}{2}\frac{\frac{h}{l}+2\sin 2\theta}{(\frac{h}{l}+\sin\theta)\cos\theta}\left(\frac{t}{l}\right) \qquad (2\text{-}12)$$

In the case of 'TW', the equations for upper and lower out-of-plane shear boundaries, equations 2-9 and 2-11, are identical and thus the method suggests that the shear modulus can be exactly determined. Under regular hexagonal conditions, the upper and lower shear modulus boundary equations for 'TL' become identical to 'TW', producing equation 2-13:

$$\frac{G_{TW}}{G_S} = \frac{G_{TW}}{G_S} = 0.577\left(\frac{t}{l}\right) \qquad (2\text{-}13)$$

Since equations 2-1, 2-2 and 2-13 are independent of in-plane load direction of regular hexagonal honeycombs, these materials can be considered isotropic in the 'LW' plane. The equations presented here are developed for honeycombs with a constant cell wall thickness. Aluminum honeycombs have double wall thickness regions due to the manufacturing method which produces a strong in-plane direction.

- **Elastic buckling strength**

Based on the perfect geometry of the honeycomb, and derived from the thin plate elastic in-plane compressive buckling theory developed by Timoshenko [6], the elastic buckling strength of the honeycomb with uniform cell wall thickness t was deduced by Gibson and Ashby [15], in Equation (2-14):

$$\sigma_c = 5.2 E_c \left(\frac{t_c}{a}\right)^3 \qquad (2\text{-}14)$$

Where $a=h$, $\alpha=30°$, $\upsilon=0.3$. Zhang and Ashby [15] also developed the elastic buckling strength for the honeycomb with one-third 2t cell walls, shown as follows:

$$\sigma_c = 7.19 E_c \left(\frac{\rho}{\rho_c}\right)^3 \qquad (2\text{-}15)$$

Where K=5.73 as four boundaries of any single cell wall are fully clamped. However, as for the condition of simply supported edges, K=3.29. Ashby mentioned that in reality the constraints on the boundaries are stronger than the simply supported but also weaker than the clamped condition [4]. Therefore a mean value, K=4, is suggested to be used for the collapsing strength, using the formula:

$$\sigma_c = 6 E_c \left(\frac{\rho}{\rho_c}\right)^3 \qquad (2\text{-}16)$$

According to another study by Wang [7] on the honeycomb elastic buckling strength, it is considered that the aggregated cell walls together resist the compressive loads and constrain each other during buckling. The critical buckling happens when a main wall, which has 2t thickness, starts to buckle. The initial buckling of the main wall is also constrained by the adjacent walls' twisting stiffness. This constraint is generated by the distributed bending moments along the two vertical edges of the main wall. Hence the calculated honeycomb collapsing strength is:

$$\sigma_c = 19.5 E_c \left(\frac{t_c}{a}\right)^3 = 5.34 E_c \left(\frac{\rho}{\rho_c}\right)^3 \qquad (2\text{-}17)$$

It may be noticed that Equation (2-16) is almost the same as Equation (2-17). This also indicates the classical elastic buckling theory of the thin plate is rather accurate to predict the honeycomb compressive buckling strength, provided that each cell wall is perfectly flat and vertical.

ρ is the average density of the honeycomb material, ρ_c is the solid cell wall material density,

➢ For uniform thickness t cell walls

$$\frac{\rho}{\rho_c} = 1,115\frac{t}{a}$$

➢ For one-third thickness 2t cell walls

$$\frac{\rho}{\rho_c} = 1,54\frac{t}{a}$$

- **Plastic Buckling Strength**

The plastic buckling strength of the honeycomb is also named the crushing strength which describes the stress level at the quasi-static crushing procedure. In an attempt to evaluate the energy absorption during honeycomb crushing, Wierzbicki [33] analyzed the collapsing behavior of an angle element in the honeycomb for some metal hexagonal honeycombs, which is undergoing bending and extensional plastic deformation, to obtain the equivalent crushing strength of the honeycomb subjected to an axial compression. Wierzbicki deduced the steady plastic collapsing strength for a metal honeycomb, as shown in the following two equations:

$$\sigma_c = 5.6\sigma_y \left(\frac{t}{a}\right)^{\frac{3}{2}} = 4.4\sigma_y \left(\frac{\rho}{\rho_c}\right)^{\frac{3}{2}} \qquad (2\text{-}18)$$

II.5.3.   The energy-balance model

A number of workers have used the Meyer indentation law to characterize the indentation response of sandwich structures. [4, 15–19] this generalized indentation takes the form:

$$F = K_i \alpha^n \qquad (2\text{-}19)$$

Where K_i and *n* are constants which can be determined by fitting the experimental data of the indentation tests and α is the indentation.

The energy-balance model is the summed of energy absorption in bending, shear and contact effects. Moreover, this model can be applied to predict the maximum impact or indentation

force (Fmax) at different impact energies. The model is based on the one degree of freedom spring-mass system shown in Figure 2-34.

The two – degrees – of – freedom spring – mass model proposed by Shivakumar et al. [24], shown in Figure 2-34, was applied to study the impact response of sandwich panels: K_i, K_b, K_s and K_m are springs representing the contact, bending, shear and membrane stiffness, respectively. In general K_m is a nonlinear spring, which can be neglected, then a global stiffness K_{bs} can be evaluated as:

$$K_{bs} = K_b K_s / (K_b + K_s) \tag{2-20}$$
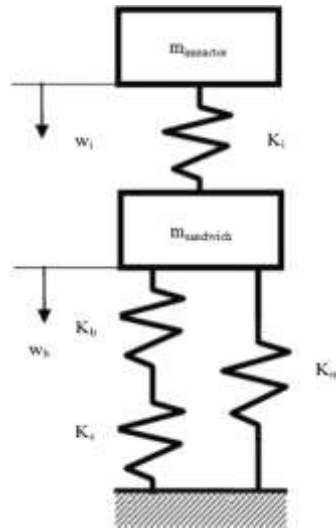
Figure 2.34: Spring-mass model for impact dynamics.

The sandwich panel was modeled in this study as a combination of two springs: a linear spring K_{bs} to account for the global deflection W_b and a nonlinear spring Ki to represent the local indentation effects. The sandwich panel, clamped around its edges, experiences the local displacement α, due to the indentation of the top face and to the core crushing, and the global displacement W_b due to the bending and the shear of the entire panel. The global and local responses of the panel can be evaluated separately, since the impact damage is small and localized around the impactor for low-velocity impacts [25].

In order to predict the impact response of honeycomb core sandwich structure with aluminum skin, the energy-balance model was used. Assume that the test responds in a quasi-static mode. When the projectile makes a contact with the structure, at the same time the structure has reached its maximum deflection. During the deflection, the sums of kinetic energy of the

projectile have been applied to deform the structure. The total energy used can be divided into two parts; the energy used to deform the structure in bending/shear and the energy dissipated in contact effects. According to the principle of the conservation of energy, the energy balance model can be derived as the following [15, 26, and 27]:

$$\frac{1}{2}mv^2 = E_b + E_s + E_c \tag{2-21}$$

Where m and v are the mass and the impact velocity of the impactor and the subscript b, s and c refer to energy dissipation in bending, shear and contact effects, respectively. The energy due to bending and shear effects at maximum displacement force W_{max} (F_{max}) is equal to:

$$E_b + E_s = \frac{F_{max}^2}{2K_{bs}} \tag{2-22}$$

Where K_{bs} is the linear stiffness including bending and shear effects.

The mathematical expression of the energy absorption due to contact effects is obtained by integrating Equation (2-22) between 0 and the maximum indentation value α_{max}:

$$E_c = \int_0^{\alpha_{max}} F d\alpha = \frac{F_{max}^{1+\frac{1}{n}}}{(n+1)K_i^{\frac{1}{n}}} \tag{2-23}$$

Finally, the total energy absorbed by the sandwich structure can be evaluated by summing the energy absorption in bending, shear and contact effects:

$$\frac{1}{2}mv^2 = E_b + E_s + E_c = \frac{1}{2K_{bs}}F_{max}^2 + \frac{F_{max}^{1+\frac{1}{n}}}{(n+1)K_i^{\frac{1}{n}}} \tag{2-24}$$

II.5.4.   Euler's Buckling Analysis

Euler's linear buckling theory is basic idea to impose an elementary unit loading on the honeycomb sandwich, and to evaluate the multipliers of this applied loading which result in incompatible stiffness matrix of the finite element model. For the unloaded structure, the stiffness matrix can be computed:

$$S^0 = \int B^T(x):K:B(x)dV \tag{2-25}$$

Where:

$S^0=$ is the stiffness matrix of the unloaded structure obtained by integration on the undeformed structure;

B(x): is the gradient of interpolation matrix.

After application of an elementary unit loading (by imposing a macroscopic strain field corresponding to out-of-plane compressive or simple shears loading for example), the stiffness matrix can be evaluated on the deformed shape:

$$S^\tau = \int B^T(x):K:B(x)dV \tag{2-26}$$

The idea is to find a multiplier of the prescribed loading that results in a stiffness matrix S^τ that has nul eigenvalue which traduces instability:

$$S^\tau = \alpha\mu^\tau \tag{2-27}$$

Where $\mu^\tau \neq 0$

With:

 * u^τ: the matrix of the eigenvectors of S^τ;
 * α: the diagonal matrix of the eigenvalues of S^τ.

The main assumption in Euler's linear buckling analysis is to look for an incompatible stiffness matrix S^τ under the form:

$$S^\tau = (I-\lambda)\, S^0(\lambda)S^d \tag{2-28}$$

Where:

 * *I*: is the identity matrix;
 * *λ*: is the diagonal matrix of the load multipliers.

By introducing Eq. (2-28) into Eq. (2-27), and by solving for nul eigenvalues: $S^\tau\, u^\tau = \alpha u^\tau = 0$ u^τ with $u\tau \neq 0$, it can be obtained:

$$\begin{cases} [S^0 + \lambda^{-1}\,(I-\lambda)\,S^d]u^\tau = 0 \text{ where } u^\tau \neq 0 \\ \Rightarrow [S^0 + \gamma^2 S^d]u^\tau = 0 \text{ with } \gamma^2 = \lambda^{-1}\,(I-\lambda) \\ \Leftrightarrow det[S^0 + \gamma_i^2 S^d] = 0 \text{ with } \gamma_i^2 \text{ corresponding to the } ith \text{ mode.} \end{cases} \tag{2-29}$$

Equation (2-29) can then be solved for γ and next for λ the diagonal matrix of the eigenvalues this immediately gives the load multipliers that lead to instability, i.e., buckling. Once λ determined, the shape of the eigenvectors u^{τ} can be evaluated with Eq. (2-27) and, most importanting, the macroscopic load applied on the RVE that leads to buckling. In other words, if the RVE is loaded with a macroscopic unit strain field E^{unit} (corresponding to a pure stress loading $\sum unit$ on the RVE), the ith loading multiplier λi associated with the I th buckling mode enables the calculation of the critical strain field:

$E^{c,i} = \lambda i E^{unit}$.

Thanks to the mechanical behavior of the equivalent medium obtained by homogenization technique, it is possible to determine the ultimate stress $\sum c, i$ corresponding to the ith mode of buckling:

$$\sum c, i = K = E^{c,i} \tag{2-30}$$

Where:

- $\sum c, i$ has only one non nul value $\sum c, i =$ in adequation with the imposed strain field $E^{c,i}$.

The failure stress limits are evaluated on the first buckling mode (the one of lowest energy).

II.5.5. The Johnson-Cook constitutive model [64]

Metals exhibit elastic and plastic behavior depending on the amount and rate of deformation they undergo. Elastic behavior of metals is usually described by Hooke's law where by the stress and strains in the material are linearly related by the modulus of elasticity up to the onset of yielding. In the case of uni-axial tension, the elastic limit can be defined as the maximum load that can be applied to a specimen without causing permanent deformation. When a material is subject to many different combinations of stress, a yield criterion is essential to determine the limit of elasticity. Many yield criteria are based on sorne scalar function of the principal stresses. Of these, the von Mises yield criterion is the most common and is given by:

$$(\sigma_1 - \sigma_2)^2 + (\sigma_2 - \sigma_3)^2 + + (\sigma_1 - \sigma_3)^2 = 2\sigma_y^2 \qquad (2\text{-}31)$$

Where σ_1, σ_2 and σ_3 are the three principal stresses, and σ_y is the yield stress of the material.

In the plastic regime, as metals deform their resistance to further deformation increases. This effect is known as strain-hardening or work-hardening and is important in metal plasticity. Under this effect, a metal is able to withstand greater loads in spite of reductions in critical cross-sectional areas within the material. For accurate modeling of material behavior under high-speed conditions, this hardening behavior must be captured at different strains across the plasticity regime.

Impact events involving metallic materials result in a temperature rise during deformation due to adiabatic heating. As a metal undergoes plastic work, heat is generated, consequently affecting the deformation mode. Shearing due to adiabatic heating is a deformation mode that is unique to high strain rates of deformation in metals and can cause shear failure. It is considered to be an important failure mode. Woodward (1990) reports that on the order of 95 % of the work done by plastic flow are converted to heat while Meyers (1994) states this fraction is 90% for most metals. This heat, if prevented from conducting (i.e. adiabatic condition), will raise the temperature of the metallic sample causing thermal softening. In a real situation, some of the heat flows while the remaining fraction causes some increase in metal temperature. In the case of those metals where the rate of thermal softening is greater than the rate of work hardening, most of the deformation takes place in the softened regions, thus producing adiabatic shear bands. In metals with low thermal conductivity, little heat is conducted and thermal softening effects are maximized. Adiabatic conditions are also a characteristic of high speed impact loading since deformation occurs over a very short time period resulting in high strain rates.

Woodward (1990) outlines a practical example showing how shearing due to adiabatic heating affects deformation by considering sharp conical and flat-faced objects impacting a metallic target. As they penetrate a body, sharp objects push material to the side. This is in contrast to flat-faced penetrators that push material out, thus producing a plug, as was shown in Figure 1.4. If shear bands exist as deformation is taking place, a metallic plug can be produced in the case of penetration by sharp conical objects. In modeling, it is thus important to consider the effect of temperature and strain rate on the flow stress. Plasticity models that are suitable for high strain rate deformation not only capture the instantaneous values of strain but also the strain rate and temperature effects on the deformation. Such a model was proposed by Johnson and Cook (1983, 1985) and is given by

$$\sigma = \left(A + B\varepsilon_p^n\right)\left(1 + C\ln\frac{\dot{\varepsilon}_p}{\dot{\varepsilon}_0}\right)(1 - T^m) \qquad (2\text{-}32)$$

Where σ is the equivalent von Mises flow stress; ε_p the equivalent plastic strain; $\dot{\varepsilon}_p$ the equivalent plastic strain rate; and $\dot{\varepsilon}_0$ is a material parameter characterizing the onset of strain rate dependence and is usually taken as 1.0 S⁻¹. *A, B,* C, *n,* and *m* are material parameters and *T* * is the homologous temperature. This temperature is defined as:

$$T^* = \frac{T_{inst} - T_{trans}}{T_{melt} - T_{trans}} \qquad (2\text{-}33)$$

Where *T inst* is the current instantaneous temperature of the metal; *T trans* is the transition temperature below which there is no temperature dependence on the flow stress and no thermal softening occurs; and *T melt* is the melting (or solidification) temperature of the metal.

This Johnson-Cook material model is a three-term multiplicative model. The first term characterizes the quasi-static behavior for $\dot{\varepsilon}_0 = 1.0$ S⁻¹ and $T^* = 0$, the second term represents the strain rate sensitivity and the third term depicts the effect of temperature on the flow stress. When modeling high speed impact events, the strain rate and temperature effects are important and must be included in the constitutive model. In most metals, large strains and high strain rates will soften the material by raising the temperature of the deforming metal and hence will affect the flow stress. In this model, the effects of strain rate and temperature on flow stress are uncoupled. This makes the strain rate sensitivity independent of temperature. In most metals, it is observed that the rate sensitivity increases with temperature. This model, however, is relatively easy to calibrate using a small number of stress-strain curves obtained from experimental tests and is weII supported in nonlinear finite element computer codes.

The fracture model proposed by Johnson–Cook takes into account the effect of stress tri-axiality, strain rate and temperature on the equivalent fracture strain. The equivalent fracture strain $\bar{\varepsilon}_{pl}$ is expressed in the following form:

$$\bar{\varepsilon}_{pl}\left(\frac{\sigma_m}{\sigma-}, \dot{\varepsilon}_{pl}, T^\wedge\right) = \left[D_1 + D_2 exp\left(D_3\frac{\sigma_m}{\sigma-}\right)\right].\left[1 + D_4\ln\left(\frac{\dot{\varepsilon}_{pl}}{\dot{\varepsilon}_0}\right)\right].\left[1 - D_5 T^\wedge\right] (2\text{-}34)$$

Where D1–D5 are material parameters, $\sigma-$ is the stress tri-axiality ratio and σ_m is the mean stress.

Chapter III: Experimental Study

This chapter presents a large experimental investigation on two types of honeycomb sandwich panels (Aluminum and Nomex core) with different cell sizes (d = 3.2, 6.4, 9.6 and 19.2 mm) subjected to quasi-static and dynamic loading conditions (compression, quasi-static indentation and low-velocity impact) to study their mechanical behavior.

The principal aims of this chapter are understand and study of the failure modes mechanism specially buckling in this type of composite and determining of corresponding critical buckling loads. Besides the critical buckling load, the effects of some key parameters on the overall energy absorption behavior, the threshold buckling load and damage of the panels are discussed, such as the honeycomb material, cell size (diameter), impact energy, solicitation's velocity and indenter geometry.

As results, it was found that these factors have large influence on mechanical behavior and the damage of these structures in terms of critical buckling load and damaged area.

In the approach presented here, the determination of the strengths of aluminum and nomex honeycomb cores relies on the assumption that the buckling phenomenon drives the failure of the structural materials. To justify this strong hypothesis, several tests are performed static and dynamic loading conditions which are presented in this section.

III.1.   Materials

Composite honeycomb sandwich panels consist of aluminum (AHS) and nomex (NHS) core bonded to Alu-Alloy 3003 face sheet (AlMnCu) by an epoxy adhesive were used in this study (Figures 3.1- 3.3). The honeycomb core is an open cell with varying a size d = 3.2, 6.4, 9.6 and 19.2 mm. The specimen preparation and testing were in accordance with ASTM standards. Each plate is measured 50x50x10 mm, with a core thickness of 8.8mm and a thickness of 1 mm for each face-sheet. Details of key properties for the investigated honeycomb sandwiches panels are given in Tables 3.1, 3.2 and 3.3.
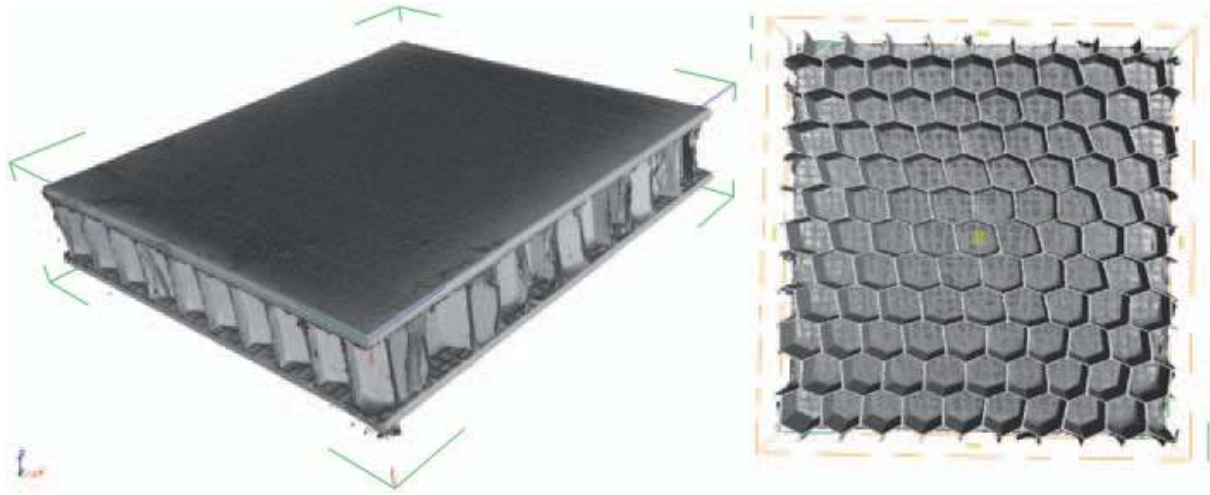
Figure 3.1: Illustration of honeycomb core material (AHC with d=6.4mm) by ct system.
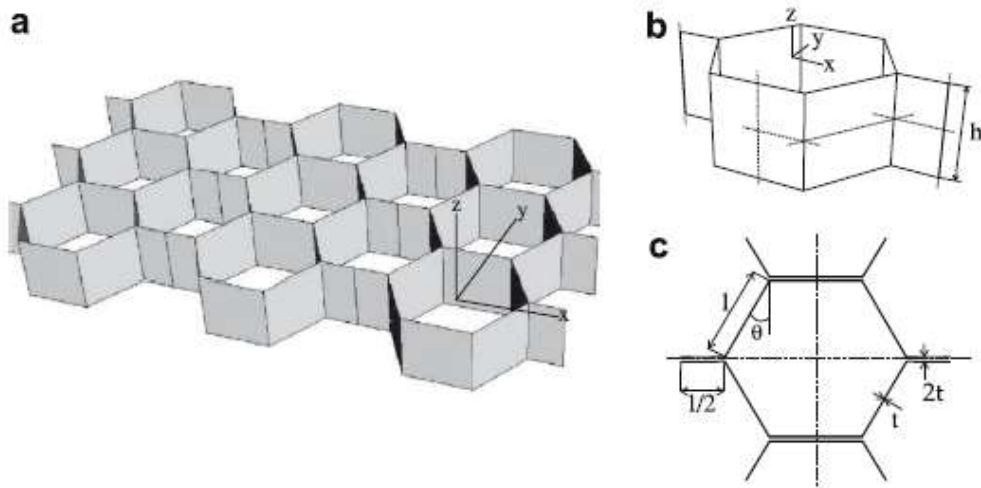
Figure 3.2: Honeycomb core structure: (a) general view, (b) honeycomb unit cell, and (c) unit cell parameters.
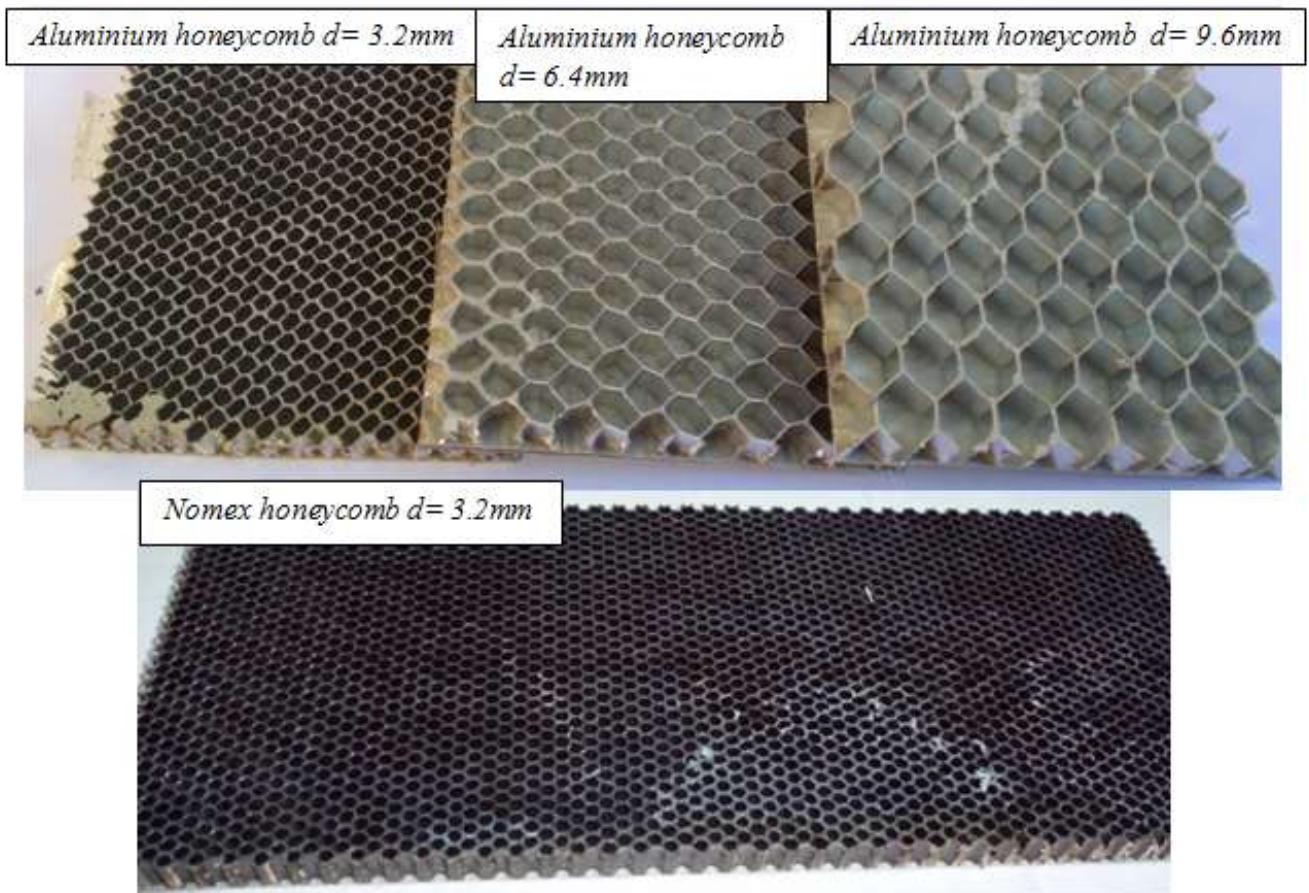
Figure 3.3: Typologies of investigated sandwiches.

Table 3.1: Physical and geometrical properties of the AHS panels.

Mechanicals properties	AHS			
Density [kg/m³]	130	82	55	29
Cell size [mm]	3.2	6.4	9.6	19.2
Wall thickness [mm]	0.06	0.08	0.08	0.08
Compression strength [Mpa]	7.00	4.25	2.24	0.69
Crush strength [Mpa]	3.38	1.66	0.90	0.26

Table 3.2: Physical and geometrical properties of the NHS panels.

Mechanicals properties	NHS			
Density [kg/m^3]	144	128	80	41
Cell size [mm]	3.2	3.2	3.2	3.2
Wall thickness [mm]	0.056	0.076	0.08	0.08
Compression strength [Mpa]	13.20	11.30	4.70	1.90

Table 3.3: Mechanical properties of the face-sheets.

Facesheet: Aluminium				
Young modulus [Mpa]	Shear strength [Mpa]	Tensil strength [Mpa]	Density [kg/m^3]	Poisson ration
70000	268	367	2,73 10^{-3}	0,33

III.2.   Experimental procedure

III.2.1.   Low velocity impact tests

The low-velocity impact tests were carried out with using Ceast Fractovis Plus a drop test machine (Figure 3. 4), able to eliminate multiple impacts. The mass of the impactor and the drop height are variable, allowing for a wide range of impact energies. The instrumented impactor, having a hemispherical tip with different diameter (10 and 20 mm), hits the centre of the specimens. A range of impact energies that varied from 8 to 220 J was achieved by varying the drop height at different velocities (v = 1.5, 2, 3, 4, 5, 6, 7 and 8 m/s) are used in this study.

The specimen was positioned between the top and bottom clamp plates, with the mid-point of the plate directly located underneath the impactor. Upon release, the free-falling impactor would fall along two smooth guided columns, and through the centre hole of the clamp plate of diameter 40mm to strike the specimen. The support fixture for the specimen facilitated circular clamped condition.

The pneumatic clamp plates prevented any movement of the specimen, without causing any buckling of the honeycomb core prior to impact. After the first impact, the rebound brake was activated to support the crosshead, and thus the impactor was only allowed

to strike the specimen once. Transient response of the samples included the velocity and deflection of the impactor, as well as load, as a function of time. Graphical plots were then generated using the data collected from the data acquisition system.
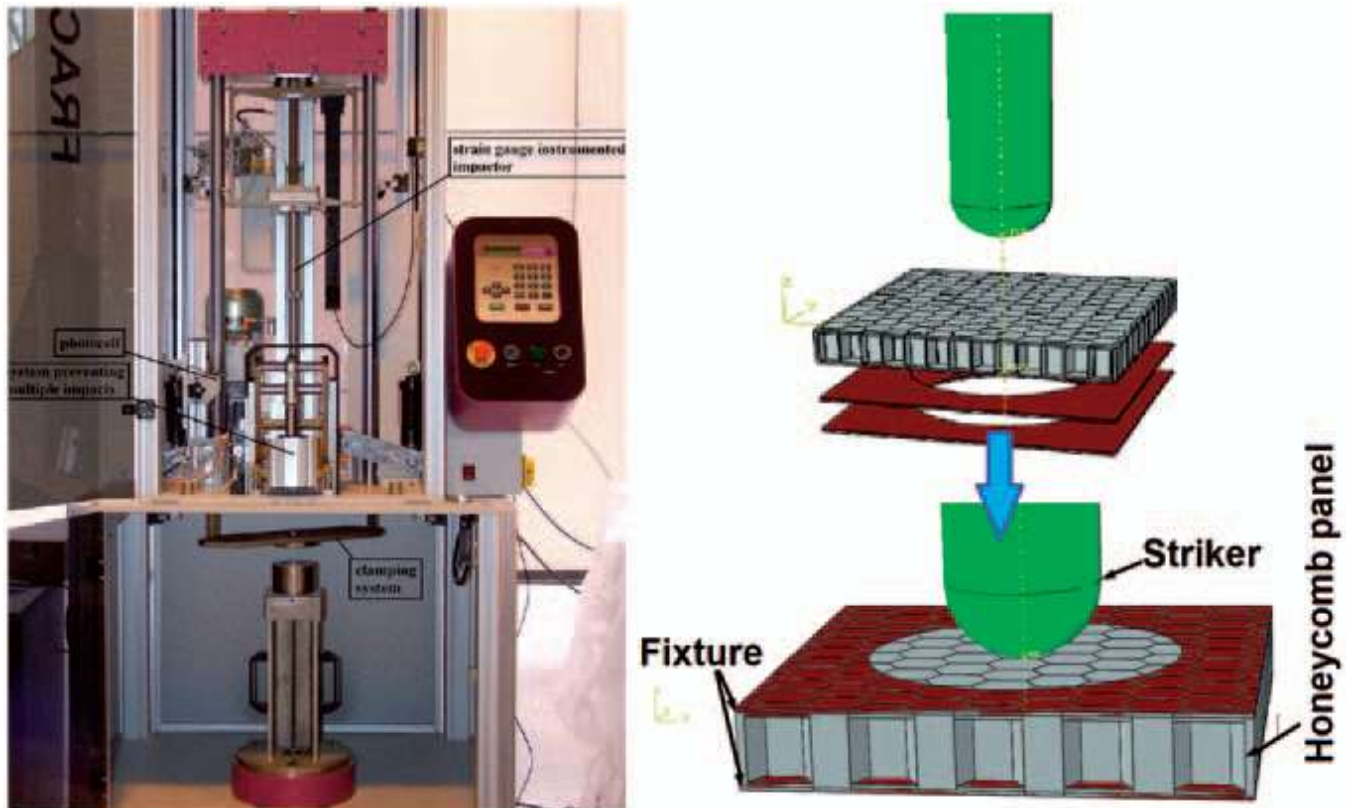
Figure 3.4: Drop – weight impact test machine (CeastFractovis Plus).

III.2.2.   3D Computed Tomography System (CT)

Radiography is one of the oldest and most widely used methods of non-destructive testing. Radiography uses radiation energy to penetrate solid objects in order to assess variations in thickness or density, and for instance to detect cracks or other internal imperfections. The test object is placed between the radiation source and a digital detector (Figure 3.5). The image on the detector show the internal features of the test object. Conventional 2D radiography is a shadowgraph of a 3D object, and information in depths and volume can be obtained observing the object with several orientations (angle).

Computerized Tomography (CT) improves upon conventional 2D radiography by producing 3D cross-sectional images of an object from flat x-ray images. In a CT system, the test component is placed upon a turntable stage that is between the radiation source and an imaging system. The sample is rotated during the examination, and the digital detector registers thousands of individual 2D x-ray images from all angles. An algorithm reconstructs

the inner-structural image processing the data into a complete 3D representation. The characteristics of the internal structure of an object including dimensions, shape, defects, and density are readily available from the whole volume obtained.
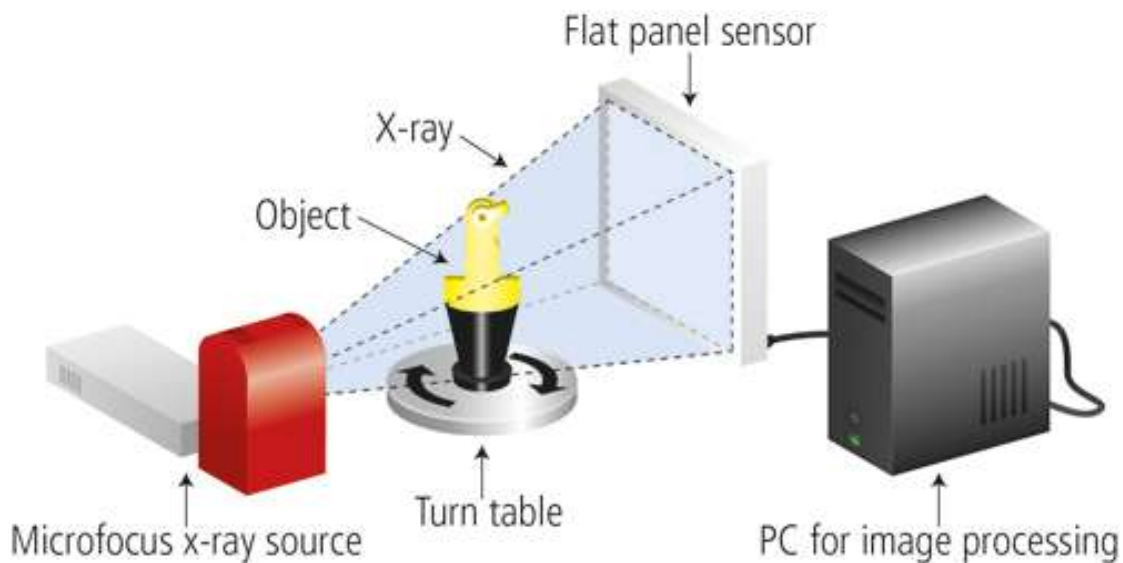
Figure 3.5: Computerized tomography (CT) configuration.

Computed tomography offers considerable advantages over conventional optical or tactile Coordinate Measuring Machines especially when measuring complex parts with hidden surface or features which are difficult to access. The metrology equipment consist computed tomography systems for high precision 3D metrology of the complete internal and external geometry of the object (Figure 3.6).
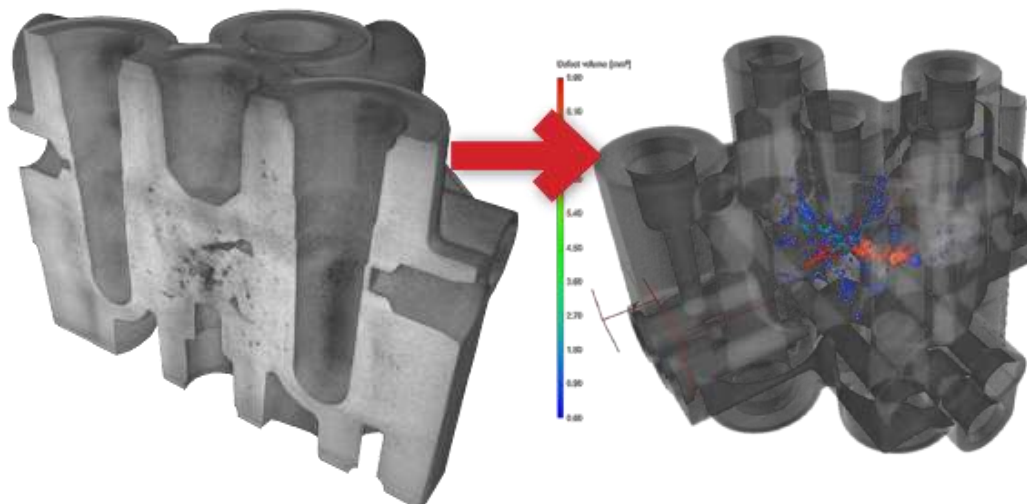
Figure 3.6: Example of application on CT system.

The Computed Tomography System scan is a non-destructive technique which allows the investigation of the internal geometries and the damage detection without perturbing the impacted specimen. The real geometry of the honeycomb sandwich was analyzed by the 3D Computed Tomography System Y.CT Vario (Figures 3.7-8) before carrying out the impact tests. The system, based on a variable focal-spot size technology, creates the cross-section images of 3D objects using X-rays. The entire set of the projections is used by computer software to reconstruct the 3D map of the absorption coefficients of the X-rays inside the sample. The results can be visualized either as cross-sections (slice by slice, in top, front and right view) or as a 3D representation of the object (Figure 3.9). A special advantage of the XCT is that the volume image can be exported for FE analysis (FEA).

Figure 3.7: 3D Computed Tomograph system (Y.CT Vario machine).

After the impact tests at different velocities (v = 1.5, 2, 3, 4, 5, 6, 7 and 8 m/s) a 3D acquisition of the impacted honeycomb panels and their internal buckling, undetectable by a visual inspection, has been carried out by a XCT system. A conical X-ray beam scanned the sample, which was rotated at increments of 0.5 $^{\circ}$/s for each rotation step until a full rotation of

360 ^{o} was achieved. Cu filters were used to improve image contrast and to correctly set detector saturation. The detector system is a flat panel with a resolution of 2048*2048 pixels.
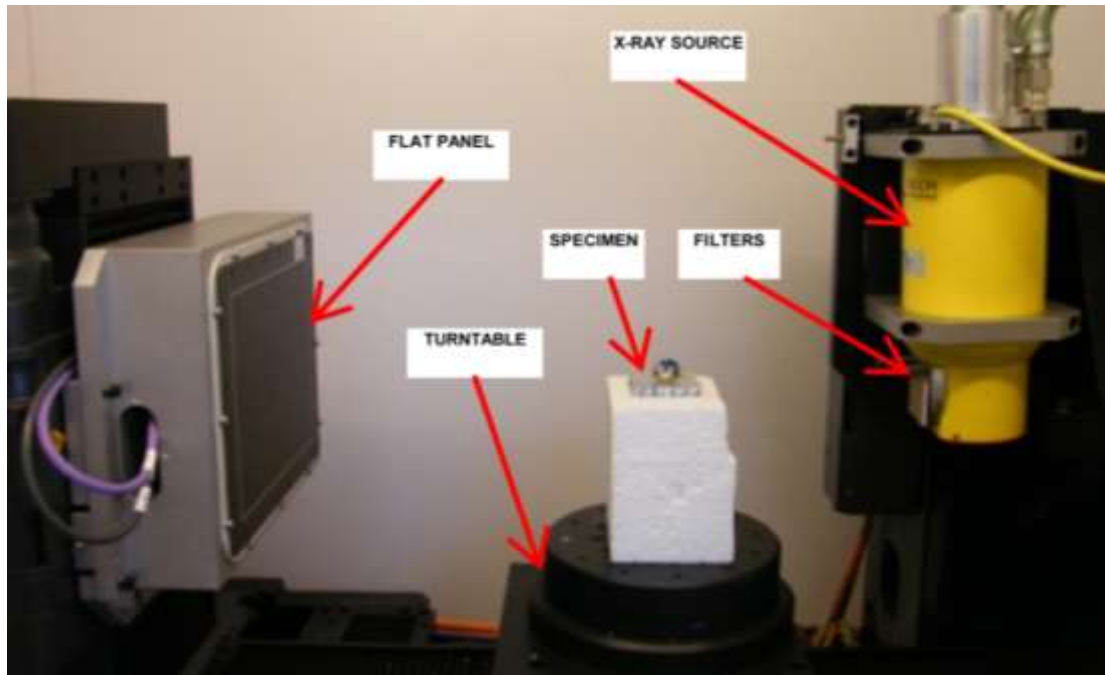
Figure 3.8: Description of computed tomography system.

Figure 3.9 shows the 3D reconstruction of an AHS by means of the CT. The system, based on a variable focal-spot size technology, creates the cross-sectional images of three-dimensional objects using X-rays. A volumetric representation of the item to be inspected is obtained as a result of the CT. Both the material inner and outer structures and the geometric dimensions of the item to be inspected are recognizable. It is important to underline that this NDT technique doesn't require cutting and polishing the samples for carrying out the X-ray measurements.

This allows a significant savings of time and the investigation of the internal damage without perturbing the impacted specimen. This unit is equipped with an X-ray source having maximum voltage and current of 225 kV and 7.1 mA, respectively, depending on the focal-spot size that can be chosen among these values: 250 mm, 300 mm, 500 mm and 800 mm. The detector system is a flat panel with a resolution of 2048*2048 pixels. The scans, reported in this section, were conducted with 250 mm focus and X-rays were set at a voltage of 210 kV and at a current of about 1.1 mA. This procedure was then repeated until a full rotation of 360° was achieved, and a total of 1440 projections were then obtained to be used in the 3D profile generation. The parameters, used for the XCT investigation, are reported in Table 3.4. The surface of the object under investigation is represented in the CT image stack by the grey value transition between air and material (Figure 3.9).

Table 3.4: *Parameters of the tomographic investigation.*

Focal-spot size (um)	X-ray voltage (kV)	X-ray current (mA)	Projections number	Integration time (ms)	Voxel size (mm)	Image size (pixels)
300	210	7.1	1080	500	0.05	2048x2048
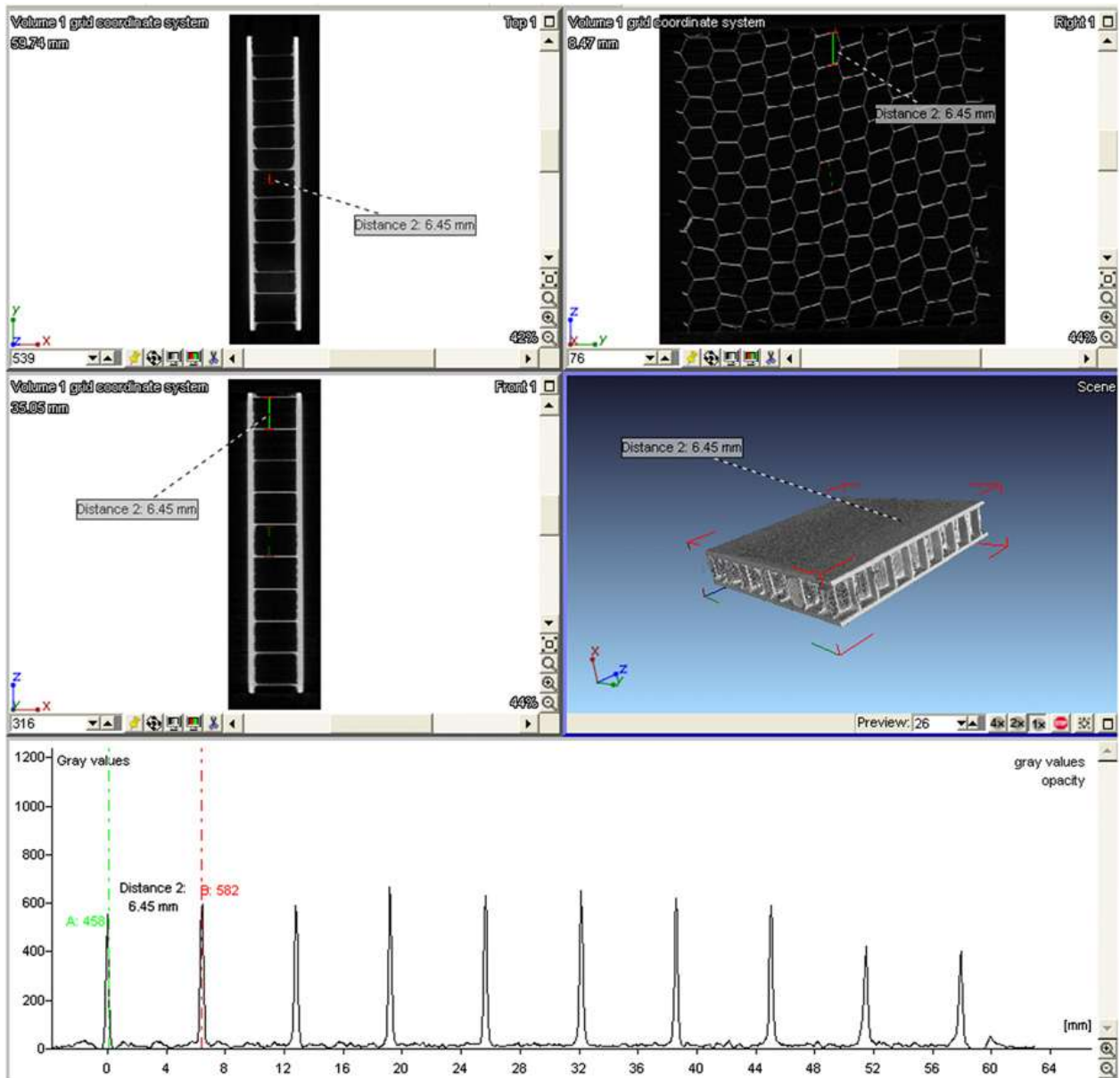
Figure 3.9: CT analysis of an aluminum honeycomb core (AHS d=6.4mm).

III.2.3. Quasi static indentation tests

A series of quasi-static indentation tests were conducted for composite honeycomb sandwiches panels described in Section 3.1 (AHS and NHS) using different steel indenters: Cylindrical, conical, hemispherical and truncated cone shown in Figure 3.11. Three samples for each kind of test were realized. Mechanical testing was realized by employing a universal testing machine model by Zwick/Roell Instruments equipped with a 100 KN load cell (Figure 3.10) at room temperature. The specimens were crushed against the fixed plate at a speed of 2 mm/min. The specimens were placed between two steel circular plates of 136 mm diameter, one of which was moved by a hydraulic system along two vertical guides. For each test, the load-indentation characteristic was recorded. After testing, the specimens were removed from the testing machine and optically examined.
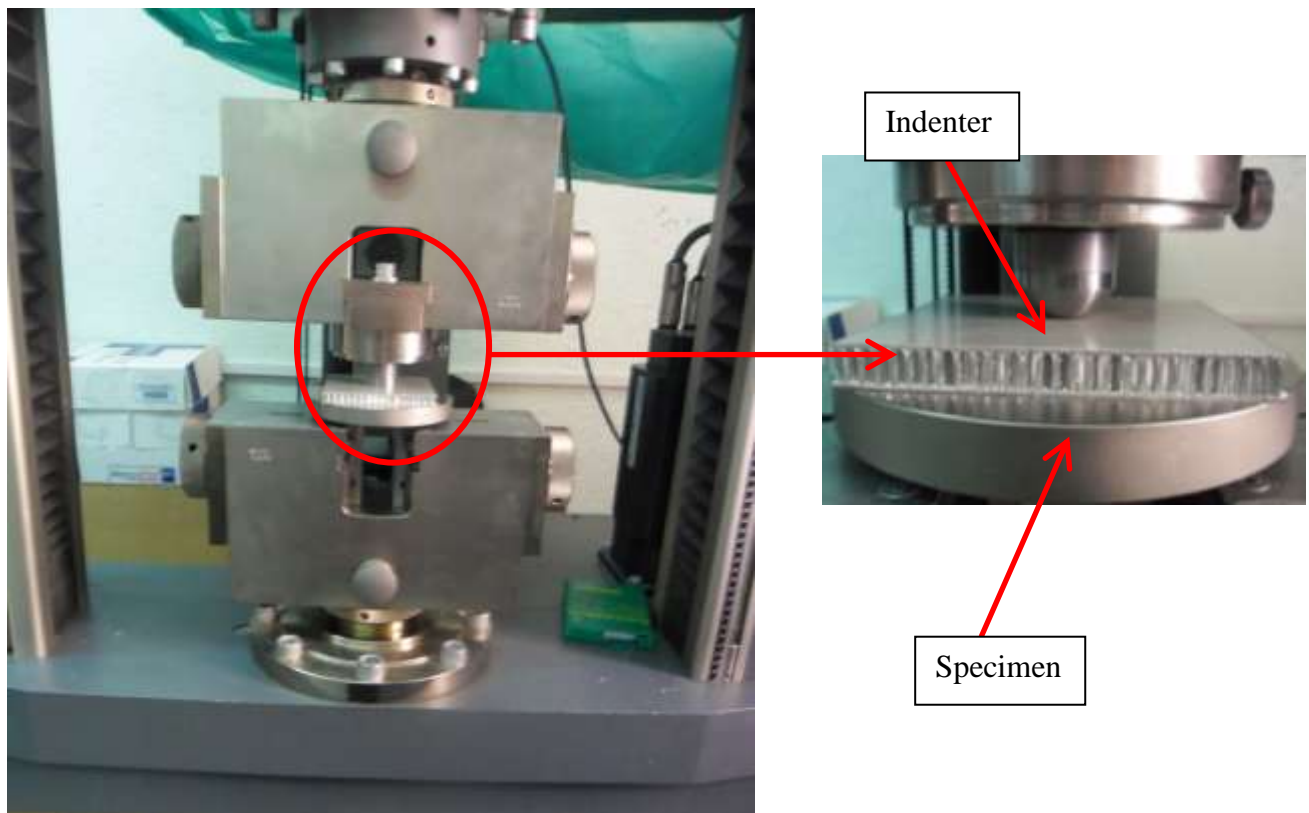
Figure 3.10: Quasi-static experiment machine (Zwick/Roell).
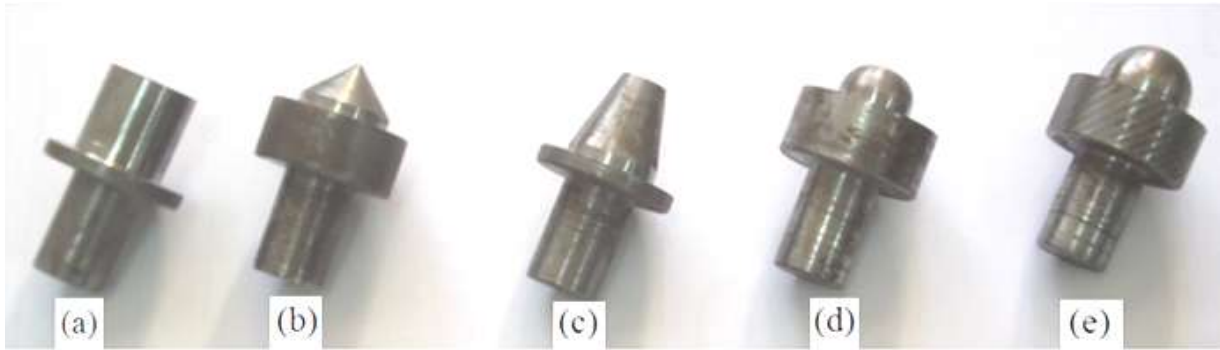
Figure 3.11: The different indenters' geometry used in this study: (a) cylindrical, (b) conical, (c) truncated cone, (d) hemispherical 16mm and (e) hemispherical 20mm.

III.2.4. Compression tests

The honeycomb sandwiches samples were compressed between two rigid platens in (T) directions: compression along the direction of cell axis. The load-displacement traces obtained from the displacement controlled at 0.5 mm/min. A **Zwick/Roell** (100 kN) (Figure 3.12) material-testing machine was employed to control the stroke rate and to record the applied axial force. The test procedure for compressive properties was as per **ASTM C 365** standards. The same materials described in section 3.1 were used to complete these tests. The dimension of the compressive specimen was 50 mm$\times$ 50 mm$\times$10 mm. During each test, the crushing behavior of the honeycomb specimen was observed carefully.

Rigid platen

Specimen
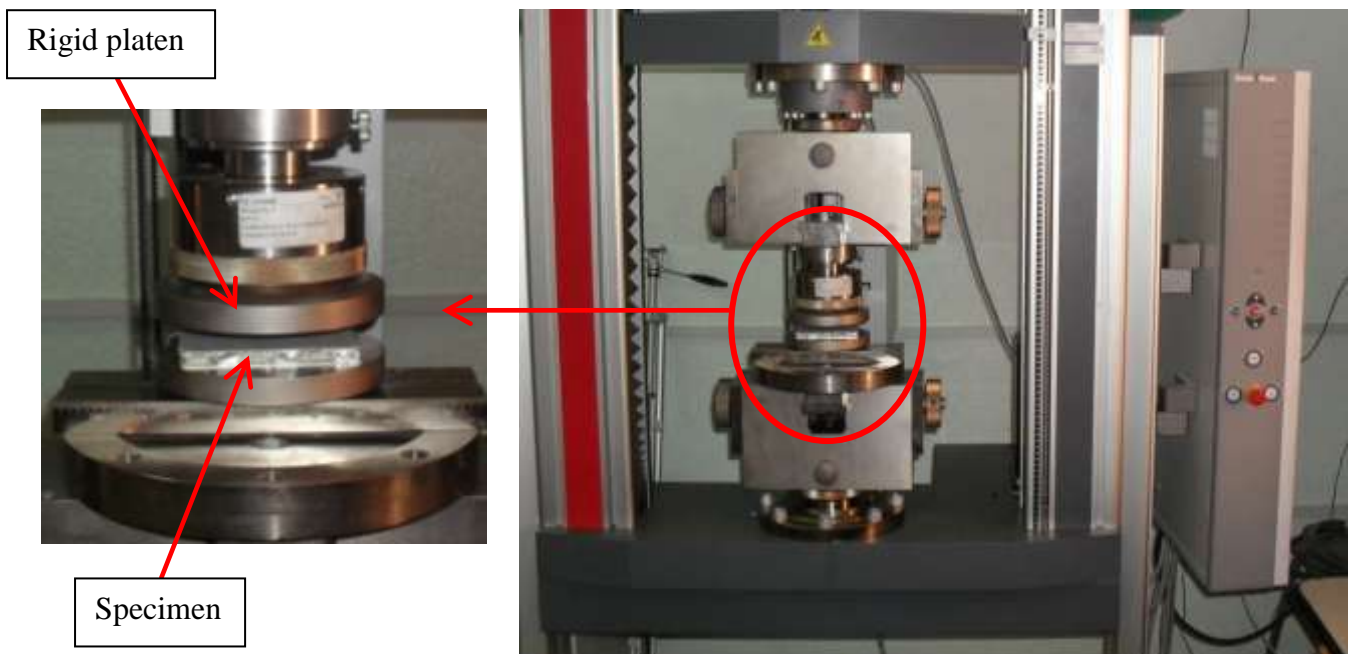
Figure 3.12: Experimental set up of the compressive test.

III.3. Experimental Results, Analysis and Discussion

The obtained results for all tests (static and dynamic) are described in detail in the following section. In meantime the effect of keys parameters on failure modes and the critical buckling load for the three loading conditions are discussed such as:

- The impact energy,
- The cell size (diameter),
- The core material (AHS and NHS),
- The impactor or the indenter geometry and diameter.

III.3.1. Low-velocity impact tests

III.3.1.1. Effect of impact energy on buckling behavior

The load–displacement curves at different impact energy for AHS panels are shown in Figs. 3.13, 3.14 and 3.15 (AHS d = 3.2 mm, d = 6.4 mm and d = 19.2 mm respectively) and for NHS are given in Figs. 3.16 (NHS, d = 3.2 mm).

The curves of the honeycomb panels have the same stiffness and a different number of load peaks: the curves for impact velocities lower than 5 ms^{-1} (lower energies) have only one load peak due to the upper skin impact failure, delamination and core crushing, the curve for v=5 ms^{-1} has a first peak due to the upper skin failure and a second peak due to the lower skin impact, the curves for impact velocities higher than 5 ms^{-1}(higher energies) have a higher second peak due to the bottom skin perforation leading to total failure of the specimens.

Figs 3.13-16 show the contact load histories of the honeycomb sandwich panels according to the changes of impact energy. The slope of the contact load histories curve increased as the impact energy was increased. As shown in these figures, the maximum contact load of the specimen with the smaller cell size (3.2mm) had a larger value than that of larger cell size (6.4 and 19.2mm). Meanwhile, the contact time of the specimen with the larger cell size was longer than that of the specimen with the small cell size. The reason is that the impacted damage area of sandwich panels with larger cell size is larger than that of the core with smaller cell size.

The curves of NHS panels have similar impact behavior, whereas they show more than two load peak and more sharp respect to the crushing of nomex. This different behavior could be explained by the shorter time between the failures of the two skins in the NHS panels.
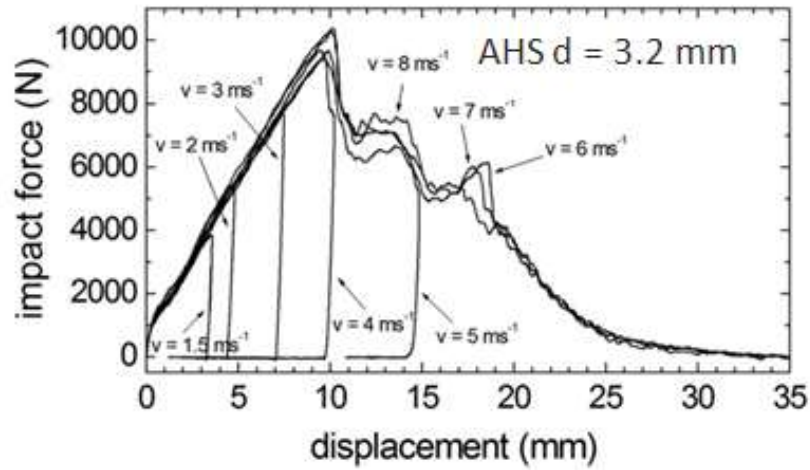
Figure 3.13: Load-displacement curves measured under impact loading (AHS d=3.2 mm).
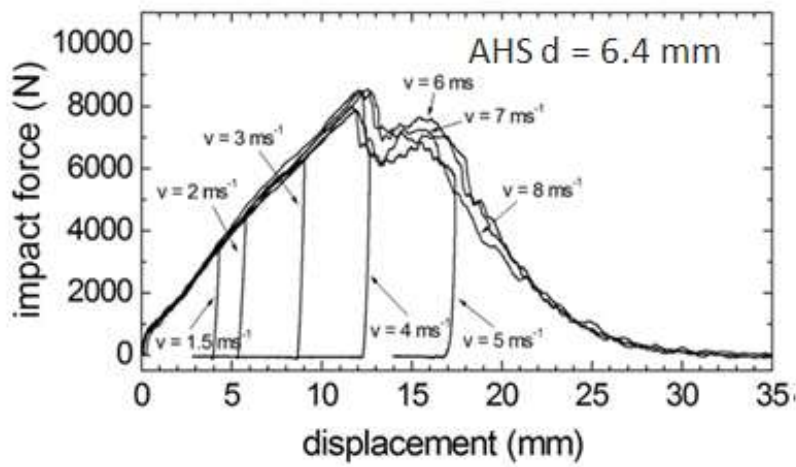
Figure 3.14: Load-displacement curves measured under impact loading (AHS d=6.4 mm).
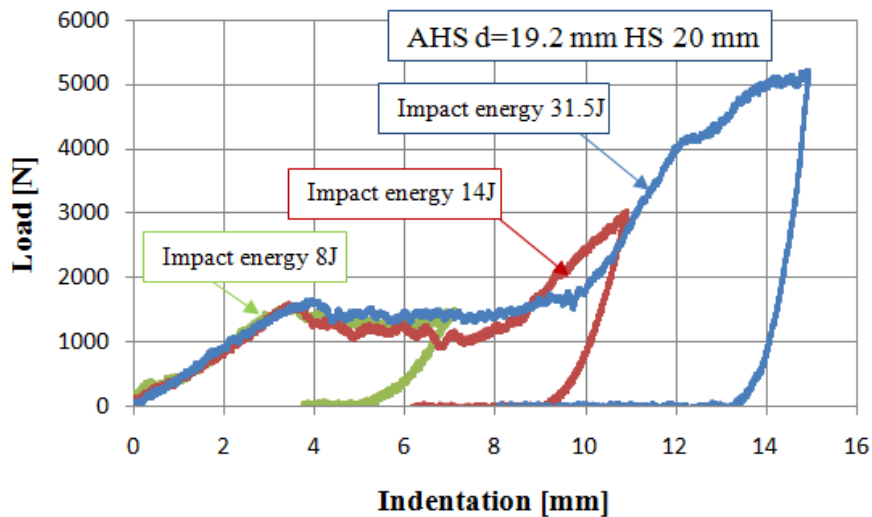
Figure 3.15: Load-displacement curves measured under impact loading (AHS d=19.2 mm)
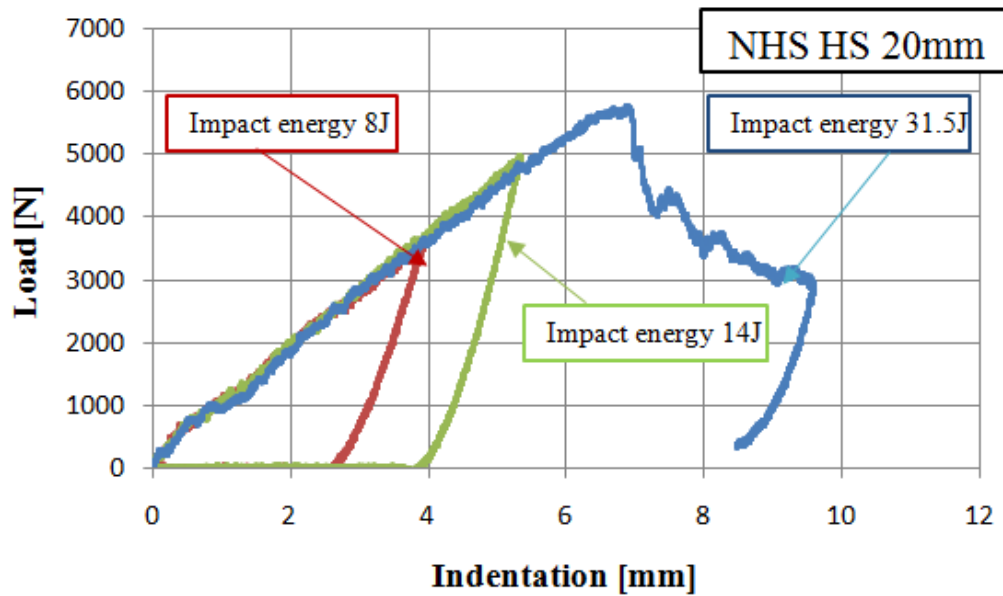
Figure 3.16: Load-displacement curves measured under impact loading (NHS d=3.2 mm; Di=20 mm).

Figures 3.13-16 also indicate that the absorbed energy at failure depends on the cell size; there is an increase of absorbed energy when the core cell size is decreased from 19.2 to 3.2 mm; however, when the core cell size is decreased, there is a reduction in the absorbed energy of the structure.

Figure 17 shows the registered threshold buckling load for AHS d= 3.2 mm and AHS d = 6.4 mm. from this figure we can see that for all impact energy the maximum buckling load it was seen for the smallest cell size (AHS d = 3.2 mm), also the critical buckling load increases at increasing the impact energy.
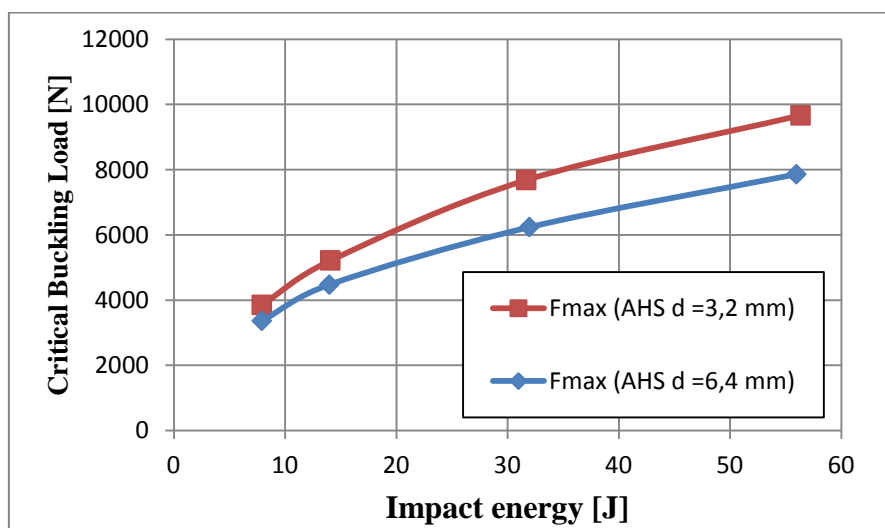
Figure 3.17: Max load- impact energy for AHS d = 3.2 mm and ahs d = 6.4 mm.

Table 3.5 reports the results of all the experimental tests in terms of absorbed energy and critical buckling load.

The same observations were observed for NHS panels (Figure 3.18).
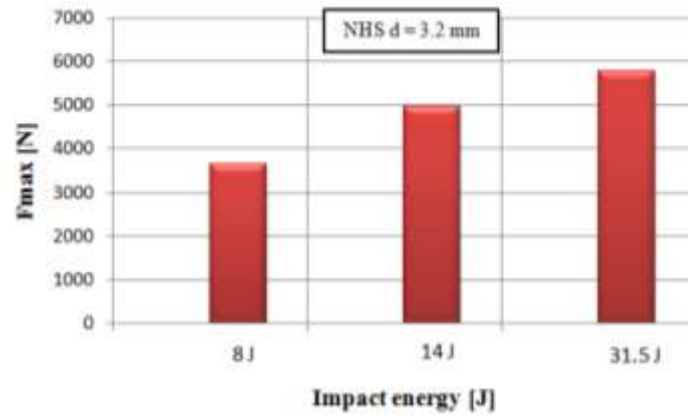
Figure 3.18: Effect of impact energy on critical buckling load (NHS d = 3.2 mm).

Table 3.5: Experimental results (impact loading).

V[m/s]	AHS (d = 3.2 mm)		AHS (d = 6.4 mm)		NHS (d = 3.2 mm)		AHS (d=19.2 mm)	
	α [mm]	F_{exp}[N]	α [mm]	F_{exp}[N]	α [mm]	F_{exp}[N]	α[mm]	F_{exp}[N]
1.5	3.12	3849	3.66	3361	4.9	3558	7,105	1586
2	4.27	5215	5.33	4476	5.1	4594	10,9	3172
3	6.89	7683	8.34	6239	6.9	5758	14,931	5221
4	9,74	9668	11,42	7862	-	-	-	-

III.3.1.2.Effect of cell diameter on the critical buckling load and deflection:

To study the effect of the cell size on impact behavior several test were carried on honeycomb sandwich panel with different cell sizes (AHS d = 3.2, 6.4 and 19.2 mm). The effect of cell size of honeycomb core on threshold buckling load is given by figure.3.19. From this curve we can see that with increasing the cell size the displacement of the impactor increases which mean that the deflection at impacted zone also increases and this can be explain with the large vide area under the upper face-sheet. In case of NHS panels, tests have been stopped at velocity lower than 5 ms[-1.] . Figures 3.19 also indicate that the absorbed energy at failure depends on the cell size; there is an increase of absorbed energy when the core cell size is decreased from 19.2 to 3.2 mm; however, when the core cell size is decreased, there is a reduction in the absorbed energy of the structure.

61
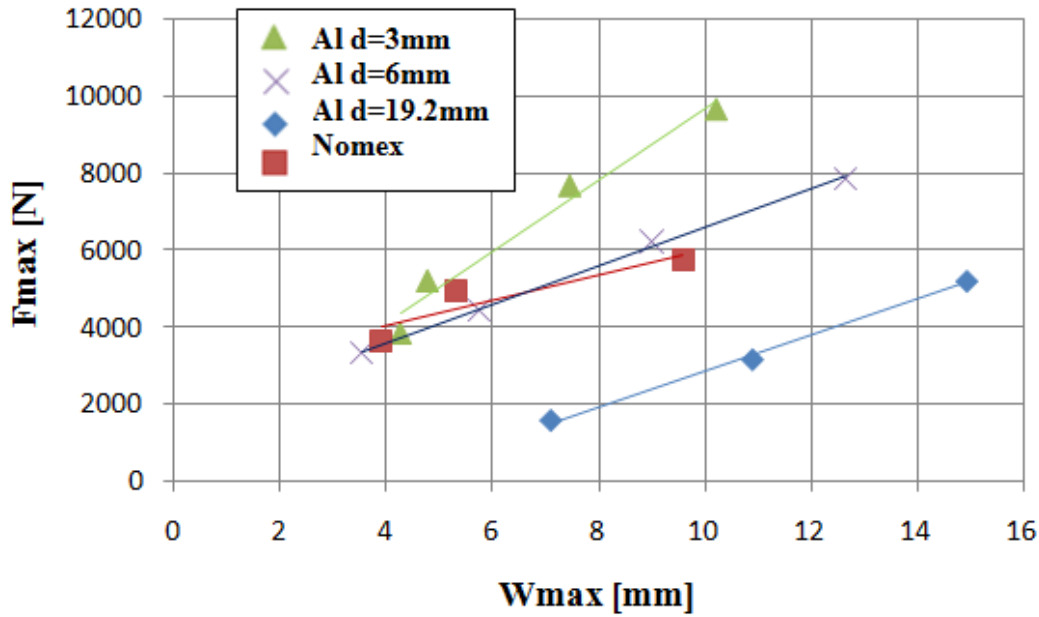
Figure 3.19: Critical buckling load-deflection (W) for all used materials.

The general observation that can be made from this figure is the impact resistance decreases with the increase of the cell size and this can be explained by the fact that the stiffness of the sandwich panel increases with the increase of the density of the core [21-36]. Also the cell size induces relevant effects on the mechanical performances of the samples under impact load. This is evident from the results shown in figure 3.19that compares the max impact load at varying the cell size at different velocity. It was found that the impact load increases with the decreasing of the cell size of the core. Damaged area decreases with the increase of density since the effect of the impacted zone becomes local due to the increase of stiffness of the panel.

III.3.1.3.Effect of impact velocity on the critical buckling load and deflection

Figure.3.20 presents the effect of impact velocity loading on the critical buckling load for AHS panel. As shown in this figure, the maximum buckling loads were obtained for the AHS d = 3.2 mm at all velocity stages. In meantime, we can see that with increasing the impact velocity the threshold buckling loads increase for all used cell sizes.
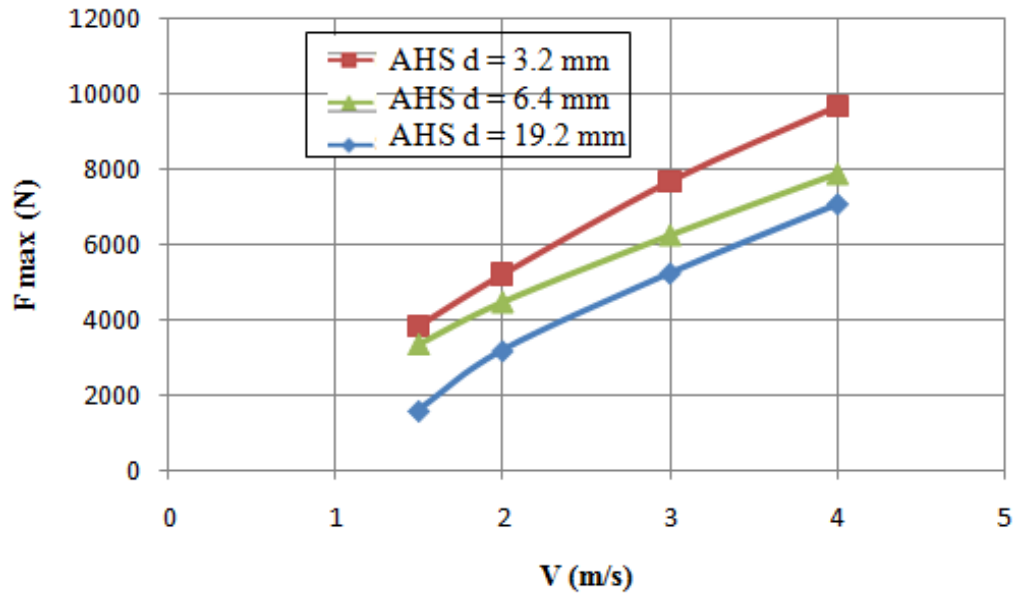
Figure 3.20: Effect of velocity and core cell size on impact critical buckling load.

III.3.1.4. Effect of impact diameter on the critical buckling load and deflection (Wb)

Figure 3.21 shows for each impactor (HS 20 mm and HS 10 mm) the absorbed impact energy and the threshold buckling load for (AHS d = 19.2 mm). Noticeable differences in the mechanical behavior of sandwich samples under impact load are evidenced at varying impactor diameter. In this figure it is possible to observe how an increase of loads is reached at increasing contact area between the impactor and specimen.
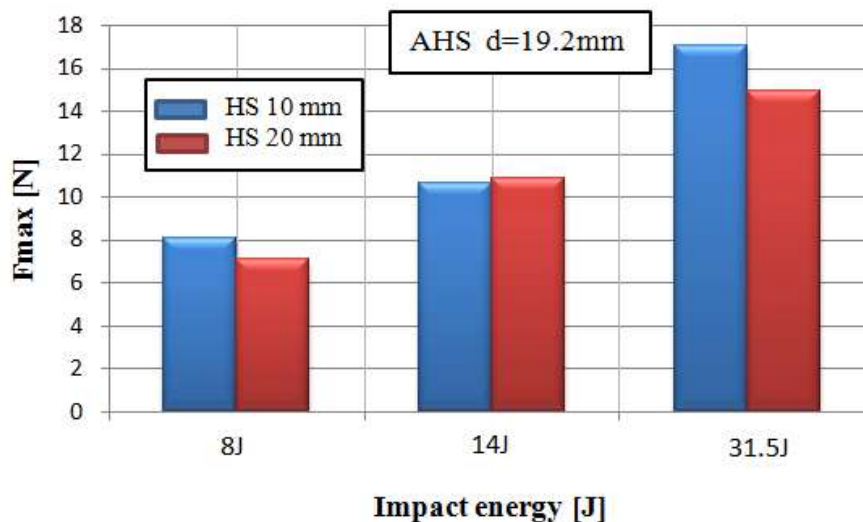
Figure 3.21: Effect of impactor diameter on the impact critical buckling load (AHS d = 19.2 mm).

However, the damaged area was proportional to the diameter of the impactor. As expected, the damaged area depends on the impactor geometry. The largest damaged areas

were observed for impactor HS 20 mm while the smallest damaged areas were observed for impactor HS 10 mm. It is noticed in Figs. 21-22 that the geometry of the impactor has significant influence on the stiffness of the honeycomb sandwich panels and the damage process. This can be explained by the fact that the impactor with the largest diameter has larger radius of curvature, which reduces the local deformation of the face and allows more penetration of the impactor without causing the failure of the face.
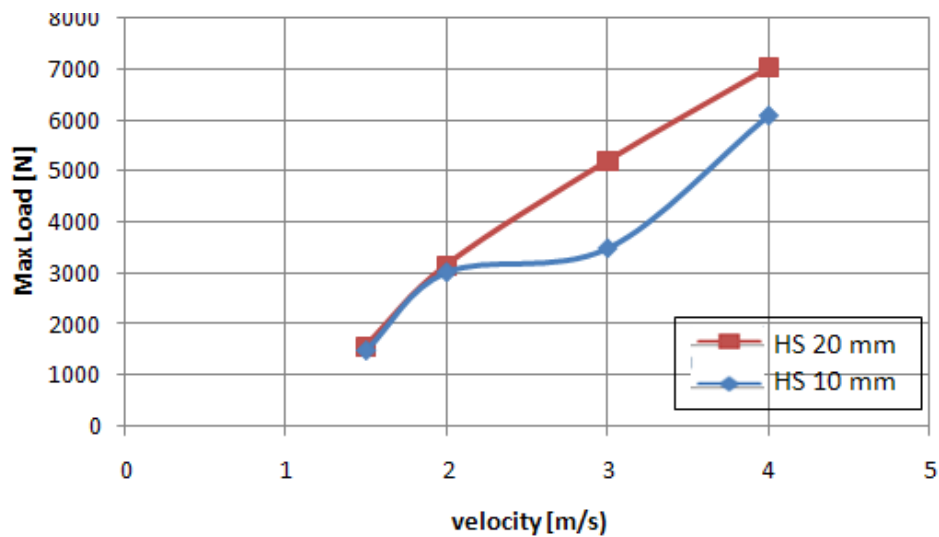
Figure 3.22: Effect of impactor diameter n the impact behavior (NHS d = 3.2 mm).

Figure 3.23: Effect of impactor diameter n the impact behavior (NHS d = 3.2 mm).

Figure 3.24: Effect of impactor diameter n the impact behavior (NHS d = 3.2 mm).

III.3.1.5. Effect of impact energy on deflection (W_b) of honeycomb sandwiches panels:

Figures 3.25 also indicate that the deflection of honeycomb sandwiches panels at failure depends on the impact energy; there is an increase in deflection (buckling) Wb of used sandwiches panels when the impact energy is decreases from 8 to 31.5J for the both used impactor.
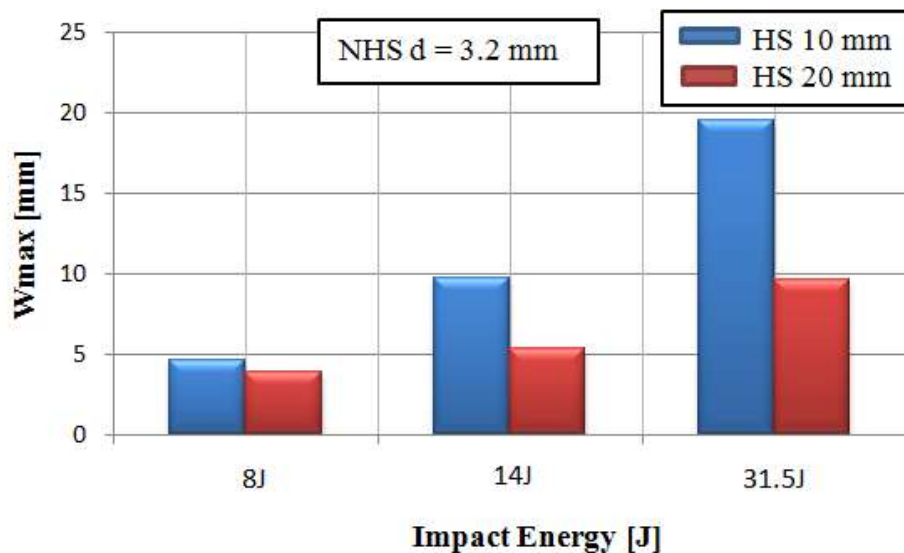
Figure 3.25: Effect of impact energy and impactor diameter on core deflection (buckling) (NHS d = 3.2 mm).

III.3.2. Tomography system results

To analyze and observe failure modes of both honeycomb sandwiches panels used in this study, the 3D Computed Tomography System was used and the results of this method are given as follow.

The vertical displacement W_b of the core at bottom face sheet interface and the impactor displacement W_i were measured by analyzing the CT images of midplanes of the panels impacted at velocities lower than 5 ms^{-1}, that didn't produce the perforation of the panels (Figs3.26-28).
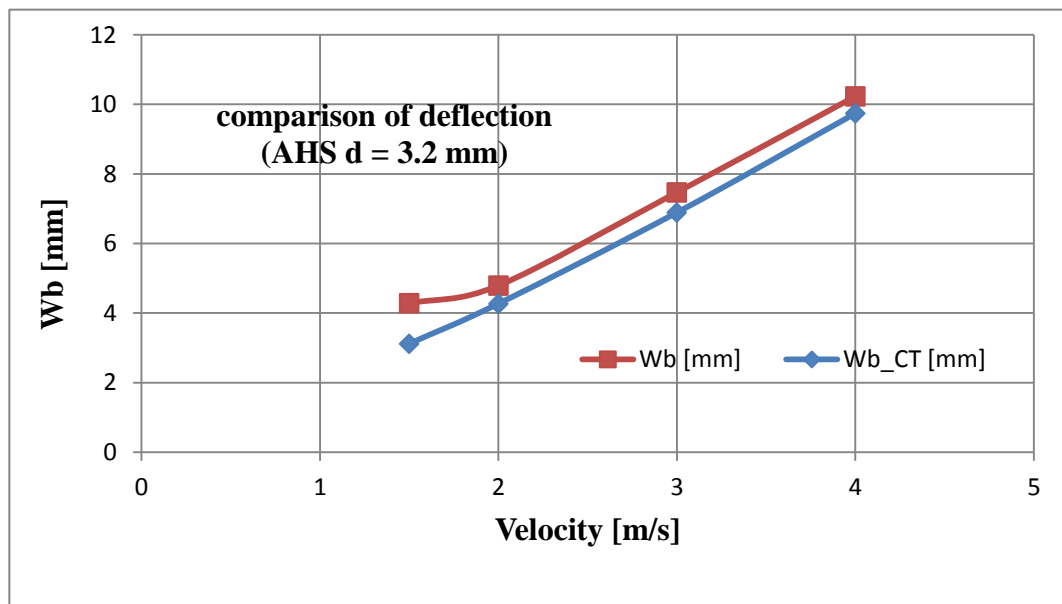
Figure 3.26: Comparison between experimental and ct results (AHS d = 3.2 mm)
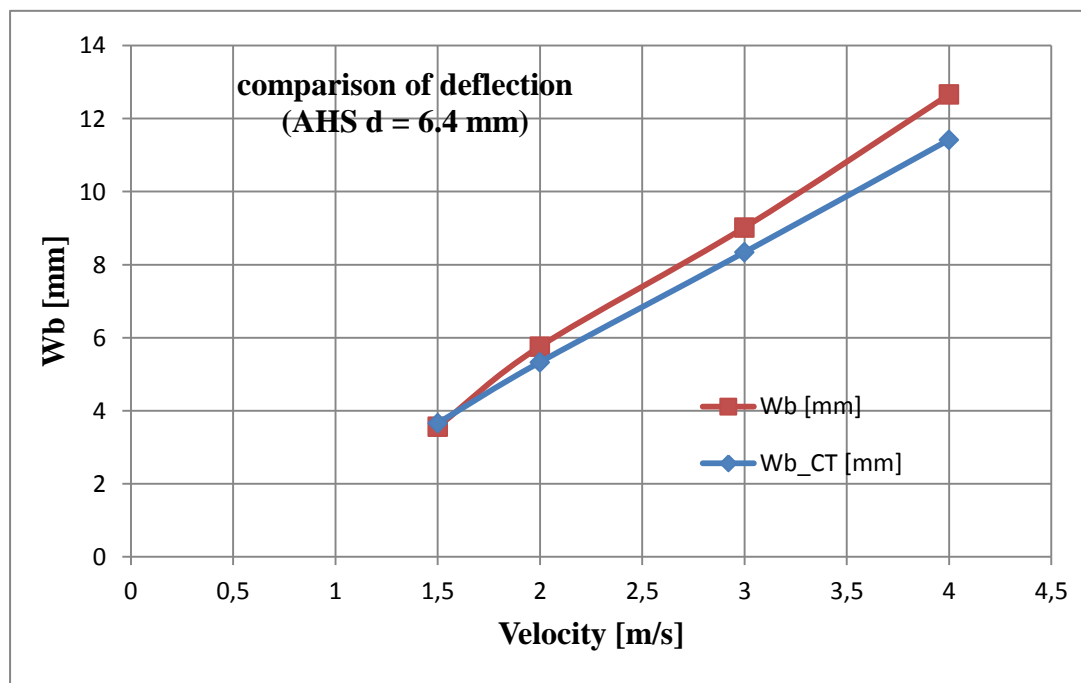
Figure 3.27: Comparison between experimental and ct results (AHS d = 6.4 mm)

66
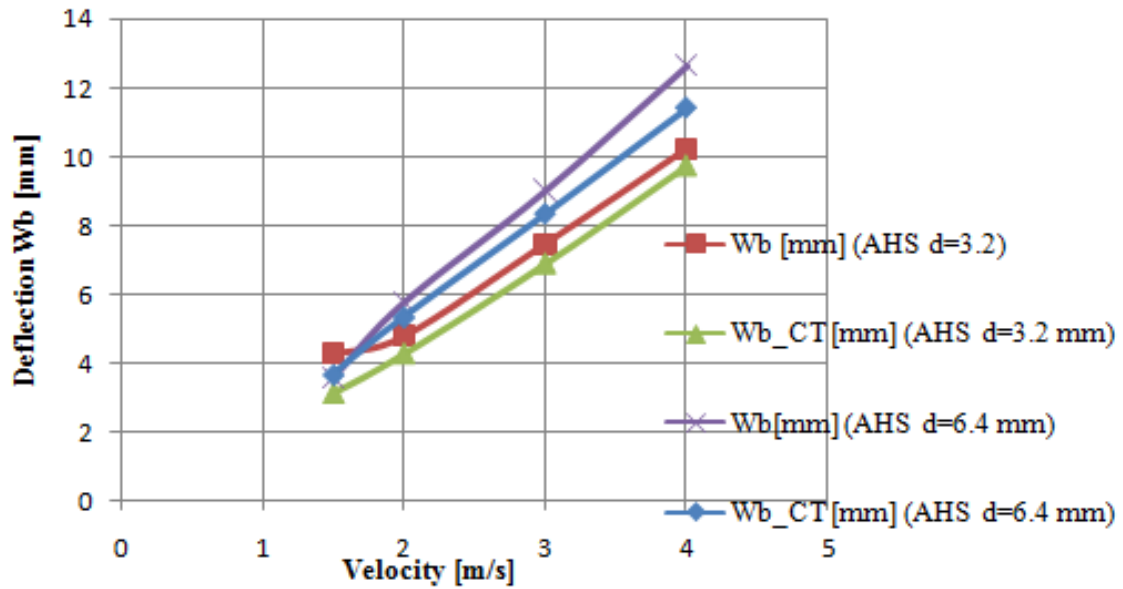
Figure 3.28: Effect of impact velocity on the middle plan core buckling (deflection) (comparison between AHS d = 3.2 and AHS d = 6.4 mm).

The tomography investigations have shown that the collapse of the panel occurs for the initial deformation of the upper skin and for the buckling of the core cells. The dominant failure mode observed during the tests was the core buckling before total perforation of the panels as demonstrated by the CT images after impact tests (Figures 3.29-33). The core buckling displacement a is obtained by the subtraction between the impactor displacement W_i and the vertical displacement W_b of the core (table 3.6).

(a)

(b)
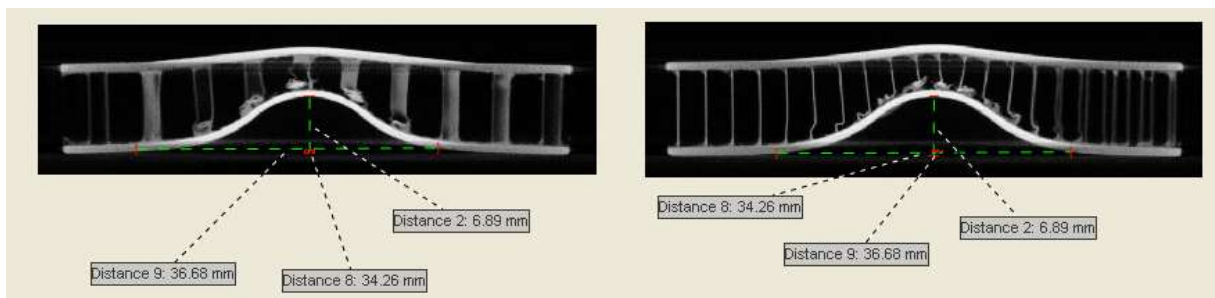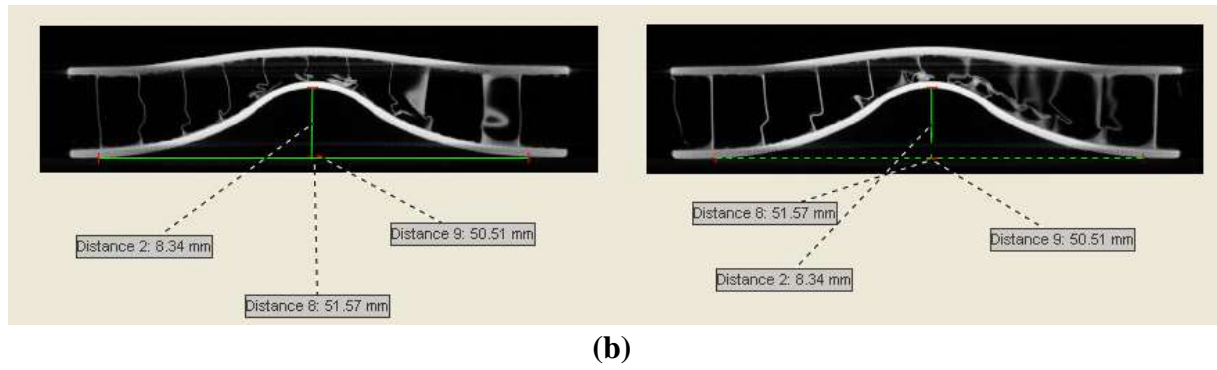
Figure 3.29: The failure mode demonstrated by the ct image: (a) AHS d=3.2mm (v=3ms^{-1}) and (b) AHS d=6.4mm (v=3ms^{-1}).

Table 3.6: Experimental Data result for Wi and Wb for d=3.2mm

V (m/s)	d = 3.2 mm		d = 6.4 mm	
	Wi (CT) (mm)	Wb (CT) (mm)	Wi (CT) (mm)	Wb (CT) (mm)
1.5	3.12	0.43	3.66	0.32
2	4.27	0.55	4.96	1.09
3	6.89	1.78	8.11	2.03
4	9.74	3.05	11.42	3.42

The dynamic response of these sandwiches is not influenced by the skin-core adhesion and depends on the quality and mechanical properties of the core as confirmed in previous studies [12-35], which demonstrated that significant impact energy is absorbed by the core material.
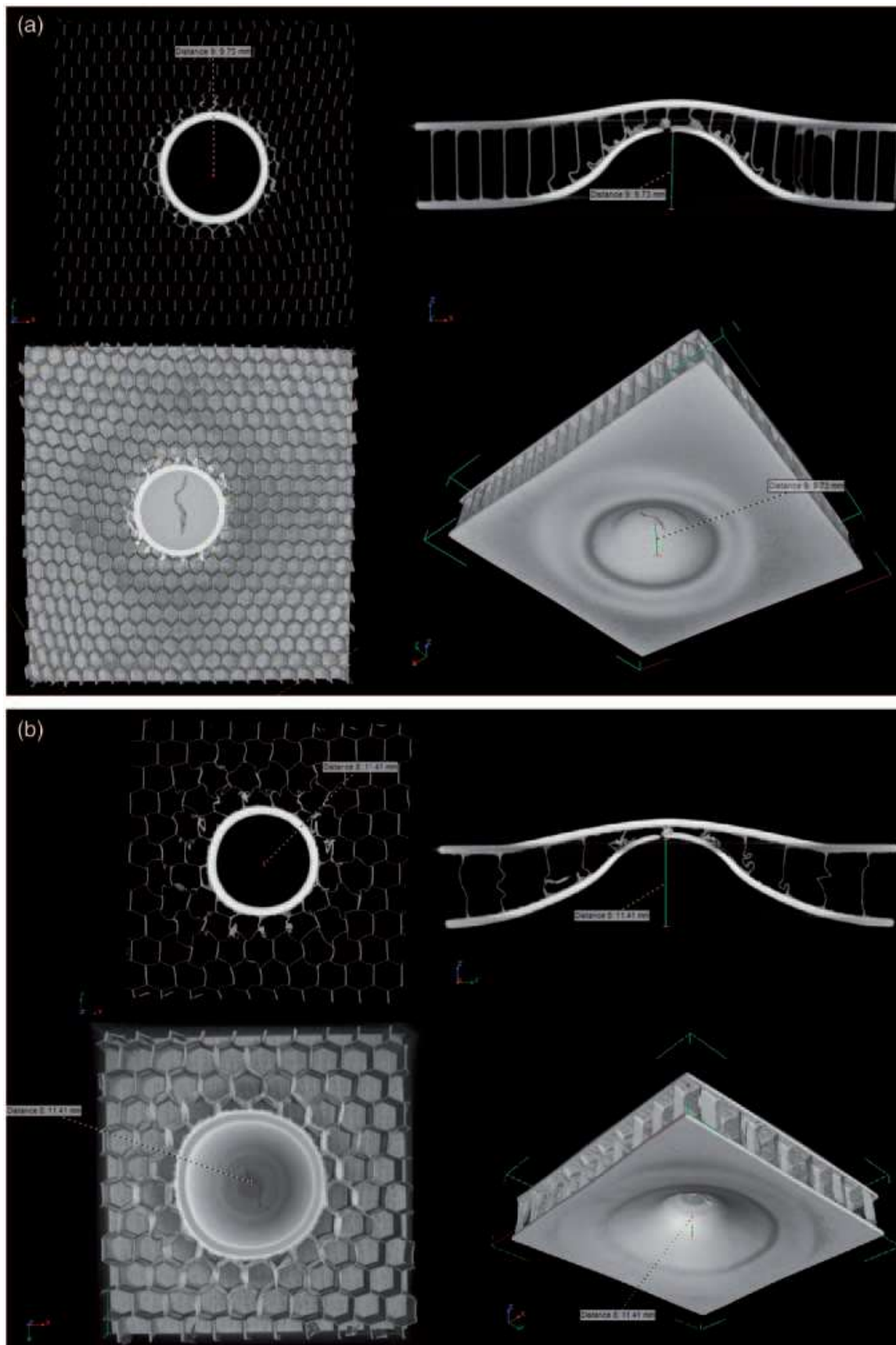
Figure 3.30: CT images of honeycomb panels after impact tests at v=4 m/s: (a) AHS d = 3.2 mm and (b) AHS d=6.4mm.
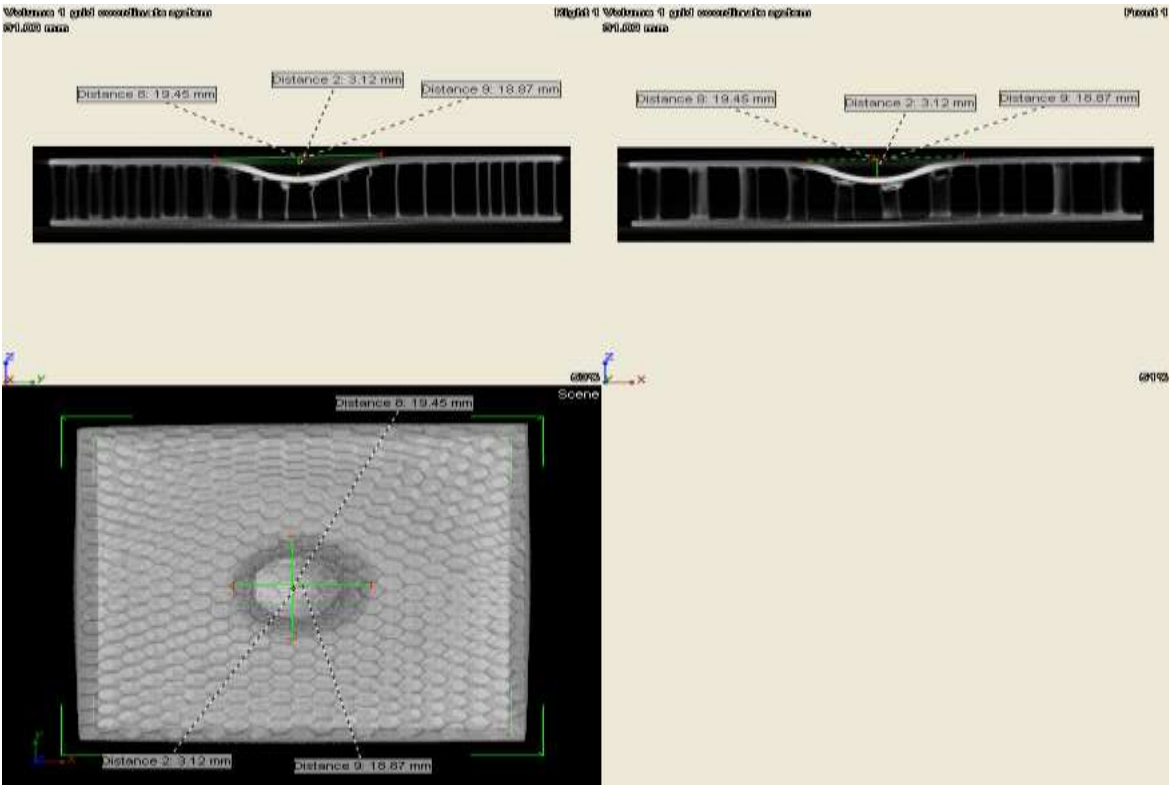
(a)
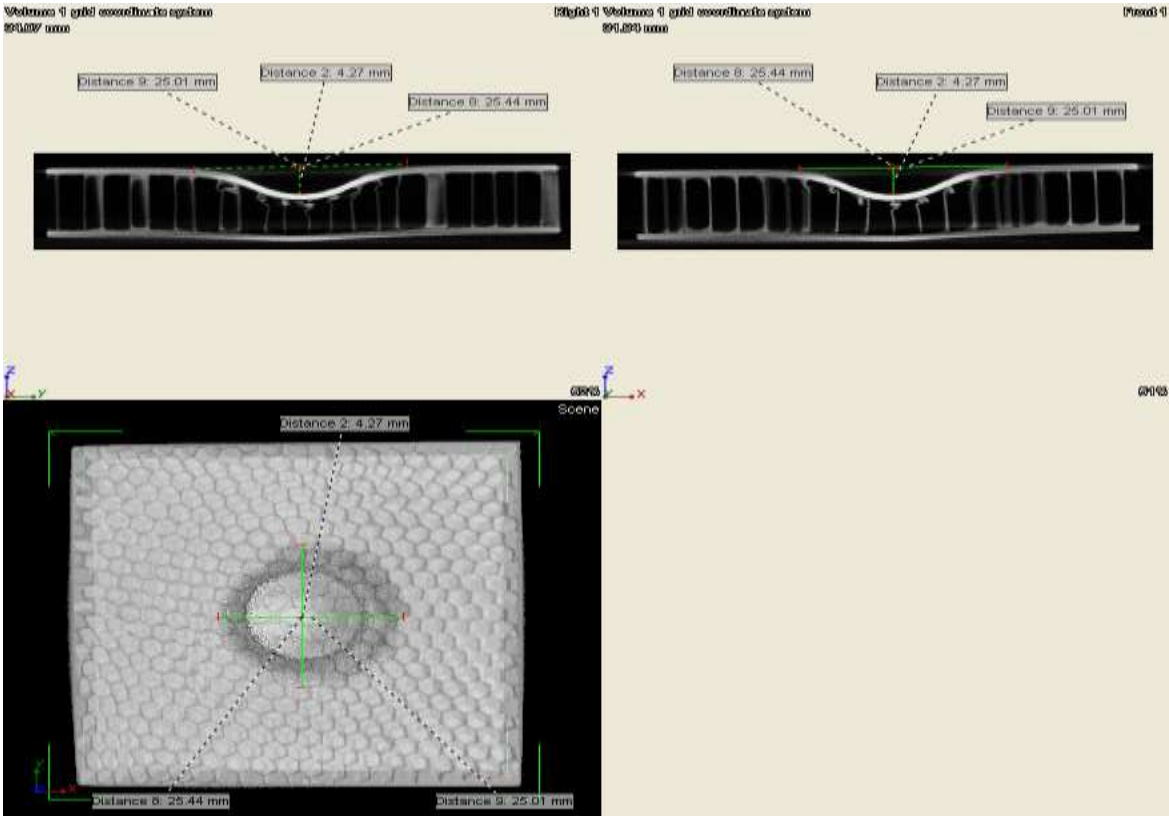
(b)
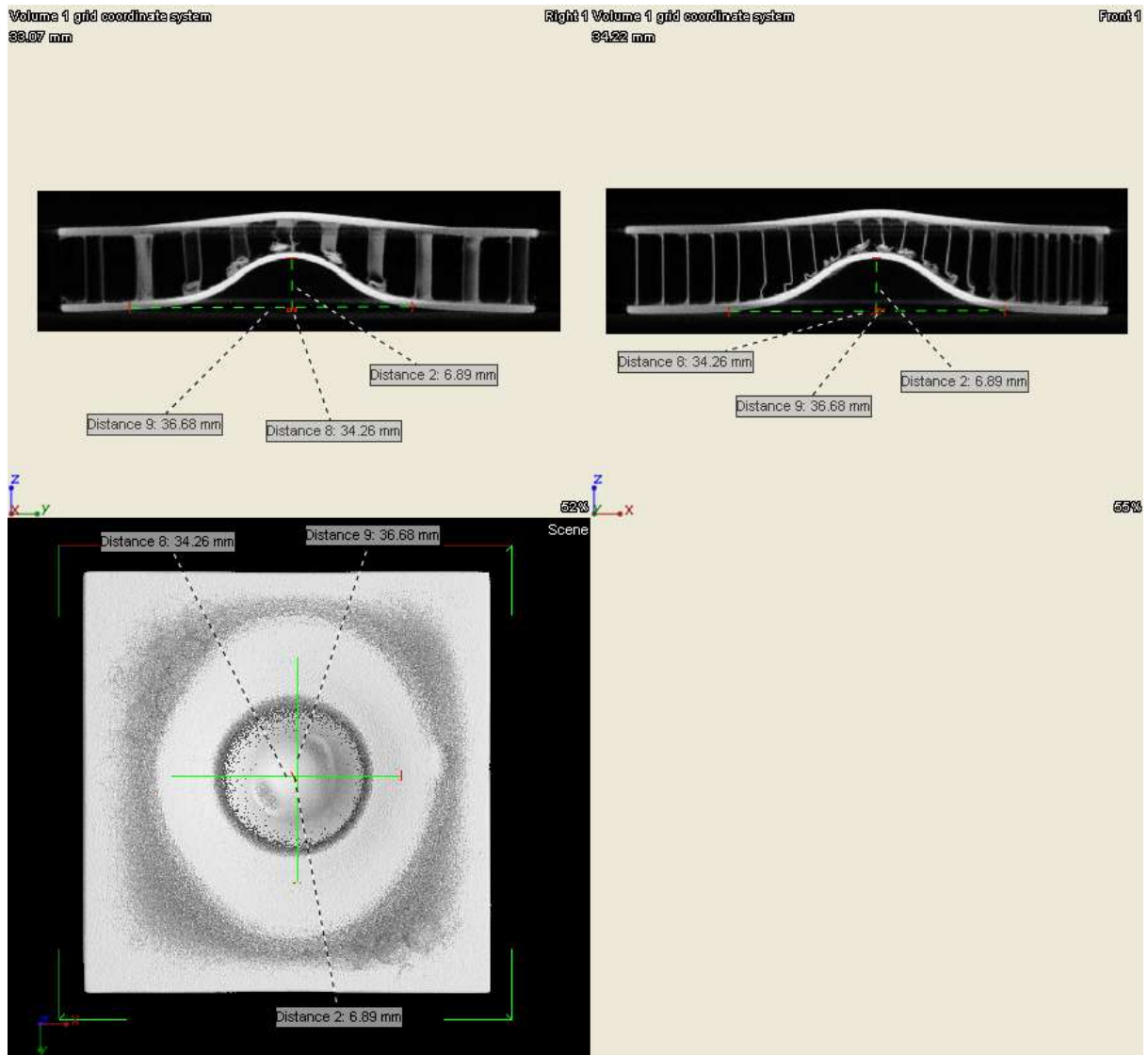
(c)

Figure 3.31: CT images of honeycomb panels after impact tests AHS 3.2 mm: (a) v = 1.5 m/s, (b) v= 2 m/s and (c) v = 4m/s
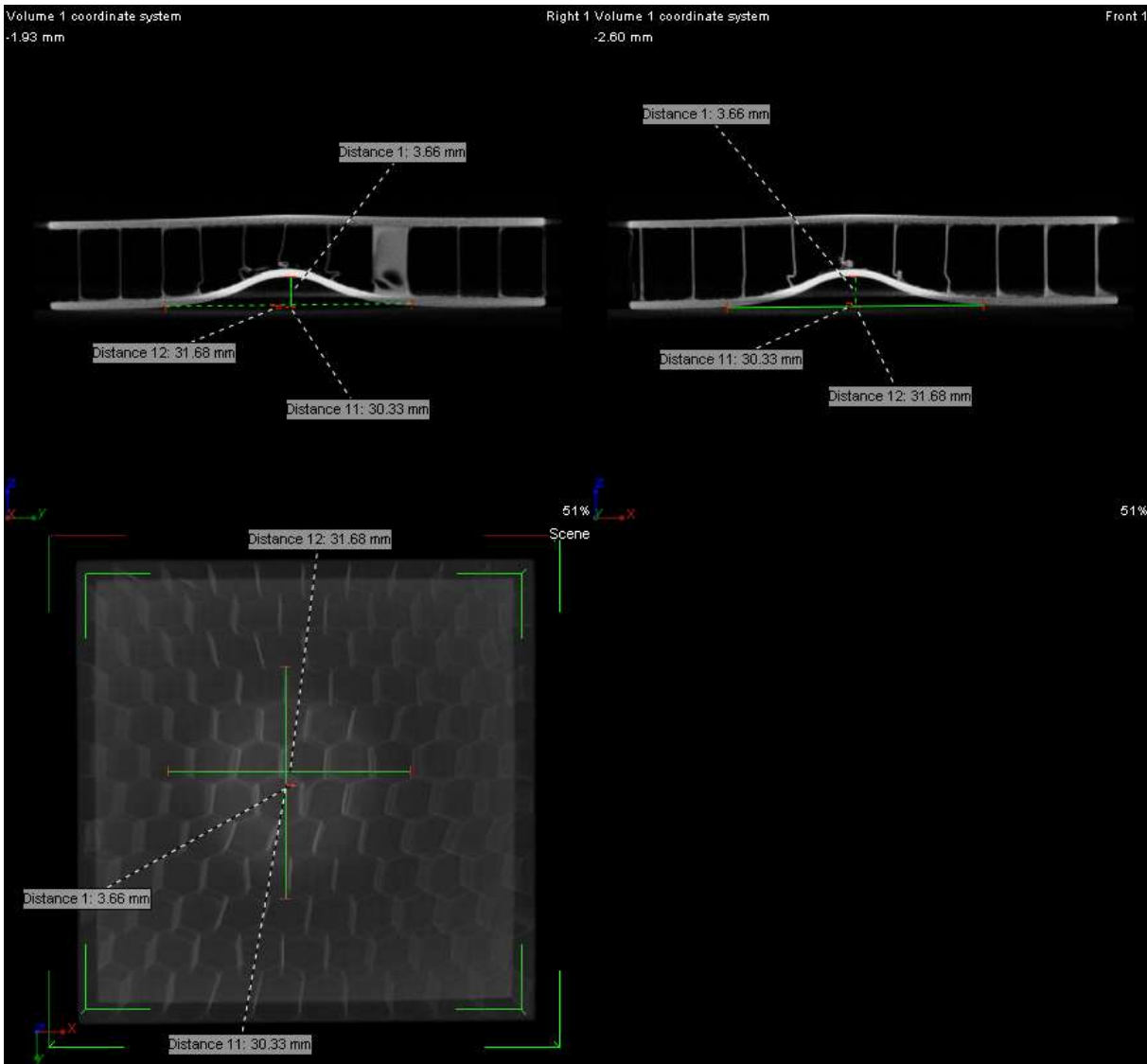
(a)
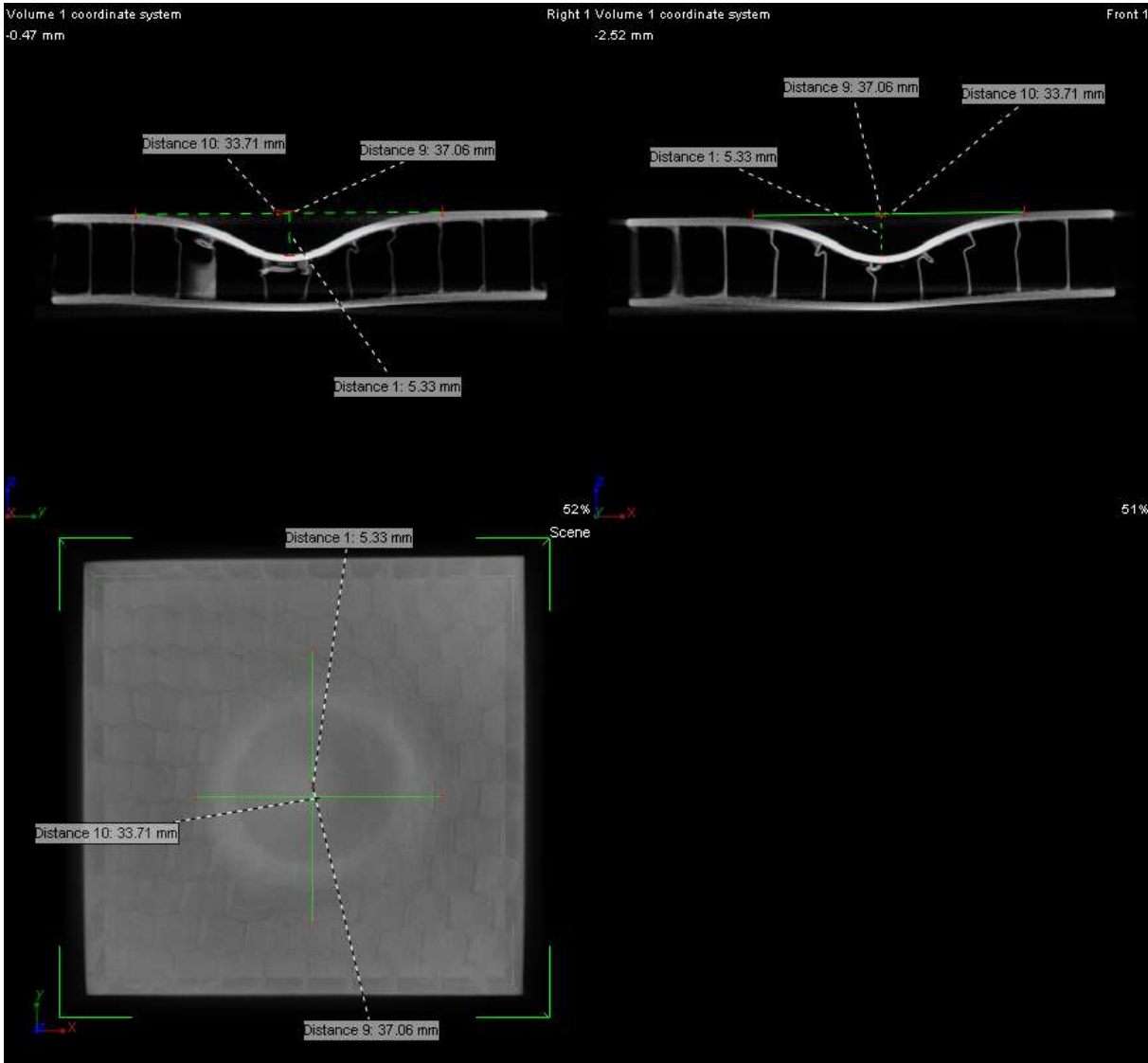
(b)
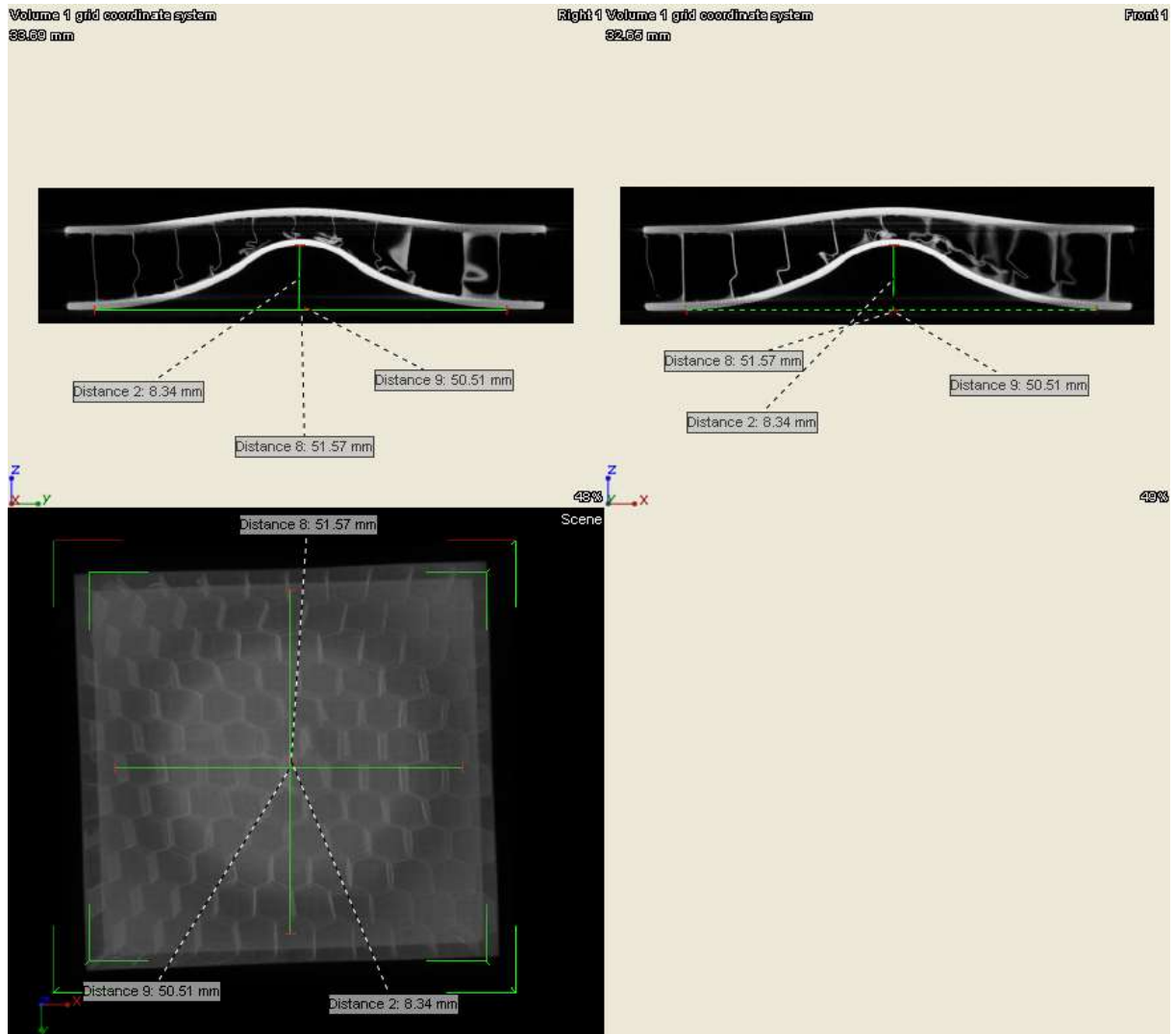
(c)

Figure 3.32: CT images of honeycomb panels after impact tests for AHS d=6.4 mm: (a) v = 1.5 m/s, (b) v = 3 m/s and (c) v = 4m/s.
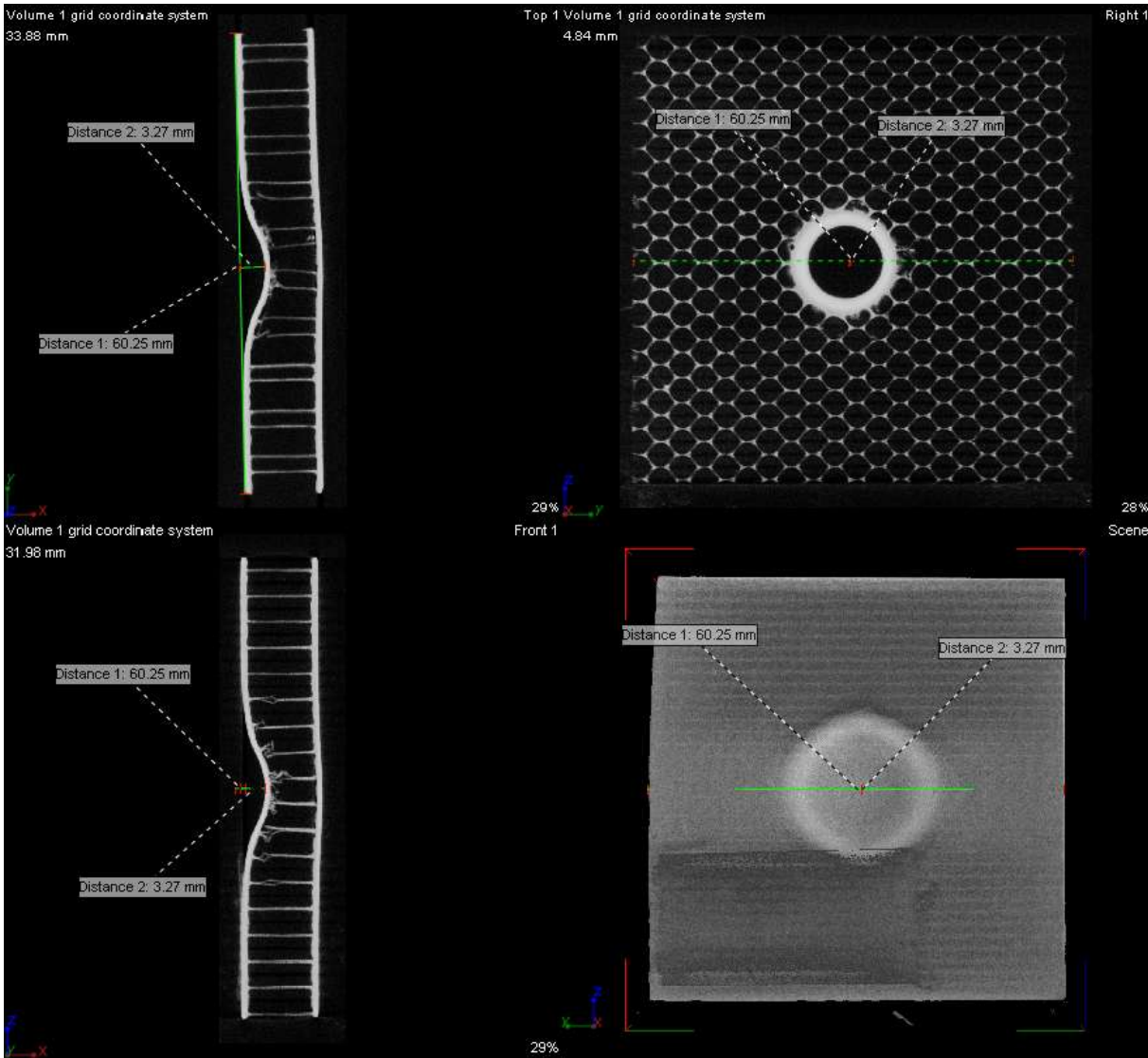
(a)
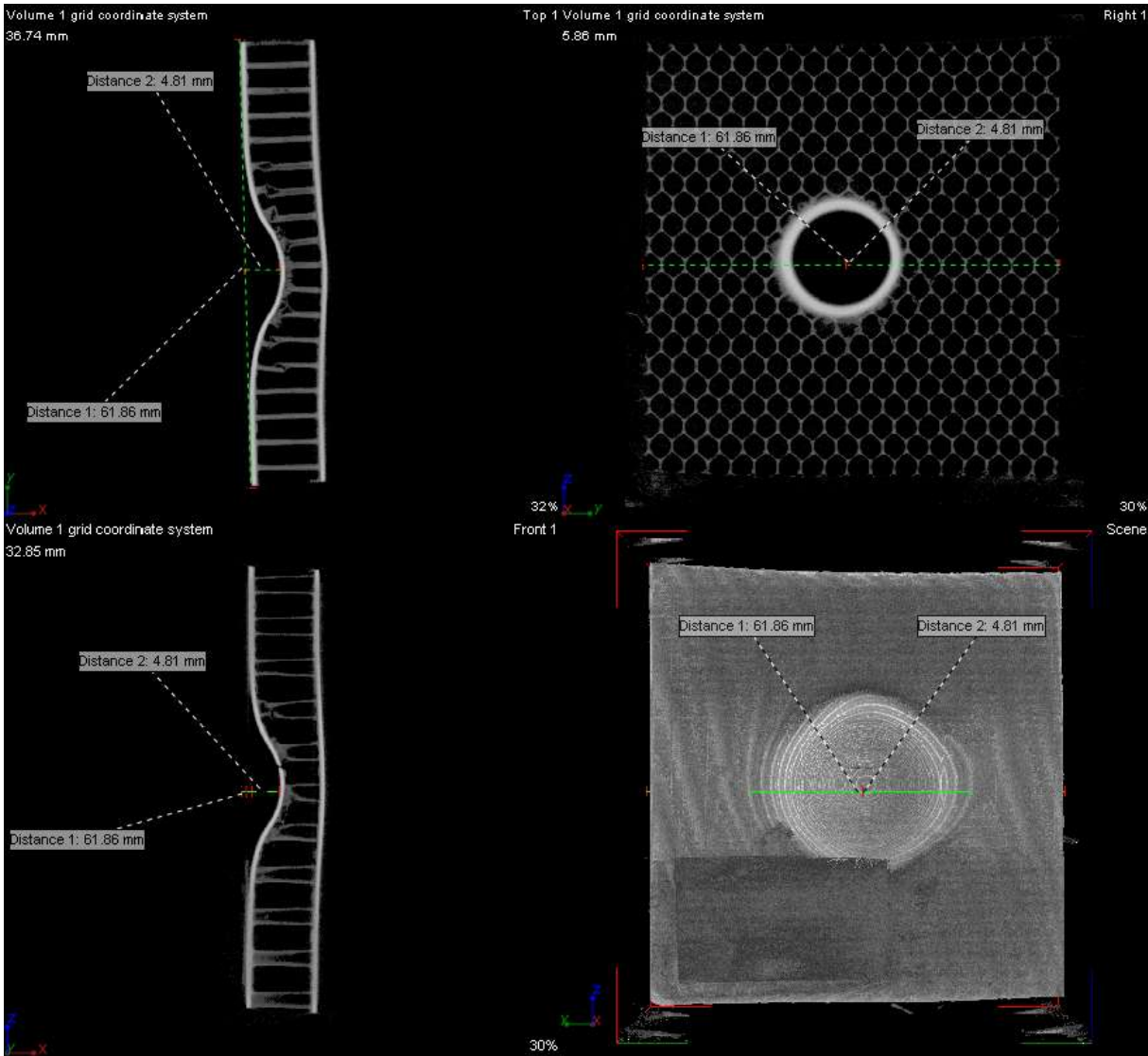
(b)
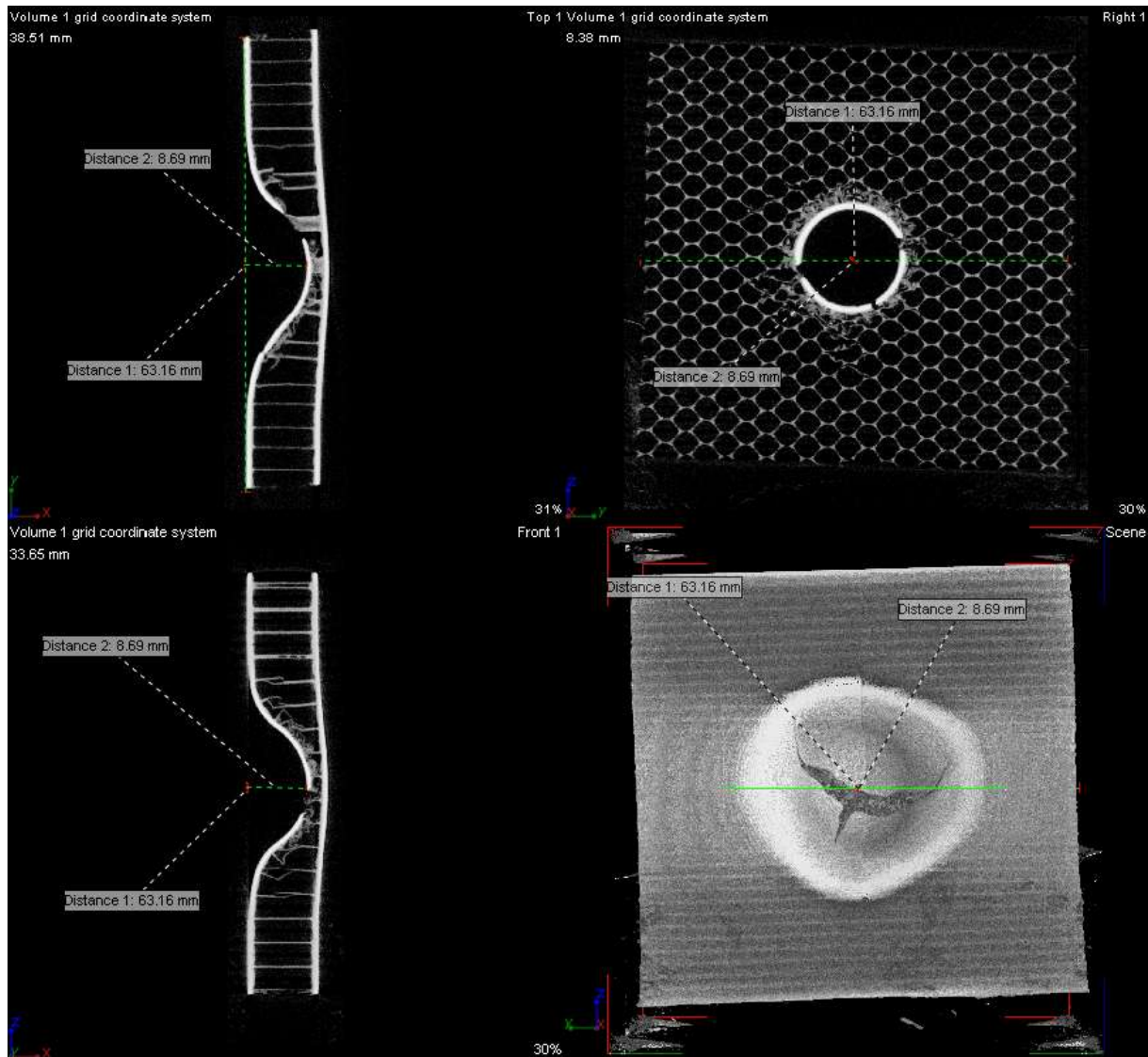
(c)

Figure 3.33: CT images of honeycomb panels after impact tests NHS 3.2 mm: (a) v = 1.5 m/s, (b) v = 3 m/s and (c) v = 4m/s

III.3.1.1. Obtained failure modes under low-velocity impact tests

Damage due to external impact applied to the sandwiches structures is the main factor underlying reduction of structural safety and integrity.

Figure 3.34 to 3.39 show the damage and buckling of the sandwiches panels according to the changes of the impact energy for used honeycomb sandwiches panels.
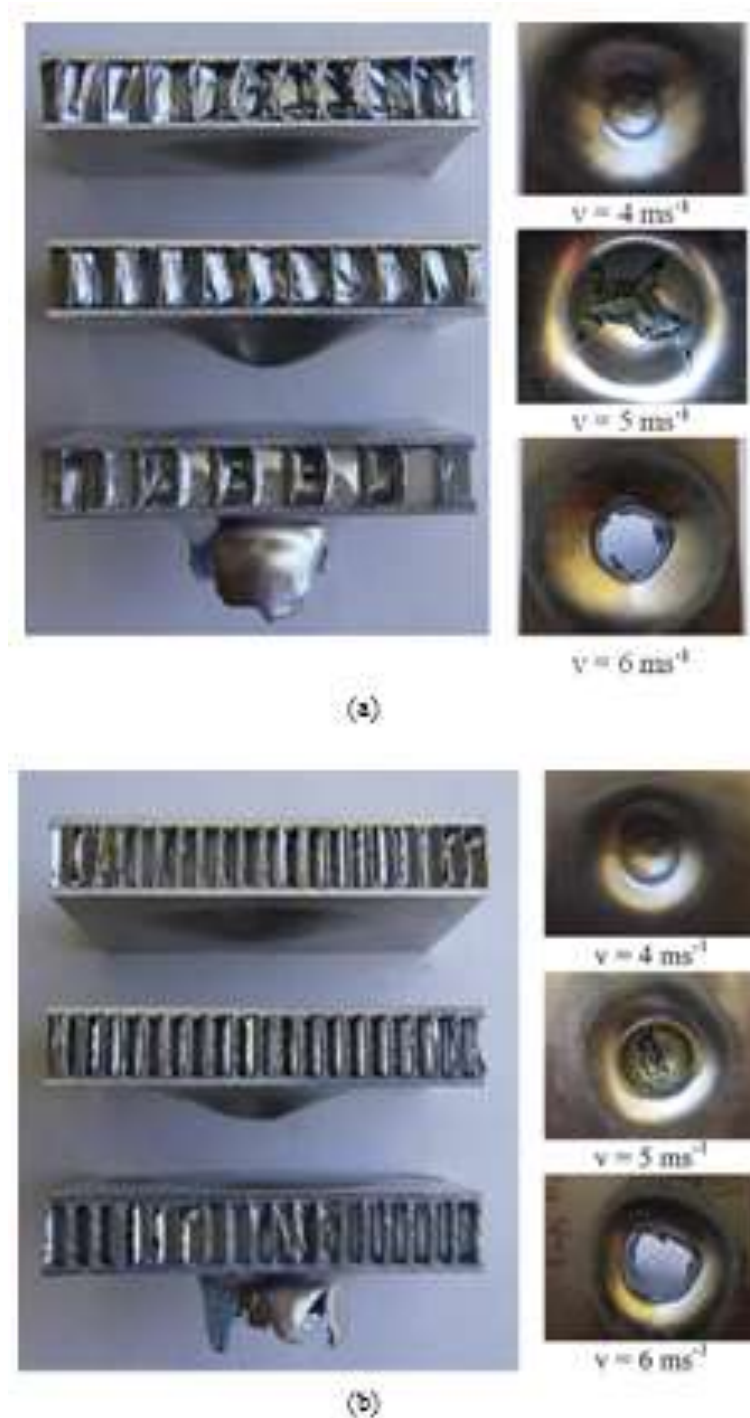
Figure 3.34: Photographs of deformed specimens at different impact velocities: (a) AHS d = 6.4 mm and (b) AHS d = 3.2 mm

The computed tomography system CT was used to observe the damage area due to local crushing failure of the core (buckling). For the sandwich specimen with cell size of d = 3.2, 6.4 and 19.2 mm respectively , as shown in Figs 3.34-3.39, de-bonding between the face-sheet and the core as well as delamination was observed, and plastic deformation by local buckling of the honeycomb core was occurred around the impact point.

Figure 3.35: Photographs of deformed specimens at different impact energies (AHS d = 19.2 mm).

Figure 3.36: Total failure of AHS d = 19.2 mm

All types of honeycomb specimens deformed in a similar pattern. No significant difference was observed in the deformation mechanism at different strain rates. During impact, crushing was initiated by elastic buckling and then progressive plastic buckling of the cell walls was observed from the lower and upper face of the specimen. Photographs of post-test specimens under impact load of two types of honeycombs are shown in Figs 3.34-3.38. It can be seen that cell walls along the impacted zone deformed in an irregular pattern but in the central portion all the cells deformed in a uniform pattern for all types of honeycomb specimens.

[21-36] do not observe any significant difference in the plastic buckling between dynamic and quasi-static. During deformation of the honeycombs, single walls deform in such a way to accommodate the deformation of the adjacent double walls. The deformation pattern of the cell walls observed in this study agrees well with the global collapse mode in [21-36].

However, it was difficult to observe the crushing pattern of the specimens because the impactor penetrated into the middle portion of the honeycomb specimens and the surrounding un-deformed cells blocked the view. Therefore, the deformation of honeycombs in indentation could only be investigated by studying the deformed honeycomb specimens after tests. Photographs of specimens were taken after impact tests (figs 3.32-3.36) and no evident difference was observed in the deformation pattern at different strain rates. For all types of honeycombs, due to a higher level of lateral constraints, honeycomb cells in the central region buckled in a regular pattern. De-bonding of the double walls was observed along the two edges of the indenter while tearing took place in single walls. During impact, crushing initiated with elastic buckling and was followed by plastic buckling of the cell walls, which was associated with debonding of the double walls. In the final stage, densification was governed by the plastic collapse. In both the quasi-static and dynamic similar buckling pattern was observed.

Figure 3.37: Photographs of deformed specimens at different impact energies (NHS d = 3.2 mm) for both impact (HS 20 et HS 10).
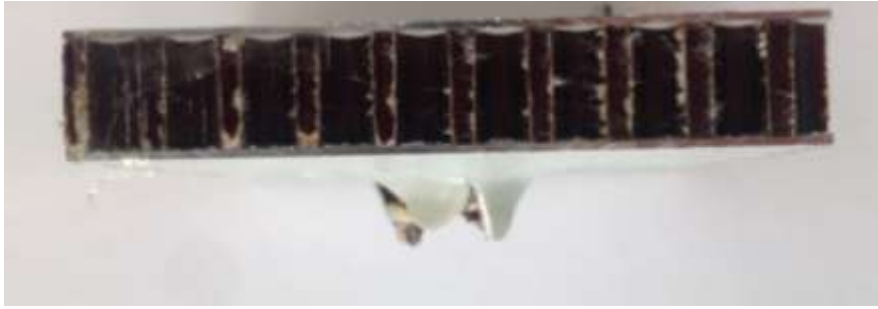
Figure 3.38: Perforation of NHS d = 3.2 mm

The computed tomography system CT was used to observe the damage area due to local crushing failure of the core (buckling) (Figure 3.39).

v = 1.5 m/s

v = 2 m/s

v = 4 m/s

v = 5 m/s
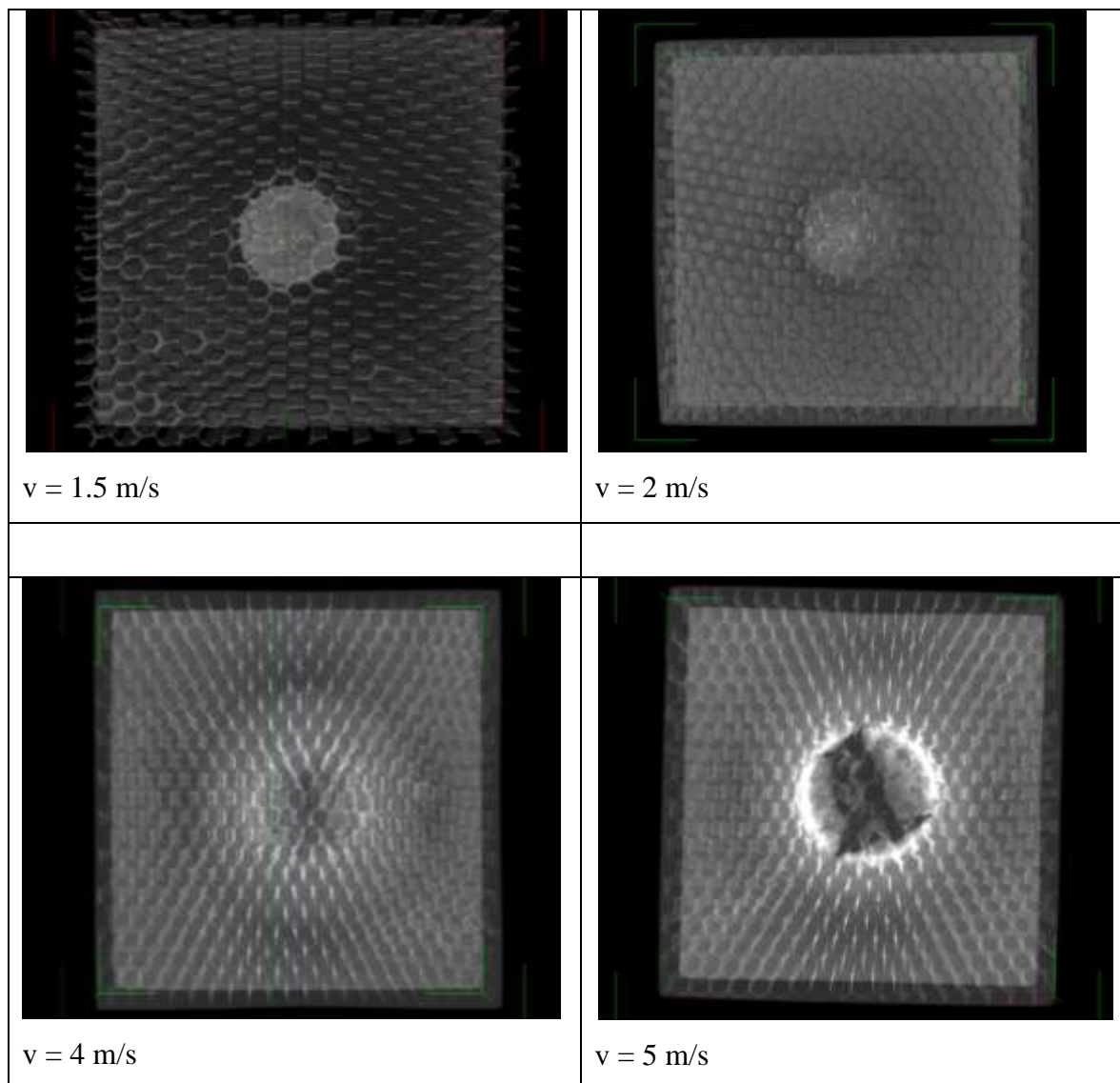
Figure 3.39: Failure evolution at different impact velocities with ct images system

III.3.3. Quasi-static indentation tests

A typical load-indentation curve obtained from indentation tests on (AHS d = 6.4 mm) panel with a hemispherical indenter (HS 20 mm) is shown in Figure 3.40. From this figure, it was observed that the load-indentation curve showed a linear behavior for low values of indentation, followed by a non-linear regime with a quick decrease in the sandwich panel stiffness caused by the extensive cells core buckling and crushing in the area under the indenter. It was seen that there are two main peaks on the load-displacement traces (Figure 3.40), the first peak mostly relates to penetration and wrinkling of the upper face-sheet and between the first and second peak, damage relates mostly to the global buckling and crushing of the core under indented zone.
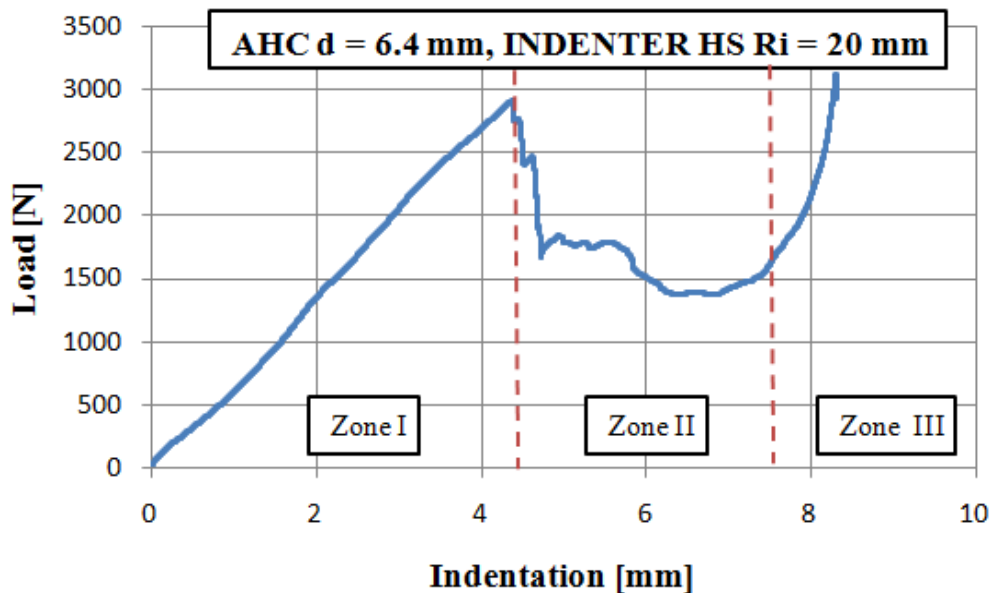
Figure 3.40: Load-indention curve of ahs d = 6.4 mm (HS 20 mm).

All the panels with different cell size and core materials present similar behavior, but the deformation between upper and lower face-sheet failure increases as the cell size increases. Also for the threshold of indentation load which are different for sandwich panels with different cell size, core materials and indenter geometry. It was found that the max indentation load increases with the decreases of the cell size of the core and it is increased when the diameter of the indenter increases. From the results, it is apparent that the indentation load and the damage for a composite sandwich panel under quasi-static indentation tests are dependent on same keys parameters which will be discussed in detail as follows.

Similar tests have been already conducted by Crupi [21] on polymeric foams with different densities and the experimental results showed that the indentation resistance depends on the indenter geometry, cells size and core's material.

[21-36] do not observe any significant difference in the plastic buckling between dynamic and quasi-static. During deformation of the honeycombs, single walls deform in such a way to accommodate the deformation of the adjacent double walls. The deformation pattern of the cell walls observed in this study agrees well with the global collapse mode in [21-36].

III.3.3.1. Effect of indenter geometry

Figure 3.41 shows for each indenter the load-indentation data for (AHS d = 3.2 mm). Noticeable differences in the mechanical behavior of sandwich samples under indentation load are evidenced at varying indenter geometry. In this figure it is possible to observe how an increase of loads is reached at increasing contact area between the indenter and specimen.

It was seen that there are similarities in the indentation failure processes in case of indenters (a) and (c). In the curves relative to honeycomb panels (AHS) two distinct regions are identified except to the curves for the tests conducted using conical indenters: an initial regime with a slight increase of the force during the gradual immersion of the indenter nose and a plateau-like regime with a slight increase of the force. The curves of the honeycomb panels relative to conical indenters show a load loss at an indentation value of about 5 mm, due to the local fracture of the upper skin in the area under the indenter.
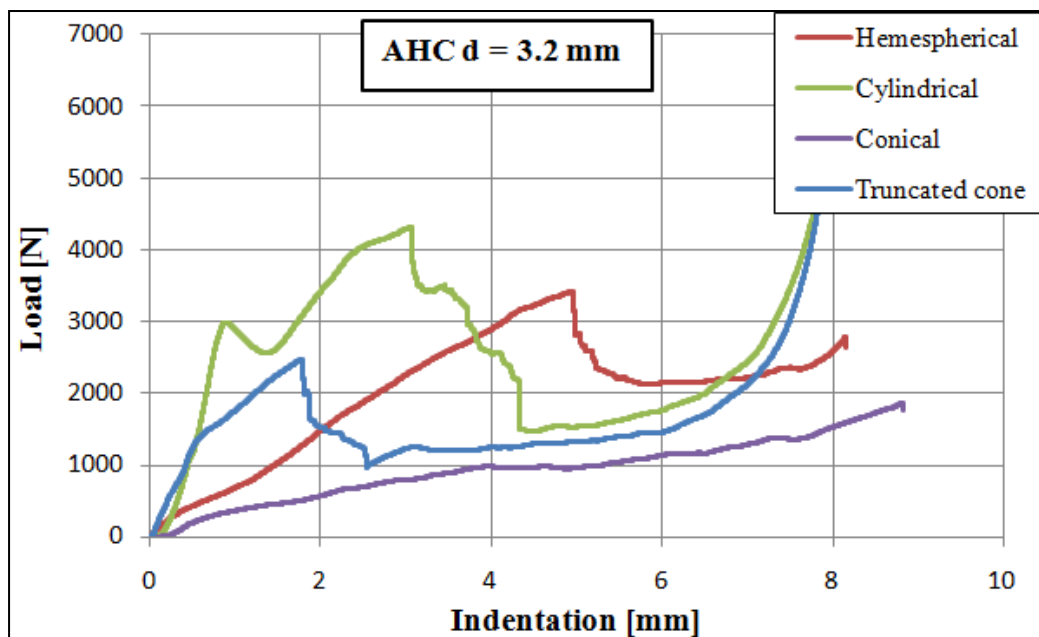
Figure 3.41: Effect of indenter geometry on indentation behavior (AHC d = 3.2 mm).

Figure 3.42 shows the damage inflicted for the different types of indenter on the same honeycomb sandwich panel. Albeit there are notable differences in the type of damage inflicted by each indenter.The indenters (a) and (d) both produced a larger area of cracking than the indenters (b) and (c). Also; it was seen that there are similarities in the indentation failure processes in case of indenters (a) and (c).

Figure 3.42: Failure modes of indentation test for each indenter.

The indenter geometry influences the shape of the damaged area on the sandwich as shown in figure 3.42. In fact, failure can be radial for the indenter (b), a crack starts at the indenter/material interface with a petals shape during the penetration, or it can be circumferential for the indenters (a), (c) and (d), the material under the indenter undergoes compressive stress and the strain interests the whole sample [21-36]. However, there is a notable difference in the total energy absorbed for the using indenters (figure 3.41). It is notable that under these loading conditions, the specimen stiffness is higher with the indenters (a) and (c) than is the case for the indenters (b) and (d), this phenomena is due to the contact geometry effects.

It is noticed in figure 3.43 that the diameter of the indenter has an influence on the stiffness of the honeycomb sandwich panels. However, the diameter has a large influence on the ultimate failure of the face. This can be explained by the fact that the indenter with the largest diameter has larger radius of curvature, which reduces the local deformation of the face and allows more penetration of the indenter without causing the failure of the face. However, the damaged area was proportional to the diameter of the indenter (see figure 3.42).

As expected, the damaged area depends on the indenter geometry. The largest damaged areas were observed for indenters (a) and (d) while the smallest damaged areas were observed for indenter (c). It is noticed in Figs. 41-44 that the geometry of the indenter has significant

influence on the stiffness of the honeycomb sandwich panels and the damage process. This can be explained by the fact that the indenter with the largest diameter has larger radius of curvature, which reduces the local deformation of the face and allows more penetration of the indenter without causing the failure of the face. However, the damaged area was proportional to the diameter of the indenter.

From the obtained results, indenter geometry has great influence on the indentation resistance and the failure mechanisms of composite sandwich panels.
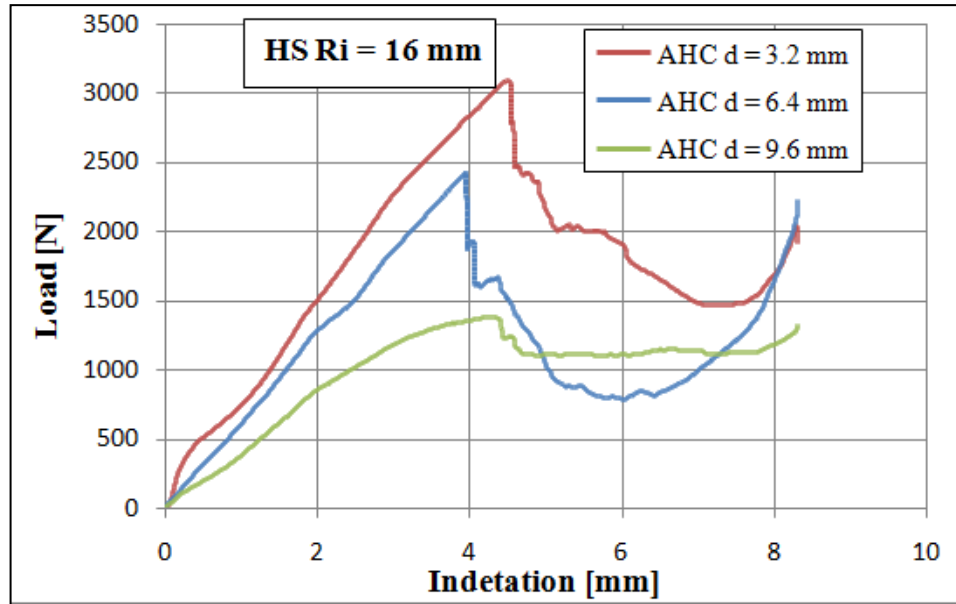
(a)
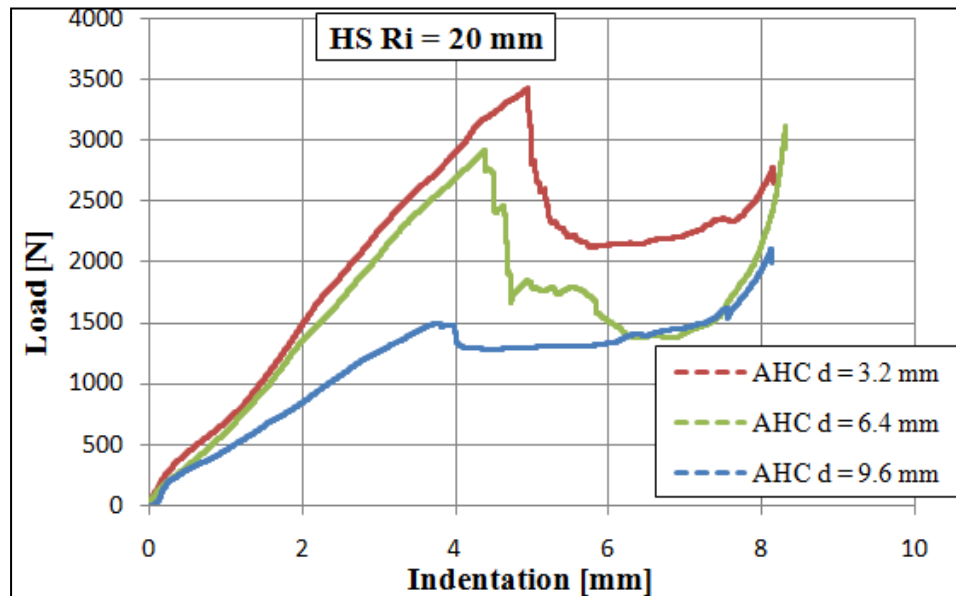
(b)

Figure 3.43: Effect of indenter diameter on indentation behavior at varying cell size: a) HS Ri = 16 mm and b) HS Ri = 20 mm.
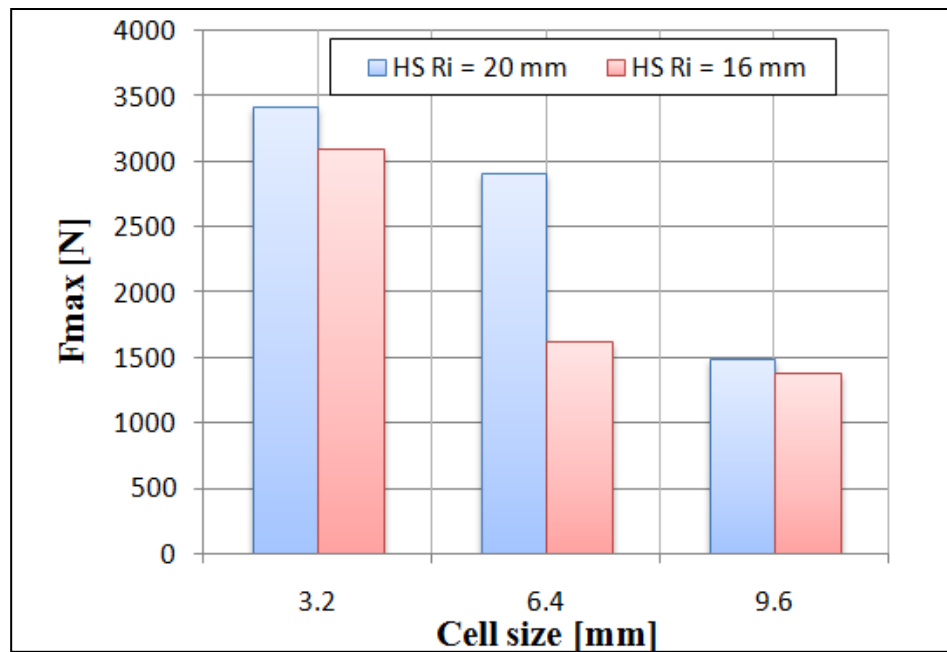
Figure 3.44: Effect of indenter diameter on Fmax of indentation at varying cell size.

III.3.3.2. Effect of the cell size of honeycomb core

To study the effect of the cell size on indentation behavior several test were carried on honeycomb sandwich panel with different cell sizes (AHS d = 3.2, 6.4 and 9.6 mm). Figures 3.45 show load-displacement curves using cylindrical, hemispherical and conical indenter, respectively. Two general observations can be made from these figures, for the same indentation displacement, the indentation resistance decreases with the increase of the cell size. The first observation can be explained by the fact that the stiffness of the sandwich panel increases with the increase of the density of the core [21-36and]. Also the cell size induces relevant effects on the mechanical performances of the samples under static indentation load. This is evident from the results shown in figure 3.46that compares the max indentation load at varying the cell size for each indenter. It was found that the indentation load increases with the decreasing of the cell size of the core. Damaged area decreases with the increase of density since the effect of the indentation becomes local due to the increase of stiffness of the panel.

Figures 3.45 also indicate that the absorbed energy at failure depends on the cell size; there is an increase of absorbed energy when the core cell size is decreased from 9.6 to 3.2 mm; however, when the core cell size is decreased, there is a reduction in the absorbed energy of the structure. This behavior is observed for all indenters.
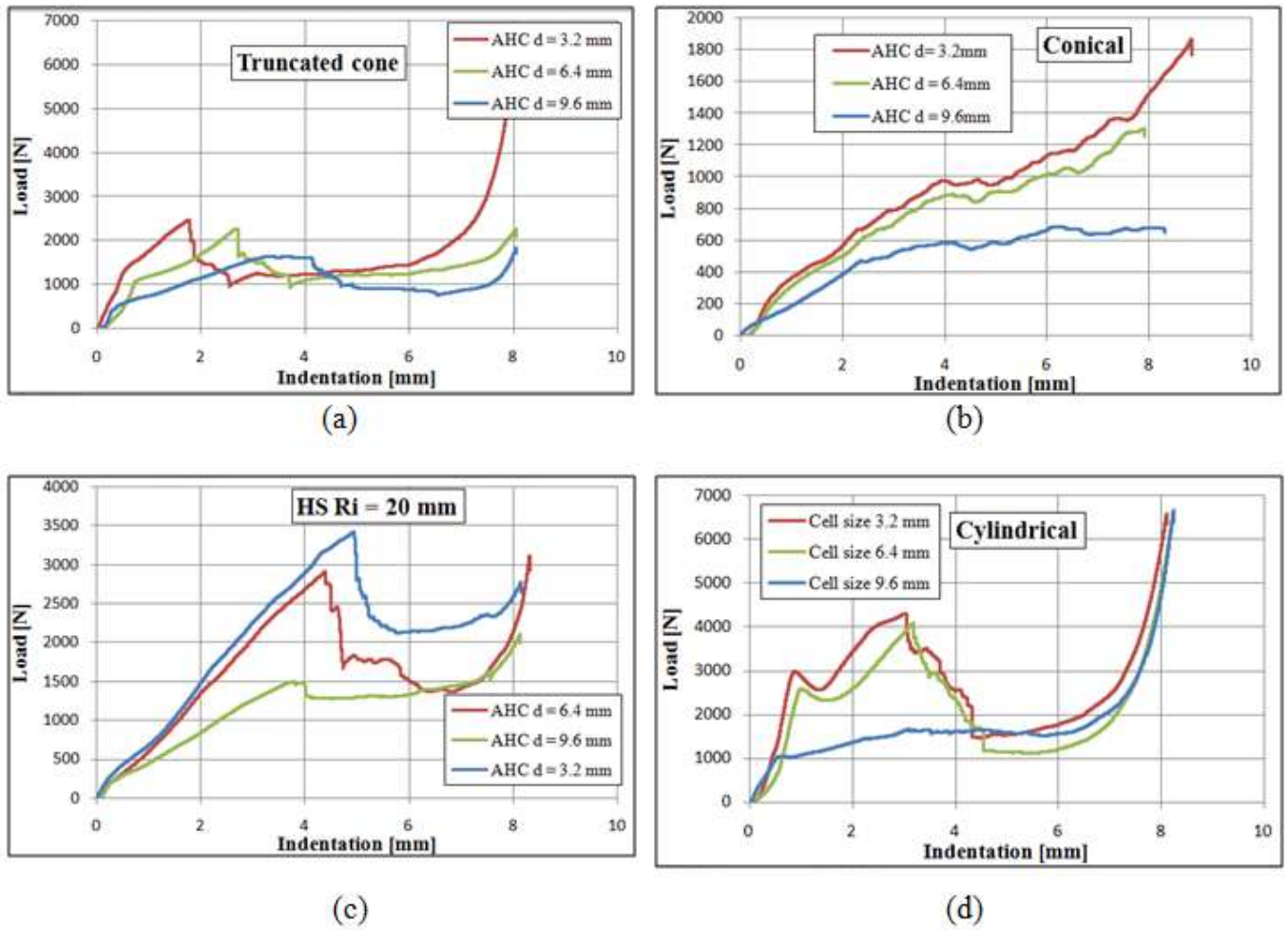
Figure 3.45: Effect of cell size on indentation behavior: a) conical b) hemispherical and c) cylindrical indenter
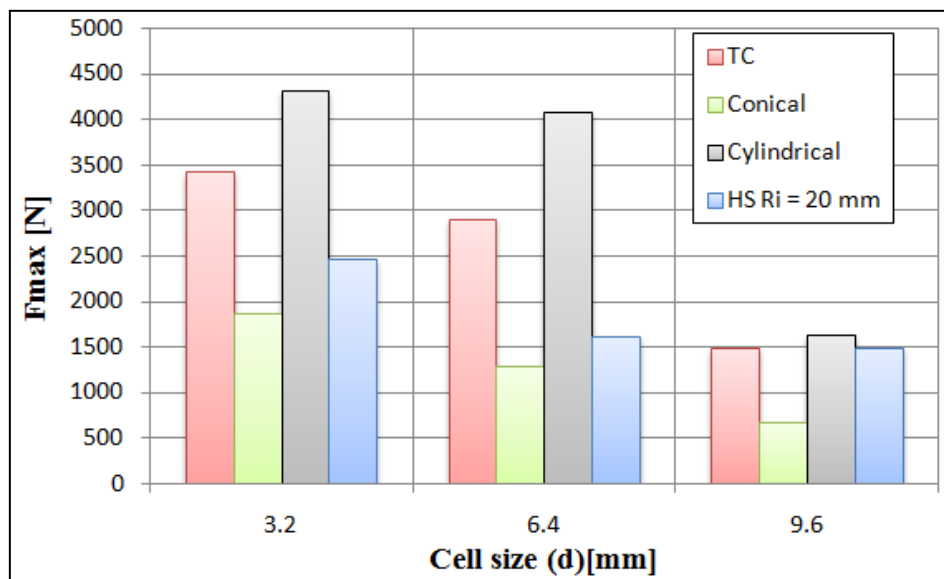
Figure 3.46: Effect of core cell size on fmax of indentation at varying cell size.

III.3.3.3. Effect of the core materials:

The effect of core material (AHS and NHS) on indentation load is illustrated in figures 3.47, which reveal load-indentation data for each indenter at same cell size. The conclusions drawn from such results are valid also for the test obtained with different values of indenter geometry, as it is possible to observe from the data summarized in Figures 3.47. For a sample with NHS the typical behavior is observed, as the one shown in Figures 3.47. On the converse, if the core is made of AHS indentation curves do not present the small drops, but a unique collapse. For the all indenters, there is considerable difference in the load versus indentation traces for the AH and NHS. In figure 3.48 it is possible to compare the critical indentation load of the two kind of core; the NHS shows almost a higher critical indentation load resistance values compared to the one exhibited from the AHS [59-61].
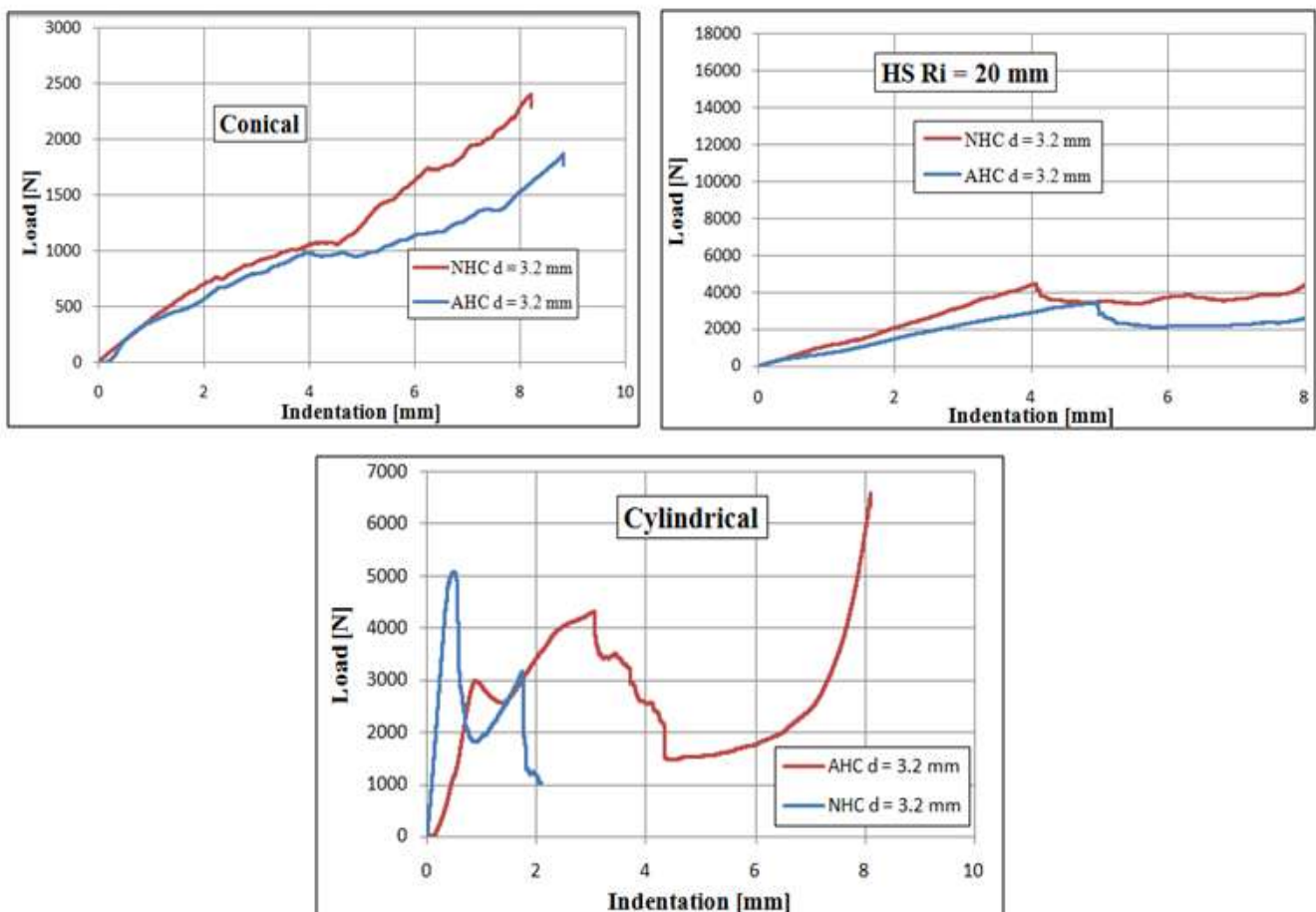
Figure 3.47: Effect of core material on indentation load at same cell size for all indenters.
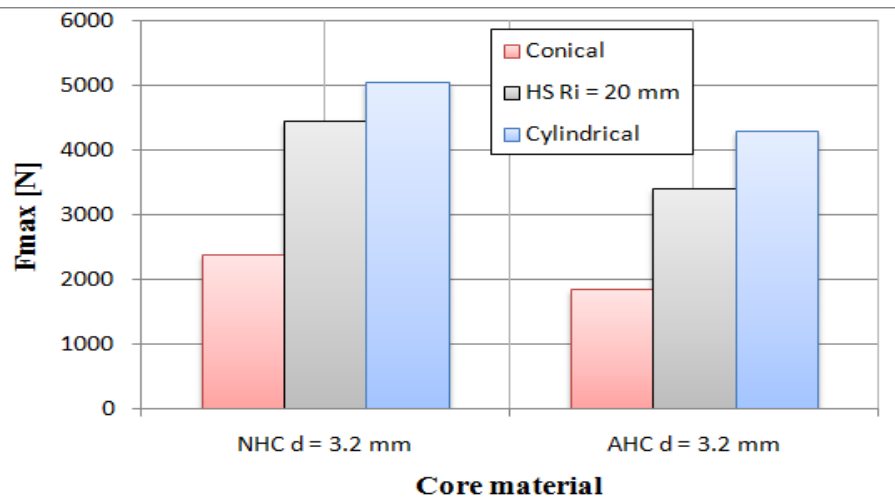
Figure 3.48: Effect of core material on Fmax of indentation at varying same cell size for each indenter.

III.3.3.4. Evaluation of failure modes

Damage in composite sandwich structures subjected to indentation load obviously depends on many factors, including face-sheet and core properties, cell size, and indenter geometry. For a given specimen type, four basic response/failure modes can be identified as the level of indentation increases: elastic recoverable deformation, local deformation/ indentation, face-sheet delamination and/or debonding from the core, and core buckling. For low levels of indentation load, the structure deform globally within the elastic range without permanent deformation. For higher load levels, local deformation appears due to core crushing followed by local bending and shearing of the upper face-sheet. The specimen undergoes permanent deformation without face-sheet failure. For even higher load levels, but below the penetration threshold, additional failure modes have been identified including extensive core indentation/cracking, face-sheet buckling, delamination within the face-sheet, and debonding between the face-sheet and core. Typical failure modes are shown in figures 3.49-3.51.
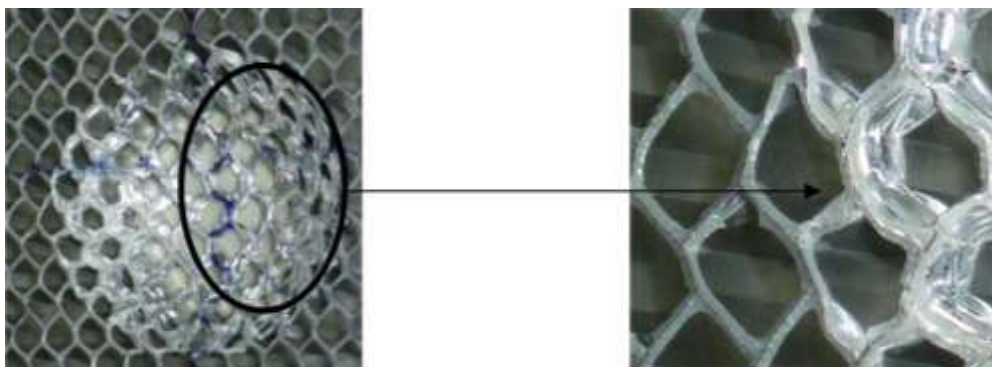
Figure 3.49: Photographs of deformed AHS specimens under quasi-static loading.

90
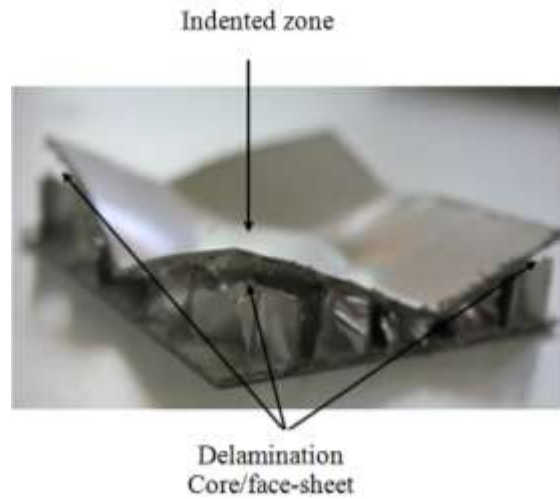
Figure 3.50: Failure modes of ahs observed during indentation: core crushing, failure of face core shear
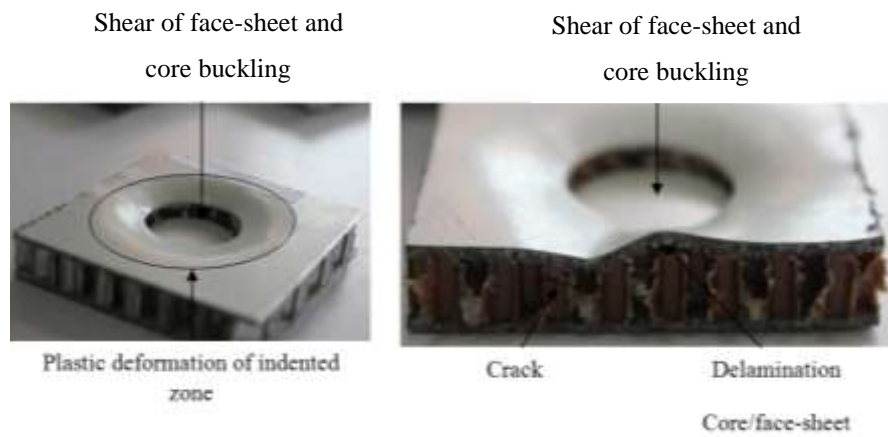
Figure 3.51: Failure modes of AHS and NHS observed during indentation: buckling, core crushing, and failure of face core shear.

III.3.3.5. Conclusions:

The indentation failure behavior of honeycomb core sandwich panels is studied by examining the effects of core, cell size and indenter geometry on indentation load. From the experimental results it is possible to draw out the following considerations:

➢ It was observed that the load-indentation curve showed a linear behavior for low values of indentation, followed by a non-linear regime with a quick decrease in the sandwich panel stiffness caused by the extensive core crushing in the area under the indenter.

➢ The failure mechanisms during indentation mechanisms depend on the indenter geometry. Damaged area depends strongly on the indenter geometry. The largest damaged areas were observed for cylindrical and hemi-spherical indenters while the smallest damaged areas were observed for conical indenters. The indenter geometry influences the shape of the damaged area on the sandwich. In fact, failure can be radial for a conical indenter (a crack starts at the pin/material interface with a petals shape during the penetration) or it can be circumferential if the indenter is cylindrical/ spherical (the material under the pin undergoes compressive stress and the strain interests the whole sample).

➢ From the obtained results, indenter geometry has great influence on the indentation resistance and the failure mechanisms of composite sandwich panels.

➢ It was found that both indenter geometry and core density have large influence on the indentation response of the sandwich panels. Several failure modes for the studied sandwich panels were identified including face failure, core failure and skin/core debonding.

➢ The load is increased when the diameter of the indenter increases.

➢ It was found that the indentation load increases with the decrease of the cell size of the core.

➢ Damaged area decreases with the increase of density since the effect of the indentation becomes local due to the increase of stiffness of the panel.

➢ The stiffness of the sandwich panel increases with the increase of the density of the core. Also the cell size induces relevant effects on the mechanical performances of the samples under static indentation load.

➢ The sandwich with high core density is much suitable for working conditions in which localized load resistance is necessary.

> ➢ There is an increase of absorbed energy when the core cell size is decreased from 9.6 to 3.2 mm; however, when the core cell size is decreased, there is a reduction in the absorbed energy of the structure.
> ➢ The nomex samples show almost a higher indentation load resistance values compared to the one exhibited from the aluminum core samples.

III.3.4. Compression tests:

Figure 3.52 shows a typical stress-strain curve obtained from the compressive test of AHS d = 6.4 mm.
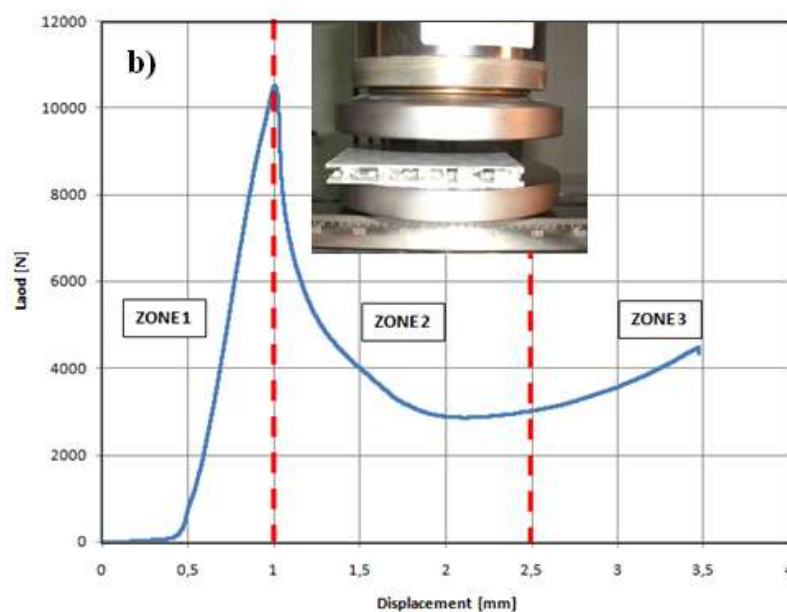
Figure 3.52: Typical stress-strain curve for an aluminum honeycomb sandwich.

The compressive deformation process can be categorized into three regions (1, 2 and 3) based on the compressive stress strain behavior.

> ➢ The figure shows that the stress strain relationship is linear in Region 1 up to the bare compressive strength. The honeycomb cell walls are in elastic buckling condition in Region I (figure 3.53).
> ➢ Later, a sudden decrease in compressive stress occurs in Region 2. In this region, core walls are in plastic buckling condition and wall folding occurs (figure 3.53).
> ➢ The compressive stress remains approximately stable in Region 3 until the densification region of the cores. This stable stress value is defined as the crushing strength. In this region, crushing and fracture of the cores Start (figure 3.53).

Depending on the core densification at the end of Region 3, an increase in the compressive stress is observed as was reported in the literature [16, 17-24].

Figure 3.53: Stages of quasi-static compression test of aluminum honeycomb: (1) initial state, (2) buckling initiation, (3) progressive folding and (4) densification.

Initial collapse occurs at a load, which is about twice of the average steady load causing progressive crushing. The amplitudes of the little peaks, which signify progressive folding collapse, are higher initially and gradually decrease as shown in Figure 3.52. Plastic collapse always occurred at one (usually top) end and the deformation front gradually progressed with continued crushing until the plastic folding deformation approached the lower end of the specimen. Then the load increased very rapidly indicating the densification of the specimen.

The load displacement graphics of NHC and AHC for different cell size, resulting from the experiment, are given in Figures 3.54. It is seen that the maximum critical buckling load value of NHC are higher than that AHC for the same cell size. Also, as the cell size increased, the critical buckling load of honeycomb panels decreased.

Besides the critical buckling load, the establishment of the incurred failure modes during the experiment is also important. As the load increased, initial honeycomb wall buckling and later regional cell wall folding and core crushing were observed in the aluminum core sandwich panels (Figs.54 (a)). The failure modes of NHC panels under compression load show similar behavior as that of AHC. But at NHC panels, which are much brittle than AHC, prior to core crushing failure, crack generation incurred (Figs.54 (b)). The failure, started as a cell wall buckling, caused cracks at greater compression loads (Figs.54) as was reported in the literature [37-43].
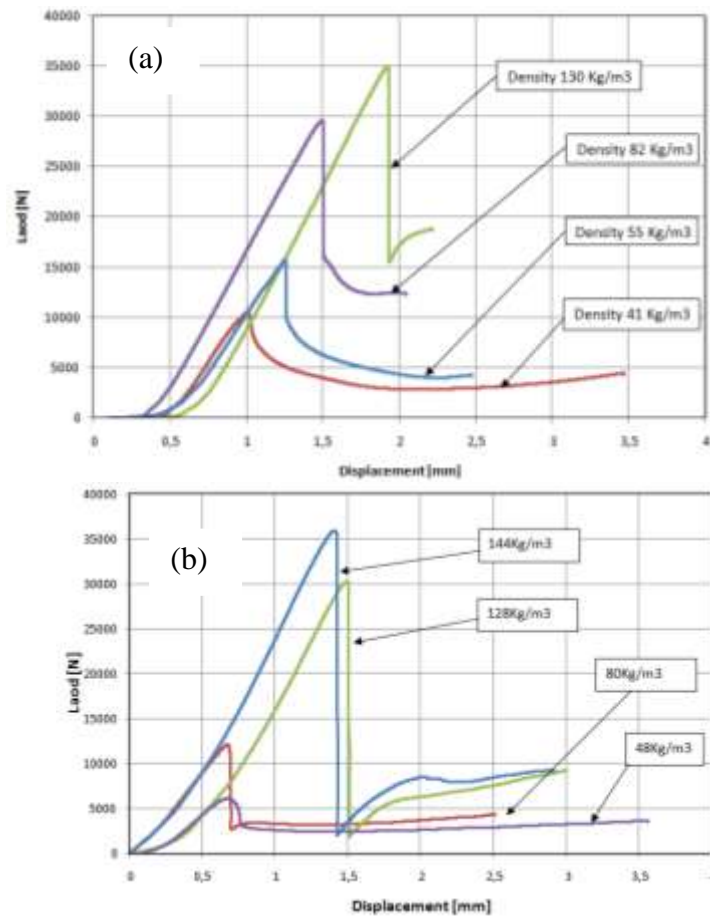
Figure 3.54*:* Load-displacement curve for honeycomb sandwich panels for different core densities: (a) AHS and (b) NHS.

The honeycomb compressive behavior intrinsically relates to the cell wall buckling behavior under compression, because in reality the vertical cell walls can never be compressed along the length direction until a pure compressive failure due to the instability of the thin structure occurs. The dominant mode of damage in these structures is the buckling of cells' walls.

For the honeycomb core compressed in the axial direction, the localization occurs in the well defined plastic collapse bands at the interface between the crushed and uncrushed structural regions.
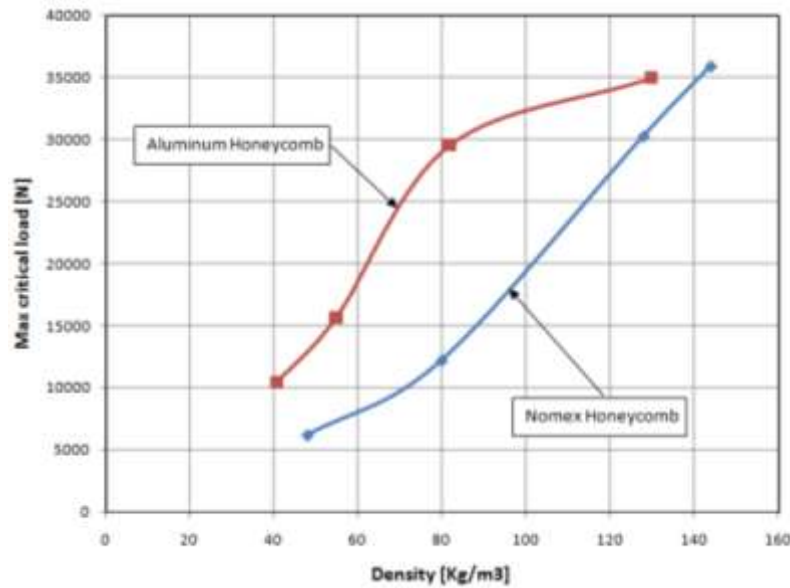
Figure 3.55: Evolution of the critical maximal load with the core density.
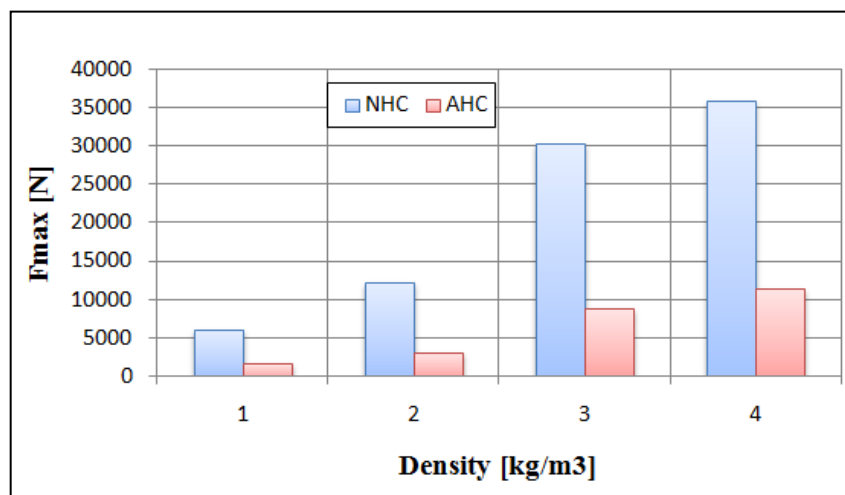
Figure 3.56: Effect of the core density on the critical buckling load.

To account for the influence of the thickness of cell wall, compression test has been made and the results of variation of load for two different wall thickness of honeycomb core at 6.4mm cell size, obtained results are given in figure. According to the results of the experiment, we find that the wall thickness of cell also has significant impact on the critical buckling load. It is established that the critical buckling load increased by the increase of the cell wall thickness. Figure 3.57 shows the evolution of load for two different cell wall thicknesses. From the obtained results, we see that the stiffness of honeycomb sandwich panels increases with the cell wall thickness.
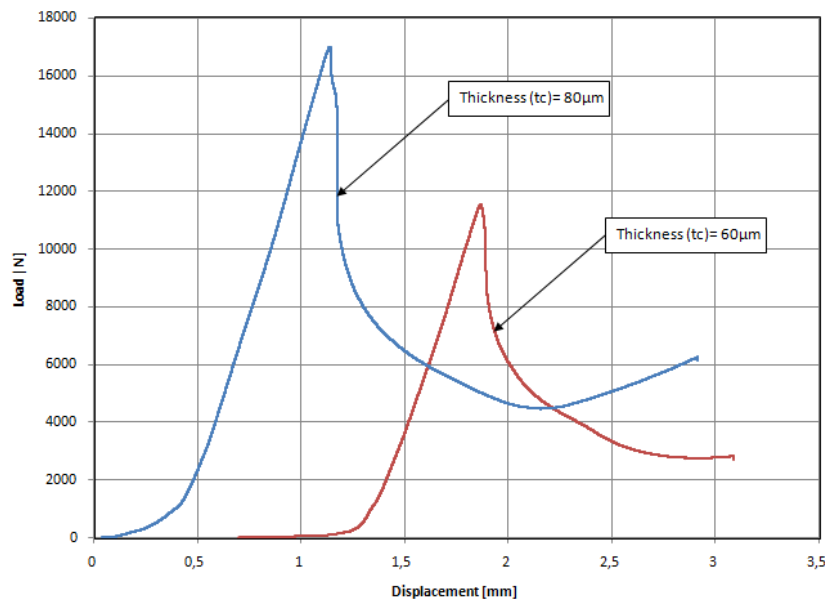
Figure 3.57: Effect of the cell wall thickness on the buckling load for aluminum honeycomb core.
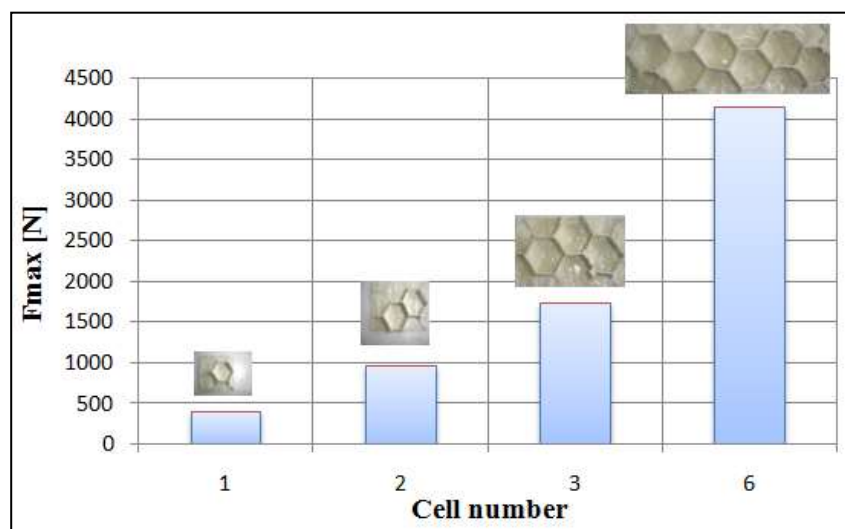
Figure 3.58: Effect of the cell number on the buckling load for AHS d = 19.2 mm.

A digital camera was used in the compressive tests to observe the deformation patterns of the two types of honeycomb specimens. All specimens deformed in a similar pattern. No significant difference was observed in the deformation mechanism at different strain rates. During compression, crushing was initiated by elastic buckling and then progressive plastic buckling of the cell walls was observed from the lower and upper interfaces of the specimen between two loading fixtures. Photographs of post-test specimens under compressive load of honeycombs are shown in figure 3.59-3.60. It can be seen that cell walls along the four edges deformed in an irregular pattern.
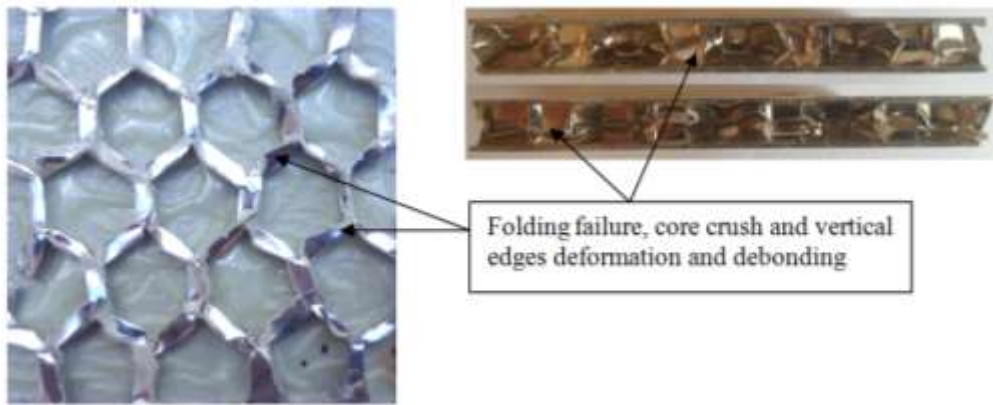
Figure 3.59: Failure mode of AHS.
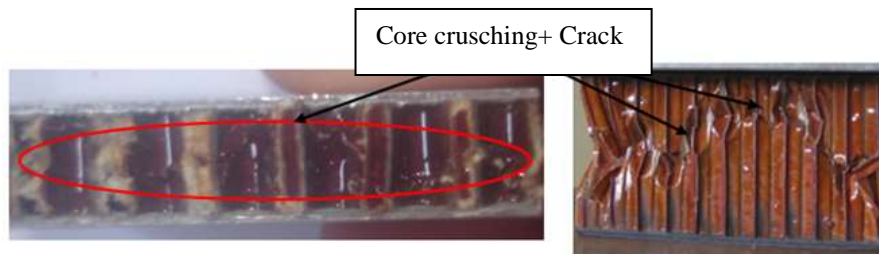
Figure 3.60: Failure modes of NHS.

III.3.4.1. Conclusions

The buckling load of sandwich plates with honeycomb core subjected to compression damage has been investigated experimentally and numerically. The cell size and wall thickness, and materials are parameters that have to be determined coherent to the usage area of the honeycomb sandwich structures optimally. The honeycomb compressive behavior intrinsically relates to the cell wall buckling behavior under in-plane compression, because in reality the vertical cell walls can never be compressed along the length direction until a pure compressive failure due to the instability of the thin structure occurs. The following are the obtained results of the study:

- The critical buckling load of aluminum panels is determined to be higher than that of nomex honeycomb panels.

- The failure modes of nomex honeycomb sandwich panels under compression load show similar behavior as that of aluminum honeycombs. However, at nomex core panels, which are much brittle than aluminum, prior to core crushing failure, crack generation incurred.

- As the core's density increased, the maximum critical buckling load increased, both for nomex and aluminum comb panels [59-61].

- It was observed that the core's height would be a crucial parameter affecting the ultimate compressive strength of sandwich panel.

- Besides the core's densities and the core height, the core wall thickness also has an important effect on the critical buckling load. The critical buckling load increased as the cell wall thickness increased.

CHAPTER IV: Theoretical Analysis of Buckling In Honeycomb Sandwiches under Different Loading Conditions

The adoption of lightweight honeycomb sandwiches requires an adequate knowledge of their response and behavior at different loading conditions which can be obtained on the basis of preliminary information obtained from the experimental tests or FEA numerical models.

Figure 4.1 shows the failure modes in sandwich structures. It has been proved that the buckling of the honeycomb sandwich panel is one of the most frequent failure modes.

This chapter focuses on development of a theoretical approach able to correlate the buckling to the failure modes of honeycomb sandwiches under different loading conditions (static and dynamic) and to estimate the critical buckling load at each loading. Experimental tests were carried out on AHS and NHS honeycomb panels in different loading conditions (compression, low velocity impact, quasi-static indentation) as we have seen in the previous chapter. The critical loads predicted by the theoretical approach were compared using the experimental data.
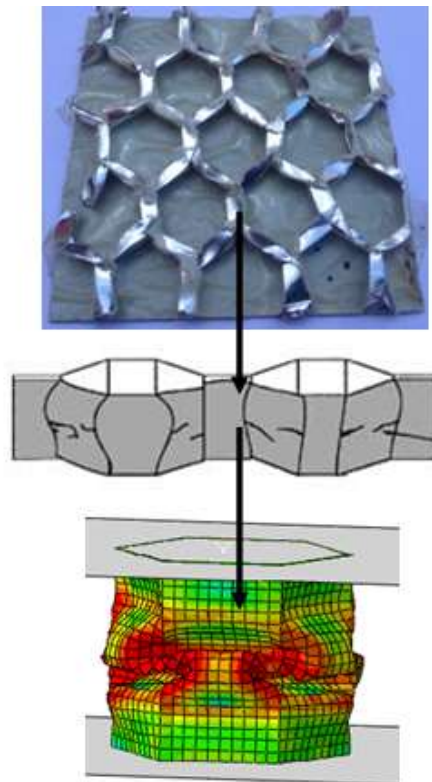
Figure 4.1: Buckling in honeycomb sandwich structures.

IV.1. Introduction

The mechanical properties of honeycomb sandwiches structures can be influenced by loading and service conditions. For that concerns the marine structures, the use of sandwiches can lead to weight reduction, providing an adequate structural strength and improving the crashworthiness. Zhang et al. [44] investigated laser-welded triangular corrugated-core sandwich panels subjected to air blast loading in order to obtain an optimal design of sandwich panel for shipbuilding. Qiu et al. [45] proposed sandwich structures for large-scale marine protective device and its anti-collision resistance to structural damage from ship impact was evaluated by FEA. The response of aluminum honeycomb panels under different loading conditions (in plane compression, bending, indentation and low-velocity impact) was analyzed by some of the many authors. An extensive series of experimental tests has been carried out and the results are reported in [21-24, and 46]. The core damage of honeycomb sandwich, caused by low-velocity impact, consists of buckling of cell walls in a region surrounding the impact point [14]. The low-velocity impact response of square sandwich plates made of carbon/epoxy skins bonded to aluminum Nomex® honeycomb was analyzed by Foo et al. [47]. The structural response in the case of low-velocity impact on Nomex® honeycomb sandwiches was predicted using a numerical approach, based on a grid of nonlinear springs, and a good correlation with experimental drop tests was achieved [48]. Dietrich et al. [49] applied the Computed micro-tomography (µ-CT) to honeycomb GFRP sandwiches. Niknejad et al. [50] introduced a theoretical relation to predict the instantaneous folding force of the first fold creation in a single cell hexagonal honeycomb under axial loading. Zhang and Ashby [30] developed a model to analyze the buckling collapse of honeycomb panels under in-plane biaxial loading. Bentouhami et al [51] focused on their study on the buckling capacities of the core components under uni-axial compression. The critical buckling loads for various core densities (cell diameter) and core materials of honeycomb panels were experimentally and numerically investigated. The effect of cell size and its materials on the behavior and damage was highlighted. It was found that the buckling load of specimen increases as the core density is increasing. In terms of stiffness and load at failure, the honeycomb sandwich panel had better mechanical characteristics than its component. The study also calculated numerically the buckling load using ABAQUS finite element analysis program. The achieved experimental and numerical results were compared with each other. In conclusion, a good correlation between theory and experiment was found.

The goal of this chapter is the development of a theoretical approach able to correlate the buckling to the failure modes of honeycomb panels under different loading conditions. The predicted critical loads were compared using the data obtained by experimental tests carried out on NHS and AHS honeycomb panels in different loading conditions (compression, low velocity impact, indentation).

IV.2. Theoretical approach

Figure 4.2 shows the failure modes in sandwich structures. It has been proved that the buckling of the honeycomb sandwich panel is one of the most frequent failure modes. A theoretical model was developed to analyze the failure mechanisms of honeycomb sandwiches subjected to different loading conditions (compressive, quasi-static indentation, low velocity impact) and to predict the critical loads for each loading condition.
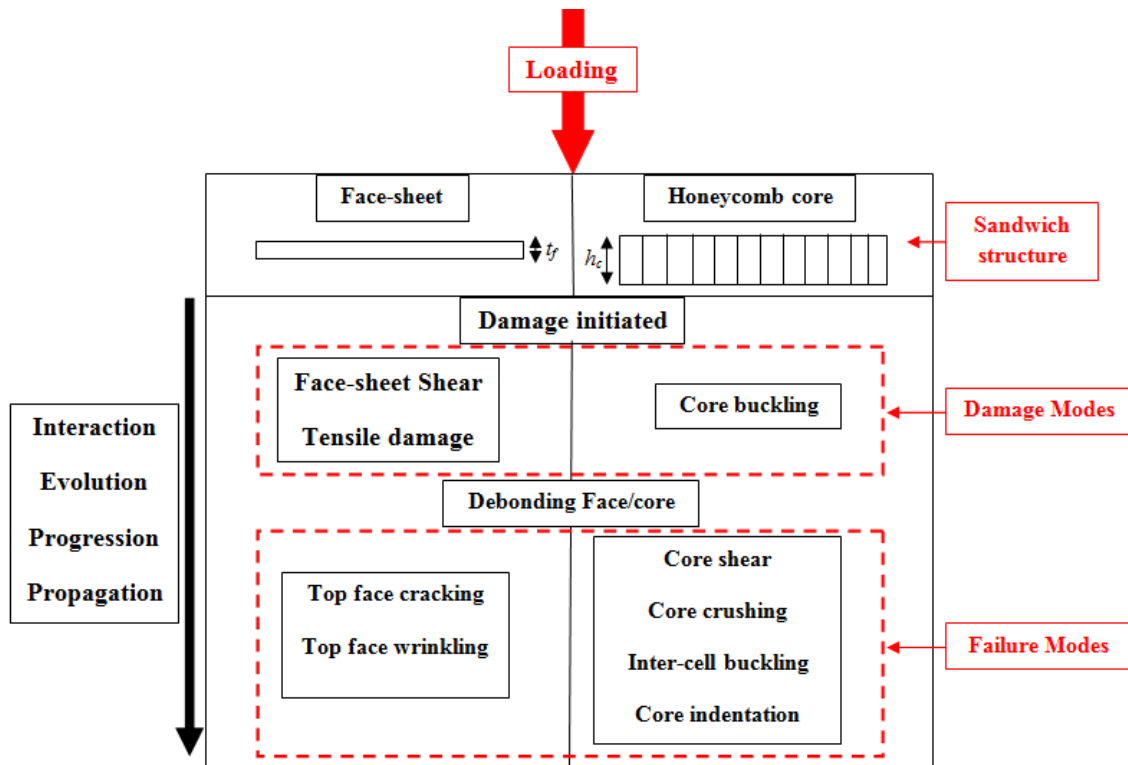
Figure 4.2: Failure process in sandwiches structures under different loading.

In this chapter we will described various mechanisms of failure which occur with honeycomb sandwich panels subjected to various loading Fig 4.2, and the honeycomb mechanics needed to evaluate the failure loads for each of these mechanisms.

If the honeycomb sandwich structure is subjected to an axial loading, every cell can be considered as a thin-walled cell shell simply supported on two ends because the face sheets are very thin Fig.4.3. When the loading arrives at critical value, how about the buckling mode?
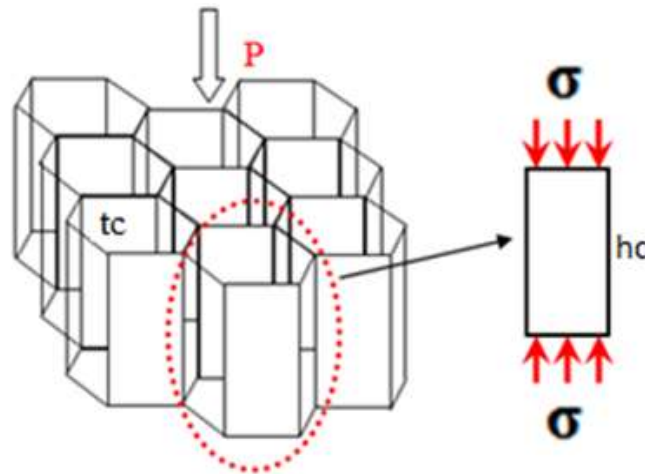
Figure 4.3: The mechanical models for investigation: the axially compressed rectangle plate with simply supported.

Practically, the core of sandwich panel is comprised of many thin walled cell shells with very small size. The σ_z may bring on the buckling of the cell shells as well as collapse of a honeycomb sandwich panel, and finally result in losing the capability of the supporting load. It has been proved that the buckling of the honeycomb sandwich panel is one of the most frequent failure forms

When the honeycomb composite is loaded in 'T' direction, it is assumed that a uniform compression is achieved on the two edges parallel to the loading direction of each wall as shown in Fig. 4.4. And also, it is assumed that cell walls and all the cell walls are deformed to the same strain. Therefore, the compressive stress of honeycomb composite is the sum of the stresses carried out by the individual cell walls.
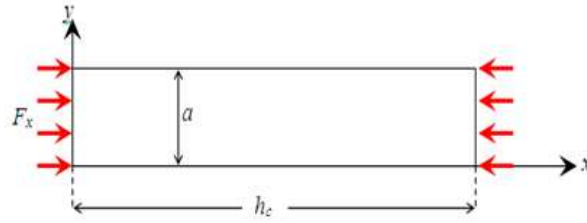
Figure 4.4: Cell wall of the honeycomb sandwich subjected to uni-axial loading.

The deformation's mechanics in 'T' direction are based on the walls buckling. Fig. 4.5 shows the buckling mechanism of an AHS under low-velocity impact loading.

Figure 4.5: Deformed honeycomb due to out-of-plane compression loading.

The honeycomb compressive behavior intrinsically relates to the cell wall buckling behavior under loading in 'T' direction, because in reality the vertical cell walls can never be compressed along the length direction until a pure compressive failure due to the instability of the thin structure occurs. The dominant mode of damage in these structures is the buckling of cell walls Fig.4.6.
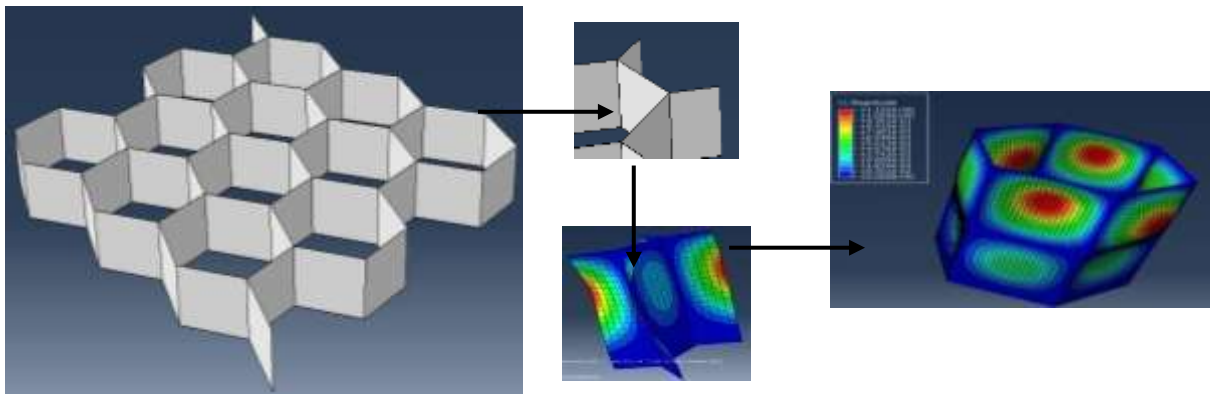
Figure 4.6: FE simulation of cell walls buckling using abaqus.

The buckling investigation on a cell wall can be substituted for that of the entire cell shell. The governing differential equation of a cell wall can be expressed as follows:

$$D \left(\frac{\partial^4 W}{\partial x^4} + 2 \frac{\partial^4 W}{\partial x^2 \partial y^2} + \frac{\partial^4 W}{\partial y^4} \right) + F_c \frac{\partial^2 W}{\partial x^2} = 0 \qquad \text{(4-1)}$$

Where w is the displacement perpendicular to the neutral face of the cell wall F_c is the axial load per unit length. D is the flexural stiffness expressed as:

$$D = \frac{E t_c^3}{12(1-v_c^2)} \qquad \text{(4-2)}$$

IV.2.1. Theoretical approach for Compression loading

Applying the governing differential equation (Eq.1) of buckling in the compression tests using the following boundary conditions:

$$\begin{cases} W = 0, \frac{\partial^2 W}{\partial y^2} = 0 & when \quad y = 0, a \\[2em] W = 0, \frac{\partial^2 W}{\partial x^2} = 0 & when \quad x = 0, h_c \end{cases}$$ Under the restriction of boundary

conditions, the solution (local buckling) of Eq.1 can be written:

$$W(x,y) = \sum_{m=1}^{\infty} \sum_{n=1}^{\infty} A_{mn} \sin \frac{m\pi x}{h_c} \sin \frac{n\pi y}{a} \qquad \text{(4-3)}$$

Thus, the critical buckling load for one wall, $F_c^{buckling}$ is given by:

$$F_c^{buckling} = K_c \frac{D\pi^2}{a} \left(\frac{m}{R} + \frac{R}{m} \right)^2 \qquad \text{(4-4)}$$

Where: $R = \frac{h_c}{a}$

The compressive load of the individual hexagonal cell of honeycomb core is the sum of the loads carried out the individual cells wall

Where K_C is end constraint factor in compression mode and its value is 5.73 [51], E_c is elastic modulus of cell walls, v is Poisson's ratio of cell walls, t_c is thickness of cell wall and h_c is length of free wall. Eq.4 is expressed for the load, $F_c^{buckling}$ on a cell wall.

Therefore, the compressive stress of honeycomb composite is the sum of the stresses carried out by the individual cell walls. The formula for a rectangular cell wall under equal uniform compression on two opposite edges, hc, was shown as following Eq.4.

The compressive load of the individual hexagonal cell of honeycomb core is the sum of the loads carried out by the individual cell walls:

$$F_c{}^{buckling} = 6K_c \frac{D\pi^2}{a}\left(\frac{m}{R} + \frac{R}{m}\right)^2 \qquad \text{(4-5)}$$

IV.2.1.1. Results

The application of the analytical model which has been developed in Eq 4-4 was used to derive the critical buckling load of the aluminum (AHS) and nomex (NHS) sandwich plate by varying the cell size and the correspondents buckling load for each size are depicted in figure 4.7.
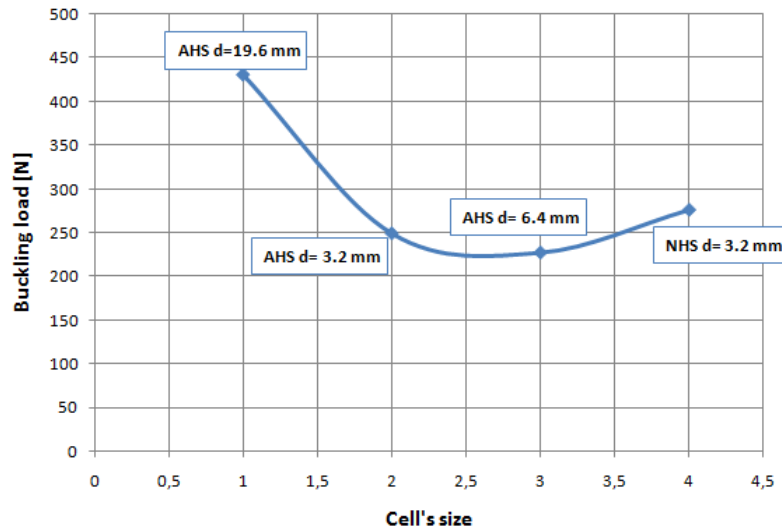
Figure 4.7: Theoretical buckling load for different cell size and core materials subjected to compression.

Table 4-1 summaries the peak load of buckling for the different used cell's size for two materials AHS and NHS.

Table 4-1:Theoretical data for compression loading.

	AHS (d=19.2mm)	AHS (d=3.2mm)	AHS (d=6.4mm)	NHS (d=3.2mm)
$F_{th\,(cell)}$[N]	431	249	227	276

Figure 4.8 shows a typical failure process in honeycomb sandwiches structures obtained from the compressive test of aluminum honeycomb sandwich panel.
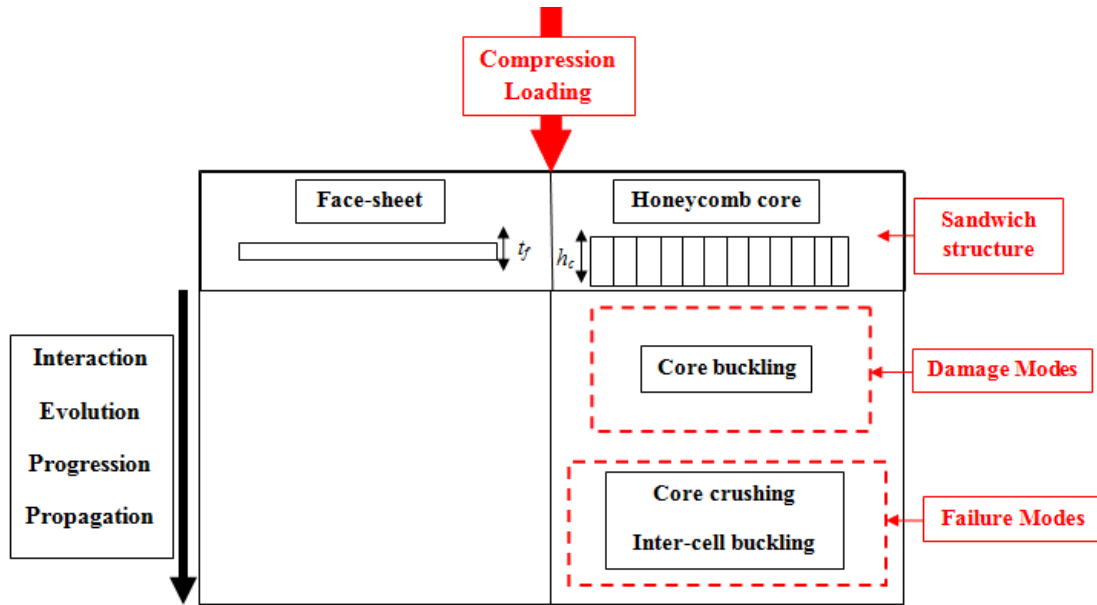
Figure 4.8: Failure process in sandwich structures under compression loading.

IV.2.2. Theoretical approach for Quasi-static indentation loading

In the case of the indentation loading on honeycomb sandwich panels, the damage force, F, at indentation distance, z, will be comprised of a component due to the honeycomb core and a component due to the facings, that is:

$$F^{In\ buck} = F_{core}^{In\ buck} + F_{face}^{In\ buck} \tag{4-6}$$

When a sandwich panel is subjected to transverse loading, it is widely accepted that the displacement of indenter is the sum of the indentation of top face-sheet and the global bending deflection [37, 43, 51-55]. All damages occurring in the experimental results are found to initiate in localized region.

Moreover, the damage initiation is independent of the boundary condition while it is dependent on the indenter radius, specimen transverse direction dimensions, cells size, and mechanical properties of the face-sheets and the core.

Two assumptions based on the preceding physical observations are used:

- External loading is taken mainly by the cells wall of the honeycomb structure.
- The contact between honeycomb and indenter is assumed to be perfect which means that the honeycomb in contact with the indenter follows the indenter shape during crushing.

The computation steps (for a spherical indenter case) are as follows:

1. Computation of polar radius (Ri).

    Since the cell wall positions are regular, their distance is a function of the diameter of the honeycomb cell. At the beginning, the indenter is considered to be in the center of the first cell to be touched to facilitate the computation by regarding only the quarter.

2. Computation of the damaged surface radius (R_i) when indenter crushes down to α_0.

    The value R_0 is calculated as a function of α and R_e (indenter radius) by using the following equation:

$$R_e = \sqrt{\alpha_0(1 - 2R_i)} \tag{4-7}$$

3. Computation of the penetration of each vertical edge (α_i).

    The penetration of vertical edges inside the damaged surface ($R_e < R_i$ is calculated using the following equation:

$$\alpha_i = \sqrt{R_i^2 - R_e^{\,2}} - R_i + \alpha \tag{4-8}$$

4. Computation of the reaction force ($F_c{}^{buckling}$).

    Knowing the penetration of each cell wall (αi) obtained by the experimental results, the reaction force for each cell wall $i(F_{ci}{}^{buckling}$ is obtained by:

$$F = \sum F_{ci}{}^{buckling} \tag{4-9}$$

5. Computation of indentation force.

    It is the sum of the reaction force of cell wall:

To have a complete indentation law, the same step is computed for several increments α_0 of indentation.
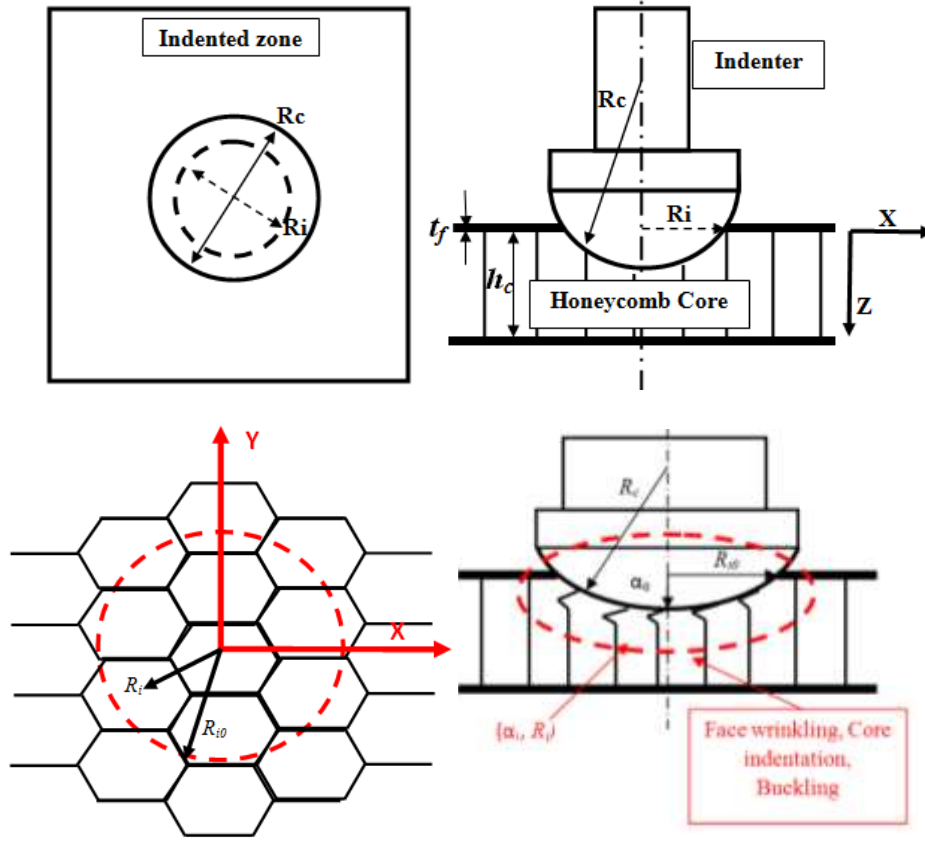
Figure 4.9: Parameters and geometrical configuration of indentation problem.

Shear stress in the top face-sheet is highly concentrated in the localized area of contact Fig.4.8. The limit load F^{shear} is given as [55, 56]:

$$F_l^{shear} = 2\pi R_e t_f \tau_f \tag{4-10}$$

Where t_f is the thickness of the face-sheets and R_e is the contact radius:

$$R_e = \sqrt{\alpha(2R_i - \alpha)} \tag{4-11}$$

and the indentation is given as:

$$\alpha = F\,\beta \tag{4-12}$$

Where β is given by

$$\beta = \frac{1}{\sqrt{\dfrac{D_f E_c}{h_c}}} \tag{4-13}$$

Where E_c and h_c are the Young modulus and thickness of the core respectively. The symbol D_f is the effective bending rigidity of face-sheet. Substituting Eqs. (11) and (14) into Eq. (10), the limit load for shear damage of the top face can be derived as:

$$F_f^{shear} = \pi^2 \beta R_i \left(t_f \tau_f \right)^2 \tag{4-14}$$

As can been seen in Eq. (14), limit load F_f^{shear} is a function of the radius of indenter R_i and thickness face t_f, and the through thickness modulus of the core h_c

Results obtained from the quasi-static tests showed that the indentation failure of the sandwich panel is mainly core dependent [46-56]. Core buckling is widely reported as the first damage mode that occurs in experiments Fig.4.11. Since honeycomb core is made of hexagonal interlinked thin walls, this damage mode will be the dominant mode for large core thickness of h_c. For this sandwich panel, the threshold load has been developed:

$$F_{cI}^{In\ buck} = \sigma_c^s K_c A_f \tag{4-15}$$

$$A_f = \pi\alpha(2R_i - \alpha) \tag{4-16}$$

$$F_c^{In\ buck} = \sigma_c^s K_c \pi\alpha(2R_i - \alpha) \tag{4-17}$$

IV.2.2.1. Results

The limit load of Eq. (17) is independent of indenter radius while experimental results show that the radius Ri may affect the limit load for core buckling.

The analysis of Eqs. (14) and (17) concludes that as the face-sheet thickness increases, the limit loads for both modes will also increase. This means increasing the face-sheet thickness will significantly increase the ultimate load. Likewise, increasing the core density will definitely leads to higher compressive strength.

The theoretical values of the critical load F_{th} predicted using eq. (4-17) for the different used cell size are reported in table 4.2 and figure 4.10.

Table 4-2: *The theoretical data for indentation loading.*

	AHS (d=3.2mm)	AHS (d=6.4mm)	NHS (d=3.2mm)
R_i [mm]	20	20	20
α [mm]	4.9	4.3	4
F_{th}[N]	3706	2891	4717
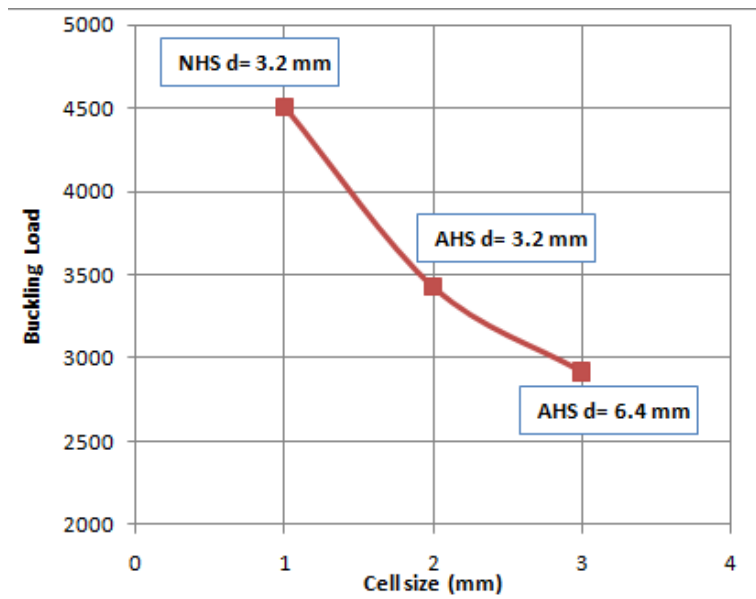
Figure 4.10: Theoretical buckling load for different cell size and core materials under quasi-static loading conditions.
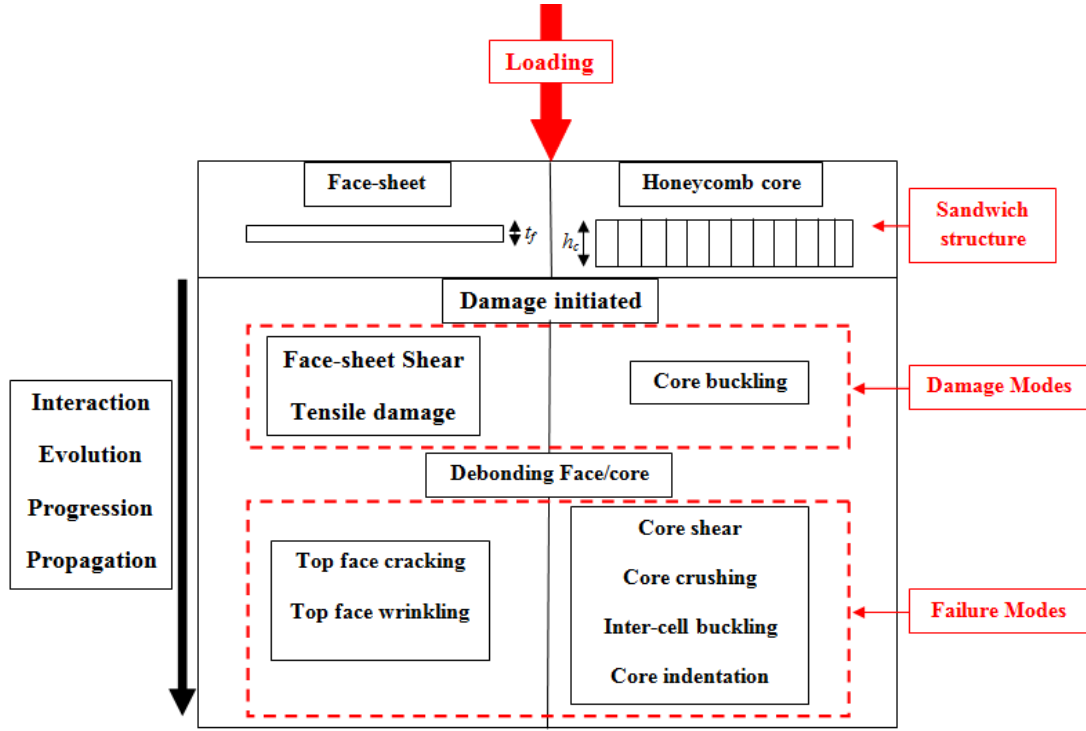
Figure 4.11: Failure process in sandwiches structures under indentation loading.

IV.2.3.Theoretical approach for Low-velocity impact loading

The developed theoretical approach is, also, able to predict the response of honeycomb sandwiches subject to low-velocity impact loading. The sandwich panel experiences the local displacement α due to the indentation of the top face and the core crushing, and the global displacement W_b due to the bending and the shear of the entire panel. The global and local responses of the panel (Figure 4.13) can be evaluated separately, since the impact damage is small and localized around the impactor for low velocity impacts [56].

The possible failure mechanisms can be summarized in Figure 4.13. The skins of the investigated sandwiches are thin, so it is possible to assess that the failure takes place because of tensile stresses.

Among the aims of this study is developing of a theoretical approach to predict the response of honeycomb sandwich subject to low-velocity impact loading.

The critical buckling load is given by:

$$F^{Im\,buck} = F^{Im\,buck}{}_{core} + F^{shear}{}_{facing} \qquad (4\text{-}18)$$

The impactor geometry influences the shape of the damaged area on the sandwich. In fact, failure can be radial for a conical indenter (a crack starts at the impactor/material interface with a petals shape during the penetration) or it can be circumferential if the impactor is cylindrical/ spherical (the material under the impactor undergoes compressive stress and the strain interests the whole sample) [57].

The limit load for shear damage of the top face can be derived as:

$$F_f^{shear} = \pi^2 \beta R_i (t_f \tau_f)^2 \tag{4-19}$$

Where β is given by:

$$\beta = \frac{1}{\sqrt{\frac{D_f E_c}{h_c}}} \tag{4-20}$$

Moreover the core critical buckling load can be calculated by the following formula:

$$F_c^{Im\ buck} = \sigma_c^d K_c A_f \tag{4-21}$$

Where A_f: is the area of damaged zone under the impactor.

$$A_f = \pi \alpha (2R_i - \alpha) \tag{4-22}$$

By substituting Eq.(22) in Eq.(21) we obtain:

$$F_c^{Im\ buck} = \sigma_c^d K_c \pi \alpha (2R_i - \alpha) \tag{4-23}$$

Kc is a constant equal generally to 1.7–2.5 [56-58]

IV.2.3.1. Results

Table 4.3 and figure 4.12 report the results of all the theoretical buckling values of AHS and NHS for different cell sizes under variable velocity of impact (1.5, 2 and 3 m/s).

Table 4-3:The theoretical data for low-velocity impact loading.

Impact velocity [m/s]	AHS (d=3.2mm)		AHS (d=6.4mm)		NHS (d=3.2mm)	
	Indentation α [mm]	Theoretical load F_{th}[N]	Indentation α [mm]	Theoretical load F_{th}[N]	Indentation α [mm]	Theoretical load F_{th}[N]
1.5	3.12	4043	3.66	3222	4.9	3404
2	4.27	5210	5.33	4269	5.1	4155
3	6.89	7560	8.34	5939	6.9	5200
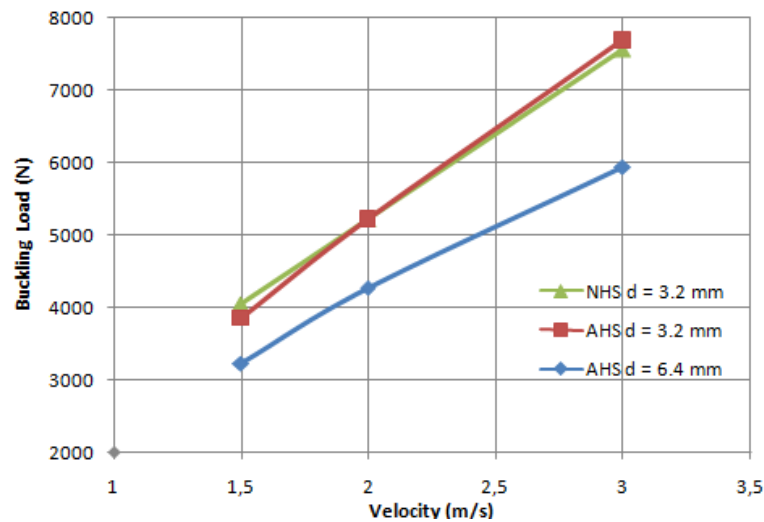
Figure 4.12: Theoretical buckling load for different cell size and core materials at different impact velocities.

The possible failure mechanisms can be summarized in Figure 4.13. The skins of the investigated sandwiches are thin, so it is possible to assess that the failure takes place because of tensile stresses.
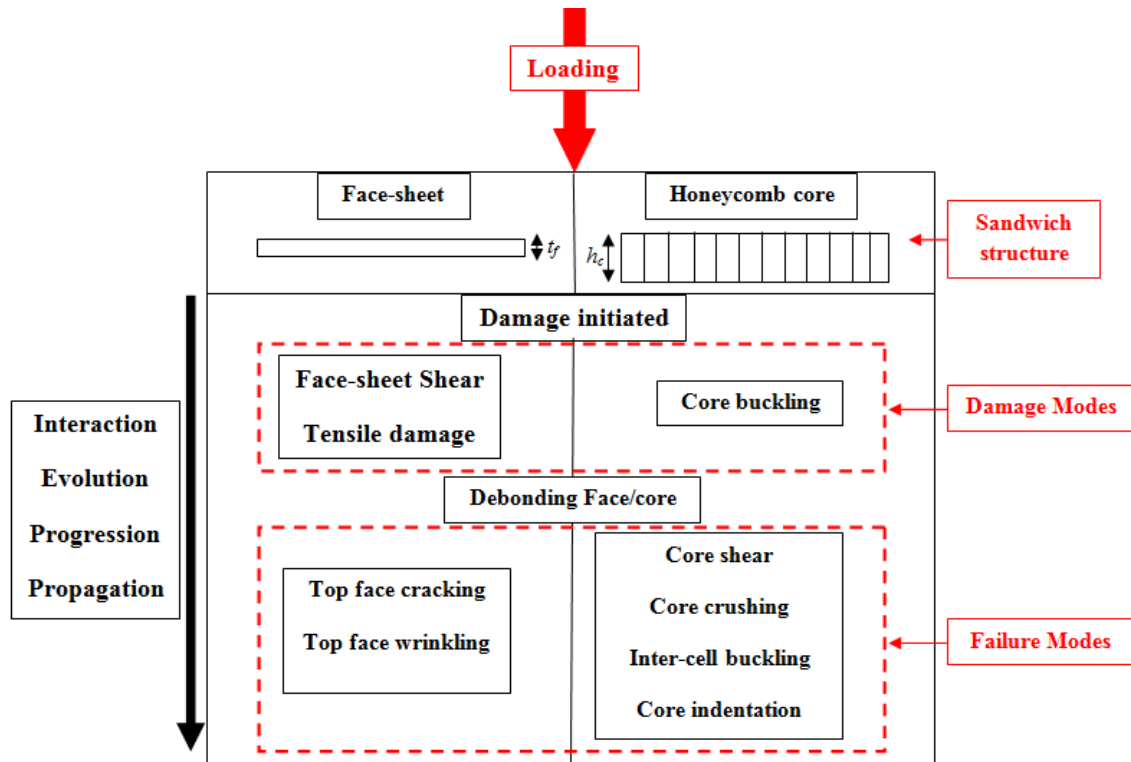
Figure 4.13: Failure process in sandwiches structures under indentation loading.

CHAPTER V: Finite Element Analysis and Results

Finite element analysis has become the prevalent method for analysis of the behaviors of solids, structures and fluid mechanics. Composite materials and structures can be modeled and successfully analyzed in finite element programs. This chapter discusses the modeling and analyzing the experimentally tested specimens utilizing numerical methods.

Aim of this chapter is the numerical study of aluminum honeycomb sandwiches (AHC) subjected to static and dynamic loading conditions using ABAQUS package program. Also, the work presented in this chapter seeks to predict damage and failure in AHC panels specially buckling of honeycomb core. In meantime, this program is used to numerically calculate the corresponding critical buckling loads. In other hand, a three dimensional (3D) reconstructions of the honeycomb panels have been carried out in order to acquire exactly the dimension and the shape of the damage (buckling).

The modeling of the penetration of a rigid hemispherical impactor through a panel of honeycomb cells is discussed in the following sections including geometry, boundary conditions, mesh sensitivity, contact interactions, and material and damage. The detailed model is described and its results are presented

V.1. Introduction

Characterization of material behavior under high strain rates is important in order to accurately model structures under severe impact conditions. Similar to the stress-strain response, damage modeling and failure mode determination are important. Modeling of complex behaviors using analytical solutions has proven to be elusive, sometimes impossible. Such problems are better handled by numerical analyses using finite element codes where well established material and damage models are implemented.

In the previous chapters, the behavior of AHC and NHC panels was investigated experimentally. In this chapter, nonlinear finite element analysis (FEA) is carried out on the thus panels. Models are developed and used to predict the buckling behavior and failure modes of the sandwich panels. Currently, there are several commercial finite element programs that can be used in the analysis and design of structures. These include SAP, NASTRAN, ADINA, ANSYS and ABAQUS, among other programs, which are capable of modeling very complex problems. Numerical FE models have been built with the commercial software ABAQUS 6.10 using two different element types: shell and solid elements. Moreover, the AHC model has been studied on different scales: on a single cell scale and on a large scale, i.e. the full model (Figs. 5.1, 5.2 and 5.3) for compression loading. The adhesive bonding between the face-sheet and the core was assumed to be perfect, and surface-based tie constraint was adopted at the face-sheet-core interfaces. By doing so, each node of the honeycomb core at the interface was constrained to have the same translational and rotational motion as the node on the face-sheet to which it was tied. The tie constraint then disallowed surfaces initially in contact from penetrating, separating, or sliding relative to one another (Figs 5.2 and 5.3).
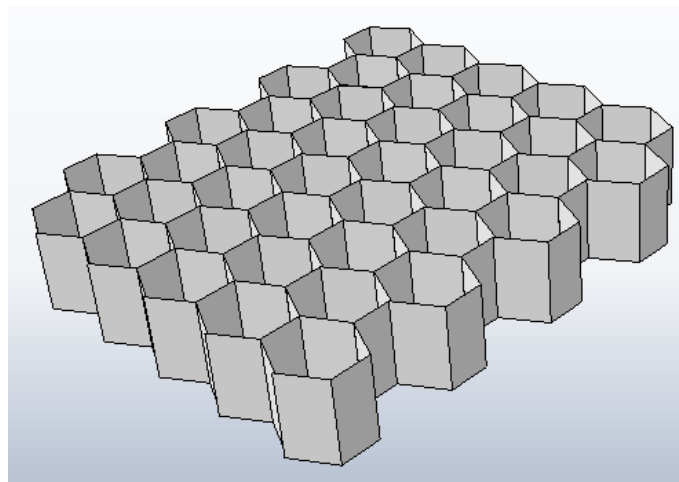
Figure 5.1: Finite element model of AHC d = 6.4 mm (gouge of cells).

Otherwise, this chapter describes the finite element analysis carried out on the sandwich panels to investigate their mechanical behavior and failure modes. The complete description of the models, including the types of elements, meshing, boundary conditions, and methods of analysis are presented in pages ahead. Moreover, the work presented here seeks to predict damage and failure in AHC panels subjected to compression, indentation and low-velocity impact.
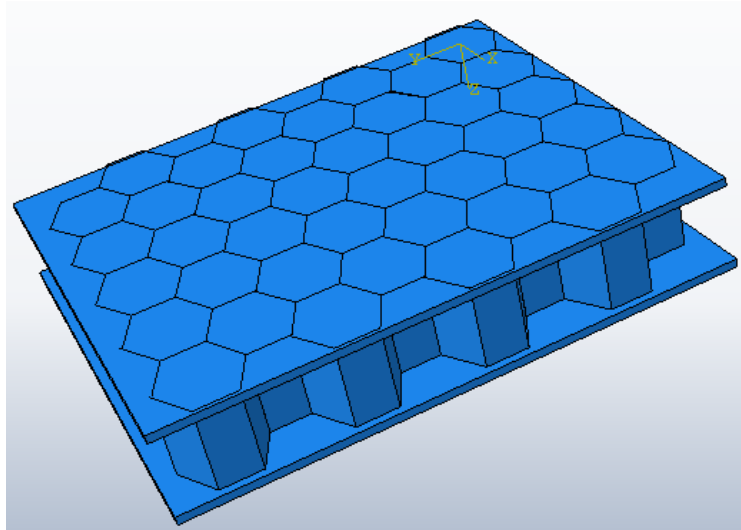
Figure 5.2: Full finite element model (AHC d = 6.4 mm).

The surface of the object under investigation is represented in the CT image stack by the grey value transition between air and material (Figure 5.3).
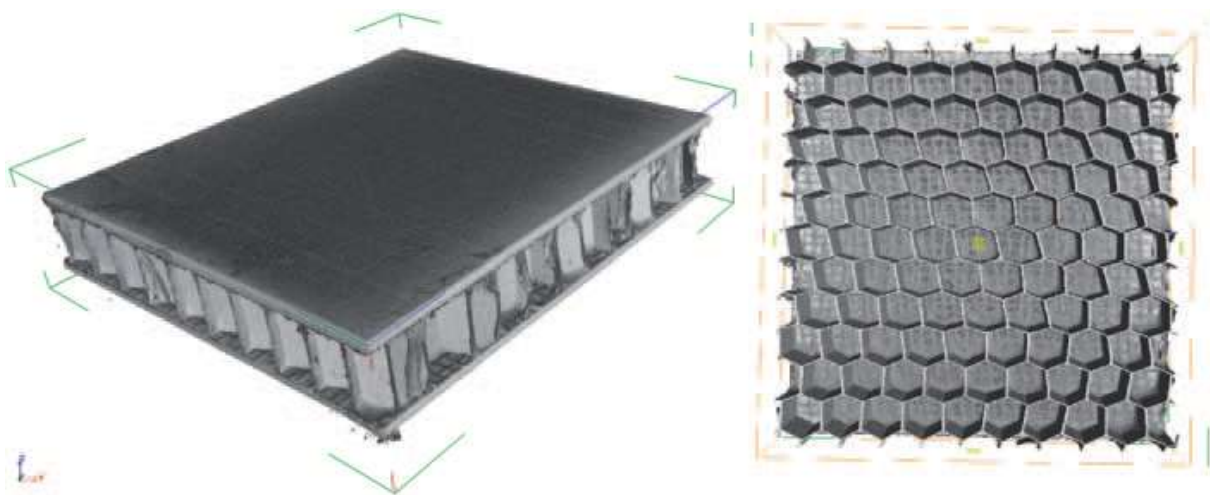
Figure 5.3: Geometry analysis of AHC d=6.4 mm.

V.2. Development of FE Model

V.2.1. FE model used for compression loading

The program used in this study is ABAQUS, which is a program by Dassault Systems. The honeycomb panels were modeled as shell elements. The element type is S4R which it is a fully integrated 4-node element that allows for finite membrane strains (designated byS4R in the ABAQUS Explicit element library) employing Gauss' integration rule. A regular mesh with nearly square elements was adopted, while the number of elements used was selected from convergence studies that follow. A number of analyses using different mesh densities (ranging from 4 to 14 elements per cell edge) were run with a coefficient of friction of zero. The results are shown in pages ahead.

For the panels tested in present study a thin film of epoxy is used to bond the face-sheet to the honeycomb. After looking into the effect of the adhesive on the calculated response it was decided that including it would make the calculation numerically cumbersome without adding significantly to the accuracy of the predictions. Thus, the top and bottom edges of the unit cell are assumed to be fixed, except that the top can translate in the Z-direction. The following periodicity conditions are used for the lateral edges of the unit cell (Fig 5.4). The displacements and rotations of points on these edges are respectively denoted by (U_{i1}, U_{i2}) and $(\theta_{i1}, \theta_{i2})$ I = 1, 3.The cell is loaded by prescribing incrementally the normal displacement of the top surfaceδ (Fig 5.4).
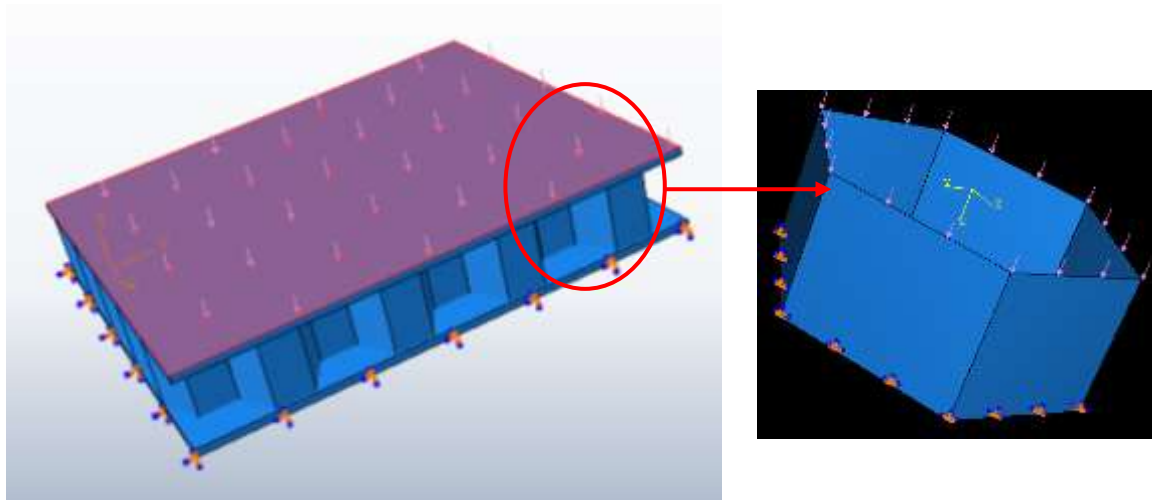
Figure 5-4: FE boundary conditions and loads.

We will start by considering just one fully periodic unit cell (Fig. 5-4 and 5-5). Progressive folding that characterizes the crushing calculations is numerically intensive so the shell element selection and the discretization adopted were guided by computational efficiency.

The following relationships are prescribed for the degrees of freedom of points on each pair of faces:

$$U_{i1} - U_{i2} = U_{i1}^{ref} - U_{i2}^{ref} \qquad and \qquad \theta_{i1} - \theta_{i2} = 0, \; i=1,3 \qquad (5\text{-}1)$$

Where U_{ij}^{ref} are displacements of conjugate points on opposite sides chosen as reference points. To support the lower surface of the sandwich panels, modeled according to the load conditions in Figure 5.4, the displacements at all joints of the sandwich layer of the lower surface in z-direction are accepted to be zero ($U_z=0$).
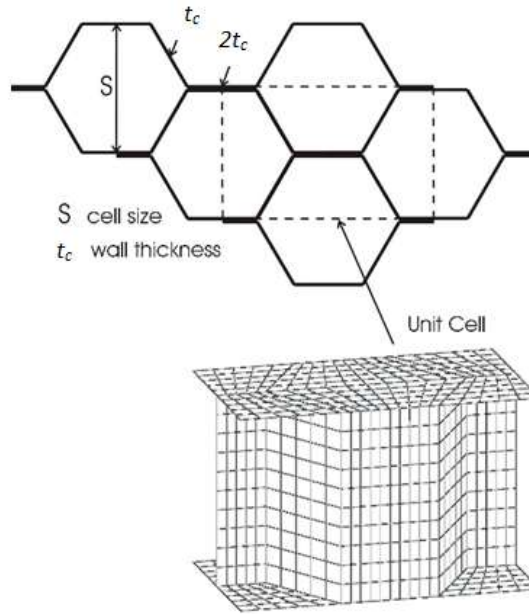
Figure 5.5: Honeycomb characteristics and unit cell definition.

A linear buckling analysis is performed by applying a unit load on the upper surface of the panel in the z-direction. As no additional adhesive is used between the surface sheet and the core, in order to apply the real boundary conditions, the cell walls are fixed. As a result, the critical buckling loads of the specimens are calculated by the multiplication of the critical buckling stress with the number of cell's wall.

V.2.1.1. The Johnson-Cook elasto-viscoplastic model

The Johnson-Cook elasto-viscoplastic model, able to predict the flow and fracture behavior of the sandwich panels, was applied to model the material behavior in the FE simulations. It

includes the effect of linear thermo-elasticity, plastic flow, isotropic strain hardening, strain rate hardening, softening due to adiabatic heating and damage. The equivalent Von Mises stress of Johnson-Cook is expressed in the following form:

$$\sigma\left(\varepsilon_{pl}, \dot{\varepsilon}_{pl}\right) = \left[A + B\left(\varepsilon_{pl}^{-n}\right)\right].\left[1 + C\ \ln\left(\frac{\dot{\varepsilon}_{pl}}{\dot{\varepsilon}_0}\right)\right].\left[1 - (T^{\wedge})^m\right] \tag{5-2}$$

Where A is quasi-static yield stress, B is the hardening constant, n is the hardening exponent, C is the strain rate sensitivity parameter and m is the temperature sensitivity parameter, $\dot{\varepsilon}_{pl}$ is equivalent plastic strain rate, $\dot{\varepsilon}_0$ is reference strain rate, ε_{pl} is the equivalent plastic strain and $T^{\wedge}$ is the non-dimensional temperature defined as:

$$T^{\wedge} = \frac{T - T_0}{T_{melt} - T_0} \tag{5-3}$$

Where T is the current temperature, T_{melt} is the melting temperature and T_0 is the reference temperature. The fracture model proposed by Johnson–Cook takes into account the effect of stress tri-axiality, strain rate and temperature on the equivalent fracture strain. The equivalent fracture strain $\Box_{\Box\Box}$ is expressed in the following form:

$$\bar{\varepsilon}_{pl}^{-}\left(\frac{\sigma_m}{\sigma-}, \dot{\varepsilon}_{pl}, T^{\wedge}\right) = \left[D_1 + D_2 exp\left(D_3\frac{\sigma_m}{\sigma-}\right)\right].\left[1 + D_4\ln\left(\frac{\dot{\varepsilon}_{pl}}{\dot{\varepsilon}_0}\right)\right].\left[1 - D_5 T^{\wedge}\right] \tag{5-4}$$

Where D1–D5 are material parameters, $\sigma-$ is the stress tri-axiality ratio and σ_m is the mean stress (see table 5.1).

Tie constraint was also applied to the interface between fixtures and skins. To simulate contact between the impactor/indenter and the panel, a general contact algorithm was introduced; using a penalty contact method in ABAQUS. Self-contact for the cellular walls of honeycomb core was also included in the FE model, so the core walls were not allowed to fold onto themselves.

Table 5.1. *Elastic and Johnson-Cook parameters for AA5052 aluminum alloy.*

Isotropic elasticity		Johnson-Cook plasticity												
E (Mpa)	ν	A (Mpa)	B (Mpa)	n	$\dot{\varepsilon}_0$	c	m	T_{melt} (K)	T_0 (K)	D1	D2	D3	D4	D5
73000	0.33	256	426	0.34	1	0.015	1	823	273	0.13	0.13	-1.5	0.011	0

Damage was modeled using the Johnson-Cook damage model given by equation (5. 2).The 5 damage parameters for AA5052 aluminum alloy are shown in Table 5.2.

*Table 5.2.*Johnson-Cook damage parameters for AA5052 aluminum alloy

D1	D2	D3	D4	D5
0.13	0.13	-1.5	0.011	0

The material is modeled as a finitely deforming solid that hardens isotropically. The model is calibrated to a bilinear stress–strain response that was fitted to measured tensile tests on the honeycomb foil. It has an elastic modulus of 73GPa, a yield stress of 256MPa, a post-yield modulus of 426MPa and is perfectly plastic at higher values.

The main elastic properties can be easily evaluated from simple considerations. Thus, the elastic modulus $E^*_3$is given by [15]:

$$\frac{E^*_3}{E} = \frac{8t}{3c} = \frac{\rho^*}{\rho} \qquad\qquad (5\text{-}5)$$

Where E is the modulus of the base material. The two Poisson's ratios are equal to that of the base material v [15].

$$\nu^*_{31} = \nu^*_{32} = \nu \qquad\qquad (5\text{-}6)$$

During the simulation, accumulation of damage in elements occurred over time. The condition of failure was met when equation (5.2) was satisfied for a value of unit y for the cumulative damage parameter D, at which point, all stresses and strains in the failed element are set to zero until the end of the simulation.

Table 5.3: Mechanical and part properties used for FEA model validation Geometric parameters of Al-5052 honeycomb used in the numerical study.

D (mm)	Density (Kg/m3)	tc (mm)	hc (mm)	Part type	Section type
3.2	144	0.8	8.8	3-D Shell	3-D Shell
6.4	82	0.8	8.8	3-D Shell	3-D Shell
19.2	29	0.8	8.8	3-D Shell	3-D Shell

For choosing the final mesh, aspect ratio of elements which has significant effect on accuracy of analysis was assigned very close to unity. The size of the element, another important parameter which affects the results of numerical simulation, was investigated by varying the number of elements over the damaged region. The refined mesh in the damaged region of the honeycomb core was required to capture buckling of the cellular walls as core crushing occurred (Fig 5.6 and 5.7). So the mesh sensitivity analyses were carried out and element size was reduced until obtaining a convergence of the results. Thus, the element size was chosen equal to 0.7 mm in order to obtain the convergence and to capture the short wave-length buckling of honeycomb walls. A regular mesh with nearly square elements was adopted, while the number of elements used was selected from convergence studies that follow.

Finally, the optimum mesh density was obtained and it consisted of 5026 shell elements for one unit cell (Figure 5.8).
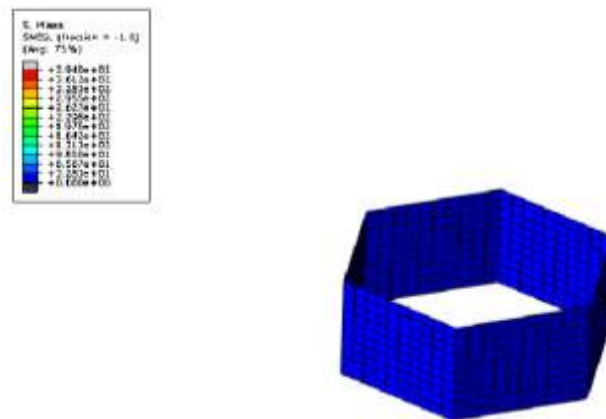
Figure 5.6: Finite element meshed for single cell scale.
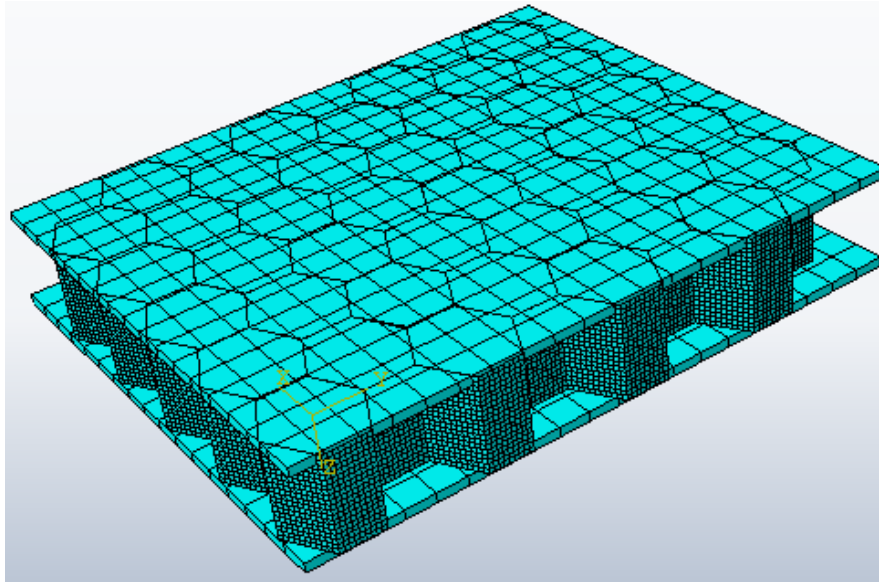
Figure 5.7: Finite element meshed model (AHC d = 6.4 m).
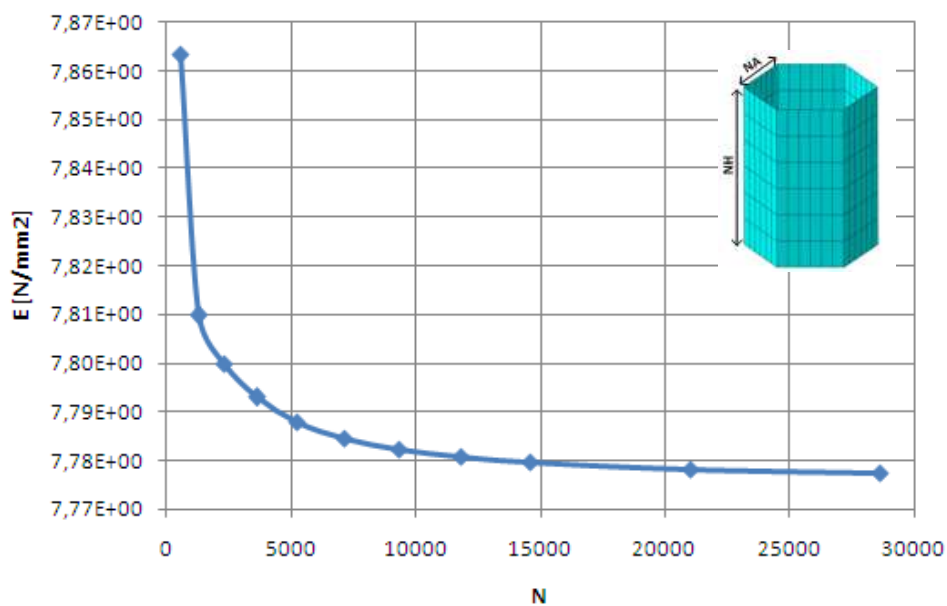
Figure 5.8: The number of elements used from convergence studies that follow (AHC d = 6.4 mm).

V.2.2. FEA model for quasi-static indentation and low velocity impact loading

Since the impact duration is quite short and impact damages are difficult to detect, Finite Element Analysis (FEA) has been widely used to simulate the damage evolution and failure mode of sandwich panels.

In this work, a three-dimensional geometrically correct finite element model of the honeycomb sandwich plate and a rigid impactor/indenter was developed using the commercial software, ABAQUS (figure 5.9). This discrete modeling approach enabled further

understanding of the parameters affecting the initiation and propagation of impact damage. The top and bottom face-sheets, as well as the honeycomb sandwich core, were meshed with shell elements (the same work like in FE Model in compression loading).

The impactor/intender was modeled as a rigid body using four-nodded linear tetrahedron continuum elements, and its motion was governed by the rigid body reference node. The impactor/indenter had a Young's modulus of 200 GPa, with a Poisson's ratio of 0.3. In the impact analysis, the 20 mm diameter steel hemispherical impactor/indenter had a density of 4 kg/m3 to reflect its actual mass in the experiment, which was 4 kg in all impact simulations. In addition, gravitational load and an initial velocity, v_0, were assigned to the impactor/indenter at its reference node. The impactor/indenter was also constrained to move only in the out-of plane direction (i.e. Z-direction) of the plate. To reduce the runtime, all simulations commenced with the impactor/indenter situated just 0.1 mm above the sandwich plate.
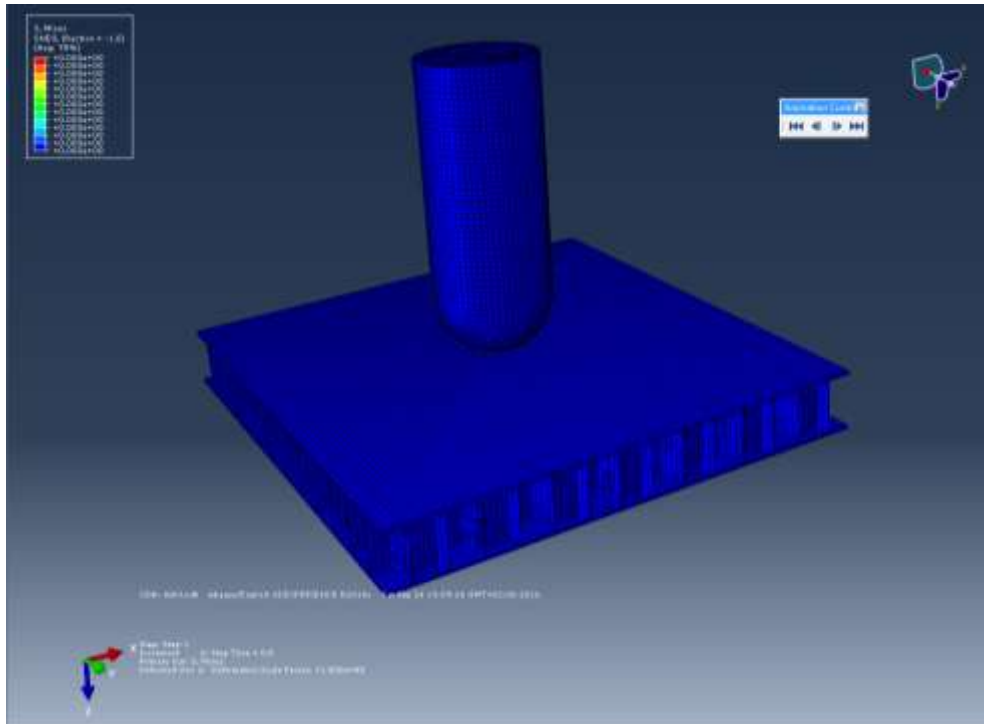
Figure 5.9: Correct finite element model of the honeycomb sandwich plate and a rigid impactor/indenter

V.2.2.1. Material and damage modeling

The Johnson-Cook plasticity model as given by equation (5.2) is used to model the behavior of the Aluminum 5052 honeycomb. This aluminum grade was chosen because the Johnson-Cook damage parameters D1, D2, D3, D4 and D5 are unavailable in the literature for the 5052

grade (see table 5.1). Damage was modeled using the Johnson-Cook damage model given by equation (5.4).

Therefore an adiabatic analysis with the Johnson-Cook plasticity model was performed. A value of 0.9 is used for the inelastic heat fraction in this analysis, indicating that 90% of the plastic work is converted to heat, as reported for most metals by Meyers (1994). The analysis also takes into effect nonlinear geometry effects. Geometries nonlinearity is related to the changes in the geometry of the deformed parts from one step to another and occurs whenever the magnitude of the displacements becomes large enough to induce nonlinearities in the stiffness matrix, consequently affecting the response of the structure.

V.2.2.2. Contact and interactions

The general contact algorithm available in ABAQUS/Explicit has been used in this study. This algorithm is easy to use, since no contacting surfaces need to be specified, and it provides a good energy balance. It enforces contact constraints using a penalty contact method, which searches for node-into-face and edge-into-edge penetrations in the current configuration. ABAQUS Explicit automatically chooses the penalty stiffness that relates the contact force to the penetration distance so that the effect on time increment is minimal, while ensuring that the penetration is not significant. The general contact algorithm is especially useful in cases where there is self-contact within a body.

A c1assical isotropic Coulomb friction model with a specified coefficient of friction between the honeycomb and impactor/indenter is used to model the tangential interaction between the impactor/indenter and deformable surfaces, as well as the tangential interaction within the honeycomb cluster in the case of self-contact. Considering the high speed impact and high strain rates, there is ambiguity regarding the level of friction present.

The value of friction coefficient for the contact between impactor/indenter and the panel was chosen equal to 0.15.

V.2.2.3. Mesh element

The mesh on the top face-sheet had to be refined adequately enough to interact with the rigid impactor/indenter, so that the impactor/indenter did not penetrate the face-sheet. In addition, the rigorous mesh in the central region of the honeycomb core was required to capture the buckling of the cellular walls as core crushing occurred.

Mesh with element size of 0.7mm was also considered for face sheets in impact region. Finally, the optimum mesh density was 238,301 shell elements (Figure 5.10). Transverse

shear deformation was expected to be significant because of high thickness-to-span ratio for the sandwich plate, and this effect was included in elements. Large-strain shell elements of ABAQUS software [65] use the Mindlin- Reissor flexural theory that includes transverse shear. The transverse shear stiffness is computed in FEA by matching the shear response for the case of the shell bending about one axis, using a parabolic variation of the transverse shear stress in each layer. It is known that hourglass control is a very useful method to minimize the problem, involved in the reduced-integration elements without introducing excessive constraints on the element's physical response. In correspondence with previous FE studies about Cook-Johnson damage modeling, enhanced hourglass option was considered in combination with element distortion control for the FE simulations. The hourglass energy, produced during the numerical simulations, is generally lower than 5% of total energy of the model [66].
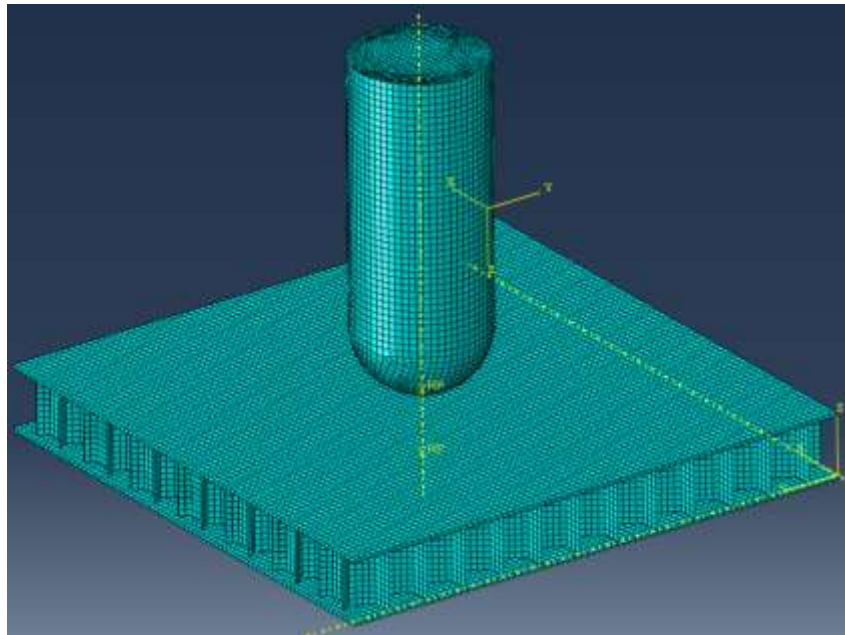
Figure 5.10: Finite element meshed model (AHC d = 6.4 m).

V.3. Results and discussion

V.3.1. Finite element compression results

This section presents a comprehensive study of the lateral compressive response of AHC panels from the initial elastic regime to a fully crushed state. These panels were laterally compressed quasi statically between two rigid platens under displacement control.

The cells of AHC buckle elastically and collapse at a higher stress due to inelastic action. Deformation then first localizes at mid-height and the cells crush by progressive formation of folds (buckling). The response densifies when the whole panel height is consumed by folds (total buckling) (Fig 5.11 and 5.12). The nonlinear behavior is initiated by elastic buckling while inelastic collapse that leads to the localization observed in the experiments occurs at a significantly higher load.

- **Buckling and initial post buckling behavior:**

The cell is loaded by prescribing incrementally the normal displacement of the top surfaceδ. A typical calculated compressive load-displacement response is shown in Fig. 5.11. Calculations of this type are performed in ABAQUS standard with a mesh of 5256 elements. The response is initially stiff and linear with stiffness E_3^* as quoted in (2). At some level of stress (F = 235 N) the walls of the cell buckle into the mode shown in Fig. 5.9. It has one half waves along the height of the cell and is symmetric about the mid-height (Fig 5.12 (a)). Interestingly, the second buckling mode shown in Fig. 5.12 (b) is anti-symmetric about the mid-height and occurs after the apparition of the first wave.

Buckling is clearly elastic as the honeycomb yields at a much higher load level (F = 235 N). The bound was developed using a long strip of foil width *hc* and thickness *t* with fixed boundary conditions along the long edges. Since the cell corners are not rigid, neighboring cells buckle in a compatible manner (see Fig.5.12), which apparently makes the structure more flexible. Elastic buckling of plates has a stable post buckling response and consequently the initial change in stiffness of the buckled structure is relatively small.
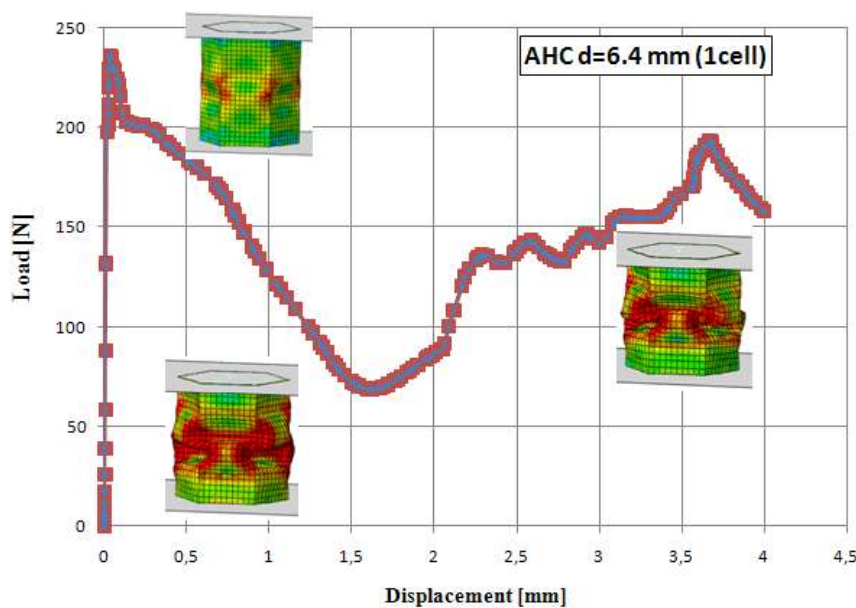
Figure 5.11: Numerical computation of buckling response from unit cell (AHC d = 6.4 mm).

130

(a)   (b)
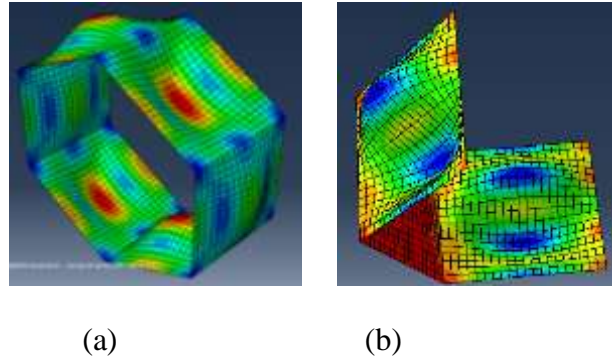
Figure 5.12: Numerical buckling modes of cell of honeycomb core before total cruching (F_{buck}^{n}=235n).
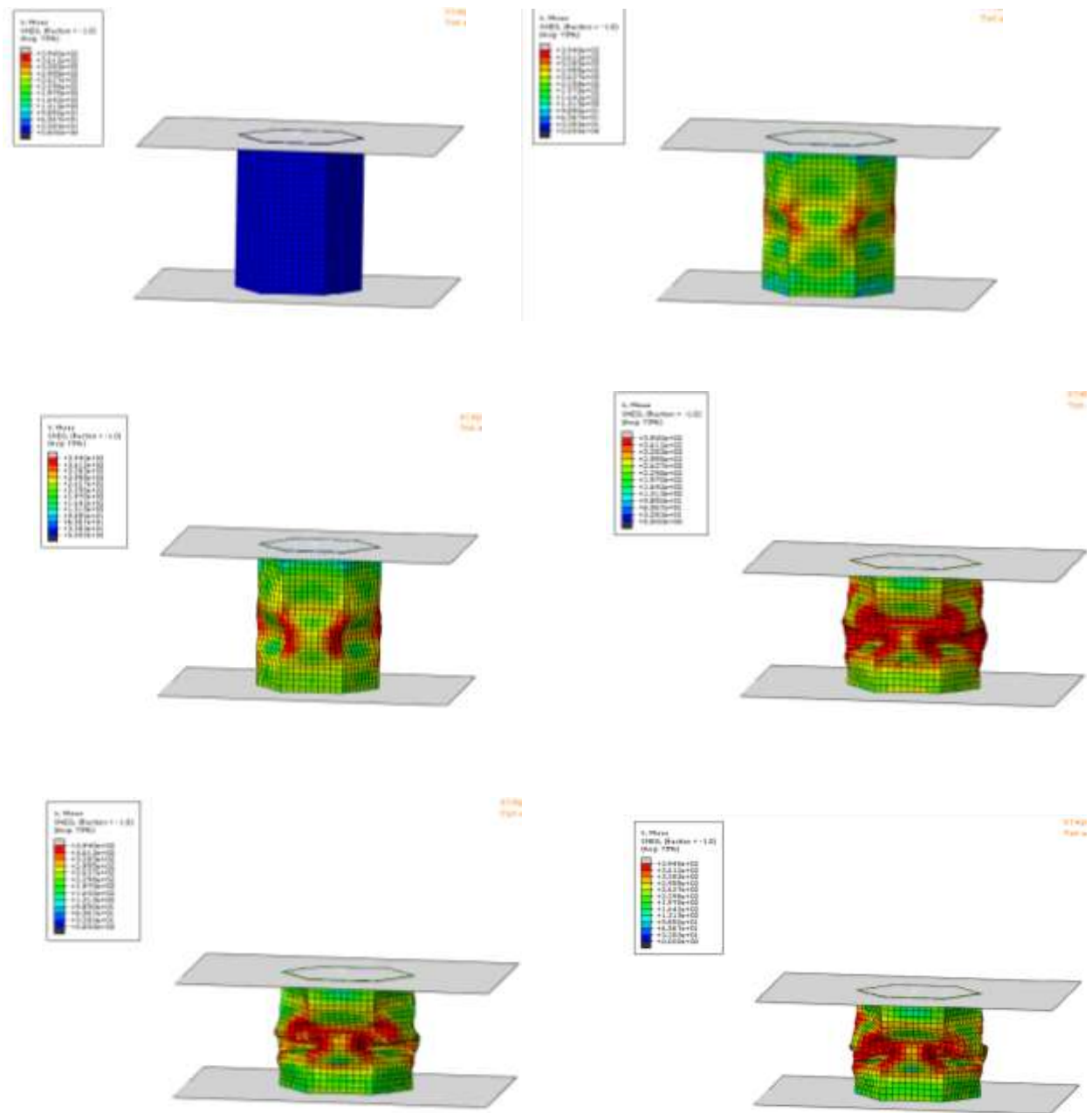
Figure 5.13: Numerical sequence from initial buckling to the total crushing configurations corresponding to perfect cell (AHC d = 6.4 mm).
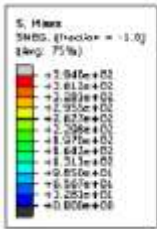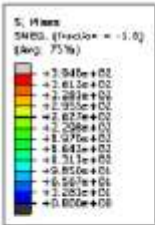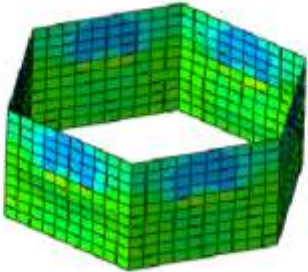
131
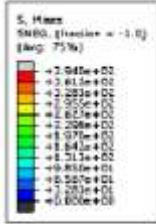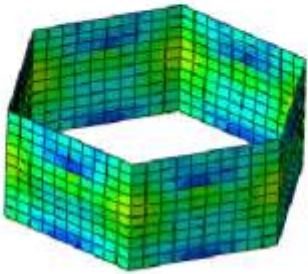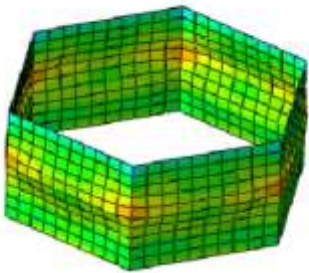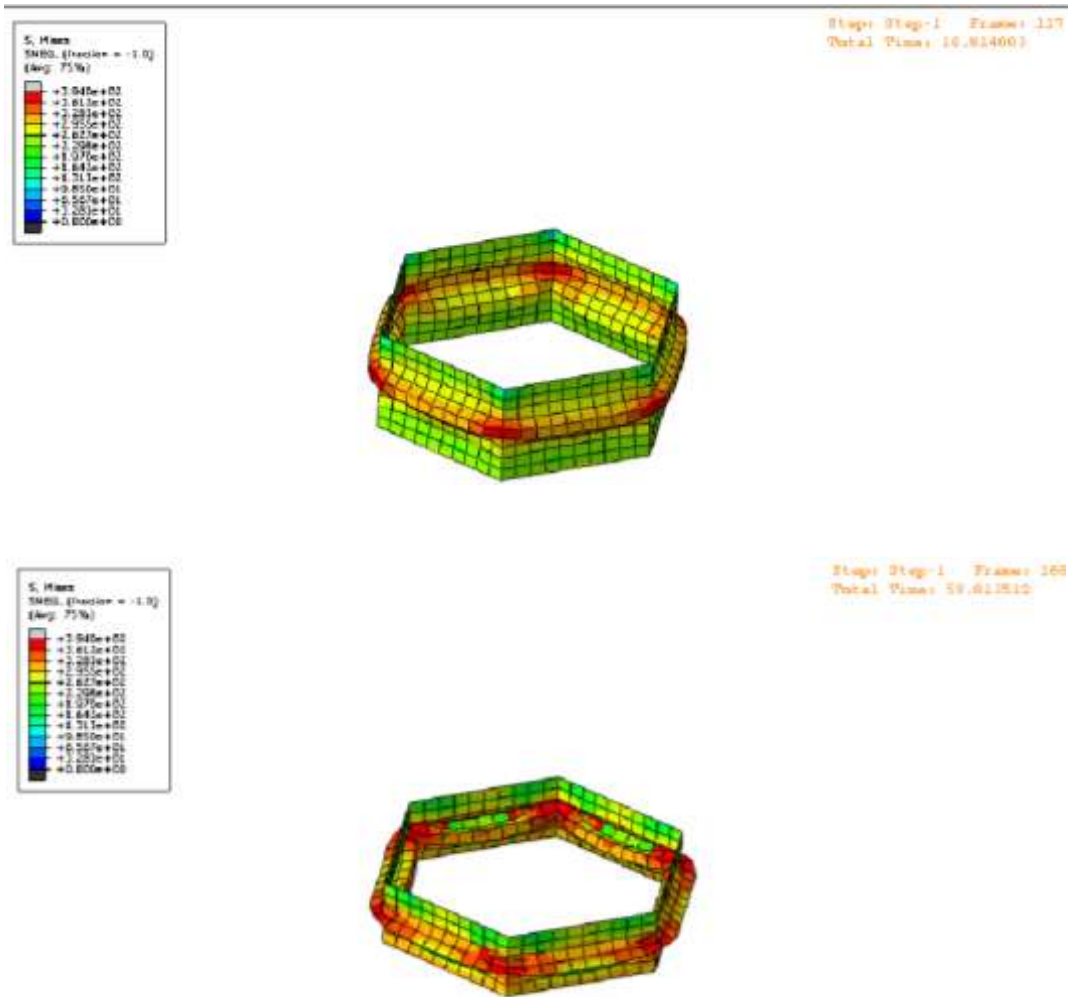
Figure 5.14: Numerical sequence from initial buckling to the total crushing configurations corresponding to perfect cell (AHC d = 19.6 mm).

The crushing involves contact between folds of adjacent cell walls as well as self-contact and consequently both sides of the cell walls were considered for contact. This process ensures that contact occurs at the actual surface of the walls.

The obtained numerical critical buckling loads for different cell size used in this study are depicted in figure 5.15.
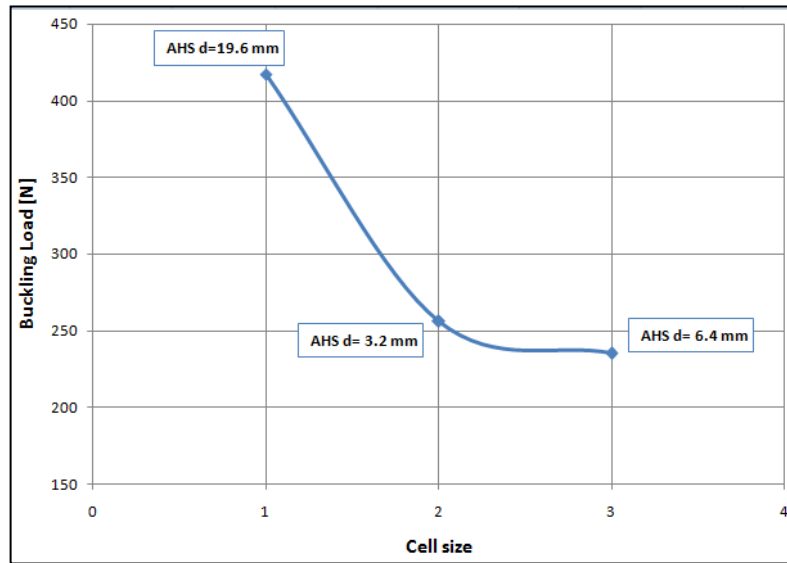
Figure 5.15: Numerical buckling load for different cell size and core materials under low-velocity impact conditions.

V.3.2. Finite element Results and analysis for low velocity impact loading

From experimental results it was found that the impactor perforated the upper skin and core and partially damage in the lower skin for impact velocity5 m/s for the both cases (AHC 3.2 mm and AHC 6.4 mm).For these reasons we have used only velocities low than 5 m/s (1.5 and 3 m/s) just to explain the buckling phenomena and influence of impact energy on damage behavior.

From this study, the significance of the velocity impact and cell size is highlighted. In detailed finite element modeling of the low velocity impact of honeycombs, carefully studying the effect of impact energy is discussed.

Figures 5.16-19 show the buckling at eight different time steps during the penetration for the case of 1.5 and 3 m/simpact with a coefficient of friction of 0.3 for tow cell sizes (AHC 3.2 mm and AHC 6.4 mm).

The FE model was able to predict correctly the deformed shape of the panels after the impact tests as shown in Figure 5.16-21. The failure mode observed during the tests was the core buckling as demonstrated by figures 5.16-21 of honeycomb panel with d= 3.2 and 6.4 mm after impact tests at v=1.5 m/s and v=3 m/s.

The plots presented are the contour plots for the equivalent plastic strain at the end of the impact event. This strain is a scalar variable that is used to represent the inelastic deformation in a material. The colored regions represent the yielded regions in the face-sheet and core. The

damage profile on the impacted face-sheets were circular in shape, while the damaged areas in the honeycomb core were localized (buckling), and concentrated mainly in the vicinity of the impact point and in the upper half of the core.
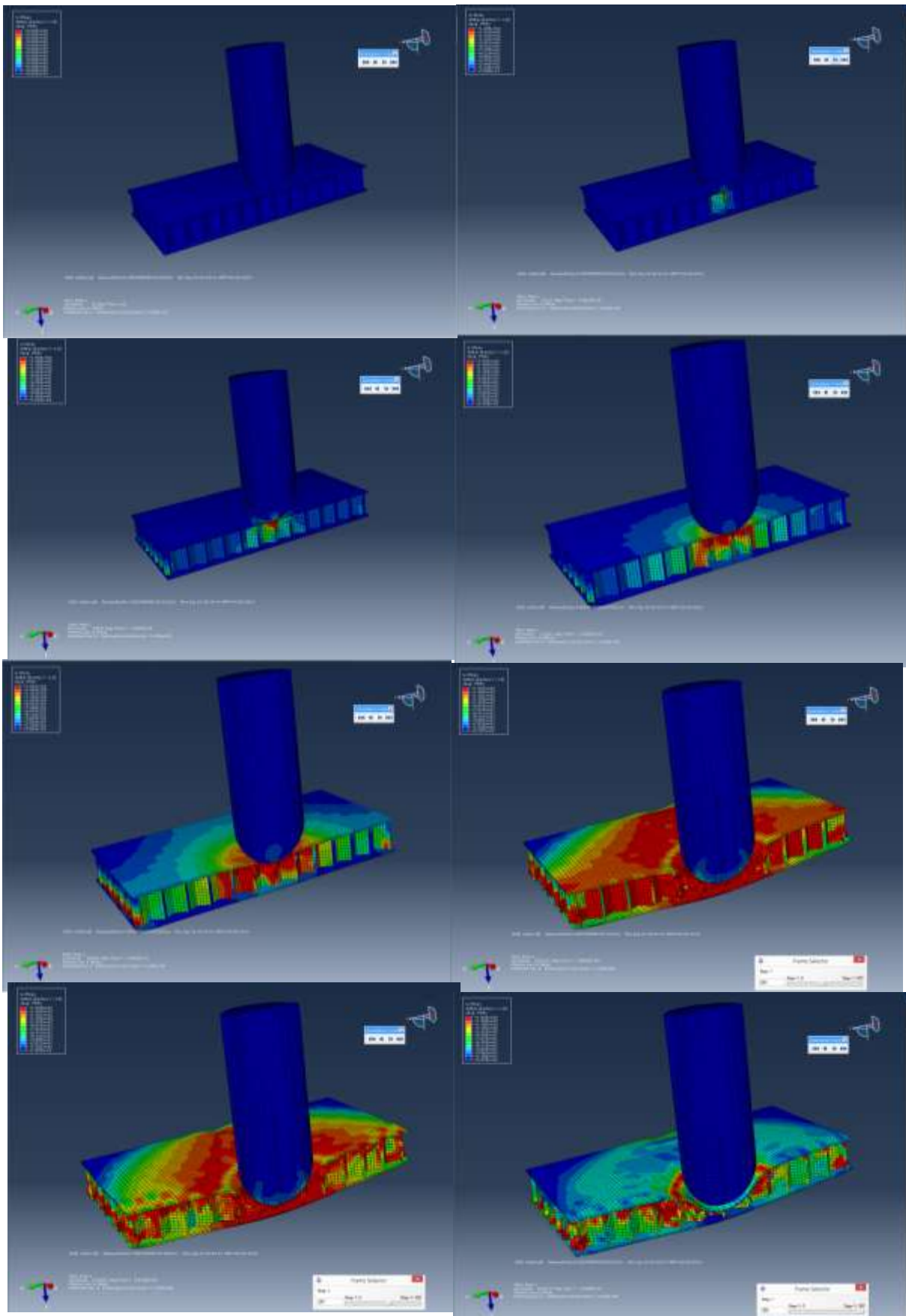
FIGURE 5.16: NUMERICAL SEQUENCE OF DAMAGE IN HONEYCOMB PANEL AFTER IMPACT (D=6.4 MM,V=3 M/S).
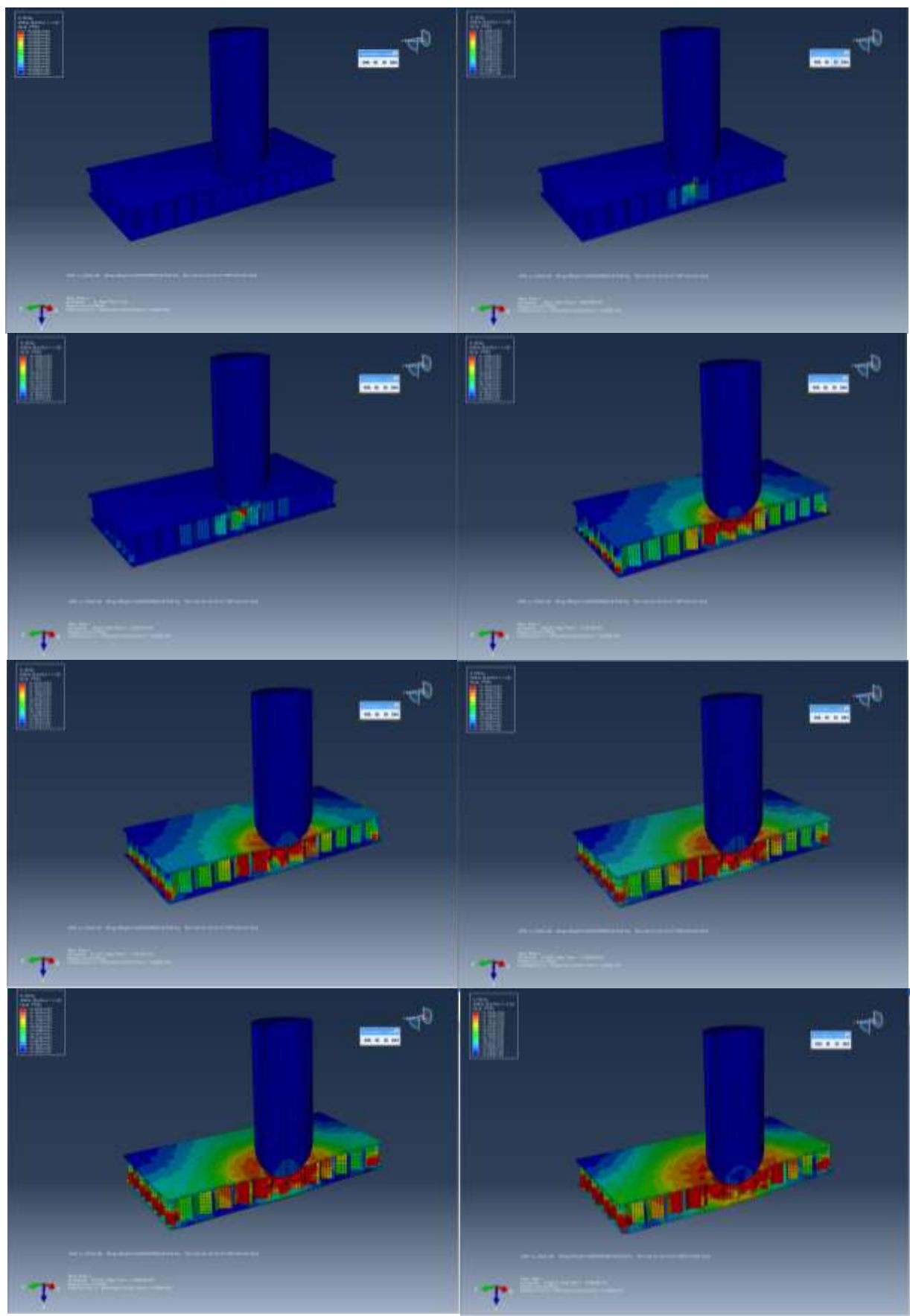
Figure 5.17: Numerical sequence of damage in honeycomb panel after impact (d=6.4 mm, v=1.5 m/s).
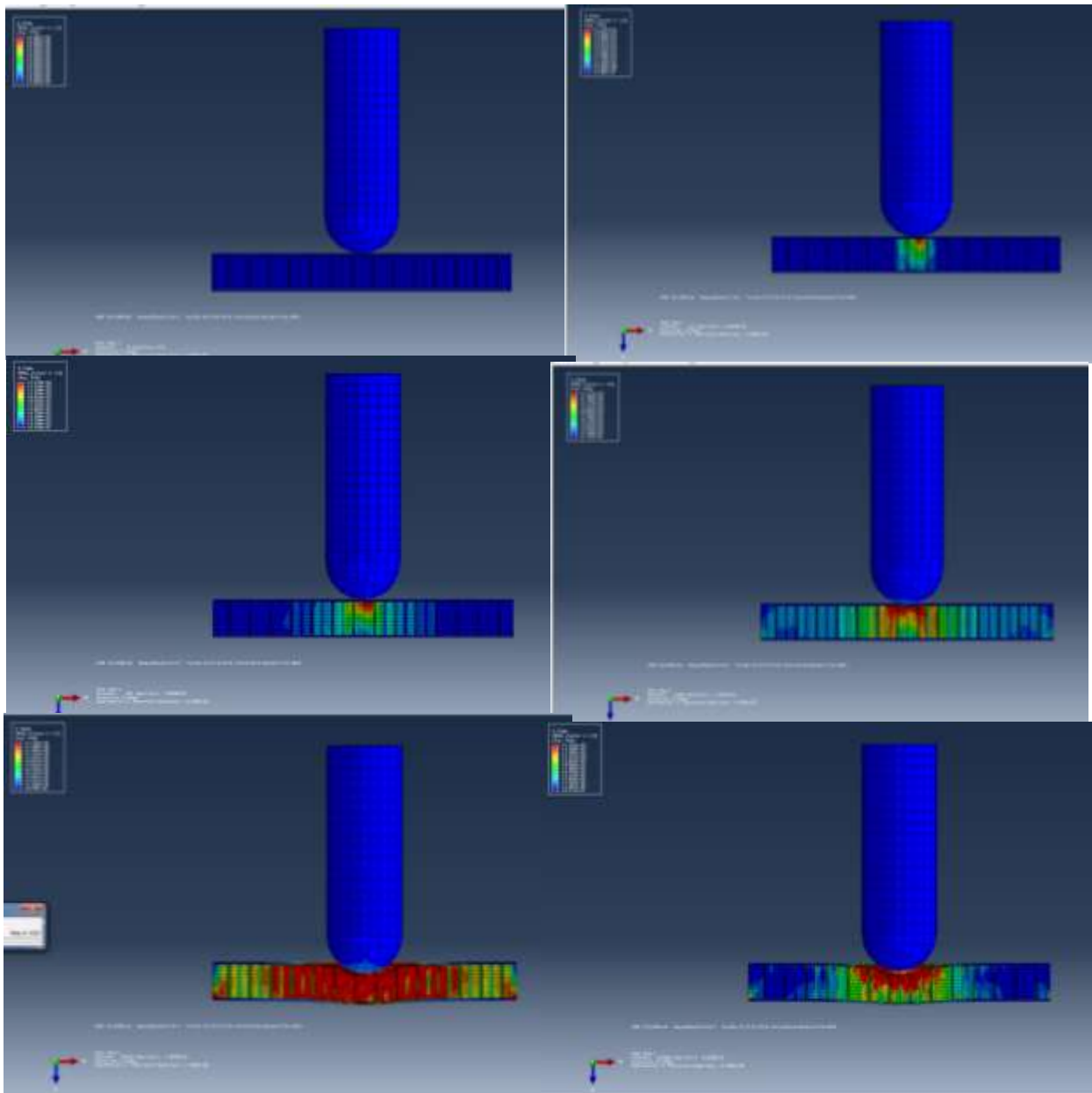
Figure 5.18: Numerical sequence of damage in honeycomb panel after impact (d=3.2 mm, v= 1.5 m/s)
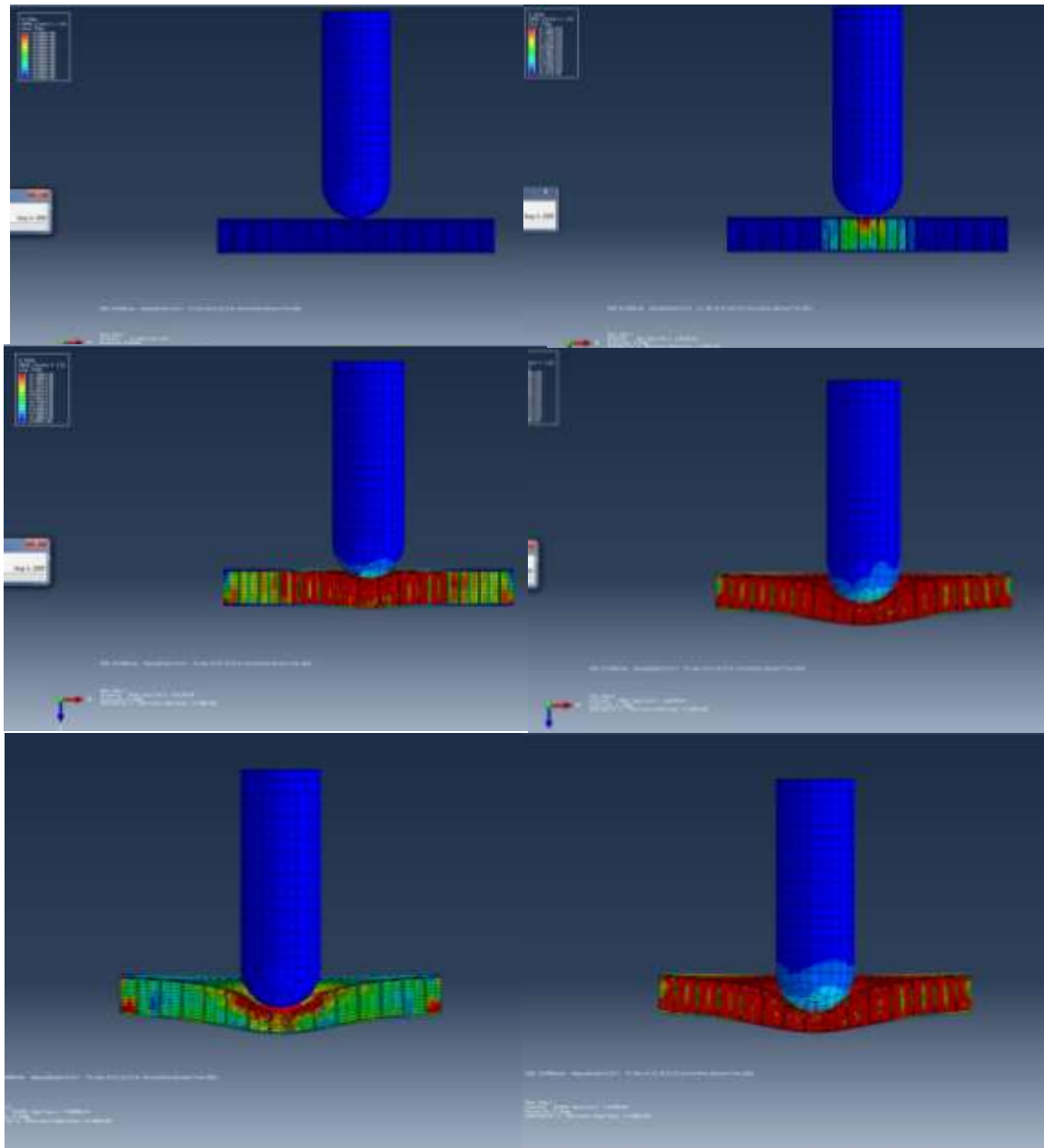
Figure 5.19: Numerical sequence of damage in honeycomb panel after impact (d=3.2 mm, v= 3 m/s)

From the results, core buckling is the most likely damage mode as the load increases as shown in Figures 5.20-21. Damage mode of core buckling is the preferred initiation mode of damage among the three damage modes as this means higher impact resistance.
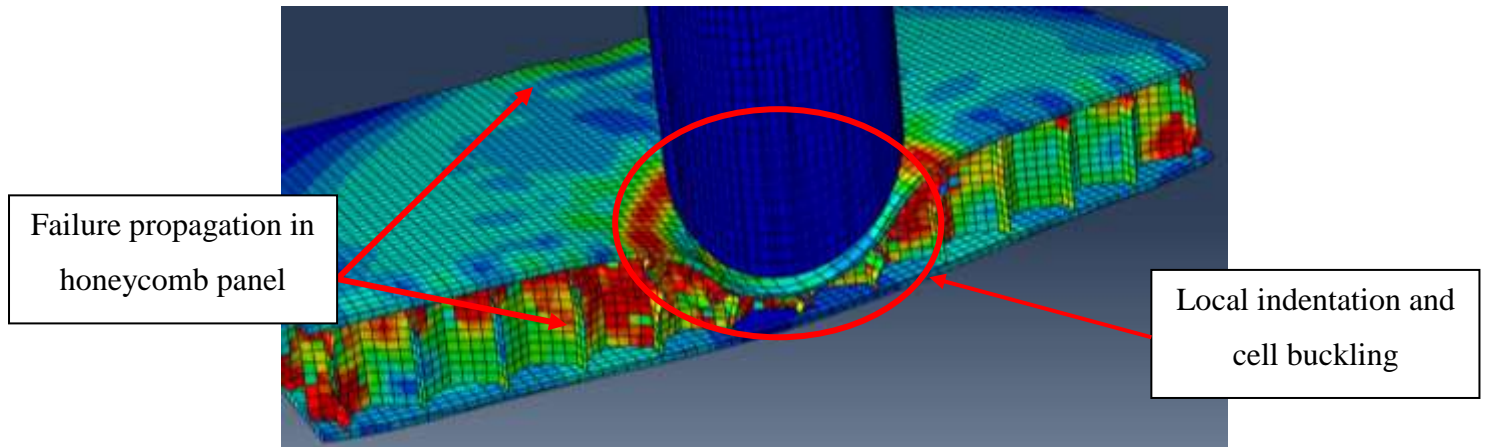
Figure 5.20: Face-Sheet failure and buckling in honeycomb panel subject to low velocity impact loading (AHC d=6.4 mm)
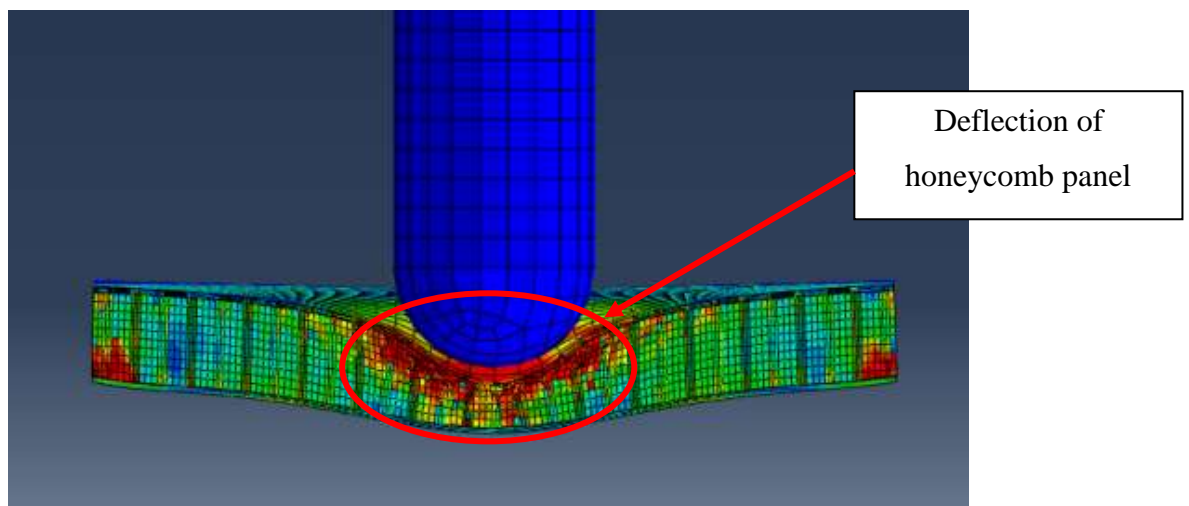
Figure 5.20: Face-Sheet failure and buckling in honeycomb panel subject to low velocity impact loading (AHC d=3.2 mm)

The vertical deflection Wi of the core was measured numerically for two velocities lower than 5 m/s, that did not produce penetration of the panels (1.5 and 3 m/s) for used honeycomb panels (AHC 3.2 and AHC 6.4 mm)and the results are illustrate by figure 5.21. The results are shown in table 5.4.
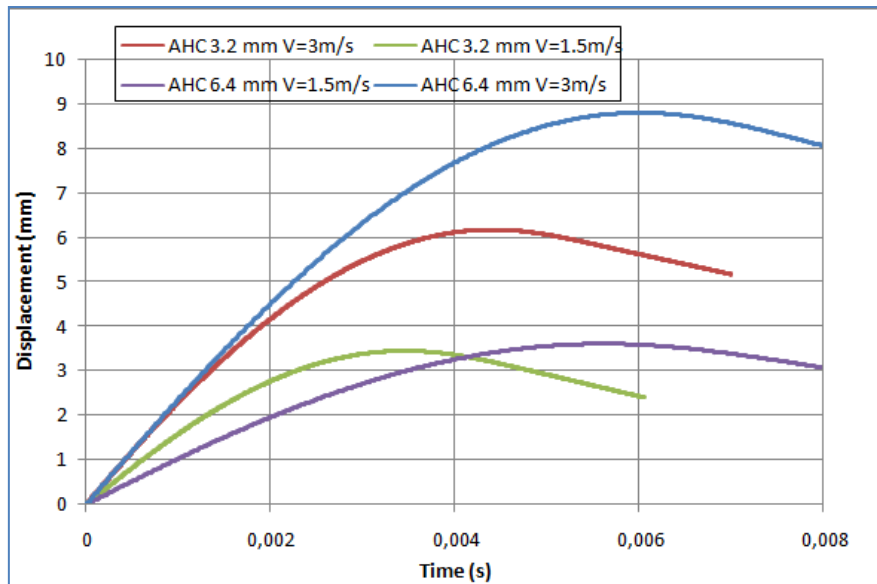
Figure 5.21: Sandwich deflection (Wb) of honeycomb panels with d=6.4 mm (v=1.5, 3 m/s).

The peak loads for the both cases (AHC 3.2 mm and AHC 6.4 mm) at different velocities of impact are depicted in figure 5.22.
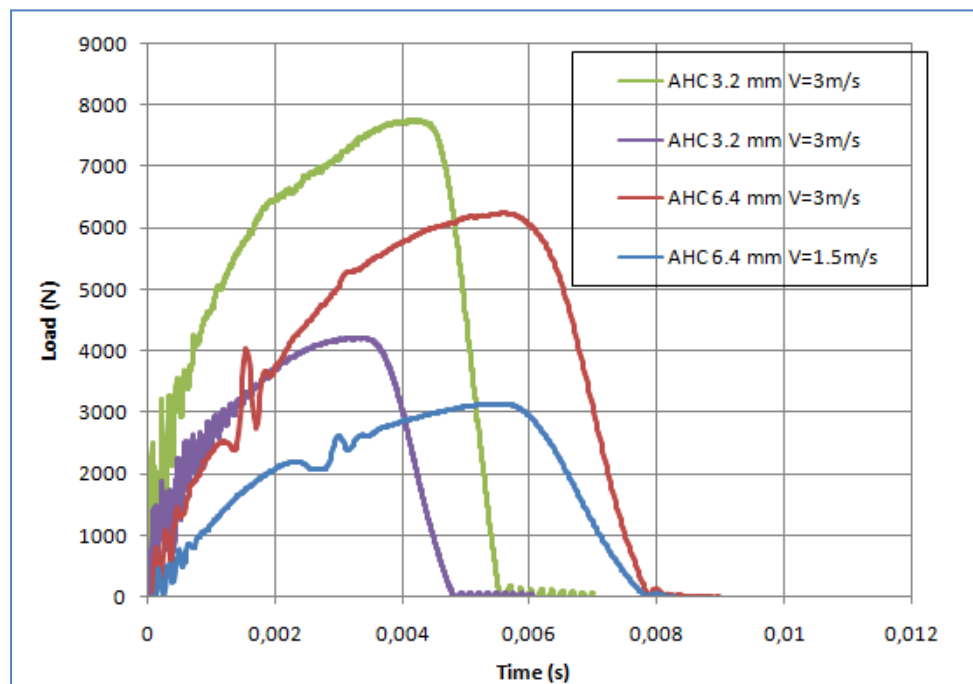
Figure 5.22: Peak load for AHC d=6.4 mm and AHC d=3.2mm (v=1.5 and3 m/s).

141

Table 5.4: *Numerical result of low velocity impact (peak loads and* Wi*).*

	Velocity 1.5 m/s		Velocity 3 m/s	
AHC 6.4 mm	Wi [mm]	3.61	Wi [mm]	8.90
	F num [N]	3103	*F num [N]*	6200
AHC 3.2 mm	Wi [mm]	3.45	Wi [mm]	6.18
	F num [N]	4213	*F num [N]*	7740

V.3.3. Finite element results and analysis for quasi-static indentation loading

Figures 5.23-24reportthenumerical load curve for AHC d=6.4mm and AHC d=3.2 mm. The analysis is carried out applying quasi-static load in the thickness direction on a 100*100 mm^2 plate. In agreement to what expected, the curves show an initial linear elastic and stiff response, then, once reached the maximum value of the force, the curve presents a sharp drop due to the beginning of the vertical edge deformation (buckling of core). During this phase the force reaches a plateau, and finally the diagram shows the condensation phase. The maximum deflections for both panels are given by Figures 5.25-26 As can be seen ; numerical results behave in accordance with experiments (Figure 5.25). As for the honeycomb core the numerical results are in good agreement with the experimental ones. Both cores initially show linear elastic and stiff response, followed by elastic–plastic behavior, without work hardening. After this phase, the material cannot absorb further energy, thus stress rises sharply without significant increase of the strain.
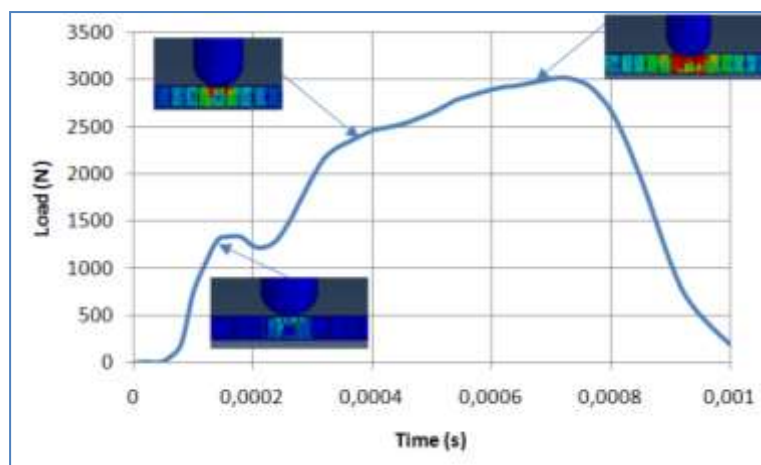
Figure 5.23: Crushing behavior of an aluminum honeycomb panel with d=6.4 mm.
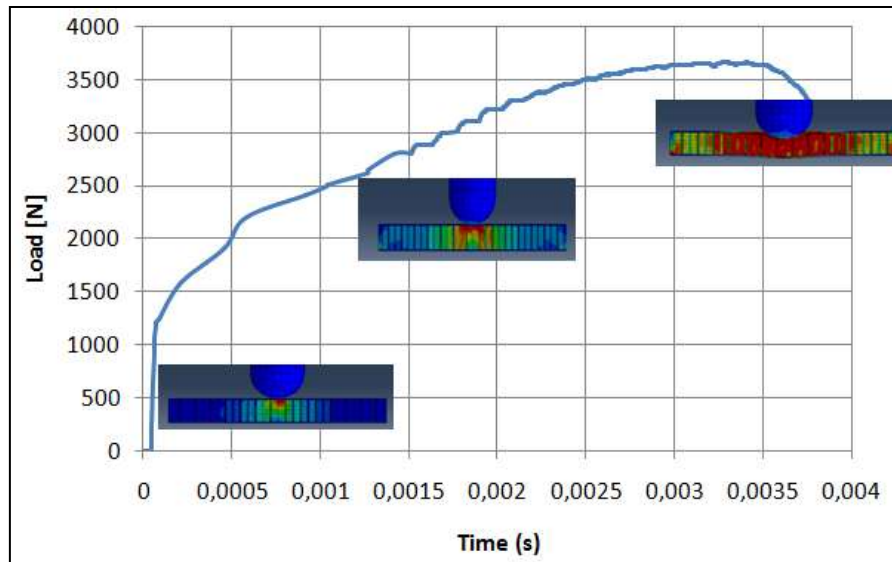
Figure 2.24: Crushing behavior of an aluminum honeycomb panel with d=3.2 mm.
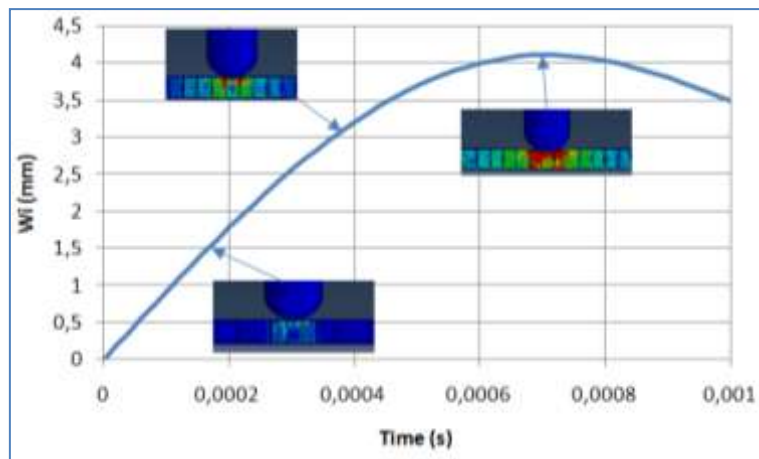
Figure 5.25: Max indentation Wi of an aluminum honeycomb panel with d=6.4 mm.
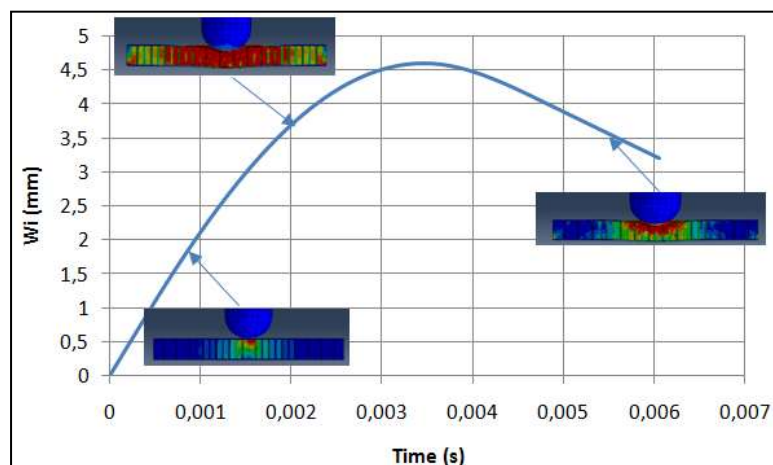
Figure 2.26: Max indentation Wi of an aluminum honeycomb panel with d=3.2 mm.
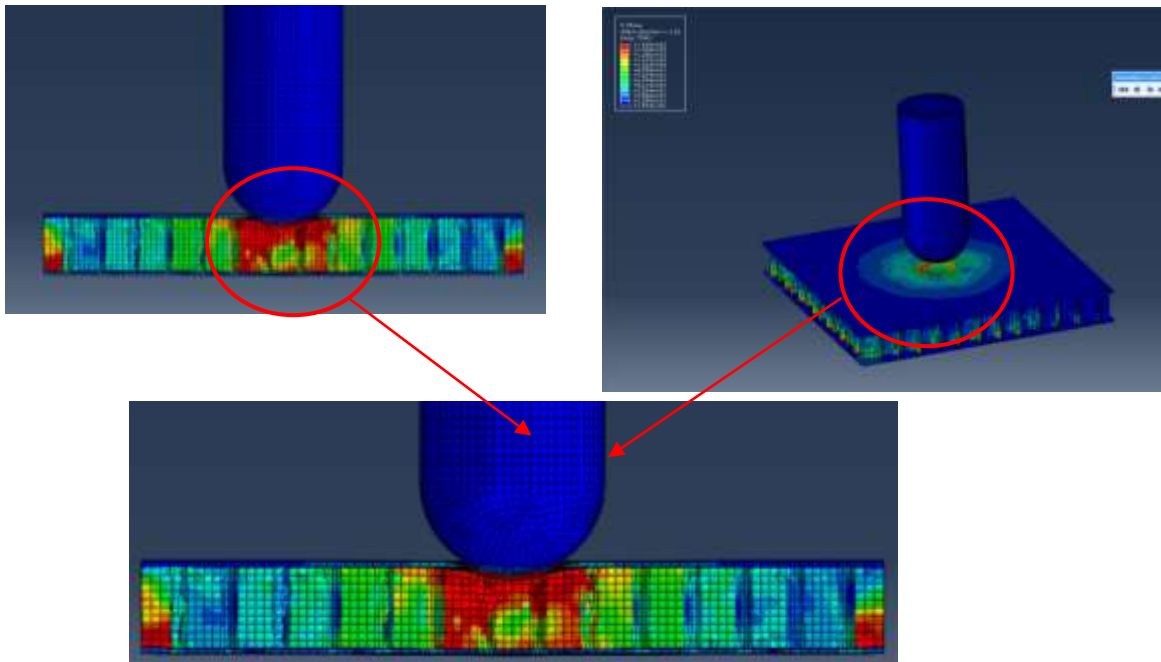
Figure 5.27: Numerical model of an AHC d=6.4 mm under quasi-static indentation loading (local indentation failure, detail of damaged area).

The results are shown in table 5.5.

Table 5.5: Numerical result of quasi-static indentation loading.

Cell size	α_{num} [mm]	F_{num}[N]
AHS (d=6.4mm)	4.1	3022
AHS (d=3.2mm	4.6	3623
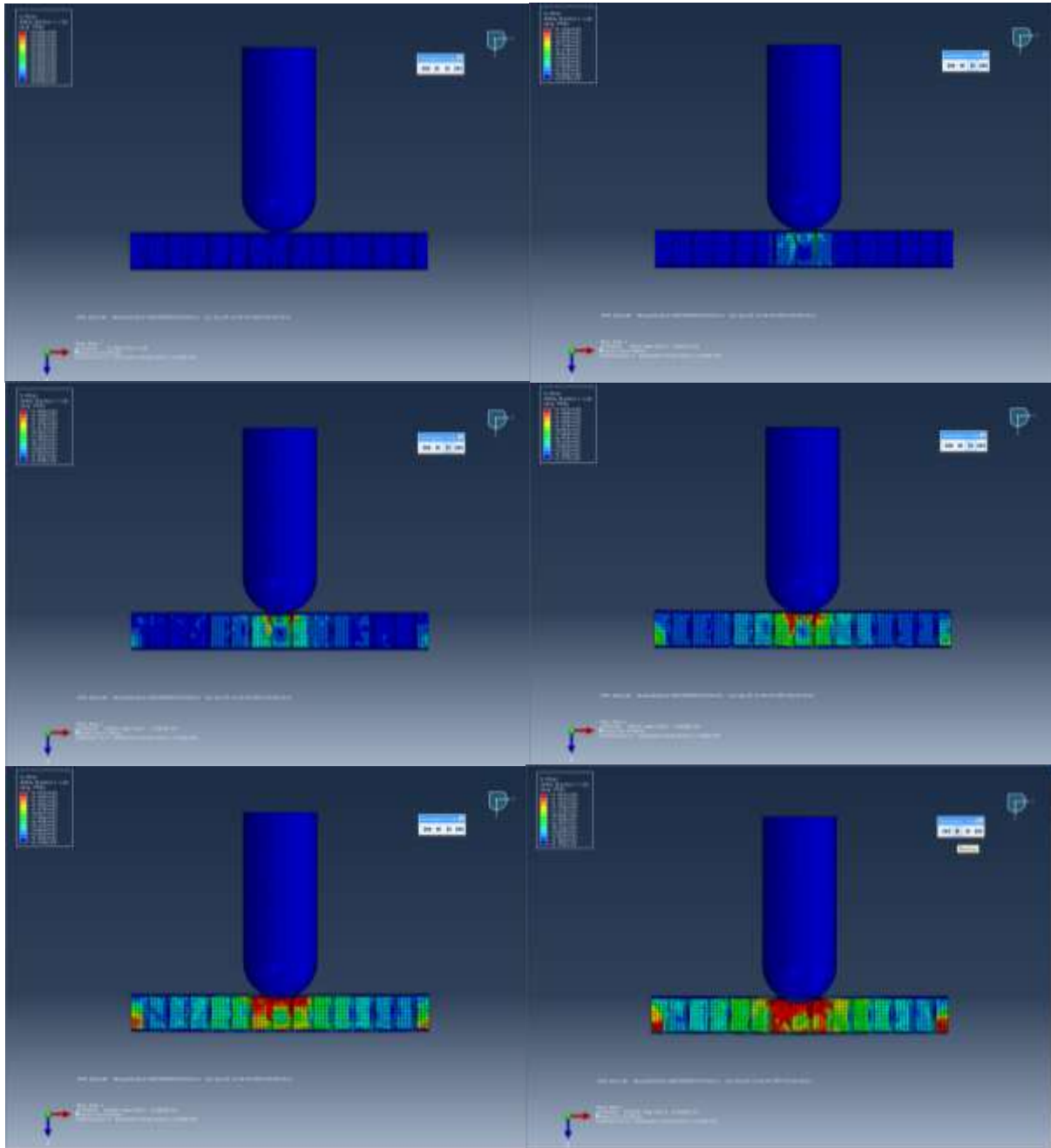
Figure 5.28: Detailed numerical damage shape at different indenter displacements (AHC d=6.4 mm).

CHAPTER VI:

Comparison of Experimental, Theoretical and Finite element analysis Results (compressive, quasi-static indentation and low-velocity impact tests).

This chapter presents the summery of our work; it covers the comparison of experimental, theoretical and finite element analysis. The critical buckling loads and failure modes, obtained for different cell sizes from experimental study are compared with those obtained theoretically with the model that was been developed in chapter IV and numerically using ABAQUS package program (chapter V). The achieved experimental, theoretical and numerical results are compared with each other and the results are provided in curves and tables.

VI.1. Comparison of experimental, theoretical and finite element analysis results of honeycomb sandwich panel subjected to compression loading conditions

As a first step, an attempt was made to validate the numerical model with experimental results obtained under compression loading. A comparison of experimental and numerical predicted data for compression test of AHS for different core cell's size (AHS 19.2, 6.4 and 3.2 mm) is given in Fig. 6.1.
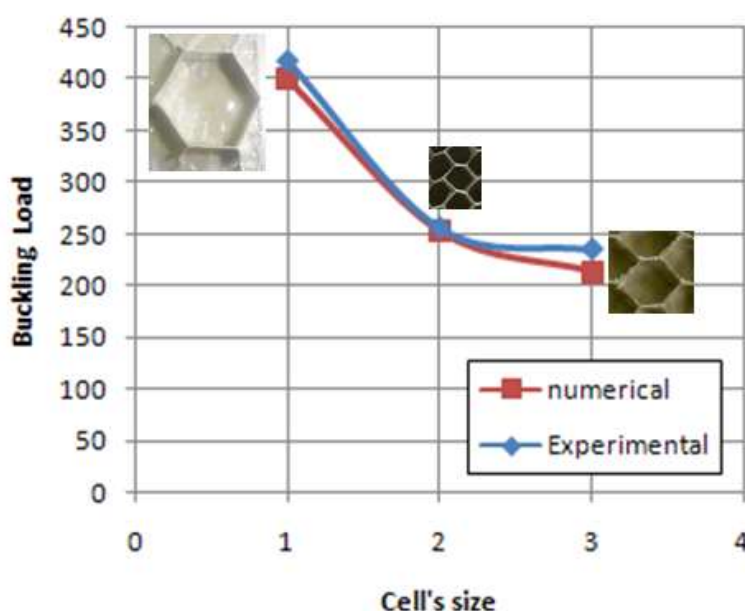
Figure 6.1: Comparison of numerical and experimental data for compression loading (AHC 19.2, 6.4 and 3.2 mm).

The sets of results demonstrate a good agreement, and this illustrates the capability of the numerical model to predict the buckling event adequately. The largest error recorded was 5.1 % for the predicted buckling load in the case of AHS 6.4 mm.

Figs 6.2-5show a typical numerical failure process in honeycomb sandwiches structures obtained from the compressive test of aluminum honeycomb sandwich panel (AHS). The compressive deformation process obtained with numerical code (ABAQUS) as some in experimental results can be categorized into core buckling and crushing. The failure, started as a cell wall buckling, caused cracks at greater compressive loads.

148

In figures6.2-4, the experimental and numerical deformation condition of AHS 19.2 mm and AHS 6.4 mm specimens under the critical buckling load are given. It is seen that the experimental and numerical deformation conditions are rather coherent.
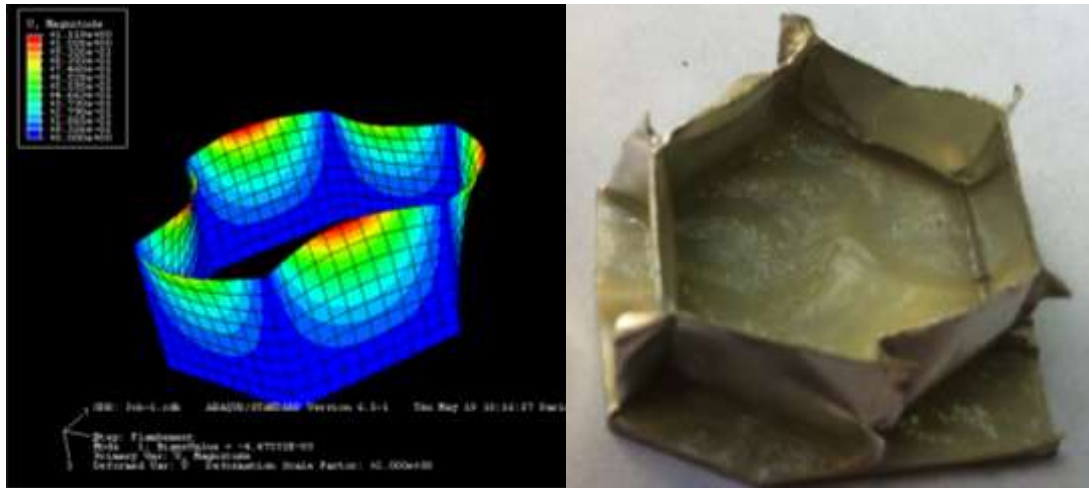
Figure 6.2: First buckling modes for domains with 1 cell (ahs d=19.2 mm)
A) Numerical and b) experimental deformation.

Honeycomb crushing involves severe local bending of and contact between the walls of the folds (buckled cells). Consequently, in contrast to the prebuckling and initial postbuckling calculations described above, crushing was performed using ABAQUS/Explicit due to the computational efficiency that it affords. The basic calculations involve the characteristic one cell had shown before with a mesh of 5850 S4 elements (convergence study chapter V).

(a) **(b)**
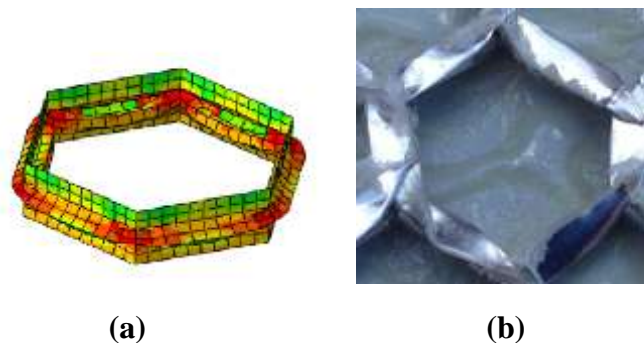
Figure 6.3: Crushing of honeycomb cell (AHC d=19.2mm):a) numerical and b) experimental deformation.

(a)   **(b)**
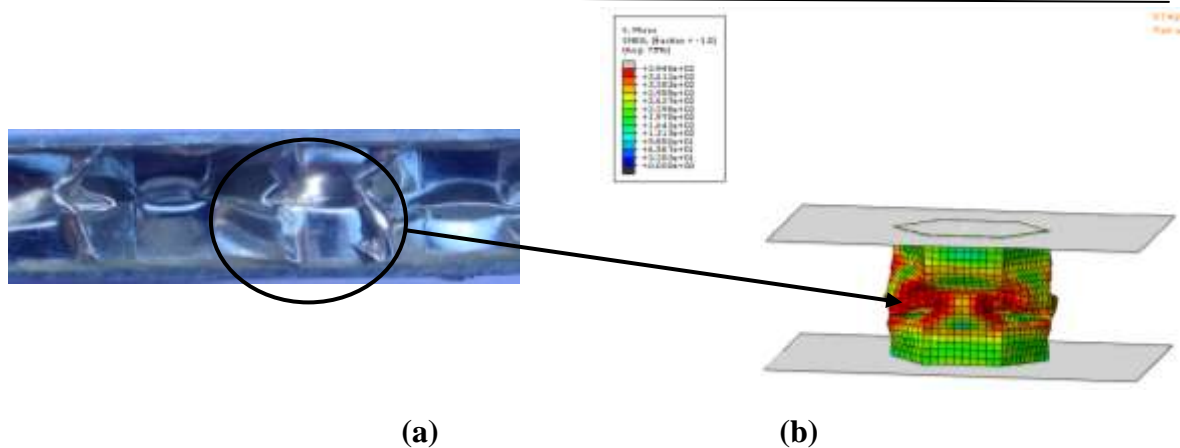
Figure 6.4: Crushing of honeycomb core (AHC d = 6.4 mm):a) experimental and b) numerical deformation.

A typical crushing response from such a simulation is shown in Fig. 6.5 along with one of the experimental responses.
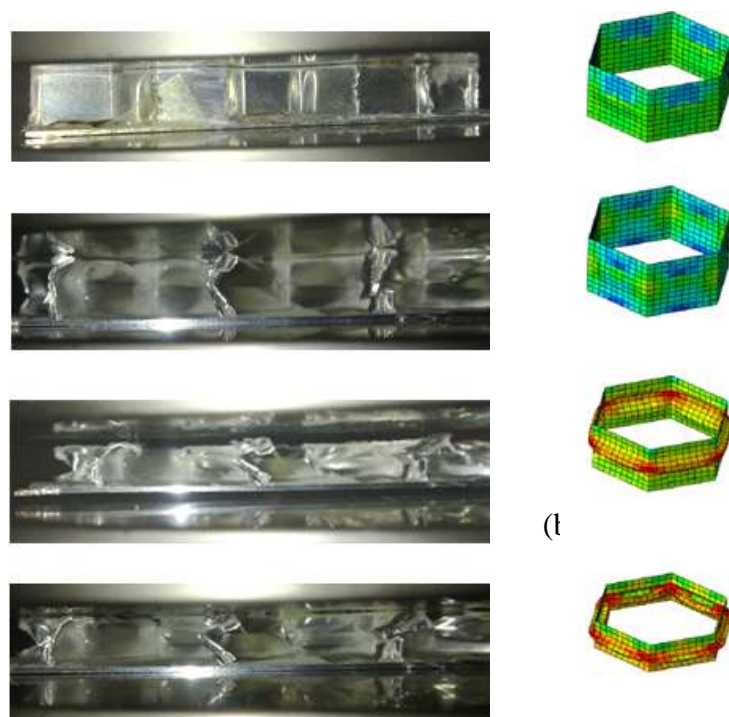
Figure 6.5: Sequence from initial buckling to the total crushing configurations corresponding to perfect cell (AHC d = 19.6 mm): (a) experimental and (b) numerical.

In meantime, an analytical model which has been developed in chapter IV was used to derive the critical buckling load of the aluminum (AHS) and nomex (NHS) sandwich plate. Fig. 6.6 depicts the peak load of buckling for the different used cell's size for two materials. Results

150

were compared with test data, as well as simulation results. The comparisons indicate that a good agreement existed between the experimental and predicted results, in terms of peak load and overall profile.
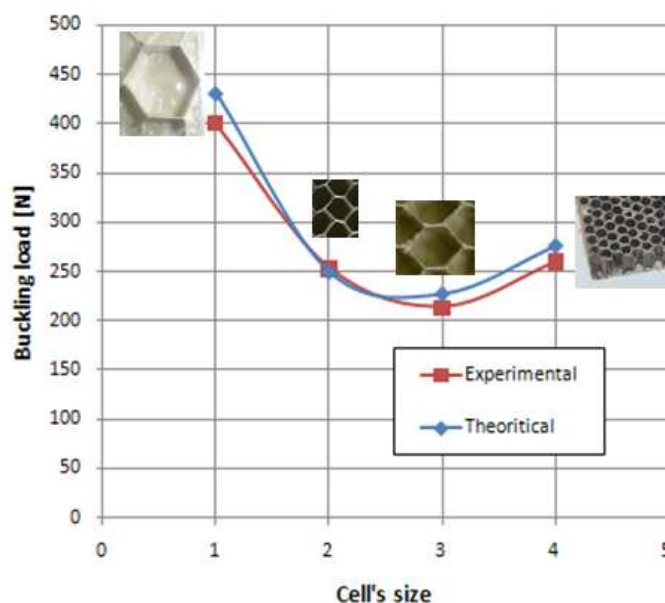
Figure 6.6: Comparison of buckling peak load obtained from theoretical approach and experimental test of compressed specimens (AHC 19.2, 6.4, 3.2 mm and NHC 3.2 mm).

The analytical model was able to predict the critical buckling reasonably well. The largest error recorded was 7.8 % for the predicted buckling load in the case of AHS 19.2 mm.

Figure 6.7 shows the summery comparison between experimental, analytical and numerical critical buckling loads for the different cell size used in our study (AHS 19.2, 6.4, 3.2 mm).

The experimental value of the critical load F_{exp} was divided to the number of the cells of the investigated sandwiches, obtaining the critical load for a single cell $F_{exp\ (cell)}$, which was compared to the value predicted by the developed theoretical approach (chapter V) using eq. (5) and the numerical model obtained with ABAQUS (chapter IV). The results are reported in Table 6.1.
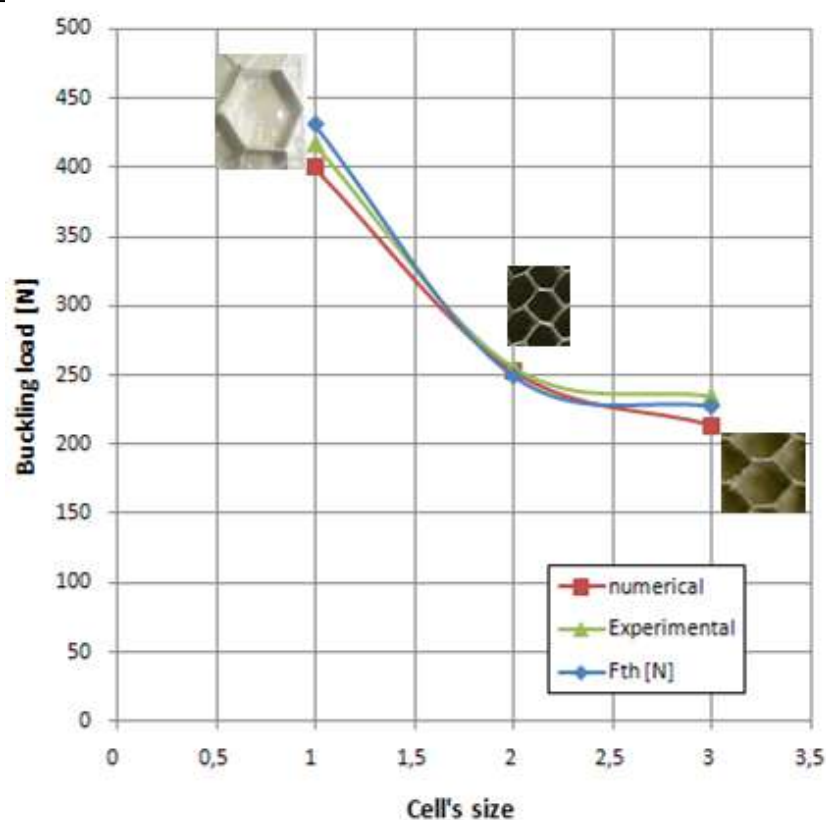
Figure 6.7: Summery of obtained buckling load under compression loading (AHC 19.2, 6.4, 3.2 mm).

Table 6-1: Summery comparison of FEA, Experimental and Theoretical data for compression tests.

Cell size	F_{exp}[N]	$F_{exp\ (cell)}$ [N]	$F_{th\ (cell)}$ [N]	Error %	$F_{num\ (cell)}$ [N]	Error %
NHS (d=3.2mm)	35921	260	276	6.1	-	-
AHS (d=6.4mm)	29569	214	227	6	225	5.1
AHS (d=3.2mm	34958	253	249	1.6	256	1.2
AHS (d=19.2mm)	4150	400	431	7.8	417	4.2

Finite element analysis and theoretical approach developed previously had reasonable agreement with experimental results with an average percentage error of 1.2% and maximum percent error of 7.8%.

VI.2. Comparison of experimental, theoretical and finite element analysis results of honeycomb sandwich panel subjected to quasi-static indentation loading conditions

The buckling load of the quasi-static indentation of a hemispherical indenter through a honeycomb cells is discussed in the following sections.

All cells have a fixed size of 3.2 and 6.4 mm and while the indenter is 20 mm in diameter. All cell walls have the same thickness of 0.08 mm.

Fig.6.8 shows peak load using a hemispherical indenter with a diameter of 20 mm. The indentation resistance decreases with increasing the cell size. This can be explained by the fact that the stiffness of the sandwich panel increases with the increase of the density of the core [16-19]. Also the cell size induces relevant effects on the mechanical performances of the samples under static indentation load.

However, the cell size has a large influence on the ultimate failure of the face. However, the damaged area was proportional to the cell size and diameter of the indenter. The maximum indentation buckling load was observed for different cell size and core materials and the results are depicted in figure 6.8.
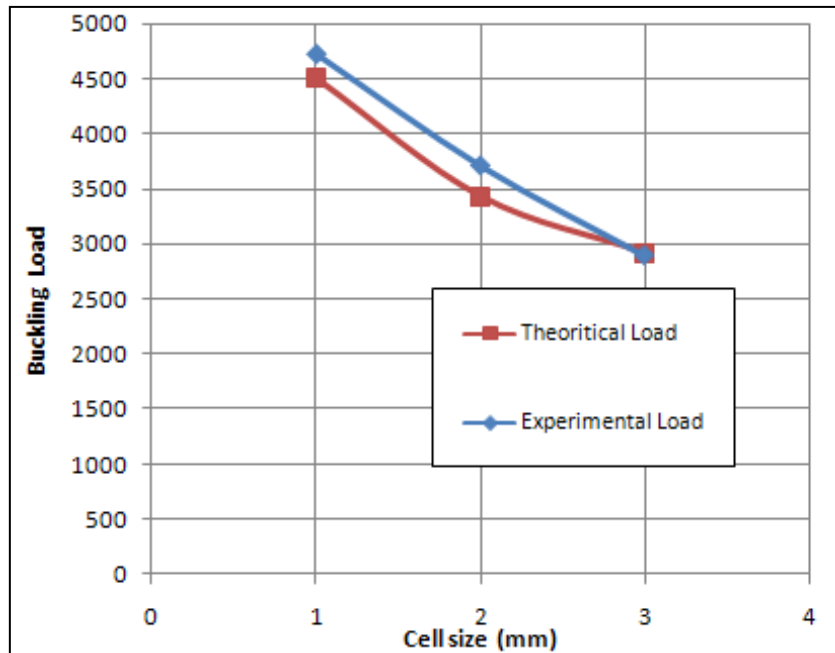
Figure 6.8: Comparison of buckling peak load obtained from theoretical approach and quasi-static indentation test (AHC 6.4, 3.2 mm and NHC 3.2 mm).

The experimental values of the critical load F_{exp} were compared to the value predicted by the developed theoretical approach (paragraph 2.2) using eq. (7) and numerical value obtained with ABAQUS.Table6.2 reports all the results.
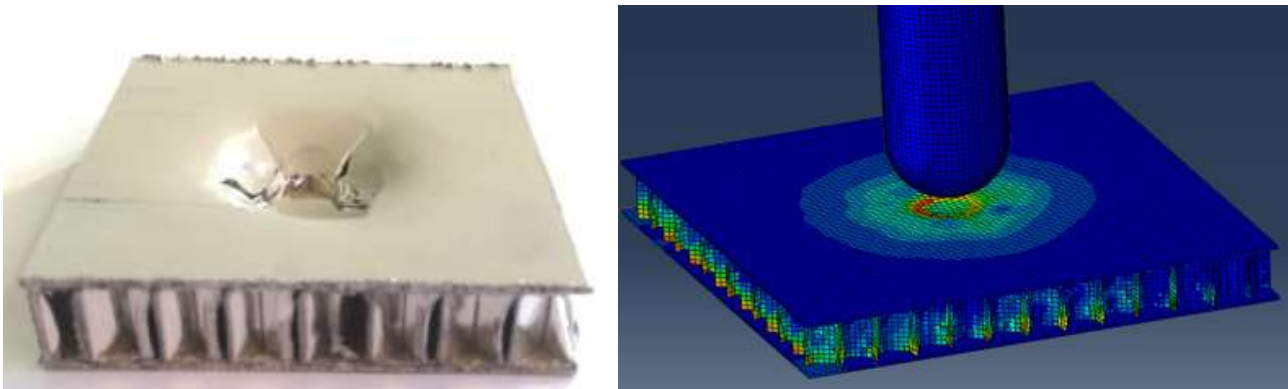
Figure 6.9: Typical failure modes observed during indentation: core crushing and failure of face.
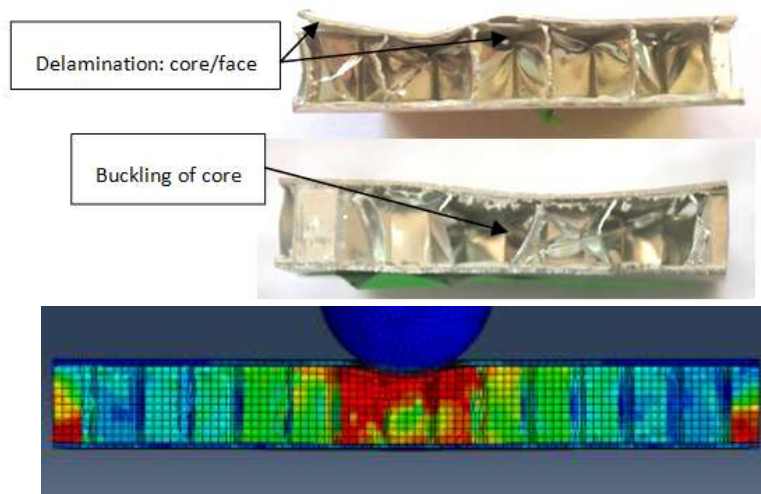
Figure 6.10: Typical failure modes observed during indentation: core crushing and failure of face.

As can be seen, numerical results behave in accordance with experiments. As for the honeycomb core the numerical results are in good agreement with the experimental ones. Both cores initially show linear elastic and stiff response, followed by elastic–plastic behavior, without work hardening .After this phase, the material cannot absorb further energy, thus stress rise sharply without significant increase of the strain.

Table 6-2: *Comparison of FEA, Experimental and Theoretical data for indentation loading.*

Cell size	R_i [mm]	α [mm]	α_{num} [mm]	F_{exp}[N]	F_{th}[N]	*Error %*	F_{num}[N]	*Error %*
NHS (d=3.2mm)	20	4	-	4500	4717		-	
AHS (d=6.4mm)	20	4.3	4.1	2914	2891	0.78	3022	3.7
AHS (d=3.2mm	20	4.9	4.6	3426	3706	8.17	3623	5.75

VI.3. Comparison of experimental, theoretical and finite element analysis results of honeycomb sandwich panel subjected to Low-velocity impact loading

The tomograms of the panels after impact tests have been compared with the results of the numerical simulations of the impact and theoretical model (Figs.6.11-13). Moreover, the FE results were validated by means of experimental data for honeycomb core with cell size of 6.4 mm.
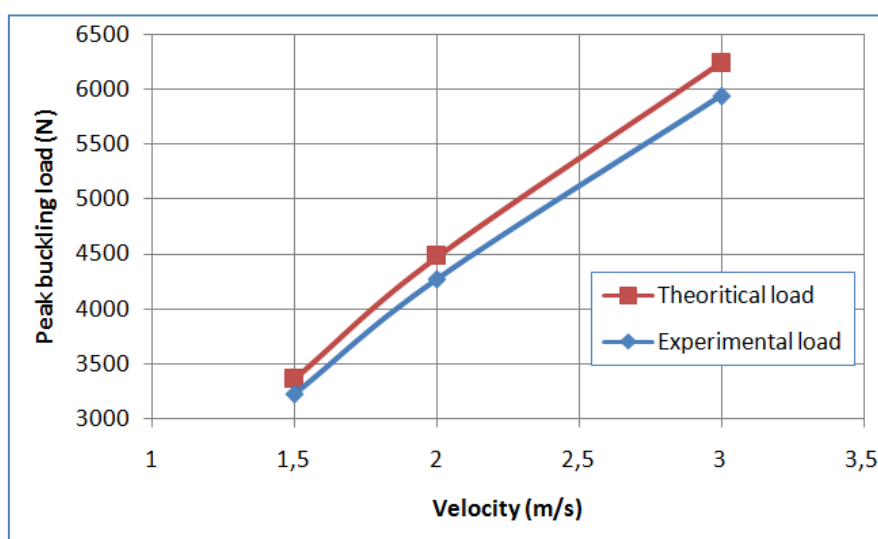
Figure 6.11: Comparison of buckling peak load obtained from theoretical approach and impact test (AHC 6.4 mm).

The observed damage initiations from the experimental results are compared with those predicted using the finite element analysis (Figs.6.14-15). A summary of the comparison is tabulated in Tables 6.3-5. The damage modes predicted using finite element analysis and that predicted using the theoretical approach gave consistent results for AHS 6.4 mm and AHC 3.2 mm.
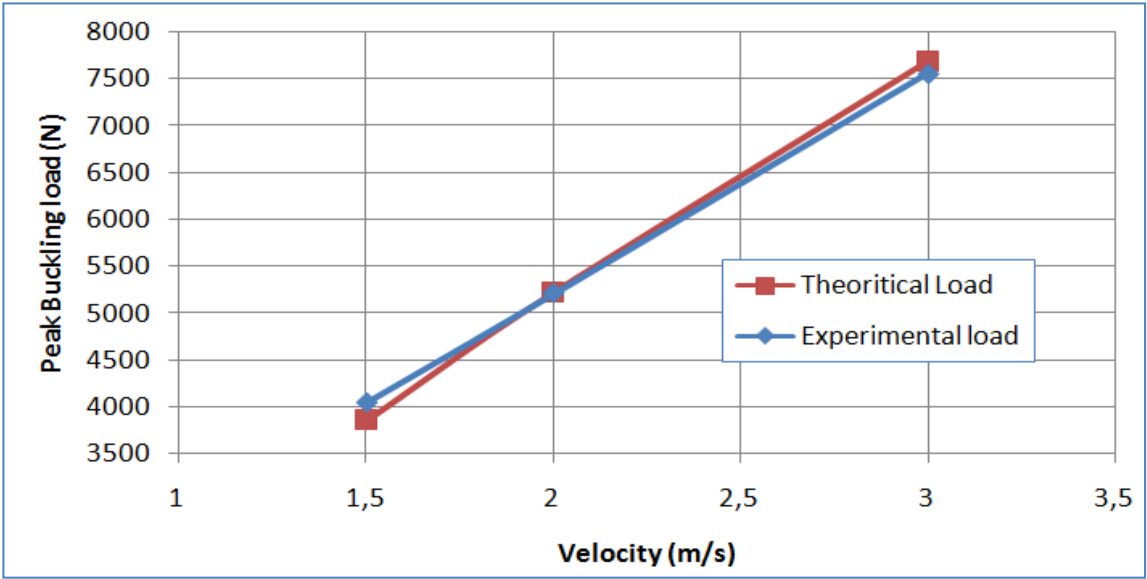
Figure 6.12: Comparison of buckling peak load obtained from theoretical approach and impact test (AHC 3.2 mm).
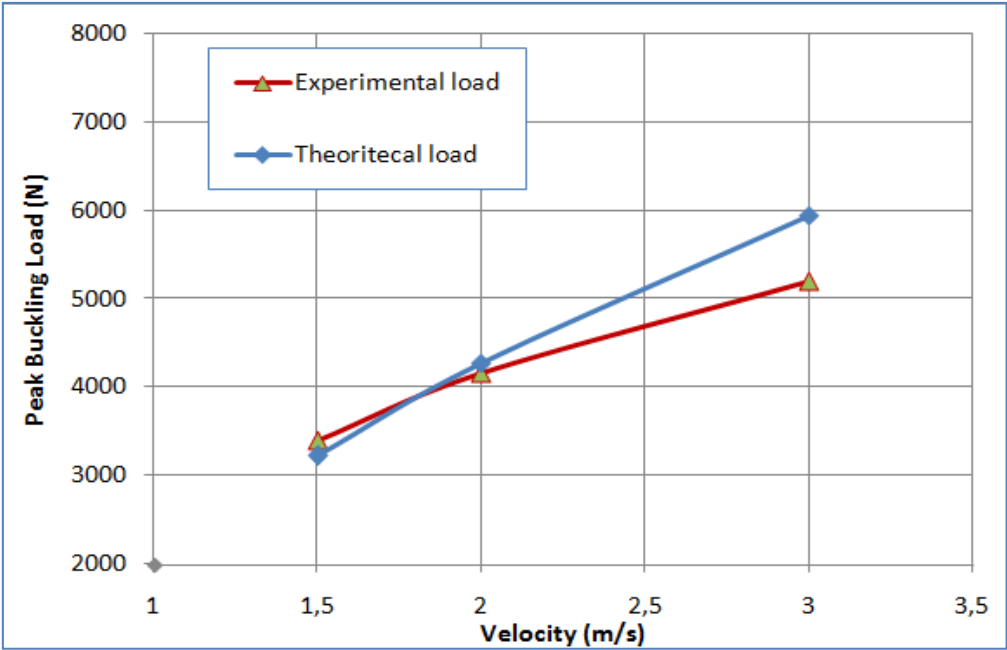
Figure 6.13: Comparison of buckling peak load obtained from theoretical approach and impact test (AHC 3.2 mm).
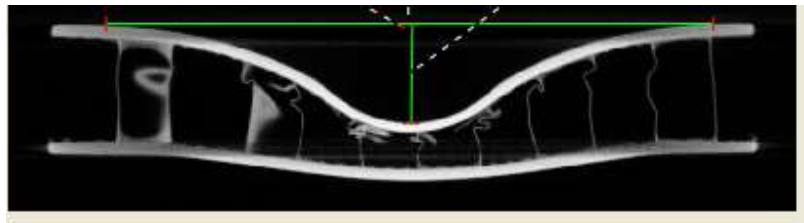
(a)
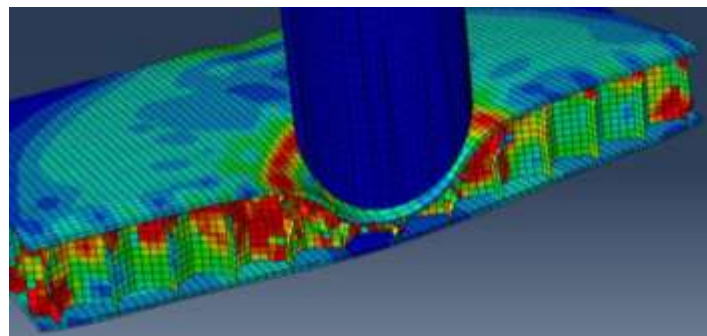
(b)

Figure 6.14: Deformed shapes of honeycomb panel (d=6.4 mm) after impact test (v=3 m/s): CT image, (b) finite element (FE) model.
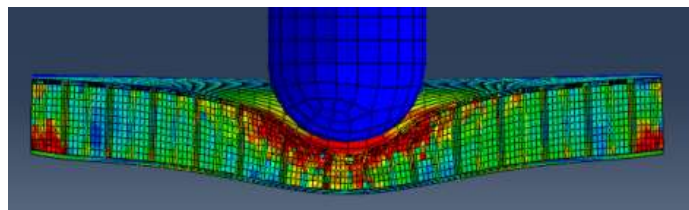
(a)
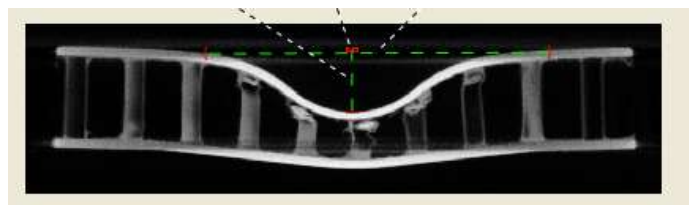
(b)

Figure 6.15: Deformed shapes of honeycomb panel (d=3.2 mm) after impact test (v=3 m/s): CT image, (b) finite element (FE) model.

The direct comparison has been done by superimposing the deformed images obtained from FE analyses and from 3D CT space reconstructions. The numerical model was also validated comparing the FE results with experimental data.

The collapse mechanism of the honeycomb sandwiches occurred for the buckling of the cells (Figures 6.14-15). The tomography investigations have shown that the collapse of the panel occurs for the initial deformation of the upper skin and for the buckling of the core cells. The dominant failure mode observed during the tests was the core buckling before total perforation of the panels as demonstrated by the CT images after impact tests (Figures 6.14-15).

The experimental values of the critical load F_{exp} were compared to the value predicted by the developed theoretical approach (paragraph 2.3) using eq. (25). Tables 6.4 and 6.5 report the results of all the experimental tests in terms of contact force peak and predicted critical loads and their comparison also the deflection of panel.

Table 6-3:Comparisonof Experimental and Theoretical data under impact loading at different velocities (NHS 3.2 mm).

v [m/s]	NHS (d=3.2mm)				
	α [mm]	F_{exp}[N]	F_{th}[N]	F_{num}[N]	δ [%]
1.5	4.9	3558	3404	-	4.3
2	5.1	4594	4155	-	9.5
3	6.9	5758	5200	-	9.6

Table 6-4: Experimental and predicted critical loads of AHS panels under impact loading at different velocities (AHS 3.2 mm).

v [m/s]	AHS (d=3.2mm)					
	α [mm]	αnum [mm]	F_{exp}[N]	F_{th}[N]	F_{num}[N]	δ [%]
1.5	3.12	3.45	3849	4043	4213	5
2	4.27	4.12	5215	5210	5247	0.1
3	6.89	6.18	7683	7560	7740	1.6

Table 6-5: Experimental and predicted critical loads of AHS panels under impact loading at different velocities (AHS 6.4 mm).

v [m/s]	AHS (d=6.4mm)					
	α [mm]	αnum [mm]	F_{exp}[N]	F_{th}[N]	F_{num}[N]	δ [%]
1.5	3.66	3.61	3361	3222	3103	1.1
2	5.33	5.16	4476	4269	4527	4.6
3	8.34	8.90	6239	5939	6200	4.8

The values of the peak force (Fmax) and deflection of honeycomb panel (Wi), obtained from FEAs and experimental tests at different impact velocities are shown in Figure 6.16 and 6.17. It can be seen that the results of FE simulations are in good agreement with experimental data. The differences are higher for impact velocity of 1.5 m/s, obtaining errors equal to about 8% while the obtained deviations are less than 2 % and 8% for deflection of the panels (Wi).
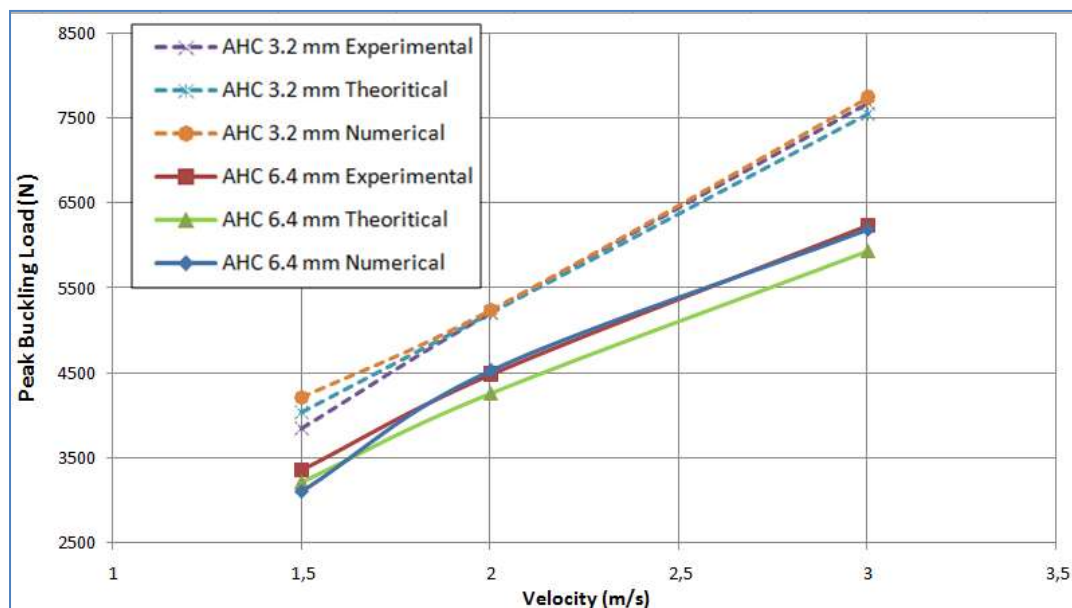
Figure 6.16: Comparison of numerical, theoretical and experimental buckling load of honeycomb panel at different velocities for AHC 3.2 mm and AHC 6.4 mm.
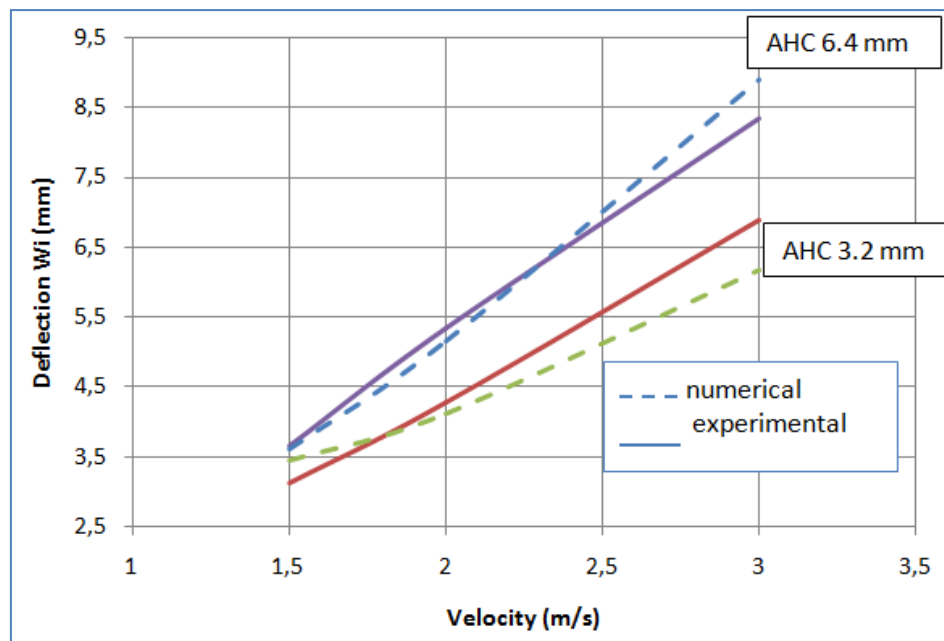
Figure 6.17: Comparison of deflection Wi numerical and experimental of honeycomb panel at different velocities (AHC 3.2 mm and AHC 6.4 mm)

CHAPTER VII:

CONCLUSIONS

Honeycomb sandwich panels are contemporary technological structures with a wide utility range. The cell size, wall thickness, core material and surface sheet materials are parameters that have to be determined coherent to the usage area and intention of the honeycomb sandwich structures optimally.

In this study aluminum and nomex honeycomb sandwich panels (AHC and NHC) with different cell size (3.2, 6.4, 9.6 and 19.2 mm) were used and the critical buckling loads were experimentally, theoretically and numerically determined by applying static, dynamic and fatigue tests on these structures (compression, quasi-static indentation, low velocity impact and repeated impact loading condition). Resulting from the performed tests, the incurred failure modes at the AHC and NHC panels were investigated and tried to determine the failure mechanisms.

The following are the obtained results of the study:

- The honeycomb compressive behavior intrinsically relates to the cell wall buckling behavior under in-plane compression, because in reality the vertical cell walls can never be compressed along the length direction until a pure compressive failure due to the instability of the thin structure occurs.

- The critical buckling load of AHC panels is determined to be higher than that of NHC panels.

- The failure modes of NHS panels under different loading conditions show similar behavior as that of AHS. However, at NHS panels, which are much brittle than aluminum, prior to core crushing failure, crack generation incurred.

- As the core's density increased, the maximum critical buckling load increased, for both for NHC and AHC panels.

- The compressive response including the buckling, collapse and crushing have been simulated numerically using ABAQUS finite element models for various domain sizes. The models idealize the microstructure as hexagonal. Buckling was confirmed to occur in the elastic regime of the material. The post-buckling response is stable and

stiff as is expected from the plate like strips that constitute the walls of the hexagonal cells.

- In view of the results presented we conclude that the compressive response of honeycomb from the initial elastic part, through buckling, collapse and crushing can be evaluated with engineering accuracy using one characteristic cell. We point out however that the crushing response requires a fine mesh for it to be accurate enough.

- As the cell size increased, the maximum critical buckling load decreased, both for NHS and AHS panels.

- The failure mechanisms during indentation mechanisms depend on the indenter geometry. Damaged area depends strongly on the indenter geometry. The largest damaged areas were observed for cylindrical and hemi-spherical indenters while the smallest damaged areas were observed for conical indenters. The indenter geometry influences the shape of the damaged area on the sandwich. In fact, failure can be radial for a conical indenter (a crack starts at the pin/material interface with a petals shape during the penetration) or it can be circumferential if the indenter is cylindrical/ spherical (the material under the pin undergoes compressive stress and the strain interests the whole sample).

- The indenter geometry has great influence on the indentation resistance and the failure mechanisms of composite sandwich panels. The load is increased when the diameter of the indenter increases.

- It was found that the indentation load increases with the decrease of the cell size of the core.

- Damaged area decreases with the increase of density since the effect of the indentation becomes local due to the increase of stiffness of the panel.

- The stiffness of the sandwich panel increases with the increase of the density of the core. Also the cell size induces relevant effects on the mechanical performances of the samples under static indentation load.

- The sandwich with high core density is much suitable for working conditions in which localized load resistance is necessary.

- There is an increase of absorbed energy when the core cell size is decreased from 9.6 to 3.2 mm; however, when the core cell size is decreased, there is a reduction in the absorbed energy of the structure.

- In detail, experimental tests have been carried out by impacting a mass at a controlled velocity (thus energy) against sandwich panels, for different levels of impact energy and recording the profile of the deformed shape of the skin in correspondence of the impact. The impact test was performed to understand and characterize the type and extent of the damage observed in a variety of honeycomb sandwich panels.

- Moreover, a theoretical model was developed to analyze the failure mechanisms of honeycomb sandwiches subjected to different loading conditions. The model is able to correlate the buckling to the failure modes of honeycomb panels under different loading conditions and to predict the critical loads for each loading condition.

- The critical loads predicted by the theoretical approach were compared using the data obtained by experimental tests carried out on NHS and AHS panels in different loading conditions (compression, low velocity impact, indentation). Their response to static loading was compared with the one obtained for AHS panels with different cell sizes. The predicted values are in good agreement with the experimental measurements.

- As final point, this study determines the effect of repeated low-velocity impact on impact-fatigue life of tow type of honeycomb sandwich structures (AHS and NHS). The following results were obtained from this study: However, the reconstruction of honeycomb geometry by means of CT analyses requires a computation time, which could be reduced with the development of CT technique and software. Thus, the next step of this study will be the comparison between the results obtained by a model, reconstructed by means of the CT images according to the developed procedure, and a FE model, realized considering an ideal geometry, in order to check the reliability of the ideal FE models, evaluating the prediction errors respect to the experimental data.

REFERENCES

1. R. Atkinson, Innovative uses for sandwich constructions, Reinforced Plastics 41, 30–33 (1997).

2. G. Belingardi, M. P. Cavatorta and R. Duella, Material characterization of a composite–foam sandwich for the front structure of a high speed train, Composite Structures 61, 13–25 (2003).

3. Um, T. J., "Mechanical Technology of World; Bonding of Composite - Lightweight Tendency of European Auto Company," Journal of the KSME, Vol. 45, No. 1, pp. 27-29, (2005).

4. Imielińska, K., Guillaumat, L., Wojtyra, R., and Castaings, M., Effects of manufacturing and face/core bonding on impact damage in glass/polyester–PVC foam core sandwich panels, Composites Part B: Engineering, Vol. 39, No. 6, pp. 1034-1041, (2008).

5. Castanie, B., Aminanda, Y., Bouvet, C., and Barrau, J.-J., Core crush criterion to determine the strength of sandwich composite structures subjected to compression after impact, Composite Structures, Vol. 86, No. 1-3, pp. 243-250, (2008).

6. Baumeister J, Banhart J, Weber M. Aluminium foams for transport industry. Materials & Design; 18(4):217e20, (1997).

7. Banhart J, Schmoll C, Neumann U. Light-weight aluminium foam structures for ships. In: Faria L, editor. Proc. Conf. materials in oceanic environment (Euromat '98), Lisbon, Portugal, vol. 1.p. 55e63, (1998).

8. Shin KB, Lee JY, Cho SH. An experimental study of low-velocity impact responses of sandwich panels for Korean low floor bus. Composite Structures;84(3):228e40, (2008).

9. H. Allen, Analysis and Design of Structural Sandwich Panels. Pergamon Press, Oxford, (1969).

10. F. Plantema, Sandwich Construction. Wiley, New York, (1996).

11. D. Zenkert, The Handbook of Sandwich Construction. Emas Publishing, Worcestershire, UK, (1997).

12. J.R. Vinson, The Behavior of Sandwich Structures of Isotropic and Composite Materials. Technomic Publishing, Lancaster, Pennsylvania, (1999).

13. E.E. Gdoutos, I.M. Daniel, K.A. Wang, J.L. Abot, Nonlinear behavior of composite sandwich beams in three-point bending, Experimental Mechanics 41 (2) 182–189, (2001).

14. Abrate S. Impact on composite structures. Cambridge: Cambridge University Press, (2005).

15. Gibson LJ, Ashby MF. Cellular solids: structure and properties. Oxford: Pergamon Press;. p. 93e271, (1988).

16. C. A. Steeves and N. A. Fleck, Material Selection in sandwich beam construction, Scripta Materialia 50, 1335–1339 (2004).

17. A. Petras and M. P. F. Sutcliffe, Failure mode maps for honeycomb sandwich panels, Composite Structures 44, 237–252 (1999).

18. Yamashita, M. and Gotoh, M., Impact behavior of honeycomb structures with various cell specifications—numerical simulation and experiment, International Journal of Impact Engineering, Vol. 32, No. 1-4, pp. 618-630, (2005).

19. Paik JK, Thayamballi AK, Kim GS. The strength characteristics of aluminum honeycomb sandwich panels. Thin-Walled Structures;35(3):205e31, (1999).

20. Abbadi A, Koutsawa Y, Carmasol A, Belouettar S, Azari Z. Experimental and numerical characterization of honeycomb sandwich composite panels. Simulation Modelling Practice and Theory; 17(10):1533e47, (2009).

21. Crupi V, Epasto G, Guglielmino E. Low velocity impact strength of sandwich materials. Journal of Sandwich Structures and Materials; 13(4):409e26, (2011).

22. Crupi V, Montanini R. Aluminium foam sandwiches collapse modes under static and dynamic three-point bending. International Journal of Impact Engineering,34:509–21, (2007).

23. Crupi V, Epasto G, Guglielmino E. Computed Tomography analysis of damage in composites subjected to impact loading. Fracture and Structural Integrity;17:32–41, (2011).

24. Crupi V, Epasto G, Guglielmino E. Collapse modes in aluminium honeycomb sandwich panels under bending and impact loading. International Journal of Impact Engineering; 43:6–15, (2012).

26. N. Barala, Cartiéb, K. Partridgeb, C. Baleyc and P. Davies. Improved impact performance of marine sandwich panels using throughthickness reinforcement: Experimental results Composites Part B: Engineering, Volume 41, 2, 117-123, (2010).

27. ASM Ashab , Dong Ruan , Guoxing Lu, ShanqingXu, Cuie Wen. Experimental investigation of the mechanical behavior of aluminum honeycombs under quasi-static and dynamic indentation. Materials and Design 74 138–149, (2015).

28. M.A. Yahaya, D. Ruan, G. Lu, M.S. Dargusch. Response of aluminium honeycomb sandwich panels subjected to foam projectile impact - An experimental study. International Journal of Impact Engineering 75 100-109, (2015).

29. A. Abbadi, C. Tixier, J. Gilgert, Z. Azari. Experimental study on the fatigue behaviour of honeycomb sandwich panels with artificial defects. Composite Structures 120 394–405, (2015).

30. J. ZHANG and M. F. ASHBY: Buckling of honeycomb under in-plane biaxial stresses, Int. J. Mech. Sci. Vol. 34, No. 6, pp. 491 509, (1992).

31. HYO S. LEE, SOON H. HONG Mechanical behavior and failure process during compressive and shear deformation of honeycomb composite at elevated temperatures Journal of materials science 37, 1265-1272, (2002).

32. Levent Aktay a, Alastair F. Johnson a,*, Bernd-H. Kroplin, Numerical modelling of honeycomb core crush behavior, Engineering Fracture Mechanics 75 2616–2630, (2008).

33. Jae-Youl Lee, Kwang-Bok Shin & Jong-Cheol Jeong Experimental and Numerical Simulation Studies of Low-Velocity Impact Responses on Sandwich Panels for a BIMODAL Tram, Advanced Composite Materials, 18:1, 1-20, (2009).

34. N. Baral, D.D.R. Cartié, I.K. Partridge, C. Baley and P. Davies, Improved impact performance of marine sandwich panels using through thickness reinforcement: Experimental results, Composites Part B: Engineering, Volume 41, Issue 2, Pages 117-123, (2010).

35. Zhibin Li, Zhijun Zheng and Jilin Yu, Low-velocity perforation behavior of composite sandwich panels with aluminum foam core, Journal of Sandwich Structures and Materials 15(1) 92–109, (2012).

36. S. Xu, J.H. Beynon, D. Ruan, G. Lu, Experimental study of the out-of-plane dynamic compression of hexagonal honeycombs, Compos.Struct. 94 (8) 2326–2336, (2012).

37. Kaman MO, Solmaz MY and Turan K. Experimental and Numerical Analysis of Critical Buckling Load of Honeycomb Sandwich Panels. J Compos Mater 44: 2819-2831, (2010).

38. Y. Aminandaand al, Experimental Analysis and Modeling of the Crushing of Honeycomb Cores. (2005).

39. Zhou, Q. And Mayer, R.R: Characterization of Aluminum Honeycomb Material Failure in Large Deformation Compression, Shear, and Tearing. (2002).

40. Mohr, D. And Doyoyo, M Nucleation and Propagation of Plastic Collapse Bands in Aluminum Honeycomb . (2003).

41. Deformation-induced Folding Systems in Thin-walled Monolithic Hexagonal Metallic Honeycomb. Mohr, D.AndDoyoyo, M. (2004).

42. Hong, S.-T., Pan, J., Tyan, T. And Prasad, P.Quasi-static Crush Behaviors of Aluminum Honeycomb Specimens under Compression Dominant Combined Loads. International Journal of Plasticity, 22(1):73-109, (2006).

43. Wilbert, W.Y. Jang, S. Kyriakides, J.F. Floccari.. Buckling and progressive crushing of laterally loaded honeycomb.International Journal of Solids and Structures 48 803–816, (2011)

44. Zhang P, Cheng Y, Liu J, Wang C, Hou H, Li Y. Experimental and numericalinvestigations on laser-welded corrugated-core sandwich panels subjected to air blastloading. Mar Struct; 40: 225-246, (2015).

45. Qiu A, Lin W, Ma Y, Zhao C, Tang Y. Novel material and structural designs for large scales marine protective devices. Mater Design; 68: 29-41, (2015).

46. Crupi V, Kara E, Epasto G, Guglielmino E, Aykul H. Prediction model for the impact response of glass fibre reinforced aluminium foam sandwiches. Int J Impact Eng; 77: 97–107, (2015).

47. Foo CC, Chai GB and Seah LK. Quasi-static and low-velocity impact failure of aluminium honeycomb sandwich panels. Proc. IMechE Part L: J Mater Des Appl; 220(2): 53–66, (2006).

48. Castanié B, Buovet C, Aminanda Y, Barrau JJ, Thevenet P. Modelling of low energy/low-velocity impact on Nomex honeycomb sandwich structures with metallic skins. Int J Impact Eng; 35: 620 – 634, (2008).

49. S Dietrich, K Weidenmann, P Elsner. 3D tomographic characterization of sandwich structures. NDT & E Int; 62: 77–84, (2014).

50. Niknejad A, Liaghat GH, MoslemiNaeini H, Behravesh AH. A theoretical formula for predicting the instantaneous folding force of the first fold in a single cell hexagonal honeycomb under axial loading. P I MechEng C - J Mec; 224 (11): 2308-2315, (2010).

51. Fan X, Verpoest I and Vandepitte D. Finite Element Analysis of Out-of-plane Compressive Properties of Thermoplastic Honeycomb. J Sandwich Struct Mater; 8: 437-458, (2006).

52. Jeyakrishnan PR, ChockalingamKn K. SK, Narayanasamy R. Studies on buckling behavior of honeycomb sandwich panel. Int J AdvManufTechnol; 65: 803–815, (2013).

53. Nurashikin S. and Hazizan A. Preparation and properties of thermoplastic honeycomb core sandwich structure with aluminum skin. J Compos Mater; 46(2): 183–191, (2012).

54. Li Z, Zheng Z and Yu J. Low-velocity perforation behavior of composite sandwich panels with aluminum foam core. J Sandwich Struct Mater; 15(1): 92–109, (2012).

55. Shitta-Bey OT, Carruthers JJ, Soutis C, Found MS. The localized low-velocity impact response of aluminium honeycombs and sandwich panels for occupant head protection: experimental characterization and analytical modeling. Int J Crashworthiness; 12(5): 549-558, (2007).

56. Zhu S, Chai GB. Damage and failure mode maps of composite sandwich panel subjected to quasi-static indentation and low velocity impact. Compos Struct; 101: 204-214, (2013).

57. Borsellino C, Calabrese L, Di Bella G. Windsurf-Board Sandwich Panels Under Static Indentation. Appl Compos Mater; 15: 75-86, (2008).

58. HooFatt MS, Park KS. Dynamic models for low-velocity impact damage of composite sandwich panels-Part B: damage initiation. Compos Struct; 52: 353-364, (2001).

59. KeskesBoualem, Z.Azari, Static and Fatigue Characterization of Nomex Honeycomb Sandwich Panels, Journal of Engineering Sciences, Doi10.5505, 287-292, (2013).

60.BentouhamiAbderrahmane, KeskesBoualem, Experimental analysis and modeling of the Buckling of a loaded honeycomb sandwich Composite, Materials and technology 49 2, 235–242, (2015).

61.Keskes B. These de doctorat (2007)

62. Onck P.R., Andrews E.W. and Gibson L.J. Size Effects on Ductile Cellular Solids. Part 1: Modelling. International Journal of Mechanical Science 43 pp.681-699, (2001).

63. Silbermann V. Mode 1 Dynamic Delamination Testing for Advanced Composite Materials. MSc Thesis. Cranfield University. (2003)

64. Simon Amine Equivalent Numerical Model for Honeycomb Subjected to High Speed Impact, A Thesis submitted to McGill University in partial fulfillment of the requirements for the degree of Master of Engineering.

65. Darılmaz K. Analysis of sandwich plates: a three-dimensional assumed stress hybridfinite element. J SandwStruct Mater; 14: 487–501, (2012).

66. Vincenzo Crupi, Gabriella Epasto, Eugenio Guglielmino, Hozhabr Mozafariand Sarah Najafian : Computed tomography-based reconstruction and finite element modeling of honeycomb sandwiches under low-velocity impacts, Journal of Sandwich Structures & Materials, Vol. 16(4) 377–397, (2014)

Abstract

Due to their high specific strength and stiffness, honeycomb sandwich structures are used in impact-resistance applications. Their structural efficiency depends to a great extent on the lightweight core separating the face sheets and providing overall high stiffness.

This study will present the Experimental, numerical and theoretical studies of composite sandwich structures

This thesis has investigated composite honeycomb sandwich materials commonly used in marine and aeronautic structures. The critical buckling loads for various core densities and materials of honeycomb composite panels are experimentally, theoretically and numerically investigated in this study.

Experimental work has investigated their failure behavior under static and dynamic loading according to the change of sum key parameters.

Otherwise, failure mechanisms in the skin and core of these structures have been identified for each loading case. In meantime, we aim to present the analytical and numerical investigation of response of composite honeycomb sandwich materials under different loading (compression, quasi-static indentation and low velocity impact) to understand how geometrical configuration affects failure mechanism of these structures. By varying the geometrical parameters (cell size, indenter and impactor geometry); core material (AHC and NHC) and loading conditions (velocity of solicitation) experimental tests were carried out. All structures tested in this work have an aluminum skin and honeycomb core (AHC and NHC).

After the impact tests at different velocities a 3D acquisition of the impacted honeycomb panels and their internal buckling, undetectable by a visual inspection, has been carried out by ka XCT system.

This work focuses on development of a theoretical approach able to correlate the buckling to the failure modes of honeycomb sandwiches under different loading conditions (static and dynamic) and to estimate the critical buckling load at each loading. The theoretical results tallied with the experimental ones and consequently it was shown that the theoretical model is a reliable predictor of buckling loads in composite honeycomb sandwich materials with defined geometry. The critical buckling loads and failure modes of the composite honeycomb sandwich materials have been determined by applying quasi-static and dynamic tests on these structures. A three-dimensional geometrically correct finite element model of the honeycomb sandwich plate is developed using the commercial software, ABAQUS. By adopting a discrete modeling approach where the cell walls and the face-sheets are explicitly modeled using shell elements, accurate prediction of the damage mechanisms and failure are possible. The finite element model which was developed in ABAQUS/CAE to validate experimental and analytical analysis produced agreeable results. The obtained numerical buckling loads have been compared with the experimental results and presented in tables.

Key words: Sandwiches Structures / low-velocity impact/ Computerized Tomography (CT)/Buckling.

ملخص

تم من خلال هذه الأطروحة مناقشة نوع من أنواع المواد المركبة ألا وهو مادةالسندويشالمركبة حيث تكون الطبقة الوسطى على هيئة عش النحل و تستخدم عادة في الإنشاءات البحرية و الملاحة الجوية و المركبات الفضائية. ومن اجل دراسة سلوك هذه الهياكل في أي تحميل خارجي سواء كان ستاتيكي أو ديناميكي, قمنا بدراسة تجريبية عميقة لهاته الهياكل في كلتا الحالتين (الستاتيكية و الديناميكية) مع تغيير بعض المعايير التي ارتأيناها مهمة في دراستنا هذه التي أعطتنا نتائج مهمة متمثلة في قوانين جديدة لتحديد آلية تحطم هذه المواد.

من خلال هذه الدراسة أيضا، تم تحديد آليات تحطم في الغطاءين(الوجهين السطحيين) و الطبقة الوسطىلهذه الهياكل لكل حالة التحميل(الستاتيكية و الديناميكية). في غضون ذلك، نهدف إلى تقديم البحوث التحليلية والرقمية لتحديد سلوك هذه المواد تحت تحميل مختلف (ضغط، ضغط مركز شبهستاتيكي وتحميل منخفض السرعة) لفهم كيفية تأثير التكوين الهندسي على آلية تحطم هذه الهياكل. من خلال تغييرشروطالتحميل(سرعة التحميل) و المعايير الهندسية (حجم الخلية،شكلالإندينترو المسبار) ونوع مادة الطبقة الوسطى لهذه الهياكلأجريت اختبارات تجريبية عليها. جميع الهياكل التي تم اختبارها في هذا العمل تتكون من غطاء منالالومنيوم إما الطبقة المركزية فكانت إما مصنوعة من الالومنيوم و إما من نومكس.

ولتحقيق الاستخدام الأمثل لهذا النوع من الماد، تم تطوير النهج النظري الذي يسمح للدراسات المعملية التي يتعين القيام بها.وبالإضافة إلى ذلك، تم استخدام نموذج نظري من اجل إيجاد قيمة قوة التحميل في كل حالة. و قورنت النتائج النظرية مع تلك التجارب، وبالتالي تبين أن النموذج النظري المستعمل في دراستنا مقبول و يمكن الاعتماد عليه من اجل تحديد آليات تحطم هذه المواد مع هندسة معرفة.أما قيمة قوة الحرجة لالتواء وسائر أشكال تحطم هذه المواد المركبة تم تحديدها من خلال تطبيق اختبارات شبه ثابتة وديناميكية على هذه الهياكل.

كما تم تطوير نموذج هندسي ثلاثي الأبعاد باستخدام البرمجيات التجارية أبكيسوقد تم مقارنة قيمة قوة الحرجة لالتواء العددية التي تم الحصول عليها مع النتائج التجريبية وقدمت في الجداول

كلمات مفتاحية: المواد المركبة/نموذج هندسي/الالتواء/آليات التحطم/